Transport-Depletion Desalination Pilot Plant

United States Department of the Interior

Office of Saline Water • Research and Development Progress Report No. 683

Research and Development Progress Report No. 683 • April 1971

Transport-Depletion Desalination Pilot Plant

By Ralph Redman, Pratt & Whitney Aircraft, East Hartford, Connecticut, for Office of Saline Water, Chung-ming Wong, Director; W. F. Savage, Assistant Director, Engineering and Development; K. C. Channabasappa, Chief, Membrane Division.

Contract No. 14-01-0001-1262

United States Department of the Interior, Rogers C. B. Morton, Secretary
James R. Smith, Assistant Secretary, Water and Power Resources

For sale by the Superintendent of Documents, U.S. Government Printing Office
Washington, D.C. 20402 - Price $2.75
Stock Number 2400-0636

As the Nation's principal conservation agency, the Department of the Interior has basic responsibilities for water, fish, wildlife, mineral, land, park, and recreational resources. Indian Territorial affairs are other major concerns of America's "Department of Natural Resources".

The Department works to assure the wisest choice in managing all our resources so each will make its full contribution to a better United States—now and in the future.

FOREWORD

This is one of a continuing series of reports designed to present accounts of progress in saline water conversion and the economics of its application. Such data are expected to contribute to the long-range development of economical processes applicable to low-cost demineralization of sea and other saline water.

Except for minor editing, the data herein are as contained in a report submitted by the contractor. The data and conclusions given in the report are essentially those of the contractor and are not necessarily endorsed by the Department of the Interior.

TABLE OF CONTENTS

VOLUME I

TABLE OF CONTENTS (Cont'd)

TABLE OF CONTENTS (Cont'd)

LIST OF FIGURES

LIST OF FIGURES

LIST OF FIGURES

LIST OF FIGURES

LIST OF FIGURES

LIST OF FIGURES

LIST OF FIGURES

LIST OF FIGURES

LIST OF TABLES

I. INTRODUCTION

Pratt & Whitney Aircraft conducted an engineering and development program for the Office of Saline Water, U. S. Department of the Interior, to design, construct, and test a transport-depletion desalination pilot plant of 10,000 gallons per day capacity. The work was divided into six major categories, as follows:

1) Review of existing transport-depletion data including that resulting from the investigation performed by Southern Research Institute, Birmingham, Alabama.

2) Generation of additional data from bench-scale and channel-evaluation tests required to adequately understand the process.

3) Design and construction of a transport-depletion pilot plant, including the evaluation of alternate design concepts for the stack.

4) Testing of the pilot plant on a feed solution of 3000 ppm NaCl, using stack sizes of both five cell pairs and forty cell pairs.

5) Design and cost study of a 500,000 gpd test-bed desalination plant using the transport-depletion process.

6) Parametric cost study of commercial-size transport-depletion desalination plants of 1, 5 and 10 million gallons per day capacity.

Consulting services and bench-scale investigations in support of this program were provided by Southern Research Institute of Birmingham, Alabama. The last two items were prepared with the assistance of Stone & Webster Engineering Corporation, Boston, Massachusetts.

II. SUMMARY

The transport-depletion data obtained by the Southern Research Institute and by the Bureau of Reclamation at Denver, Colorado and at Webster, South Dakota, was reviewed. This data review made it possible to develop a design methodology for the pilot plant, and to identify the additional data required to adequately predict the performance of a transport-depletion stack. The data review with the additional information resulting from bench-scale evaluations performed at Southern Research Institute, indicated that optimum stack performance would be achieved with higher solution velocities, smaller membrane spacing, and longer path lengths than were being used up to that time. A channel-evaluation program was performed by Pratt & Whitney Aircraft to evaluate turbulence-promotion screens and solution inlet and exit configurations suitable for a thin-channel pilot-plant design. Nine turbulator screens and four solution inlet configurations were evaluated.

An evaluation of over twelve different stack design concepts and variations was completed which resulted in the selection of a forty-cell-pair plate-and-frame design with four separate channels for the pilot plant. Each channel had separate electrodes, electrode-rinse streams and manifolding. Path lengths of 33.5, 67, and 134 inches could be obtained by connecting these channels in various series and parallel arrangements. Membrane spacing was 30 mils. The spacer screens were 40 inches long by 22 inches wide. They were of unitized construction with an epoxy-impregnated Fiberglas frame containing a Vexar 15 PDS-129 polypropylene turbulator screen.

A stack assembly of five cell pairs was first tested to demonstrate the design concept. This was followed by the testing of the complete forty-cell-pair stack. Both tests were performed with a feed solution of 3000 ppm NaCl. The forty-cell-pair stack was tested over a range of channel velocities from 2 to 5.75 in/sec, current densities from 5 to 50 ma/cm^2, product-to-waste ratios of 1/1, 4/1, 8/1 and 12/1, path lengths of 33.5, 67, and 134 inches and stack flow capacities from 4000 to 28,800 gpd. Current efficiencies ranged from 36 to 70 percent. Product concentrations as low as 120 ppm were produced. Cell pair areal resistances from 20 to 280 ohm-cm^2 were measured.

A design and cost study of a 500,000 gpd transport-depletion test-bed plant was performed by Pratt and Whitney Aircraft and its subcontractor Stone & Webster Engineering Corporation, which showed that the test-bed plant would cost $1,401,700 to construct and would produce potable water at a cost of $1.81 per thousand gallons. The test-bed plant is not the optimum design. A parametric cost study and a series of projected cost estimates for commercial plants of 1, 5 and 10 mgd capacities showed potable water costs ranging from $1.27 per thousand gallons for a 1-mgd plant to $0.811 per thousand gallons for a 10-mgd plant.

II. DESCRIPTION OF TRANSPORT-DEPLETION PROCESS

A. Qualitative Description

The transport-depletion process for desalting water is one variation of the electrodialysis process. The electrodialysis method of desalination makes use of the property of certain membranes to selectively conduct ions of a particular electrical charge when driven by an electrical field. Membranes are available which transport in solution, either positively-charged ions only (cation membranes), or negatively-charged ions only (anion membranes). A conventional electrodialysis stack consists of a series of parallel alternating cation and anion membranes, spaced typically 20 to 60 mils apart by means of suitable frames, and held between two electrodes. The ion separation is accomplished by placing an electrical field across the two electrodes and causing the saline solution to flow through the compartments between the ion-selective membranes. This process is illustrated schematically in Figure 1 which shows a cross-section of an electrodialysis stack fed by a sodium chloride solution. Sodium ions attracted by the cathode pass freely through the cation membrane, but are restricted from passing through the anion membranes. Chloride ions attracted by the anode pass freely through the anion membranes, but cannot pass through the cation membranes. This process causes one set of alternating compartments, D, to become ion-depleted (product water) and the other set of alternating compartments, E, to become ion-enriched (concentrate or waste water).

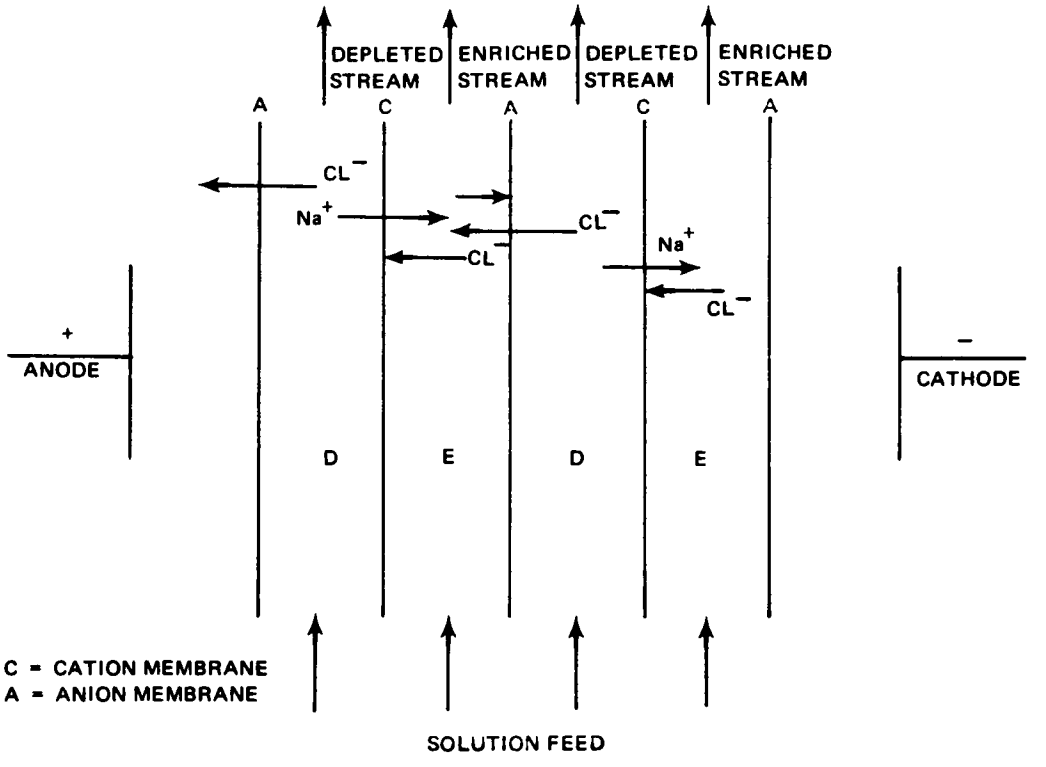

Figure 1 Schematic of Electrodialysis Process

In the transport-depletion process, all of the anion membranes are removed and replaced by neutral membranes. A perfect neutral membrane is defined as having the same ion-transport properties as water. An ion-separation process similar to conventional electrodialysis still occurs, as illustrated in Figure 2, except that sodium ions are no longer restricted by the membrane sheets from moving towards the cathode. The chloride ions, however, are still restricted from free passage across the membrane stack by the cation membranes.

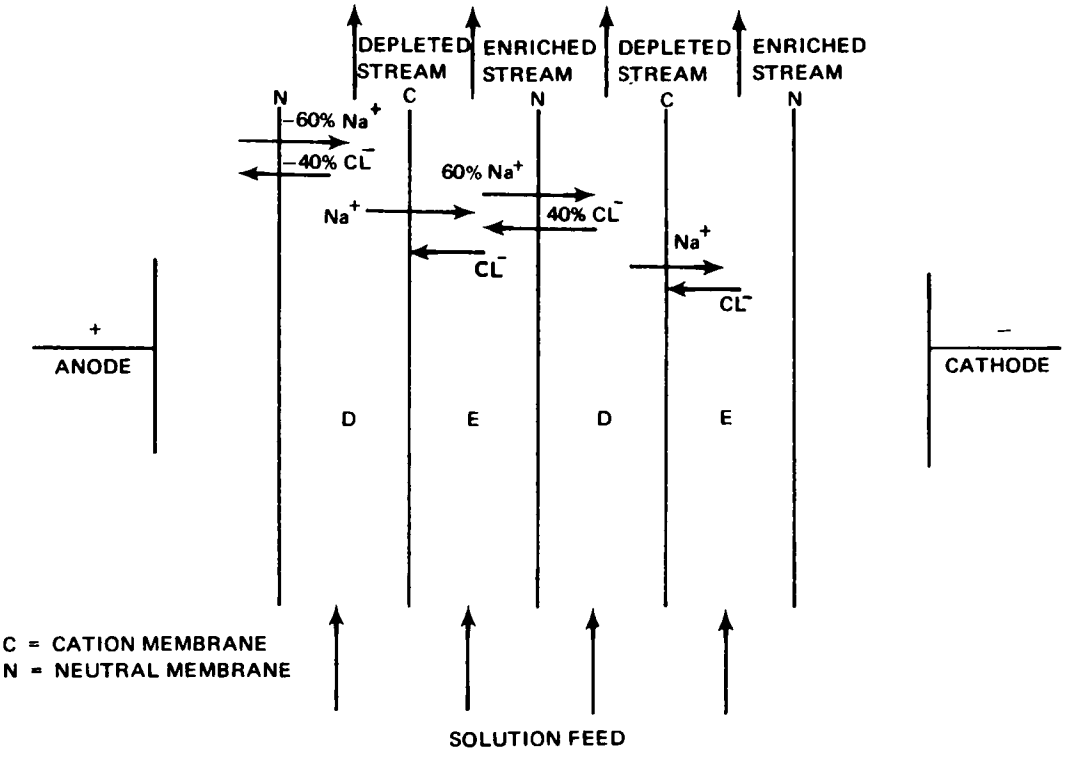

Figure 2 Schematic of Transport-Depletion Process

The transport-depletion process can be understood by examining the properties of an idealized "cell pair". The cell pair is the basic repeating unit of a transport-depletion stack. It is composed of a cation membrane, a neutral membrane, a depleted stream and an enriched stream arranged as shown in Figure 3. This basic structure is repeated many times to form a stack. In the idealized cell pair shown in Figure 3, the membranes are assumed to be impermeable to water. Furthermore, the cation membrane permits passage of sodium ions only, and the neutral membrane permits passage of sodium ions and chloride ions in exactly the same ratio as these ions are transported by an electrical current in a salt-water solution.

In a sodium chloride solution the transference number of the sodium ion, i.e., the fraction of the total current carried by sodium, is 0.39. Likewise, the transference number of the chloride ion is 0.61. This means that in both the neutral membrane and the depleted and

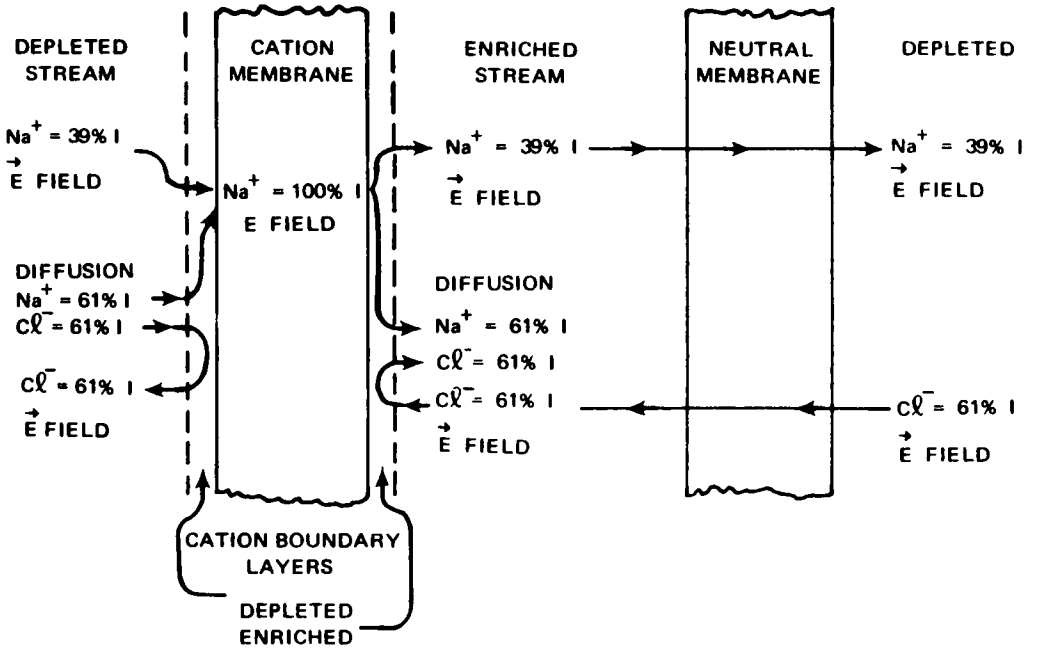

Figure 3 Schematic of Transport-Depletion Cell Pair

enriched streams, 39 percent of the current is carried by sodium ions moving towards the cathode (to the right in Figure 3) and 61 percent of the current is carried by chloride ions moving towards the anode (to the left in Figure 3). In the cation selective membrane, however, all of the current must be carried by the sodium ions, since this membrane permits passage of cations only.

The discrepancy between the rate of ion transport in the cation membrane and in the adjacent solutions results in the formation of concentration boundary layers on both surfaces of the cation membrane. In the depleted-stream boundary layer the flow of current, I, causes a net removal of sodium ions to the right (into the cation membrane), and chloride ions to the left (into the depleted stream bulk), both at a rate proportional to 61 percent of I. The continuous removal of sodium chloride from the boundary layer by current flow creates a concentration gradient which causes a net diffusion of sodium chloride from the depleted stream bulk into this boundary layer.

A similar situation exists in the enriched-stream boundary layers. In this case the flow of current, I, causes a net enrichment of sodium ions from the cation membrane and chloride ions from the enriched stream bulk, at a rate proporational to 61 percent of I. The net increase of sodium chloride is removed by diffusion from the boundary layer into the enriched stream bulk.

Thus, there is a diffusive flow of sodium chloride to the membrane on the depleted-stream side and away from the surface on the enriched-stream side. Therefore, the effect of the cation membrane is to stimulate the flow of sodium chloride from the depleted stream to the enriched stream, at a rate proporational to 61 percent of I.

No similar separation process occurs at the neutral membrane. It is required only to prevent the enriched and depleted streams from mixing together, while allowing current to flow across the cell pair by the transport of ions in either direction. It should be noted that no concentration boundary layers exist next to the neutral membrane, since its ion-transport properties in the ideal case are the same as those of the salt solution.

The use of neutral membranes in place of the anion membranes offers several potential advantages and one prime disadvantage. The disadvantage is the reduced current utilization that is possible with neutral membranes. In the transport-depletion process, only 61 percent of the current in the ideal case is useful in removing salt from the product stream. Some of the advantages which the transport-depletion process offers are as follows:

1) The enriched-stream concentration boundary layer adjacent to the anion membrane is eliminated. Salt precipitation within this layer normally limits the current density and enriched-stream concentration for the electrodialysis process. A combination of higher current density and higher waste-stream concentration can be achieved with the transport-depletion process.

2) The depleted-stream concentration boundary layer adjacent to the anion membrane is eliminated. This lowers the stack electrical resistance and tends to reduce power consumption. Water splitting which also can occur in this layer, producing extraneous hydrogen and hydroxyl ion transport across the stack, is markedly reduced.

3) The pH of both the depleted and enriched streams tends to remain neutral, because of the lack of hydrogen and hydroxyl ion transport. Operation at high current density may cause the enriched stream to become acidic rather than basic, because of the transport characteristics of the two membranes. An acidic enriched solution is less susceptible to precipitation.

4) The neutral membrane does not appear to be as susceptible to fouling as is the anion membrane.

5) Material cost of the neutral membrane is negligible when compared to that of anion membranes.

B. Analytical Description

Analytical expressions which define the relationships between geometric and operating parameters are required in order to design a transport-depletion stack and to understand its performance. The basic relationships are the same for both transport depletion and electrodialysis, however, the values of many of the parameters may differ. These relationships can best be developed by examining the properties of the basic repeating unit of the stack, the cell pair. The properties of the cell pair can then be used to determine the performance of the entire stack.

1. General Equations for Cell-Pair Performance

Faraday's law, as related to the transport-depletion process, states that the effective or useful current passed through a cell pair is directly proportional to the number of equivalents of salt transported through the membranes. Using Faraday's constant this can be written as

$$\text{equivalents passed per second} = \frac{\text{effective current, amperes}}{\text{96,500 coulombs/equivalent}} \quad (1)$$

This equation indicates the maximum desalination that can be achieved with a given current, if all of the current passing through the cell pair is effective in transporting salt. In fact, all of the current used is not effective, and the term "coulomb efficiency" is used to describe the effectiveness of the current in producing the desired desalination. Coulomb efficiency is defined as

$$\eta_I = \frac{\text{effective current}}{\text{actual current passed through cell pair}} \quad (2)$$

Using the definition of effective current as expressed in Equation (1) by Faraday's law, coulomb efficiency can be written as

$$\eta_I = \frac{\text{(equivalents passed per second)}\ \text{(96,500 coulombs/equivalent)}}{\text{(actual current passed through cell pair)}} \quad (3)$$

The coulomb efficiency obtainable with a particular set of membranes is determined primarily by the difference in transport number of the membranes. The transport number of a membrane is defined as the fraction of the current carried through the membrane by an ion of a particular charge. Thus, a perfect cation membrane has a cation transport number of $t_C^+ = 1.0$, and a perfect anion membrane has a cation transport number of $t_A^+ = 0$. The transport number of a neutral membrane immersed in a NaCl solution would ideally be about $t_N^+ = 0.39$, which is the cation transport number of Na^+ in water at typical brackish-water concentrations. The upper limit of coulomb efficiency for the transport-depletion process with perfect neutral membranes in a sodium chloride solution is ideally 61 percent, derived as follows:

$$\eta_I = t_C^+ - t_N^+ = 1.0 - 0.39 = 0.61 \quad (4)$$

In practice, the coulomb efficiency is reduced below this ideal value by other processes which occur in the transport-depletion stack. These deleterious processes include:

1) Back-diffusion across the membranes can occur due to the concentration gradient between the enriched and dilute streams. Back-diffusion across most cation membranes is negligibly small. Back-diffusion across presently-available neutral membranes can be significant and must therefore be considered.

2) Osmotic water transport across the membrane may occur but is usually negligible for either membrane.

3) Extraneous ion conduction in the form of H^+ (or H_3O^+) and OH^- conduction may occur but has not been detected in the transport-depletion process. It would certainly occur under extreme combinations of very high current densities and very low depleted-stream concentrations.

4) Other causes of decreased coulomb efficiency include mechanical defects such as holes or rips in membranes, and solution leakage between enriched and dilute compartments.

The actual current required to achieve a desired degree of demineralization can be expressed in terms of geometric and operating parameters by combining Equations (1) and (2), and noting that the equivalents of salt transported per unit time equals the solution flow rate times the change in salt concentration.

$$\text{equivalents of salt per second} = \Delta N q \tag{5}$$

Where

ΔN = change in concentration, equivalents/liter

q' = volumetric flow rate through depleting compartment of cell pair, liters/sec

The combination of Equations (1), (2) and (5) results in the following expression of Faraday's law.

$$\eta_I I = \Delta N q' \times 96{,}500 \tag{6}$$

Where

I = actual current passed through cell pair, amperes

A more useful form is derived by using the following definitions.

$$i = \frac{I}{w' l' \times 10^{-3}} \tag{7}$$

$$V_{oc} = \frac{q'}{w' d' \times 10^{-3}} \tag{8}$$

Where

i = average current density across cell pair, ma/cm^2

w′= width of channel or flow path, cm

l′= length of channel or flow path , cm

V'_{oc} = open-channel solution velocity, cm/sec

d′= channel depth (membrane spacing), cm

The substitution of Equations (7) and (8) into Equation (6) results in

$$\eta_I \, i \, l' = \Delta N \, V'_{oc} \, d' \times 96{,}500 \tag{9}$$

For sodium chloride, one equivalent equals 58.45 gm, therefore

$$\Delta N = \frac{\Delta ppm}{58.45 \times 10^3} \tag{10}$$

Where

Δppm = change in concentration of NaCl, ppm

When using a sodium chloride solution, Equation (9) now becomes

$$\eta_I \, i \, l' = \frac{\Delta ppm \, V'_{oc} \, d' \times 96{,}500}{58.45 \times 10^3} \tag{11}$$

Using engineering units and rearranging Equation (11), current density can be expressed by

$$i = 4.19 \left(\frac{d}{l}\right)\left(\frac{V_{oc} \, \Delta ppm}{\eta_I}\right) \tag{12}$$

Where

i = average current density, ma/cm^2

d = channel depth (membrane spacing), inches

l = channel length, inches

V_{oc} = open-channel solution velocity, inches/sec

Δppm = change in depleting stream NaCl concentration, ppm

η_I = coulomb efficiency for cell pair, fractional

Equation (12) shows that the current density required to achieve a given demineralization effect is strictly a function of cell-pair geometric parameters (d and l) and operating parameters (V_{oc}, Δppm and η_I). This equation also holds for a stack with any number of cell pairs. It can, of course, also be used to calculate the coulomb efficiency of a stack when the other parameters are known.

Another useful form of Equation (6) can be derived in a manner similar to Equation (12) by noting that

$$q' = \frac{Q'}{n} \qquad (13)$$

Where

Q' = total depleting-stream flow rate through the stack, liters/sec

n = number of depleting compartments in the stack

Using engineering units, and combining Equations (13) and (10) with Equation (6), results in

$$I = \frac{0.104\ Q\ \Delta ppm}{n\ \eta_I} \qquad (14)$$

Where

I = current through cell pairs in stack, amperes

Q = total depleting-stream flow rate through stack, gpm

Δppm = change in depleting-stream NaCl concentration, ppm

n = number of depleting streams in stack

η_I = coulomb efficiency of stack cell pairs, fractional

Equation (14) is useful in evaluating the overall current utilization of a particular stack, In this case, the current I is the total current to the stack electrodes, and η_I then becomes the total current utilization for the stack. Stack current utilization not only includes the effects of cell-pair losses but current leakage through the manifolds, and other losses due to any current path other than through the cell pairs.

2. Cell Pair Resistance

The resistance of a cell pair determines the electric field required to produce the current necessary to achieve the desired demineralization. This resistance is best expressed as an areal resistance, for it then becomes independent of stack area. Since the resistance of a cell pair is dependent upon the concentration of the solutions in the two compartments, its value will vary from location to location as the solution concentrations vary. The value stated in describing the areal resistance of a cell pair therefore represents the average or effective areal resistance over the entire cell pair area.

The resistance of a cell pair can be considered as being made up of eight component resistances connected in series. These eight resistances correspond to eight regions in the cell pair, namely, two membranes, two bulk solutions, and four concentration boundary layers. A perfectly neutral membrane will not have any concentration boundary layers associated with it, and in this case, only six regions need be considered. In practice, however, a completely neutral membrane rarely exists, if ever.

The areal resistance of a cell pair is expressed as follows:

$$R_{CP} = R_C + R_N + R_{DB} + R_{CB} + \Sigma R_{BL} \qquad (15)$$

Where

R_{CP} = cell-pair areal resistance, ohm-cm^2

R_C = cation-membrane areal resistance, ohm-cm^2

R_N = neutral-membrane areal resistance, ohm-cm^2

R_{DB} = depleted-bulk-stream areal resistance, ohm-cm^2

R_{CB} = concentrate-bulk-stream areal resistance, ohm-cm^2

ΣR_{BL} = sum of boundary-layer areal resistance, ohm-cm^2

In the following paragraphs, these terms are discussed in further detail.

Membrane Resistance – Two types of membranes are of interest for the transport-depletion process, ion-selective membranes (usually cation selective) and neutral membranes. Ion-selective membranes exhibit fairly uniform resistance characteristics, regardless of the solution concentrations adjacent to them. This suggests that ions are transported across the membrane by traveling through the lattice of the membrane material and are therefore little affected by the solutions from which they come. Neutral membranes for the most part behave like sponges, i.e., they exhibit a resistance characteristic similar to that of a solution indicating that the solutions have saturated the membrane. The membrane in this case does little more than impede mixing of the two solutions on either side. The resistance of both ion-selective and neutral membranes is best determined by actual measurement. Neutral-membrane resistance data must be correlated with solution concentrations over the range of interest.

Bulk Stream Resistance – The resistance of the streams between the membranes is a function of the concentration of the solutions and the characteristics of the turbulence-promotion screen which may be present in the solution channel. The turbulence-promotion screen reduces the compartment volume effectively occupied by the solution, and also reduces the cross-sectional area of solution between the membrances that is available for current conduction. The specific resistance of a solution can be described as:

$$\rho = \frac{1000}{\Lambda N} \tag{16}$$

Where

ρ = specific resistance, ohm-cm

Λ = equivalent conductance of salt in solution, (mho/cm) / (equivalents/cm^3)

N = concentration of solution, equivalents/liter

The resistance per unit area of a bulk solution is therefore

$$R_B = \rho d' = \frac{1000\, d'}{\Lambda N} \tag{17}$$

Where

R_B = areal resistance of bulk solution, ohm-cm^2

d'= channel depth (membrane spacing), cm

A factor must be introduced to this equation which accounts for the effective reduction in area due to the presence of a turbulator screen. The general form of the equation remains.

$$R_B = \frac{K\, d}{ppm} \tag{18}$$

Where

K = constant which includes effects of turbulator screen, equivalent conductance, and dimensional corrections

d = membrane spacing, inches

ppm = concentration of solution in bulk stream, ppm

Boundary Layer Resistance - Boundary-layer resistance can form a significant if not insurmountable barrier to the successful operation of a stack. The boundary layers must be treated in such a way that significant concentration polarization does not occur. Otherwise precipitation on the concentrate side of the membrane, and/or a layer of very-high-purity water on the depleted side can lead to extremely high resistances and loss of performance.

The concentration boundary layers are formed as a result of a change in transport number at the membrane-solution interface. This discontinuity of transport numbers results in either the depletion or buildup of ions at the interface, which, in turn, creates a concentration gradient in the boundary layer. Continuity of ion conduction across the boundary layer is maintained by the diffusion process resulting from this concentration gradient.

The resistance of each boundary layer is a complex function of the geometry of the solution channel and turbulator screen, current density, flow velocity, transport numbers of the solution and membrane, and bulk solution concentration and composition. The resistances of the two concentrate-stream boundary layers can usually be neglected, except where precipitation has occurred. However, the resistances of the dilute-stream boundary layer can be substantial, especially in the case of the dilute-stream cation-membrane boundary layer. The resistance of the dilute-stream neutral-membrane boundary layer can be neglected as long as the neutral-membrane transport number is close to that for a true neutral membrane. Thus it is the dilute-stream cation-membrane boundary layer which may develop a substantial resistance and it should therefore receive maximum attention when estimating repeating-cell-pair resistance.

Correlations of experimental resistance data appear at this time to provide the most practical means of estimating boundary-layer resistance. Direct calculation of these resistances is impossible without adequate knowledge about the thickness and concentration profile of the boundary layer. A qualitative description of the boundary layer is very useful nevertheless. It should suggest the system variables that are important in describing boundary-layer resistance, and may even suggest a functional form for the correlation equations.

The resistance of a boundary layer can be expressed as the sum of many increments of resistance.

$$R_{BL} = \left| \int_{o}^{d_{BL}} \frac{1000\, dx}{\Lambda(N)\, N_{(x)}} \right| \qquad (19)$$

Where

R_{BL} = a real resistance of the boundary layer, ohm-cm^2
dx = thickness of boundary layer increment
$N_{(x)}$ = solution concentration at location (x)
$\Lambda(N)$ = equivalent conductance at concentration $N_{(x)}$
d_{BL} = thickness of boundary layer

This integral cannot be evaluated without making further assumptions about the boundary layer thickness d_{BL} and the shape of the concentration gradient $N_{(x)}$.

Usually, a linear concentration profile is assumed and Equation (19) can then be evaluated as:

$$R_{BL} = \left| \frac{1000\, d_{BL}}{N_{(x)}\,(N_B - N_M)} \ln \frac{N_B}{N_M} \right| \qquad (20)$$

Where

N_B and N_M = solution concentrations at boundary-layer limits
N_B = concentration of bulk solution
N_M = concentration at membrane interface

Equation (20) is still not directly useful for calculating boundary-layer resistance, since the thickness of the boundary layer d_{BL} is not known. Furthermore, it cannot be accurately calculated, particularly when a turbulator screen is present in the channel. Nevertheless Equation (20) can form the basis for several interesting qualitative statements about the expected behavior of the boundary layer resistance with changes in operating and geometric parameters.

1) Reducing the thickness of the boundary layer will decrease its resistance. This suggests the use of turbulence-promotion devices and high solution velocities to minimize the effective thickness of the boundary layer.

2) Boundary-layer resistance increases rapidly when the solution concentration at the membrane interface approaches zero. This effect is consistent with the limiting-current-density effect experienced with conventional electrodialysis, and suggests the use of any device or combination of parameters that will minimize boundary-layer thickness.

3) If it is recalled that the boundary-layer concentration gradient is established as a result of current flow which tends to increase the concentration gradient, and the resulting diffusion process which tends to decrease the gradient, another equation can be written as follows:

$$i = K\frac{dN}{dX} = K\frac{(N_B - N_M)}{d_{BL}} \qquad (21)$$

Where

i = current density
K = constant
dN = concentration gradient across boundary layer
dX = thickness of boundary layer

Equation (21) can be combined with Equation (20) to eliminate N_M. The result is

$$R_{BL} = \left| \frac{1000\,K}{\Delta(X)\,i} \ln \left[\frac{N_B}{N_B - \frac{i\,d_{BL}}{K}} \right] \right| \qquad (22)$$

Examination of this equation indicates that boundary-layer resistance may increase rapidly with increasing current density. Further, a limiting current density may exist which corresponds to the membrane interface concentration approaching zero. This limiting current density may be increased by decreasing the thickness of the boundary layer.

In practice, the concentration at the membrane surface will not reach zero at high current densities. Instead, as the concentration approached 10^{-7} equivalents per liter, hydrogen ions present in the water would be transported across the cation membrane in significant numbers. This would result in a shift in the pH of the solution; the depleted stream would become basic, and the concentrate stream would become acidic. No significant pH shift has been observed yet in experimental observations of the transport-depletion process. This suggests that if a limiting current density actually exists, it has not been reached with the current density, flow velocity, and bulk-solution-concentration conditions that were present in any of the test cases.

3. Electrical Performance of Stack

The electrical performance of a stack may be described as a combined function of the performance of the repeating cell pairs, electrode compartments and the stack geometry. It is convenient to construct and examine the properties of an equivalent electrical circuit of a stack. Such an equivalent circuit is shown in Figure 4a. In this figure

R = resistance of one cell pair
r = resistance of solution inlets and exits to one cell pair,
δ = resistance of manifolds for length equal to thickness of one cell pair
$R_{external}$ = resistance of all external current flow paths between anode and cathode terminals

The external resistance, which includes stack headers and other system piping, can be made so high that the external leakage current can be neglected in a well-designed system.

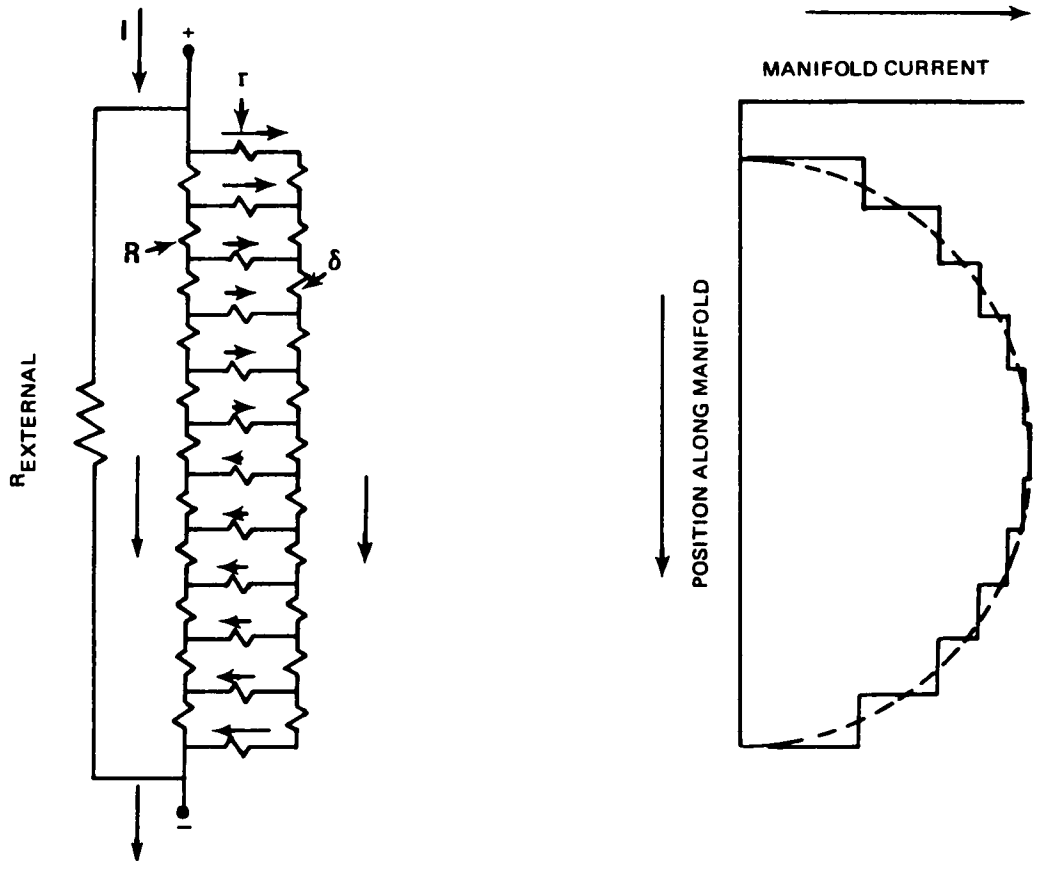

Figure 4 Equivalent Electrical Circuit for Stack

Stack Current - Stack manifold leakage currents can be significant and they should therefore be included in the evaluation of stack performance. It is desirable to minimize these leakage currents since any current which bypasses the cell-pair stack does no useful work and only increases the power required to achieve a given demineralization effect. The relative magnitude of the manifold leakage currents is indicated in Figure 4b. Since the leakage varies with position along the manifold length, its calculation is somewhat complex. It is useful to employ the concept of a manifold leakage factor which is defined as the fraction of the total current not doing useful work.

$$L = \frac{I_M}{I_T} \tag{23}$$

Where

L = manifold leakage factor
I_M = effective manifold leakage current, amperes
I_T = total stack current, amperes

Total stack current can now be expressed as

$$I_T = I_{CP} + I_M = \frac{i A'_e}{1000} + L I_T \tag{24}$$

$$\text{or } I_T = \left(\frac{1}{1 - L}\right) \frac{i A'_e}{1000} \tag{25}$$

Where

I_{CP} = current through cell-pair stack, amperes
i = average current density in cell-pair stack, ma/cm^2
A'_e = effective area of cell pair, cm^2

In engineering units, Equation (25) can be written as

$$I_T = 6.452 \times 10^{-3} \left(\frac{1}{1 - L}\right) i \; w \; l \tag{26}$$

Where

w = channel width, inches
l = path length, inches

An expression for the leakage factor has been derived by Mandersloot and Hicks[1]. The result is given below as a function of the resistance factors shown in Figure 4a.

$$L = \frac{R}{R + \delta} \left[1 - \frac{\tanh \frac{n}{2} \sqrt{\frac{R + \delta}{r}}}{\frac{n}{2} \sqrt{\frac{R + \delta}{r}}} \right] \tag{27}$$

Where n = number of cell pairs directly connected to a common manifold

[1] W.G.B. Mandersloot and R.E. Hicks, "Leakage Currents in Electrodialytic Desalting and Brine Production", Desalination, 1 (1966),178-193

Examination of Equation (27) shows that for a stack with an infinite number of cell pairs connected by the same manifolds, the leakage factor is

$$L_{n=\infty} = \frac{R}{R + \delta} \tag{28}$$

That is, the resistance of the liquid connections between the channels and the manifolds is not important. However, for most real stacks with a finite number of cell pairs, this resistance is important and can be used advantageously to minimize manifold leakage.

Stack Voltage - Stack voltage is the potential difference which must be applied across the electrodes of a stack to achieve the desired demineralization. It consists of the sum of the potentials across each electrode compartment and across the repeating cell pairs.

$$V_T = nV_{CP} + V_{EC} \tag{29}$$

Where

V_T = total stack voltage
n = number of repeating cell pairs
V_{CP} = voltage across each cell pair
V_{EC} = voltage across the two electrode compartments

The cell-pair voltage is

$$V_{CP} = i\ R_{CP} \times 10^{-3} \tag{30}$$

Where

i = average current density, ma/cm^2
R_{cp} = repeating cell-pair areal resistance, ohm-cm^2

The voltage drop across the electrode compartments cannot be accurately calculated directly. It is often convenient to assume that this voltage drop is proportional to the voltage drop across a cell pair. This assumption should be valid where electrode overpotentials are low and leakage currents are small. The expression for stack voltage now becomes

$$V_T = \frac{i\ R_{cp}}{1000} \quad (n + n_a + c) \tag{31}$$

Where

n_{a+c} = equivalent number of cell pairs represented by two electrode compartments

4. Hydrodynamic Performance of Stack

Knowledge of the basic hydrodynamic properties of a stack, such as pressure drop and flow distribution through the various cell pairs, is important to successful design and operation of the stack. These properties can usually be estimated analytically to a fair degree of accuracy. Such calculations are useful in preliminary design work, since they indicate the magnitude of potential sealing problems, and may suggest which designs are superior from this standpoint. Exact calculations are not necessary for an economic evaluation since pumping energy requirements represent a very small fraction of the total requirements. However, from a practical sealing and structural integrity standpoint, it is important to be able to estimate these hydrodynamic properties.

The pressure drop through the stack includes header losses, manifold losses and spacer-screen losses. Header losses can be estimated if the geometry is simple. Further these losses can be kept very low, so that exact estimates are not necessary.

Manifold losses can be estimated by assuming the manifolds to be a very rough pipe containing a series of fluid sinks. For good distribution to the various cell pairs, the pressure drop in the manifolds should be reasonably small and the velocity can be assumed to decrease linearly down the manifold, becoming zero at the last cell pair. The accuracy of this calculation will depend upon the alignment of the manifold and on the manufacturing tolerances of the spacer-screen assembly, since these two factors determine the roughness of the manifold "pipe".

Spacer-screen losses include both channel losses and solution inlet and outlet losses. The accuracy of calculations of inlet and outlet losses depends to a great extent on the geometry of the inlet or outlet and the state of the flow at the entrance and exit to each inlet or outlet. Calculations are usually based on the assumption of linear flow at the entrance of the inlets. Turbulence in this region can affect the flow through the inlet, and thus affect the pressure drop. It is therefore desirable to verify any calculations of inlet and outlet pressure losses with correlations of experimental results.

Pressure drop through the flow-channel portion of the spacer screen is usually difficult to calculate, due to the presence of a turbulence-promotion screen. An empirical approach to the estimation of this loss is therefore desirable. Experimental data is desired for each screen and channel geometry of interest, over a range of flow velocities.

The overall pressure loss in a stack is simply the sum of the component losses.

$$\Delta P_{total} = \Delta P_{headers} + \Delta P_{manifolds} + \Delta P_{inlets\ and\ exits} + \Delta P_{channels}$$

5. Experimental Performance Data

It is apparent from the previous discussion that certain cell-pair and stack-performance parameters are best estimated by the use of empirical correlations of experimental data. The parameters which best lend themselves to an empirical approach are:

1) cell-pair coulomb efficiency,
2) cell-pair areal resistance, and
3) spacer-screen pressure loss.

The first two items are concerned with the electrical performance of a cell pair. The behavior as regards both coulomb efficiency and cell-pair resistance is desired as a function of the membrane type, channel geometry, solution concentration and composition, solution velocity, and current density. This data must be obtained with an actual transport-depletion stack. The third item, spacer-screen pressue loss, can be evaluated as a function of channel geometry and solution velocity, using a simple channel designed for hydrodynamic experiments.

IV. DATA REVIEW

This section describes the results of the review of existing transport-depletion data and the subsequent generation of additional data necessary for a more complete understanding of the process. A review of existing data generated by Southern Research Institute of Birmingham, Alabama, relating to the development of the transport-depletion process was conducted, as a requirement of the contract program. In addition, other transport-depletion data obtained by the Bureau of Reclamation, Denver, Colorado, and at Webster, South Dakota was reviewed. As a result of this initial review, it was concluded that additional data was desirable to confirm certain conclusions, and to improve the understanding of the process. Additional membrane and bench-scale evaluations were performed by SRI, and a channel hydrodynamic evaluation program was conducted by Pratt and Whitney Aircraft.

The objectives of the data review were to

1) Identify the effects of operating parameters on the performance of the transport-depletion process,
2) Determine some preliminary design requirements for the design of the 10,000 GPD pilot plant, and
3) Develop a design methodology for the pilot plant, including a performance-prediction method suitable for scale-up studies of large commercial-size transport-depletion plants.

A. Description of Existing Data

The existing data that was reviewed is contained in the following reports:

1) Quarterly Progress Reports Numbers 1 through 8 by Southern Research Insititute to OSW covering the work performed under Contract 14-01-0001-698 and dated January 1966 through December 1967.

   The SRI reports describe the results of experiments using two bench-scale stacks that were specifically designed for transport-depletion operation. These two stacks were designated as HV-A and HV-B units and had typical channel dimensions of 22 x 3 x 0.062 inches and 55 x 3 x 0.036 inches, respectively.

2) Bureau of Reclamation Report Number WC-34, "An evaluation of the Transport-Depletion Process with a Natural Brackish Water", July 10, 1967.

   The evaluations conducted by the Bureau of Reclamation were made on natural brackish water using equipment specifically designed for the conventional sheet flow electrodialysis process. Details of this equipment were not available.

3) Webster Engineering and Developmental Report Number 29, "Pilot Plant Demineralization of Webster, South Dakota Water Using the Transport-Depletion Process", June 1967. The transport-depletion experiments at Webster, South Dakota, were performed using

three stacks, all designed for conventional electrodialysis operation. These stacks were an Asahi Acilyzer, an Ionic Stackpack, and an Aqua-Chem WD 6-2. Design descriptions of these stacks were not available.

B. Results of Review of Existing Data

Studies of the available transport-depletion electrical performance data indicated that:

1) Coulomb efficiencies considerably lower than 60 percent have been repeatedly recorded for the transport-depletion process, and

2) Repeating-cell-pair areal-resistance values varying from 70 to 800 ohm-cm^2 have been recorded.

A comprehensive evaluation of the data was performed to ascertain whether a practical set of operating conditions could be specified to achieve high coulomb efficiency combined with low repeating-cell-pair resistance.

1. Factors Influencing Coulomb Efficiency

The primary factors which affect the coulomb efficiency of a transport-depletion cell pair are as follows:

1) Membrane ion-transport characteristics,
2) Salt diffusion through the membranes,
3) Extraneous ion transport,
4) Solution leakage past or through the membranes, and
5) Current leakage past the membranes.

A change in the transport characteristics of the neutral membrane and salt diffusion (back-diffusion) due to the concentration gradient across the membranes are the probable primary causes for lower coulomb efficiency in the transport-depletion process. Extraneous ion transport (hydrogen or hydroxyl) would cause a shift in the pH levels of the depleted and enriched streams. The investigators indicate that such shifts were not present for the bulk of the data recorded, nor was there any mention of solution and current leakage.

The latter two factors can usually be controlled to low levels by proper geometric and mechanical design of the membrane stack.

The most notable correlation of the SRI and Bureau of Reclamation data was the reduction of coulomb efficiency as the average concentration of the depleted stream decreased. The shift of the ion transport characteristics of the neutral membrane towards cation selectivity as the solution concentration decreases, as recorded by SRI, could explain this observation. Apparently the regenerated cellulose type of neutral membrane is inherently cation-selective. This inherent cation selectivity is normally masked by the transport properties of a concentrated solution, but becomes more influential as the solution concentration decreases.

Further correlations were obtained by comparing data recorded using sodium chloride solutions that were similar with respect to cut and feed concentrations and the following information was obtained:

1) The coulomb efficiency decreases as the product-to-waste flow ratio increases,

2) The coulomb efficiency decreases as the current density increases,

3) The coulomb efficiency decreases as the solution velocity decreases,

4) The coulomb efficiency decreases as the membrane spacing decreases.

These correlations are based on the limited data available and may not all be significant. However, the effects are to be expected if back-diffusion is present.

Back-diffusion is the product of the membrane diffusion coefficient and the concentration gradient. The diffusion coefficient is a material property which has been measured by SRI for a limited number of membranes and for a limited number of conditions. The diffusion coefficient of the A. H. Thomas neutral membrane is three orders of magnitude greater than that of the Ionac MC-3142 cation membrane. An increase in the product-to-waste flow ratio lowers coulomb efficiency because of increased back-diffusion through the neutral membrane. An increase in current density lowers coulomb efficiency because salt concentration adjacent to the membranes increases - therefore increasing back diffusion. As velocity increases, coulomb efficiency increases because the boundary layers are decreased. Therefore, decreasing the concentration gradient causes back-diffusion. No reason is known for the lower coulomb efficiency recorded as spacing is decreased. The reason is believed to be related to boundary-layer conditions.

The effects of alternate turbulator screens on coulomb efficiency could not be readily compared using existing data.

Limited data was recorded using enriched-stream acidification which showed a decrease in coulomb efficiency. The reason is not known.

2. Factors Influencing Cell-Pair Resistance

The major elements which determine cell-pair areal resistance and their typical resistance values are as follows:

1)	cation membrane (Ionac MC-3142)	12 ohm-cm^2
2)	neutral membrane (A.H. Thomas 4465-A.2-4.9)	16 to 90
3)	enriched stream (35-mil thickness)	5 to 30

4)	depleted stream (35-mil thickness)	20 to 75
5)	enriched boundary layers	less than 1
6)	depleted boundary layers (optimum conditions)	1 to 5

The data indicates that significant performance improvement can be obtained if the resistance of the depleted boundary layer can be reduced under a practical set of stack operating conditions. Data recorded in SRI Report No. 6 under Contract 14-01-0001-698 indicate cell-pair resistances of approximately 70 ohm-cm^2 for a cut of from 0.06N to 0.03N at current densities of 11 and 38 ma/cm^2. This apparently indicates that the depleted boundary layer resistances were less than 10 ohm-cm^2. Many examples can be cited from the SRI data in Report No. 4 where repeating-cell-pair resistance reached 500 to 800 ohm-cm^2, which would be consistent with boundary-layer resistances in excess of 200 ohm-cm^2. It is of interest to explore the conditions that minimize this boundary layer resistance.

The data suggests that high solution velocity can minimize cell-pair resistance. The effect of increasing solution velocity is to reduce the boundary thickness, producing two desirable effects:

1) The depleted boundary-layer resistance is directly proportional to thickness, hence a reduction in thickness by a factor of from 2 to 5 would reduce resistance by a factor of from 2 to 5.

2) The resistivity of the depleted boundary-layer solution is a function of the salt ion concentration. At a given current density, a definitive concentration gradient must be established within the layer to supply the required positive ions to the cation membrane. If the boundary-layer thickness is halved, the concentration difference between the bulk solution and membrane surface should also be halved. This essentially doubles the average ion concentration within the boundary layers, causing a corresponding decrease in cell-pair resistance.

Path lengths in excess of 55 inches are apparently required to achieve the limiting resistance at 2500 to 500 ppm cut using reasonable current densities. This implies that velocities in excess of 10 cm/sec (4 inches/ sec) are required for a 55 inch or shorter path length at the same cut conditions.

A lower current density should also reduce the boundary-layer resistance by reducing the required concentration gradient in the boundary layer, thus increasing the average boundary-layer concentration. The data does not clearly indicate this anticipated effect.

A more effective turbulator screen will also reduce the boundary-layer resistance by reducing the thickness of the boundary layer at a given solution velocity. Little data exists to determine the most effective type of turbulator screen.

The prime resistances, excluding boundary-layer resistance, are the depleted-stream bulk resistance and the neutral-membrane resistance. A significant reduction in either of these resistances will cause a marked reduction in cell-pair resistance.

The depleted-stream bulk resistance can be reduced by reducing the spacing between the membranes. The minimum spacing will be determined by the mechanical limitations of designing and constructing a satisfactory spacer screen.

The resistance of the regenerated cellulose type of neutral membrane is a function of the concentration of the surrounding solution. The membrane apparently acts like a sponge filled with salt solution. Current is conducted through the membrane by ionic transport as in the bulk solution, thus the conductivity of the membrane is proportional to the concentration of ions (conductors) present. Little data exists on satisfactory alternate neutral membranes with improved resistance properties.

A product-to-waste flow ratio of at least 4 to 1 is desired to reduce cell-pair resistance by lowering the enriched-stream bulk resistance. The upper limit is not defined by the data, but should be determined by such factors as salt precipitation and increased back-diffusion through the membranes.

Natural or synthetic brackish water which includes less soluble salts than sodium chloride introduces a precipitation problem which can cause a marked increase in resistance as a function of current density. Insufficient data is available to perform a detailed evaluation of ths problem. However, it is expected that the same factors which reduce boundary-layer resistance, high velocity and a more effective turbulator screen, will also reduce this problem by lowering the maximum concentration in the enriched boundary layers next to the cation membrane.

3. Summary

All existing data has been obtained on stacks of conventional design although the SRI stacks were specifically intended for the evaluation of the transport-depletion process. The SRI data contains detail design descriptions whereas this type of data was not available for other experiments.

It appears desirable to operate at high flow velocities to minimize cell-pair resistance and maximize coulomb efficiency. The advantage of high velocity is to reduce the boundary-layer thickness, which reduces the concentration difference required in a given boundary layer to achieve the necessary concentration gradient. This improves both coulomb efficiency and cell-pair resistance at the expense of increased solution pumping power.

A long path length is required to achieve the desired degree of cut at high solution velocities with a current density of 10 to 30 ma/cm^2.

Reduced membrane spacing offers lower resistance, but reduced coulomb efficiency may limit this reduction. It appears that the pump power penalty is not significant with this

change, however data is needed to confirm this assumption. Geometric limitations with respect to spacer-screen design will probably govern the minimum achievable membrane separation.

Significant coulomb efficiency improvement can be obtained if a true neutral membrane or a membrane with a slight anion selectivity can be used. Reduced membrane resistance will also offer performance improvements.

Salt precipitation problems when operating on brackish water will perturbate the quantitative results but not the basic qualitative results. Sufficient data has not been generated to fully appreciate and explore the problems of brackish-water operation.

Additional data is desired to define the coulomb efficiency and cell-pair resistance as a function of solution velocity and path-length variations, adjusting the current density to obtain a fixed cut. Variable-path-length data at a fixed cut is required to separate the effects of current density and solution velocity.

The neutral membrane presently being used has poor transport and resistance characteristics. The identification and selection of a better neutral membrane would be desirable.

C. SRI Bench Rig and Membrane Evaluation Data

A number of experimental membrane and bench-rig demineralization evaluations were performed by SRI to obtain the additional data required for the performance-prediction method and for the pilot-plant design.

The major objectives of the bench-rig experiments were to determine the specific effects of solution velocity, product-to-waste flow ratio, path length, and membrane-spacing variations on coulomb efficiency and cell-pair resistance. The same feed solution concentration of 2500 ppm NaCl was used in all cases. Also, current density was adjusted to achieve the same product concentration of 500 ppm in all cases except for the membrane spacing evaluations. In these cases, a product concentration of 500 ppm could not be achieved when the membrane spacing was doubled because of a maximum current density limitation. Therefore, comparative cases were run at two membrane spacings with the current density adjusted to achieve a product concentration of 1500 ppm.

Table 1 lists the nominal conditions for the SRI bench-rig experiments. All experiments used Ionac MC-3142 cation membranes and A.H. Thomas 4465-A2-4.9 neutral membranes.

TABLE 1

Nominal Conditions of SRI Demineralization Runs with HV-B Stack

Path Length Inches	Membrane Spacing Inches	Solution Velocity cm/sec	Product-to-Waste Ratio	Product Concentration ppm
55	0.036	3	4/1	500
55	0.036	5	4/1	500
55	0.036	7	4/1	500
55	0.036	10	4/1	500
55	0.036	10	1/1	500
55	0.036	10	8/1	500
44	0.036	3	4/1	500
44	0.036	5	4/1	500
44	0.036	7	4/1	500
44	0.036	10	4/1	500
33	0.036	3	4/1	500
33	0.036	5	4/1	500
33	0.036	7	4/1	500
33	0.036	10	4/1	500
55	0.036	7	4/1	1500
55	0.036	10	4/1	1500
55	0.072	7	4/1	1500
55	0.072	10	4/1	1500

Nominal feed solution was 2500 ppm NaCl

A description of these demineralization experiments, including the detailed results, was contained in SRI Report No. 6 which was included in Pratt and Whitney Aircraft Report No. 7 to OSW, Contract 14-01-0001-1262. A detailed description of the SRI HV-B stack used for these experiments was given in SRI Report No. 6 to the Office of Saline Water, Contract 14-01-0001-698.

The results of these experiments tended to verify the previous prediction that cell-pair areal resistance asymptotically approaches a minimum value as solution velocity is increased. Current density appears to have little effect on resistance over the range of experimental values used. Correlations of this data are discussed in detail in Section IV. E. below.

Twenty membranes were studied by Southern Research Institute to determine their potential for use as neutral membranes in the pilot-plant stack. Nine samples were of regenerated cellulose materials and eleven samples were reverse-osmosis membranes. The transference

number (t+), electrical resistance, wet thickness, and in most cases the diffusion constant for these twenty samples were measured and compared. The results were contained in SRI Reports Numbers 4, 5, 6, and 7, which were included as part of Pratt & Whitney Aircraft Reports Numbers 5, 6, 7, and 8, respectively, to the Office of Saline Water, Contract 14-01-0001-1262.

In general, the results of these evaluations indicated that the Zephyr Z cellulose membrane made by Union Carbide appeared to have the best combination of properties for initial use in the pilot-plant program. It is readily available and its width of 22 inches does not unduly restrict the size of the pilot-plant stack design. The unheat-treated reverse-osmosis membranes were modified cellulose acetate type obtained from several sources. They appear to be attractive neutral membrane candidates but require further investigation.

The electrical resistance of one regenerated cellulose membrane, A.H. Thomas dialyzer tubing, 4465-A2-4.9, was measured when the membrane was between NaCl solutions of different concentrations. The purpose was to provide information about the resistance of neutral membranes under concentration conditions similar to those in an operating transport-depletion stack. These experiments were described in detail in SRI Report Number 6 which was included as part of Pratt & Whitney Aircraft Report Number 7 to the Office of Saline Water, Contract 14-01-0001-1262. The results indicate that the resistance of a neutral membrane between solutions of different concentration is best approximated by its resistance in a solution with a concentration equal to the direct average of the two solution concentrations. This is not a perfect correlation and some arguments can be made for using the log mean average of the two solutions. The data correlation is further discussed in Section IV. E. below.

D. P&WA Channel Evaluation Rig Data

A channel evaluation program was conducted by Pratt & Whitney Aircraft to investigate the hydrodynamic characteristics of various solution inlet configurations and turbulence-promotion screens. The channel evaluation rig constructed for this purpose was capable of testing samples of various thicknesses and configurations under a wide range of channel velocities that might be encountered in the pilot plant. Nine different turbulator screens and four inlet and exit configurations were tested during this program. The inlet configuration and turbulator screen used in the final stack design were also evaluated during the tests.

1. Channel Evaluation Rig

Figure 5 shows a system schematic and component breakdown of the rig. Figure 6 is a photograph of the assembled rig. Two flat 0.75-inch thick Plexiglas sheets contain the solution channel which is defined by a stainless steel spacer of appropriate thickness. Vinyl gasket material was used as a seal between the spacer and plastic plates. The combined thickness of the spacer and vinyl gaskets determined the thickness of the channel. A sealing load was provided by bolts located around the edge of the channel.

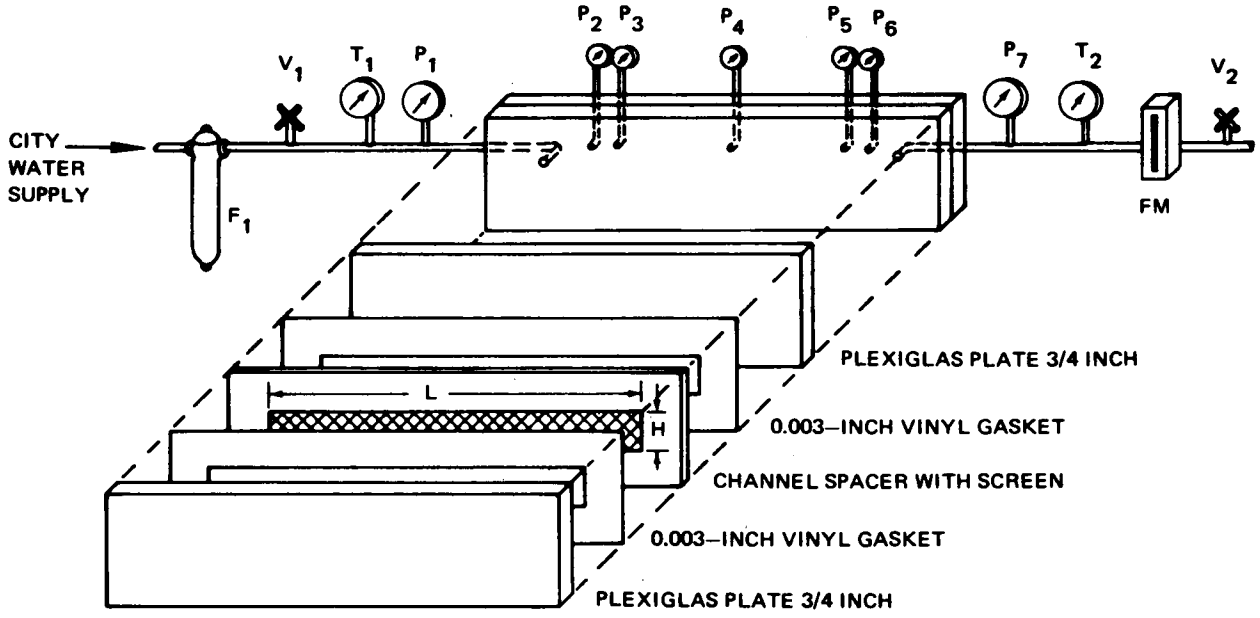

F_1–FULL FLO FILTER MODEL BRX10
V_1–HOKE FLOW–CONTROL VALVE MODEL PY276K
V2–MARSH FLOW–CONTROL VALVE MODEL 1900FFG
T_1 AND T_2 – CHROMEL–ALUMEL THERMOCOUPLES
P_1 THROUGH P_7 MARSH PRESSURE GAGES, 0-60 PSI
FM–FISHER PORTER FLOWMETER

L = CHANNEL LENGTH = 30 INCHES
H = CHANNEL HEIGHT = 3 INCHES

ACCURACY ±0.20 PERCENT OF FULL SCALE

Figure 5 Schematic of Channel-Evaluation Rig

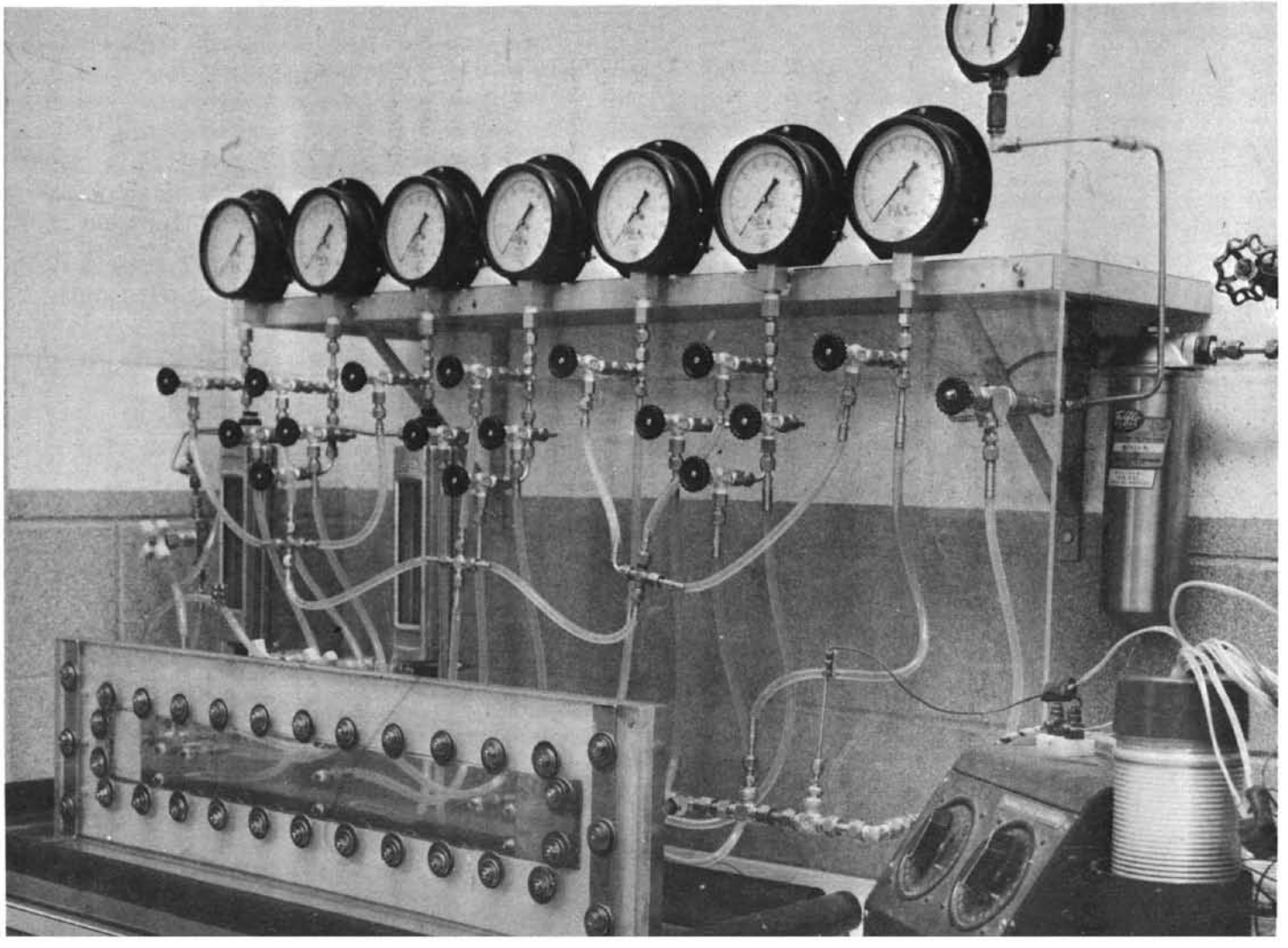

Figure 6 Photograph of Channel-Evaluation Rig

Static pressure taps were located along the length of the channel and in the inlet and exit lines, as shown in Figure 5. Pressure was read on Marsh gages equipped with a bleed circuit for air removal. Solution flow rate was controlled with a stainless steel needle valve. Flow rates were measured with a Fisher & Porter glass-tube flowmeter with an accuracy of 2 percent of full range.

2. Solution Inlet Evaluations

The solution inlet configurations that were evaluated are shown in cross-section in Figure 7. The last configuration shown was chosen for the final stack design.

The results of the inlet tests are plotted in Figures 8 and 9 as a function of open channel velocity. The channel dimensions used to calculate this velocity were the same as in the final pilot-plant design (0.030 inch spacing and 4.5 inches wide).

The first two inlets (tubular and grooved) were two inches long and one inch wide. The data in Figure 8 has been adjusted to reflect the full two-inch width of the final pilot-plant design. No adjustment was made to correct for length, however, since pressure loss is a combination of end losses which are constant, and frictional losses which depend upon inlet length. The relative magnitude of these losses is not known. The data shown in Figure 8 represents the best results obtained with these two inlets.

The first inlet consisted of a row of polypropylene tubes cemented together. During the tests, there was considerable leakage around the outside of the tubes which resulted in non-repeatable pressure losses depending upon the amount of clamping pressure used. No further consideration was given to this configuration.

The second configuration (grooved inlet) that was tested represents an attempt to completely support the flexible neutral membrane. It was hoped that the stiffer cation membrane could be clamped against the open-groove side of the inlet without difficulty. The tests showed that the cation membrane had extruded into the grooves which caused erratic and unrepeatable pressure losses. In some cases this effect was sufficient to completely block off all flow.

The last three inlets tested were two inches wide by 0.5 inch long, the same as in the final pilot-plant design. The molded-tube design consisted of a series of 15-mil tubular passages which became easily plugged during the tests. The molded-slot design was rejected because of frequent wall collapse under sealing pressure and subsequent flow restriction. Both of these designs were difficult to fabricate and assemble into the spacer screen.

The last configuration represents the spacer-comb type that was selected for use in the final pilot-plant design. This inlet is described in detail in Section V.B.1. It is an integral part of the spacer-screen assembly. The outer walls are the outer two sheets of epoxy-impregnated Fiberglas 10 mils thick which make up the frame of the spacer-screen assembly. These sheets are spaced in the inlet area by a comb of the same materials 10 mils thick to form slots which are 10 mils deep and 80 mils wide. The results of testing this inlet configuration are shown in Figure 9. Pressure loss was repeatable and there was no sign of wall collapse. This and the

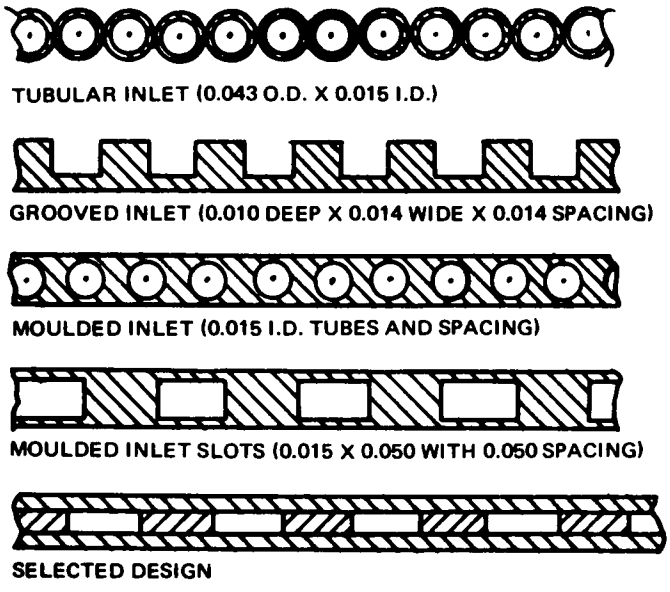

Figure 7 Inlet Configurations

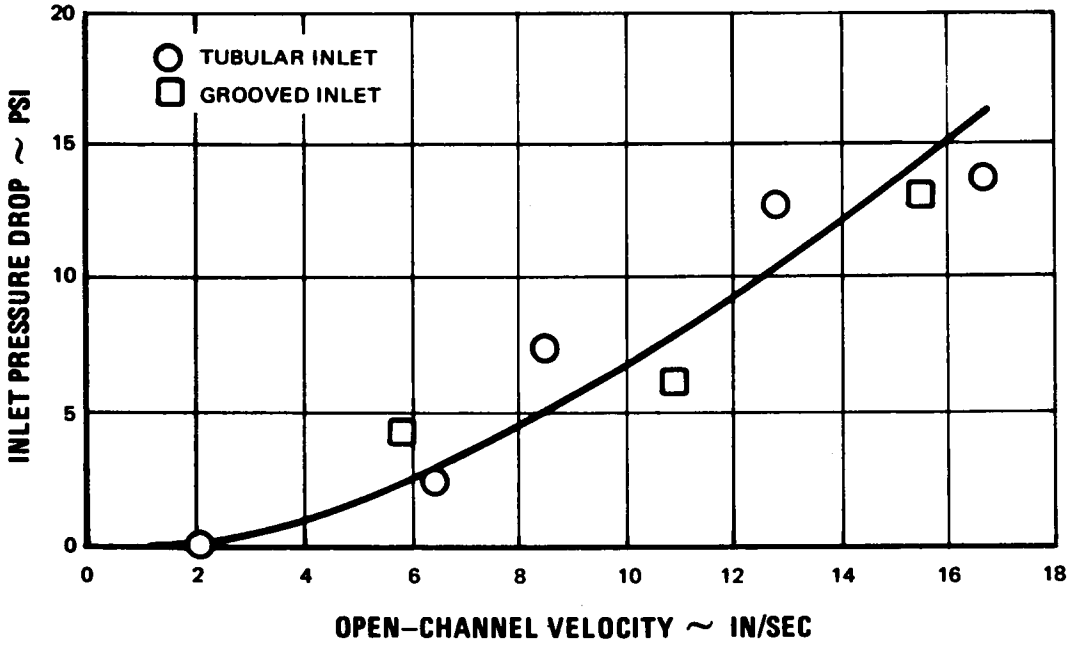

Figure 8 Inlet Pressure Drop

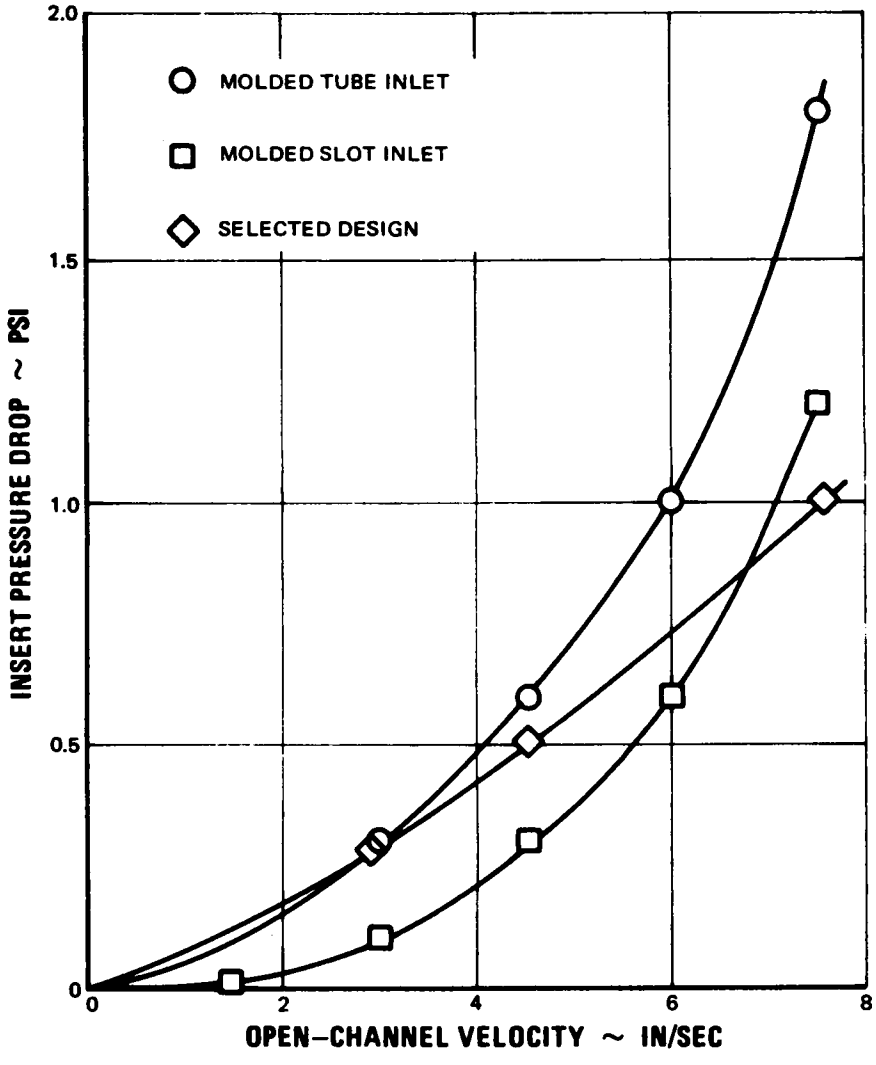

Figure 9 Inlet Pressure Drop

extreme ease of fabrication were the major reasons for selecting this configuration for the final design.

3. Tubulator Screen Evaluations

Several candidate turbulator screens were tested to evaluate their pressure-loss and turbulence-promotion characteristics. Table 2 lists these screens and the channel depth and flow orientation used during the tests. All screens except the Vexar series were woven fabrics. The Vexar screens consisted of nonwoven strands with thermally-bonded intersections. All screen samples were tested over a range of channel velocities from about 1 to 10 inches per second with no inlet or exit inserts in the channel.

TABLE 2

Turbulator Screens

Manufacturer's Designation	Mesh Size	Fiber Diameter, mils	Material	Angle of Intersecting Strands, deg.	Channel Depth, mils	Flow Orientation
Vexar 20 PDS-129	12 x 12	20	polpropylene	90	44	→ XXX
Vexar 30 CDS-89	8 x 8	30	polyethylene	90	63	→ XXX
Prodesco # 12	33 x 24	12 8	polypropylene	90	45	→ 33 / 24
10 x 10 polyproplyene	10 x 10	15	polypropylene	90	38	→ #
8 x 10 polyproplyene	8 x 10	20	polypropylene	90	43	→ 10 / 8
10 x 10 polyproplyene	10 x 10	20	polyrpopylene	90	45	→ #
12 x 12 polyproplyene	12 x 12	20	polypropylene	90	45	→ #
Vexar 15 PDS-129	12 x 12	15	polypropylene	90	38	→ XXX
Prodesco # 12	33 x 24	12 8	polypropylene	90	38	→ 33 / 24
Vexar 15 PDS-129	12 x 12	15	polypropylene	90	28	→ XXX
Vexar 15 PDS-89	8 x 8	15	polypropylene	98	24	→ XXX

Figures 10 and 11 show the results of the initial evaluations. In most cases, there was an almost linear increase in pressure loss with increasing velocity. Also, where the same screen was tested with different channel thicknesses, pressure loss increased as the channel thickness decreased. The results show that the screen pressure losses were about the same order of magnitude as those of the 0.5-inch long inlet (Figure 9).

An attempt was made to evaluate the effectiveness of the screens as a turbulence-promotion device. The injection of both tracer dye and air bubbles was tried. Both methods showed that all screens rapidly distributed the flow across the full width of the channel. Dispersion of the tracer dye and breakup of the air bubbles was so rapid, however, that no evaluation of the turbulence-promotion characteristics of the screens could be made.

After the channel dimensions of the pilot-plant design had been finalized, further testing was performed using two Vexar screens of different mesh size. A channel thickness was used for these tests which matched the final spacer-screen dimensions as closely as possible. The results of these tests are shown in Figure 12. The screen chosen for the final pilot-plant design, Vexar 15-PDS-129, resulted in a lower pressure loss than that of Vexar 15-PDS-89. Pressure loss with both screens was higher than in the earlier tests due to the reduced channel thickness.

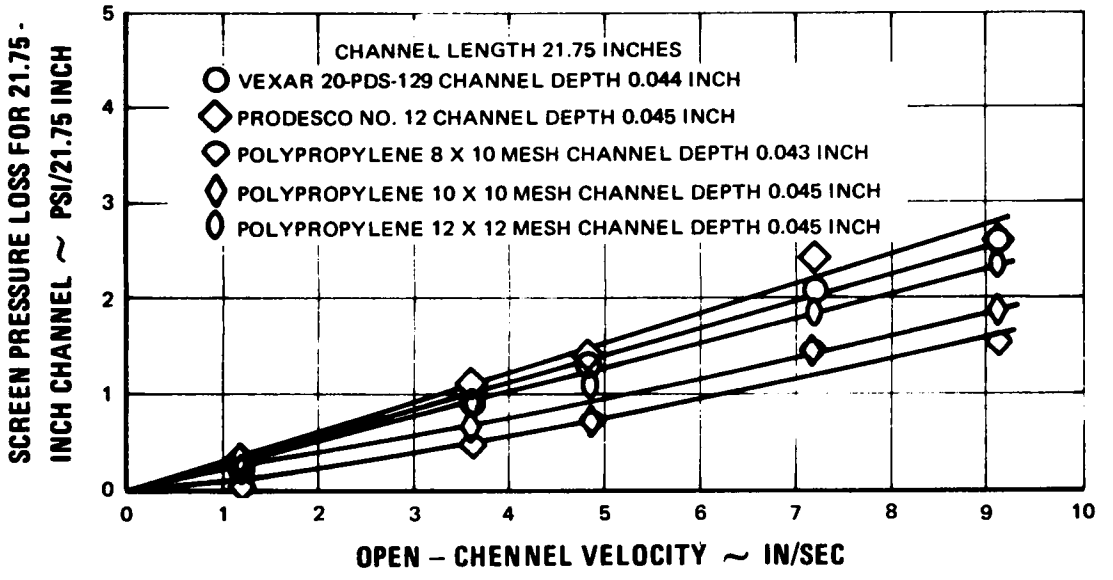

Figure 10 Screen Pressure Loss vs Channel-Flow Velocity

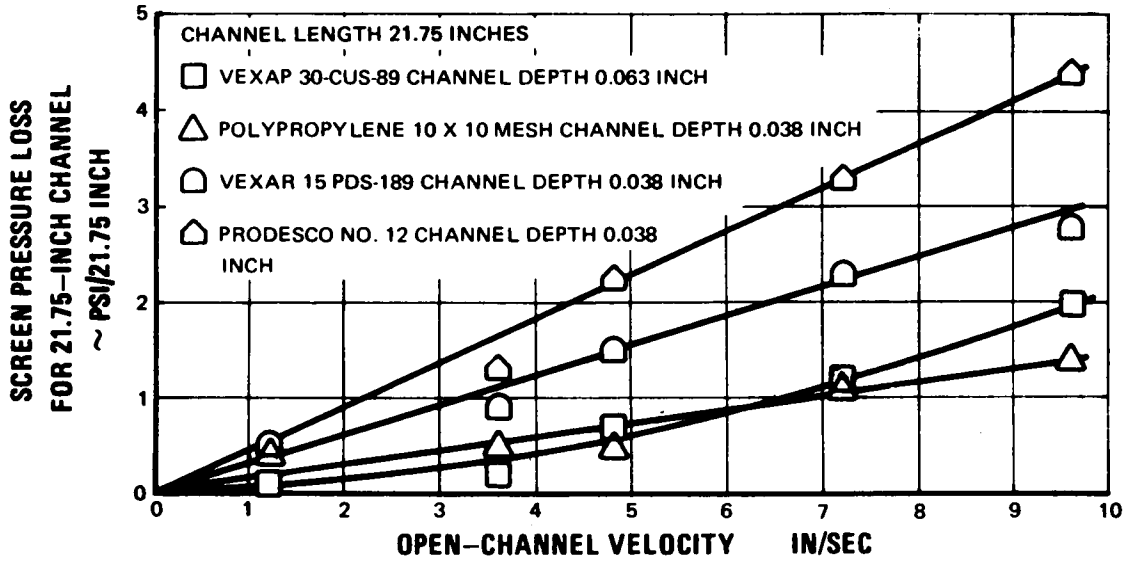

Figure 11 Screen Pressure Loss vs Channel-Flow Velocity

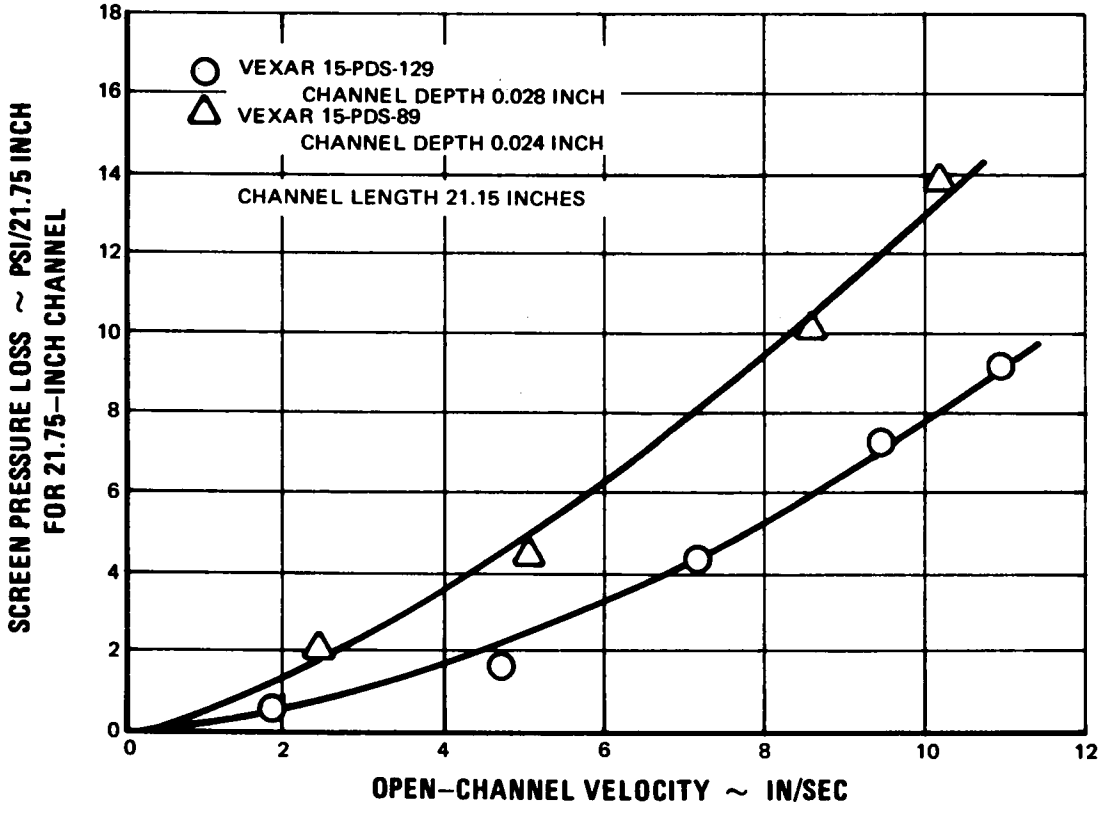

Figure 12 Screen Pressure Loss vs Channel-Flow Velocity

E. Performance-Prediction Method

In Section III. B. above, analytical expressions were derived for the electrical and hydrodynamic performance of a transport-depletion stack. These expressions, together with certain data correlations, constitute a performance-prediction method suitable for use in the design of the 10,000 gpd pilot plant, and in parametric studies of commercial-size transport-depletion plants. In this section, data correlations used to describe coulomb efficiency, cell-pair resistance and stack-pressure-loss characteristics are presented.

Overall correlation expressions for resistance and coulomb efficiency were examined, and empirical relationships describing the various components of these two factors were obtained, which explained the SRI data in a reasonable manner. The correlations presented here represent the best fit of several attempts to correlate the available performance data.

Although the expressions for coulomb efficiency and cell-pair resistance represent combinations of empirical expressions, these expressions should be usable to a certain extent outside the range of the data used in obtaining the correlations, since the correlations were set up in such a way as to be physically reasonable. The expressions may not be correct, however, if extrapolation is attempted very far from the range of the experimental data.

1. Coulomb Efficiency Correlation

As described previously, coulomb efficiency of the cell pair is determined primarily by three factors:

1) Thecation-membrane transport number,

2) The neutral-membrane transport number, and

3) Back-diffusion of salt through the neutral membrane.

Each factor may be described empirically, using data generated by Southern Research Insittute or data available from the membrane manufacturers.

Cation-Membrane Transport Number – The cation transport number of the cation membrane is very close to 1.0, except when very high salt concentrations tend to cause a decrease in transport number. A value of $t_c^+ = 0.99$ is given for the transport number of Ionac MC-3142 cation membranes in SRI Report Number 1 to the Office of Saline Water, Contract 14-01-0001-698. Literature from Ionac indicated a transport number of $t_c^+ = 0.94$ in 0.5N NaCl/1.0N NaCl solution. In more dilute solutions a better transport number is expected. A value of

$$t_c^+ = 0.98 \tag{32}$$

was used in calculations to predict coulomb efficiency. This value should be reasonably accurate over the range of interest.

Neutral-Membrane Transport Number - The transport number of A.H. Thomas dialyser tubing, the neutral-membrane material used in most experimental demineralization runs by SRI, was correlated with the concentration of the dilute streams. Correlations with an average concentration did not fit as well in the overall coulomb efficiency correlation. Figure 13 shows the neutral-membrane transport-number data and the empirical curve fit of this data. The expression for neutral-membrane transport number represented by this curve fit is

$$t_N^+ = 0.4 + 0.6e^{-2.04 \times 10^{-3}\ ppm_D} \qquad (33)$$

where ppm_D =log mean average concentration on the dilute side of the membrane in ppm of NaCl. This expression results in a transport number close to ideal ($t_N^+ = 0.4$) for concentrations greater than about 2000 ppm NaCl. As the concentration approaches zero, the transport number approaches that of a perfect cation exchange membrane ($t_N^+ = 1.0$).

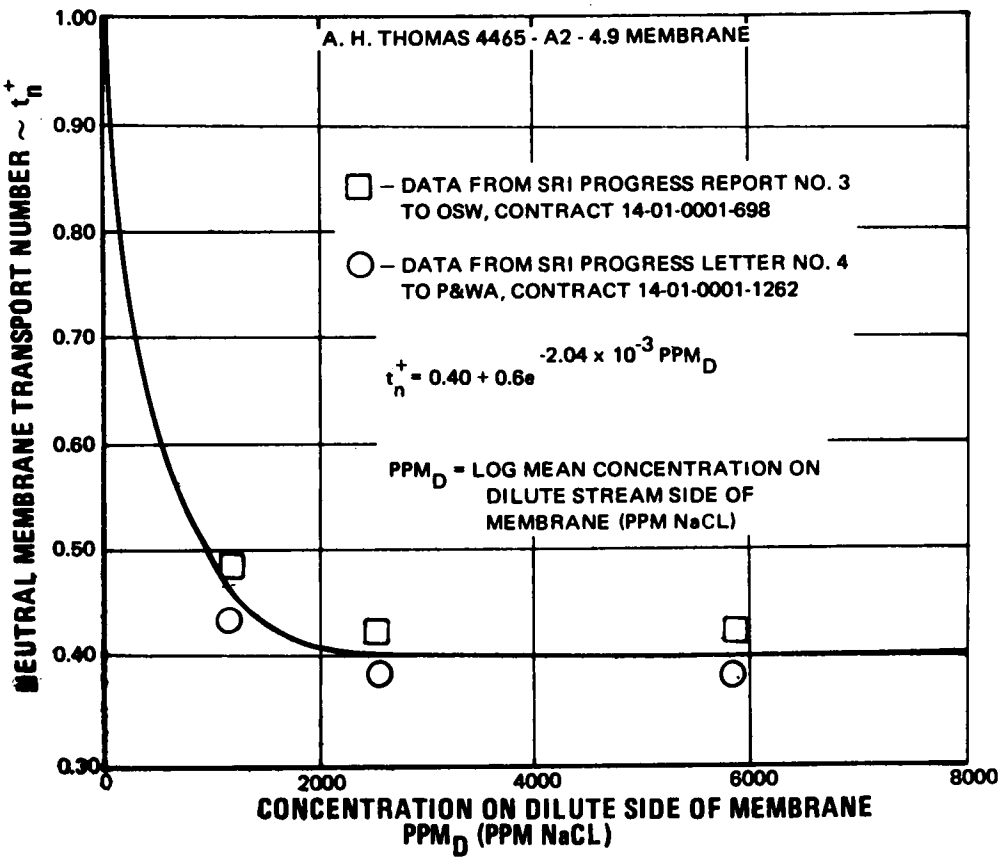

Figure 13 Neutral Membrane Transport Number vs Concentration

Back-Diffusion Through Neutral Membrane - Diffusion through a membrane in general can be expressed as

$$J_o = D\frac{dc}{dx} \tag{34}$$

Where

J_o = diffusion rate, eq/cm^2 sec
D = membrane diffusion constant, cm^2/sec
dc = concentration difference across membrane, eq/cm^3
dx = thickness of membrane, cm

In engineering terms related to a neutral membrane in a cell pair,Equation (34) can be expressed as

$$J_o = \frac{6.74 \times 10^{-9} D (ppm_E - ppm_D)}{dn} \tag{35}$$

Where

ppm_E = log mean average of enriched-stream concentration, ppm NaCl

ppm_D = log mean average of depleted-stream concentration, ppm NaCl

dn = thickness of neutral membrane, inches

Values of J_o, dc and dn can be found in reports published by SRI from which values for the diffusion constant can be calculated.

Southern Research Institute Report Number 1 to the Office of Saline Water, Contract 14-01-0001-698, Table I, lists the following data:

$J_o = 46 \times 10^{-5}$ eq/cm^2 hr

dc = 1.5 N NaCl

$d_N = 18 \times 10^{-3}$ cm = 7.1×10^{-3} inch

This data results in a membrane diffusion constant of

$D = 15.3 \times 10^{-7}$ cm^2/sec

Southern Research Institute Report Number 4 to Pratt & Whitney Aircraft (included in Pratt & Whitney Aircraft Report Number 5 to the Office of Saline Water, Contract 14-01-0001-1262), Table II, lists the following data:

J_o = 32×10^{-5} eq/cm^2 hr

dc = 1.5N NaCl

d_N = 8.2×10^{-3} inch

The resulting value of the diffusion constant is:

D = 12.45×10^{-7} cm^2/sec

The averages of these values for D and d_N are:

D = 13.9×10^{-7} cm^2/sec

d_N = 7.64×10^{-3} inch

Coulomb Efficiency Prediction Equation – The overall expression for coulomb efficiency may be calculated from the expressions described above and the previously derived relationship for current density, Equation (12).

The basic expression for coulomb efficiency as a function of the membrane-transport numbers and back-diffusion through the neutral membrane is

$$\eta_I = (t_c^+ - t_N^+) - \frac{J_o F \times 10^3}{i} \qquad (36)$$

Where

t_c^+ and t_N^+ = membrane transport numbers

$\frac{J_o F \times 10^3}{i}$ = decrease in coulomb efficiency due to back-diffusion across neutral membrane

J_o = salt diffusion rate as defined by Equation (35), eq/cm^2 sec

F = Faraday constant, 96,500 coulombs/eq

i = average current density in cell pair, ma/cm^2

The general expression for coulomb efficiency is derived by substituting the appropriate expressions for the salt diffusion rate, Equation (35), and current density, Equation (12), into Equation (36) and rearranging. The resulting expression is

$$\eta_I = \frac{t_c^+ - t_N^+}{1 + \frac{0.154\ Dl\ (ppm_E - ppm_D)}{d_N\ d\ Voc\ \Delta ppm}} \tag{37}$$

When the Ionac MC-3142 cation membrane and the A. H. Thomas 4465-A2-4.9 cellulose-casing neutral membrane are used, the appropriate membrane constants can be inserted into Equation (37).

The final expression for coulomb efficiency when using this membrane pair is

$$\eta_I = \frac{0.58 - 0.6e^{-2.04 \times 10^{-3}\ ppm_D}}{1 + \frac{2.82 \times 10^{-5}\ l\ (ppm_E - ppm_D)}{d\ V_{oc}\ \Delta ppm}} \tag{38}$$

This expression for coulomb efficiency was compared with experimental determinations of coulomb efficiency obtained by Southern Research Institute to assess its accuracy in predicting coulomb efficiency. Figures 14 through 27 illustrate the correlation of values calculated using this expression with experimental data obtained under a variety of conditions.

Figures 14 through 21 include data obtained on the SRI HV–A demineralization stack. This stack has a path length of 22 inches and a membrane spacing of 0.62 inch. Figures 22 through 27 contain data obtained using the SRI HV–B stack which has a path length of 55 inches and a membrane spacing of 0.036 inch. The HV–B stack can also be run with path lengths of 22, 33, and 44 inches by isolating sections of the segmented electrodes. The effect of membrane spacing can be evaluated using the HV–B stack by using multiple spacers between membranes. Figures 25, 26 and 27 show the effect of membrane spacing (channel depth), product-to-waste flow ratio, and solution velocity when operating at fixed feed and product solution concentrations.

2. Cell-Pair Resistance Correlation

The areal resistance of a cell pair can be expressed as the sum of several component resistances as described in Section III.B. above.

$$R_{cp} = R_o + R_{BL} \tag{39}$$

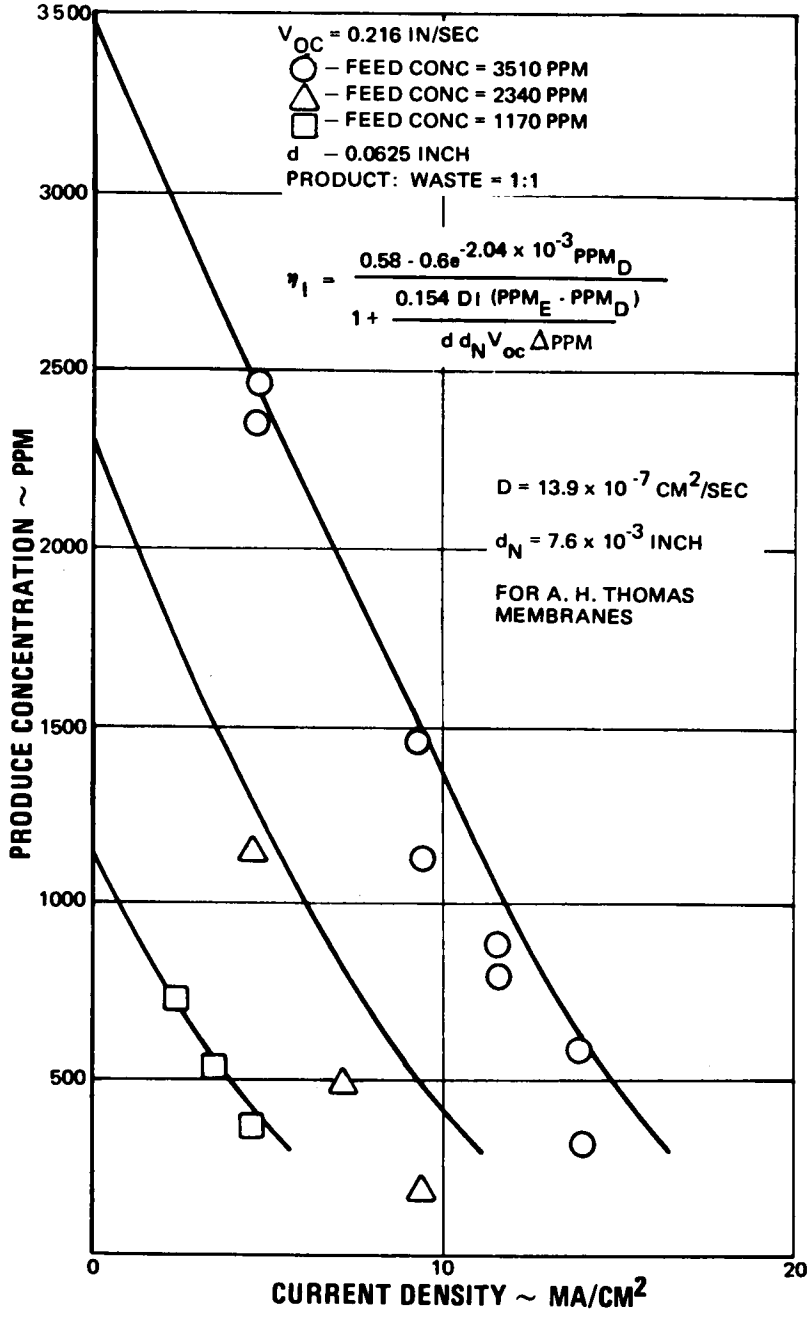

Figure 14 Coulomb Efficiency Correlation. Data from SRI Report No. 2 to OSW, Contract 14-01-0001-698

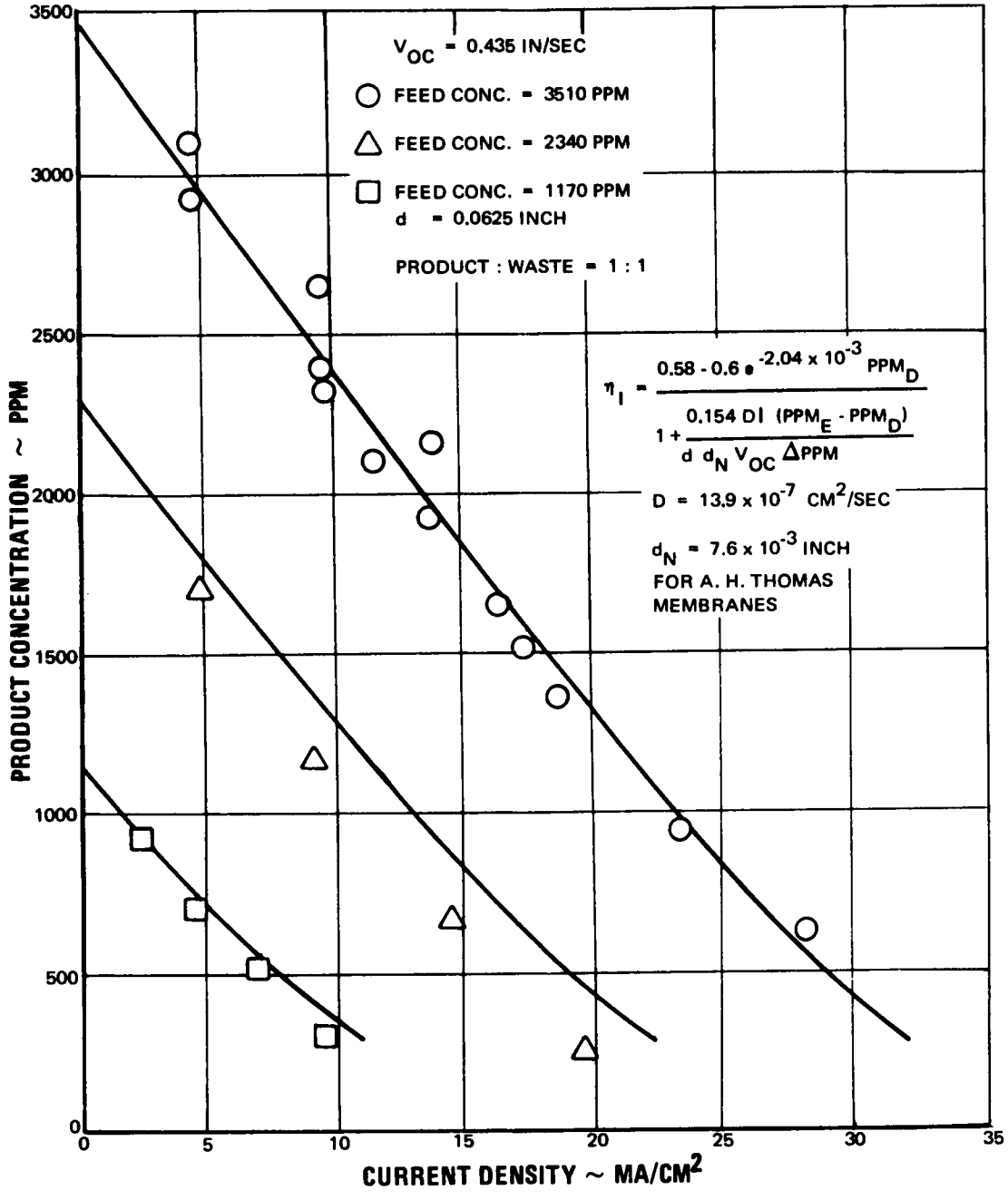

Figure 15 Coulomb Efficiency Correlation. Data from SRI Report No. 2 to OSW, Contract 14-01-0001-698

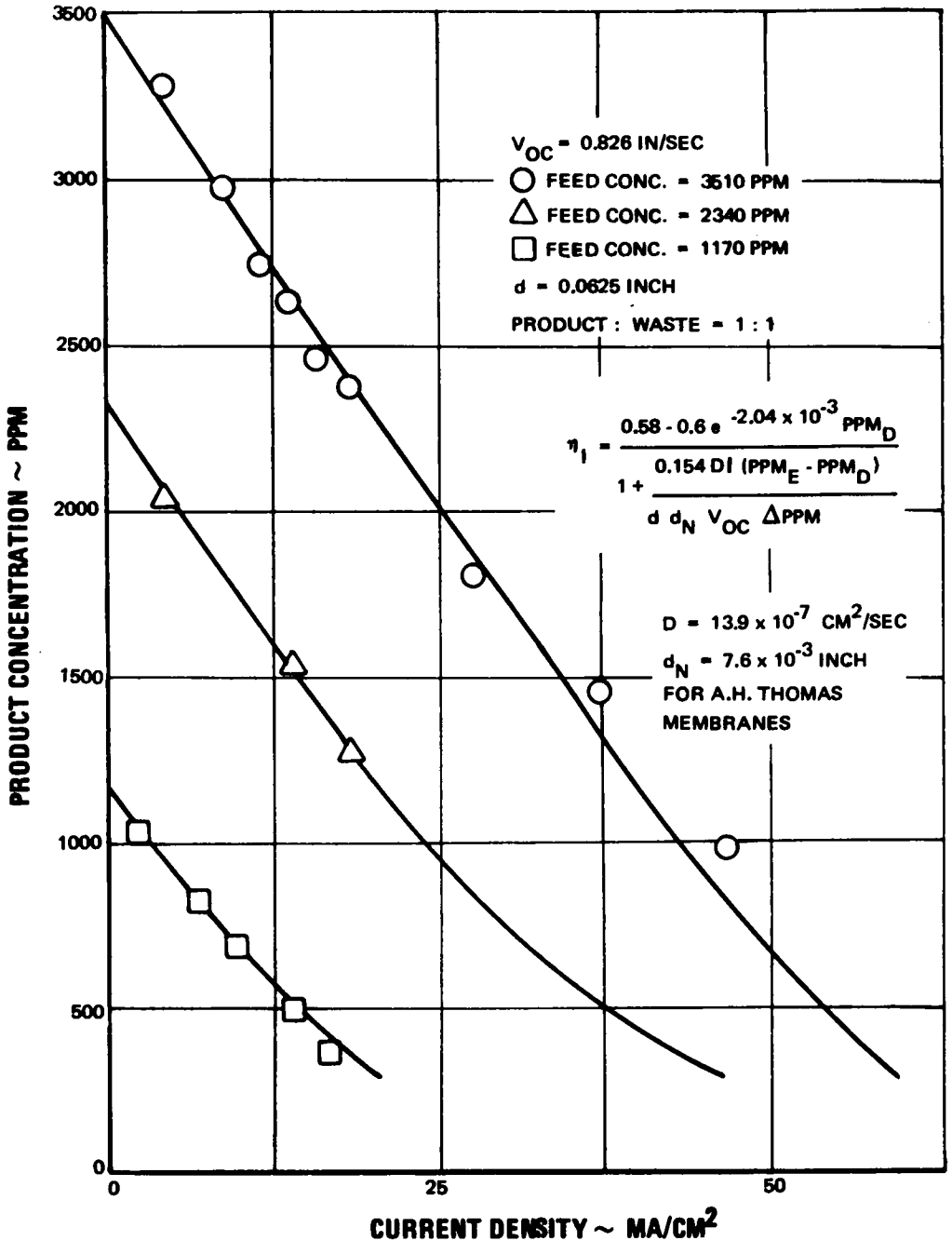

Figure 16 Coulomb Efficiency Correlation. Data from SRI Report No. 2 to OSW, Contract 14-01-0001-698

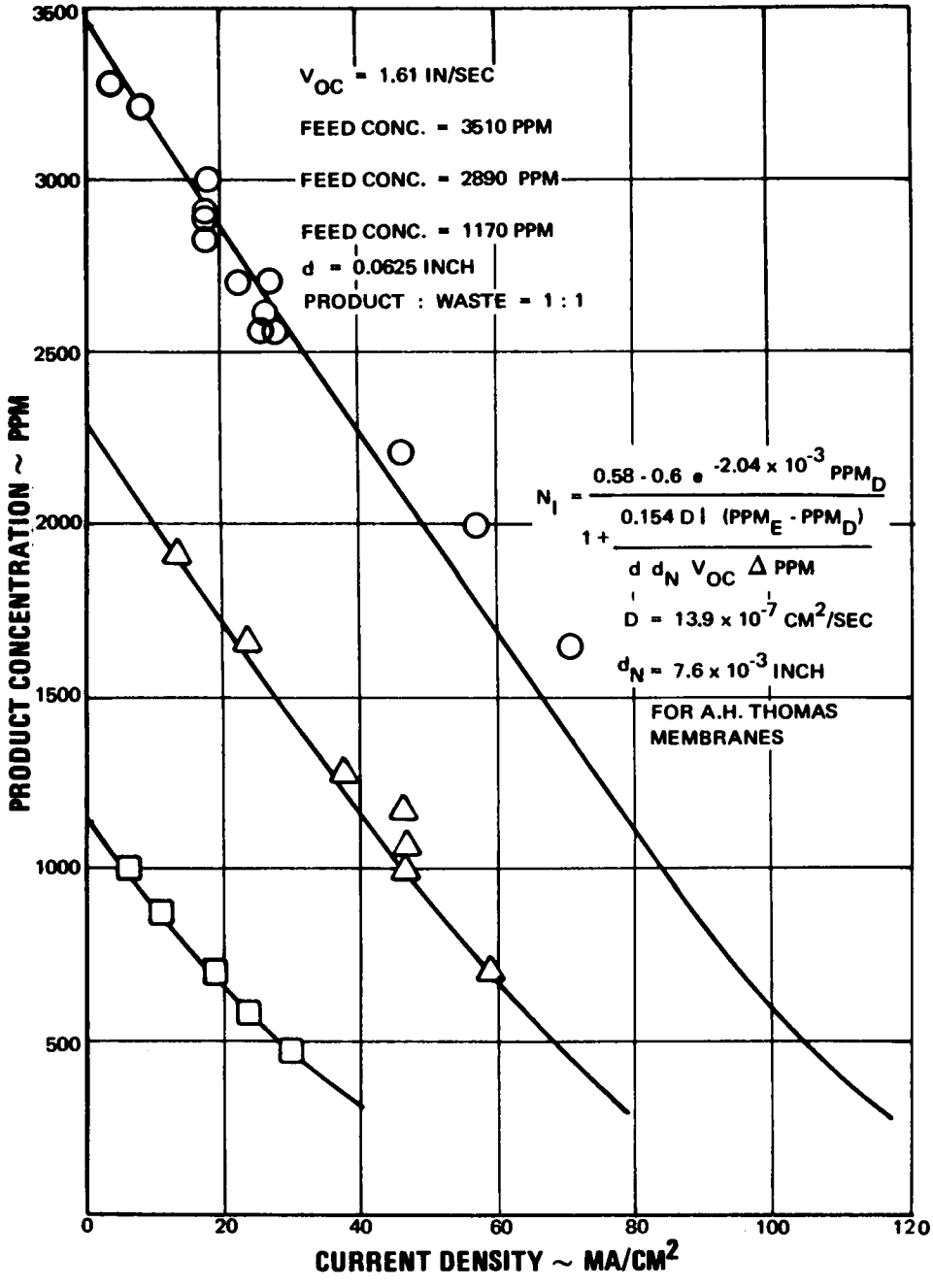

Figure 17 Coulomb Efficiency Correlation. Data from SRI Report No. 2 to OSW, Contract 14-01-0001-698

where

$$R_o = R_N + R_C + R_{DB} + R_{EB} \quad (40)$$

and

R_{CP} = cell-pair areal resistance, ohm-cm^2

R_{BL} = boundary-layer areal resistance, ohm-cm^2

RN = neutral-membrane areal resistance, ohm-cm^2

R_C = cation-membrane areal resistance, ohm-cm^2

R_{DB} = depleted-bulk areal resistance, ohm-cm^2

R_{EB} = enriched-bulk areal resistance, ohm-cm^2

Overall expressions for predicting cell-pair resistance were developed by correlating functional relationships describing the resistance of the various components with the available data. Functional relationships for the resistance of each membrane and each solution stream were first established. The difference between the calculated total of these resistances and the measured cell-pair resistances was then attributed to boundary-layer resistance.

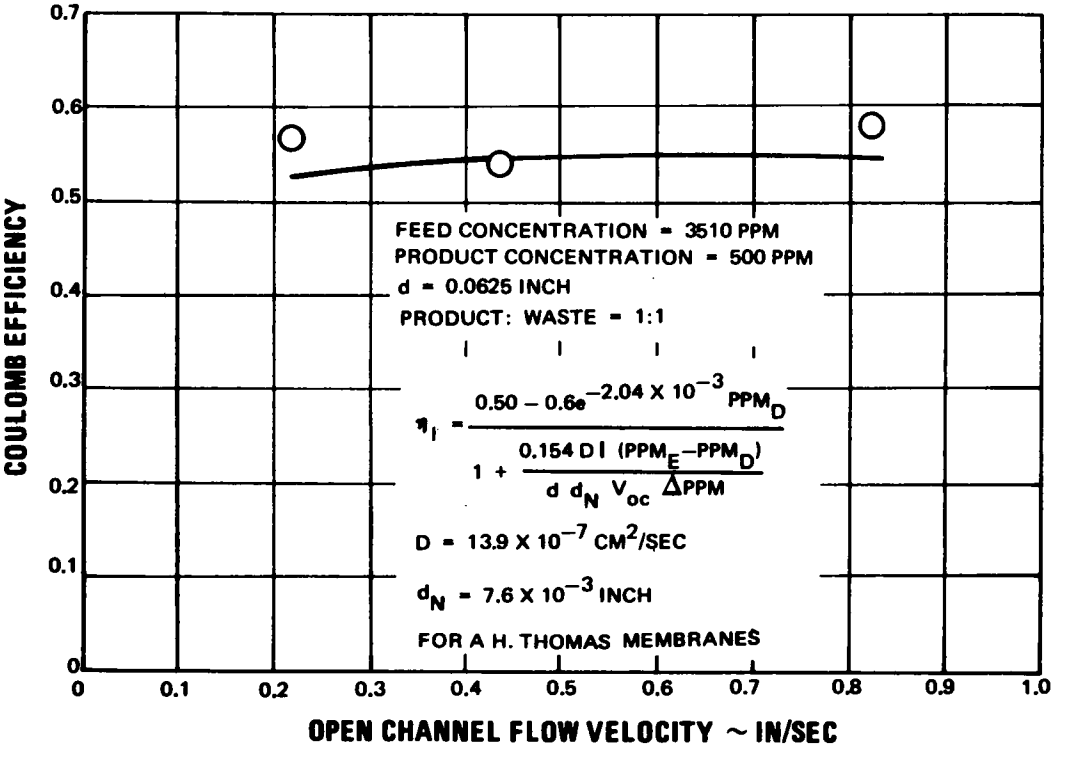

Figure 19 Coulomb Efficiency Correlation. Data from SRI Report No. 4 to OSW, Contract 14-01-0001-698

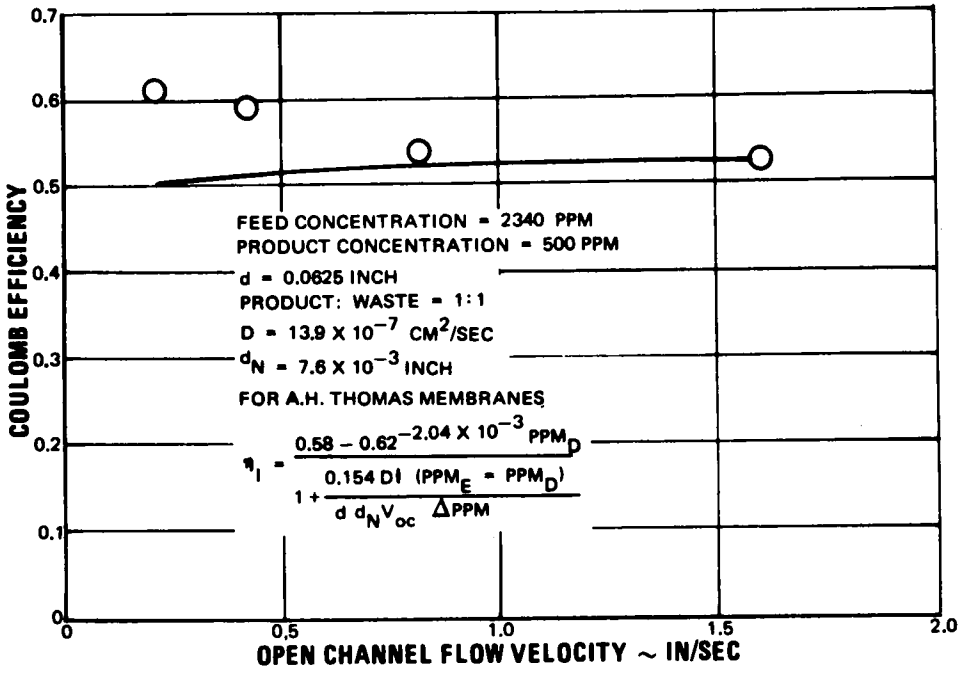

Figure 20 Coulomb Efficiency Correlation. Data from SRI Report No. 4 to OSW, Contract 14-01-0001-698

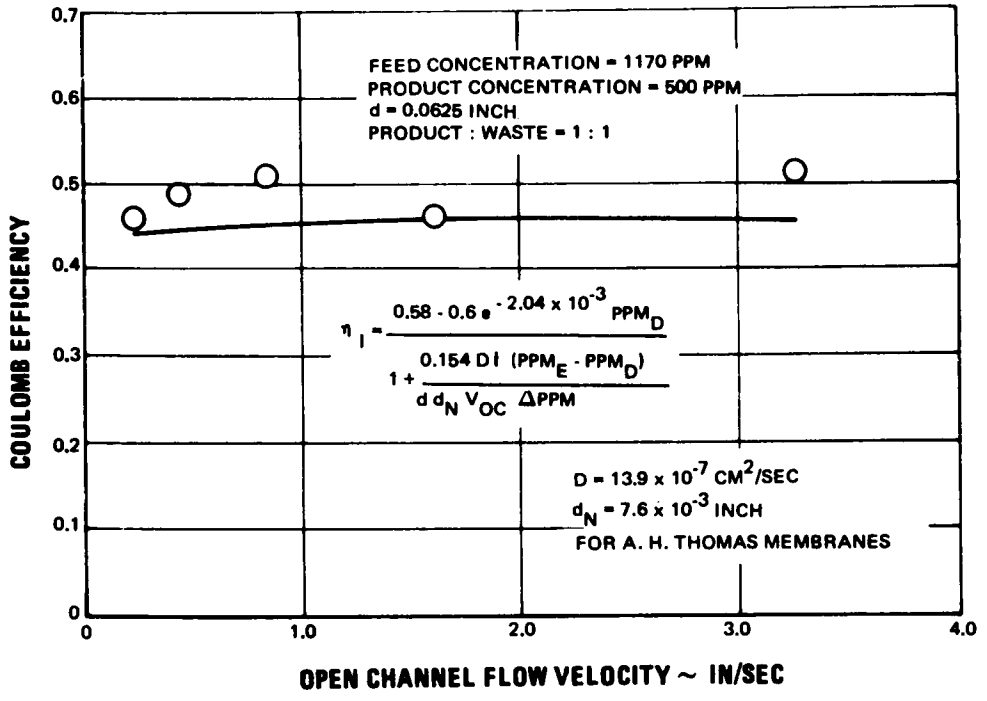

Figure 21 Coulomb Efficiency Correlation. Data from SRI Report No. 4 to OSW, Contract 14-01-0001-698

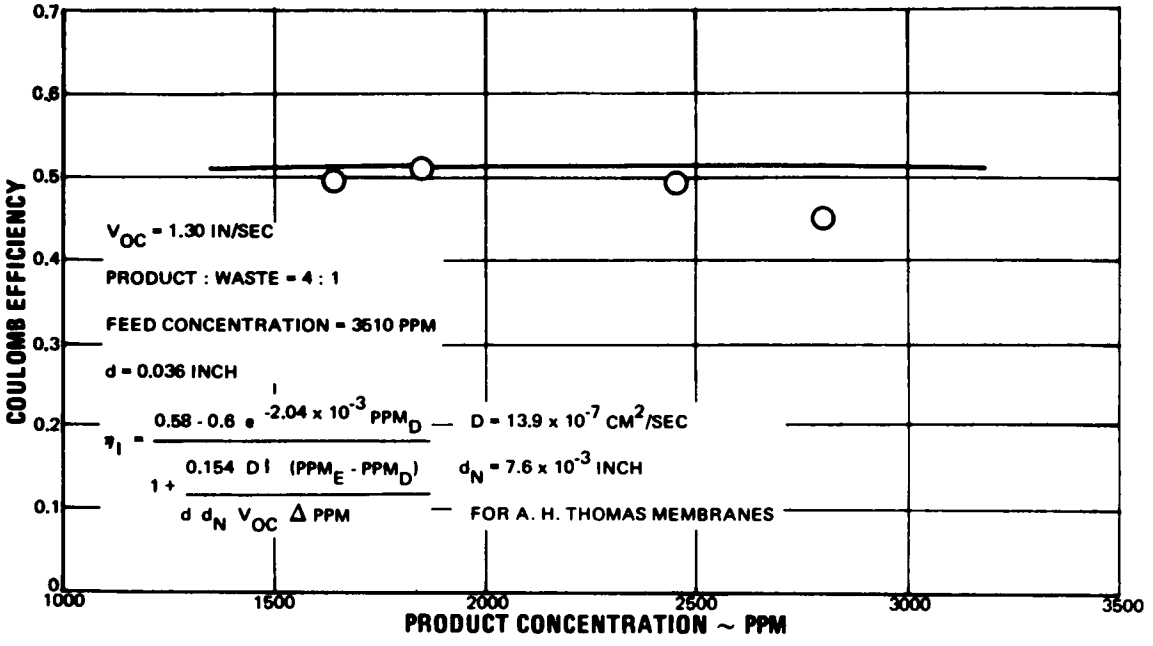

Figure 22 Coulomb Efficiency Correlation. Effect of Product Stream Concentration. Data from SRI Report No. 6 to OSW, Contract 14-01-0001-698

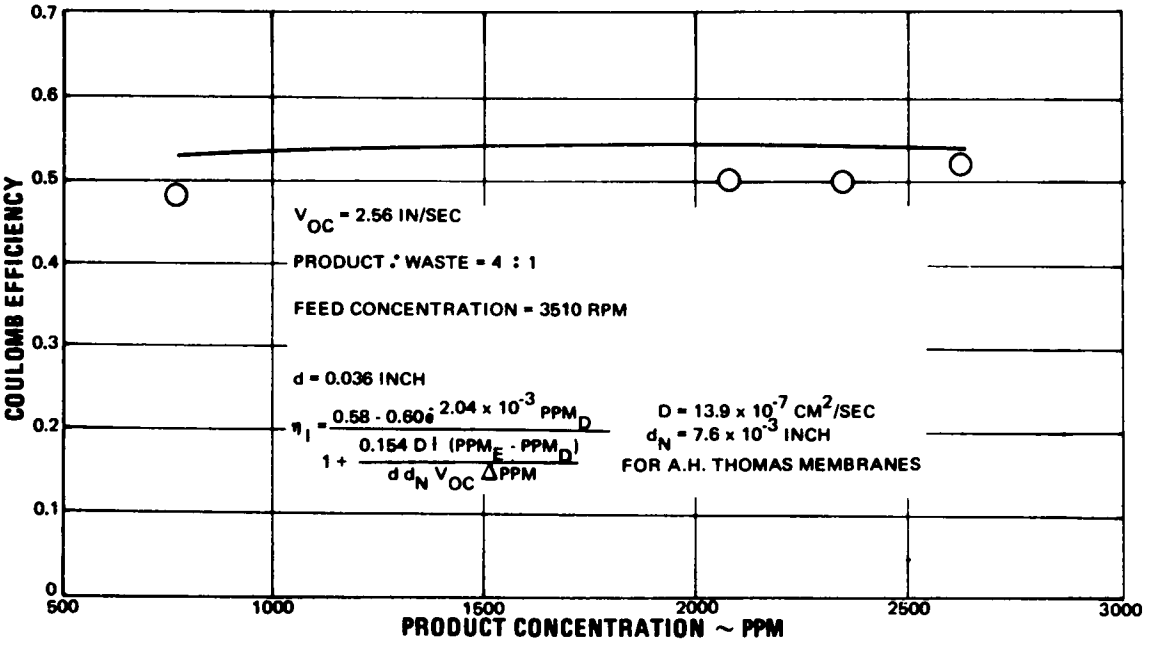

Figure 23 Coulomb Efficiency Correlation. Effect of Product Stream Concentration. Data from SRI Report No. 6 to OSW, Contract 14-01-0001-698

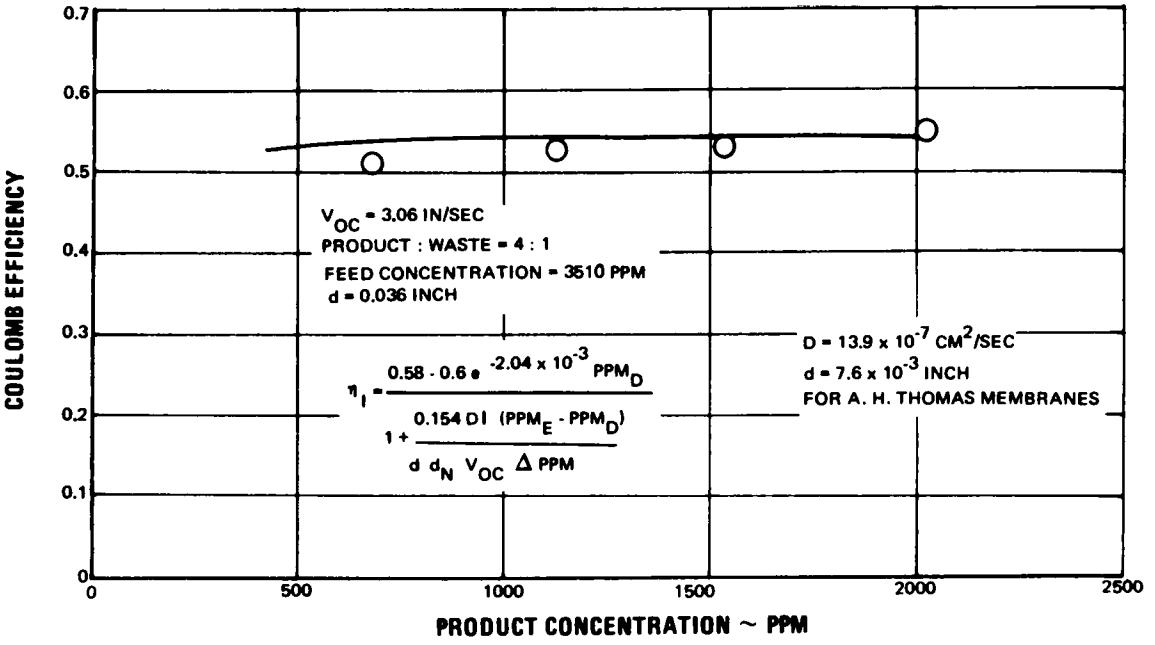

Figure 24 Coulomb Efficiency Correlation. Effect of Product Stream Concentration. Data from SRI Report No. 6 to OSW, Contract 14-01-0001-698

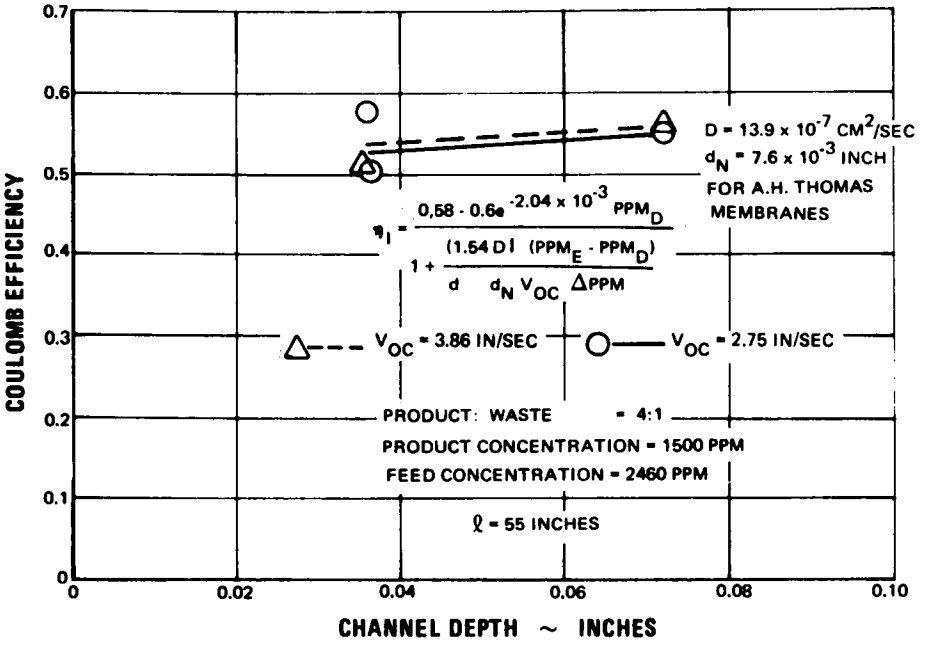

Figure 25 Coulomb Efficiency Correlation. Effect of Channel Depth. Data from SRI Report to P & WA, Contract 14-01-0001-1262

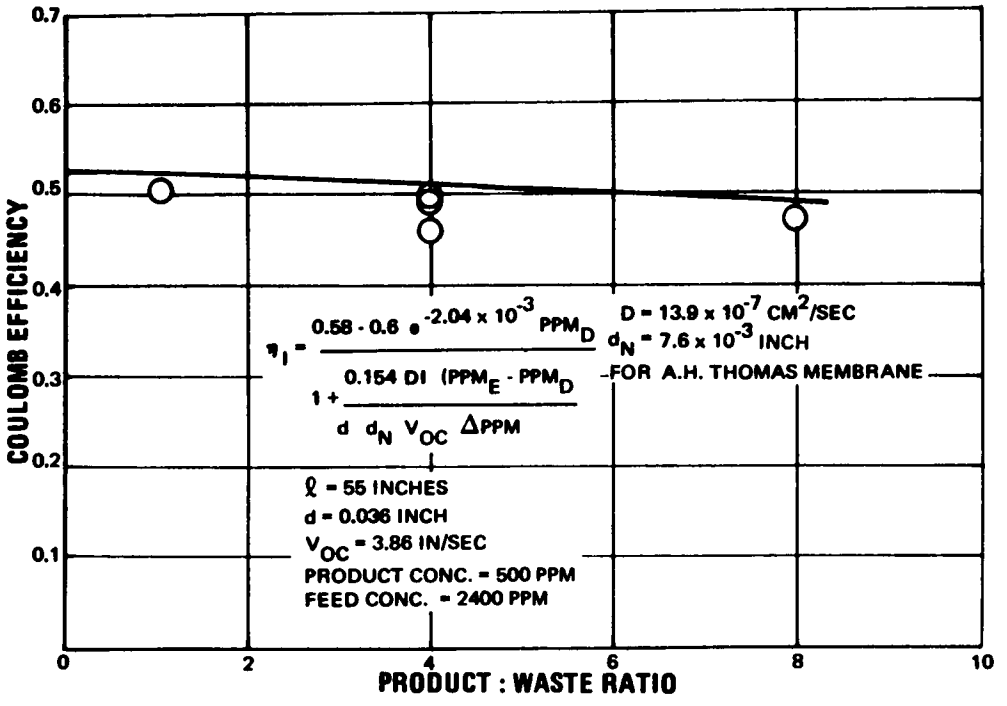

Figure 26 Coulomb Efficiency Correlation. Effect of Product:Waste Ratio. Data from SRI Report No. 6 to P &WA, Contract 14-01-0001-1262

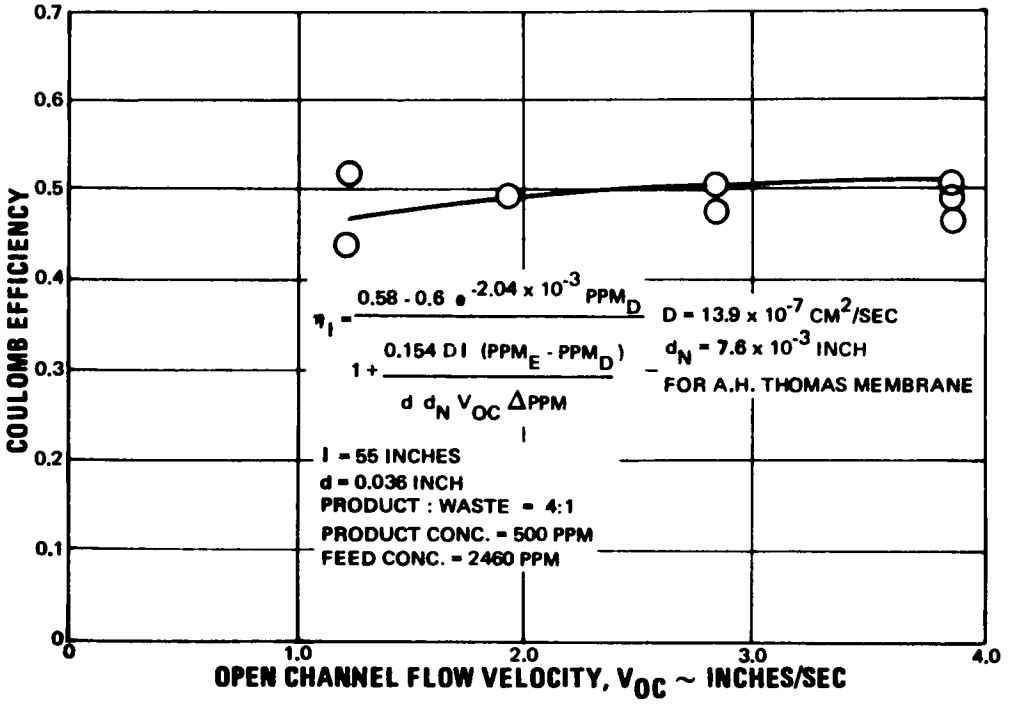

Figure 27 Coulomb Efficiency Correlation. Effect of Flow Velocity. Data from SRI Report No. 6 to P &WA, Contract 14-01-0001-1262

The correlation of this difference led to an appropriate expression for boundary-layer resistance as a function of operating parameters.

Neutral-Membrane Areal Resistance - The resistance of the neutral membrane was obtained as an empirical correlation of data obtained by Southern Research Institute. This resistance correlation is that of A. H. Thomas dialyser tubing. Regenerated cellulose neutral membranes are thought to act like a sponge. If this is the case, a correlation of the form

$$R \propto \frac{1}{ppm} \tag{41}$$

should exist, since this is the form of the expression for resistance of a bulk solution. The best correlation of SRI data was obtained with the correlation equation

$$R_N = \frac{5.15 \times 10^4}{ppm_S} + 5.5 \tag{42}$$

Where

ppm_S = direct average of log mean average concentrations on either side of membrane, ppm NaCl

Resistance values calculated from this equation were plotted in Figure 28, along with the available experimental data. It is expected that the resistance of any regenerated-cellulose type neutral membrane would correlate in a similar way qualitatively.

Cation-Membrane Areal Resistance – The resistance of the Ionac MC-3142 cation-selective membrane remains constant at about 12 ohm-cm^2 regardless of the solution concentration, according to data contained in SRI Report No. 3 to the Office of Saline Water, Contract 14-01-0001-698. Therefore in all calculations it was assumed that

$$R_C = 12 \text{ ohm-cm}^2 \tag{43}$$

Areal Resistance of Depleted and Enriched Solution Streams – General expressions for bulk solution resistance are described in Section III. B., Equations (17) and (18). The combination of these two equations results in an expression for bulk solution resistance

$$R_B = K \frac{1000\, d'}{\Lambda N} \tag{44}$$

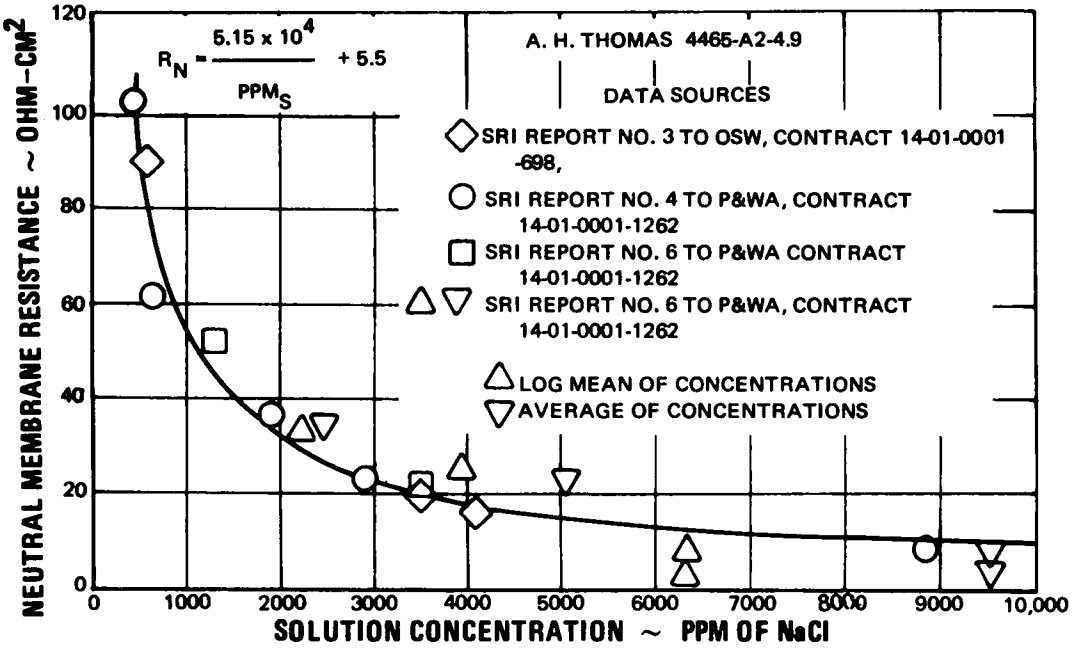

Figure 28 Neutral Membrane Resistance

Where

d' = membrane spacing, cm

Λ = equivalent conductance of salt in solution, (mho/cm)/(equiv./cm^3)

N = concentration of solution, equiv./liter

K = appropriate factor to account for presence of turbulator screen

Two assumptions were made to establish a useful form of this equation; a constant equivalent conductance of Λ = 116 cm^2/ohm-equiv., and a 50 percent increase in resistance over that of the bulk solution due to the presence of a turbulence-promotion screen in the channel. The first assumption produces the most accurate results where the concentration is low (Λ = 116 cm^2/ohm-equiv. at 1500 ppm NaCl), thus being most accurate where resistance is significantly high. The second assumption is based on information from SRI where such an increase in resistance due to the presence of a screen material was experienced.

In engineering units, the resistances of the depleted and enriched bulk streams are therefore given by

$$R_{DB} = \frac{1.92 \times 10^6 d}{ppm_D} \tag{45}$$

$$R_{EB} = \frac{1.92 \times 10^6 d}{ppm_E} \tag{46}$$

Where

R_{DB} and R_{EB} = areal resistances of depleted-bulk and enriched-bulk solution streams respectively, ohm-cm^2

ppm_D and ppm_E = log mean average concentrations of depleted-bulk and enriched-bulk solution streams respectively, ppm NaCl

d = membrane spacing (channel width), inches

Boundary-Layer Resistance – The general form of the boundary-layer resistance was chosen as as a result of the analysis of the boundary-layer resistance phenomenon discussed in Section III. B., and intuitive judgment of the primary factors which might influence this resistance. The general form is

$$R_{BL} = \frac{A\, i^B}{V_{oc}^C \; ppm_D^D} \tag{47}$$

Where

A, B, C, D are appropriate correlation constants

The final expression for boundary-layer resistance, which results in the best average correlation of the available data, is

$$R_{BL} = \frac{2.44 \times 10^8}{V_{oc}^{0.75} \, ppm_D^2} \qquad (48)$$

Where

V_{oc} = solution velocity, in/sec

ppm_D = log mean average concentration of depleted solution, ppm NaCl

Current density appears to have little effect on resistance. This is demonstrated by the data plotted in Figure 29 where resistance values obtained at three different path lengths are plotted against solution velocity. In each case, the same feed concentration was used and current density was adjusted to maintain the same product concentration. There is no correlation between current density and cell-pair resistance over the range of the available data.

Velocity does appear to correlate with cell-pair resistance, however, as shown in Figures 29 through 32. Also the bulk-stream resistance of the depleted stream appears to influence resistance to a great extent, as shown by these same figures which represent data obtained with several different feed-solution concentrations. The curves in Figures 29 through 32 show the degree of correlation obtained with Equation (48). The best correlation is obtained at the higher velocities (above 4 cm/sec) where boundary layer resistance is the lowest. The higher velocities also appear to be of most interest for the transport-depletion process.

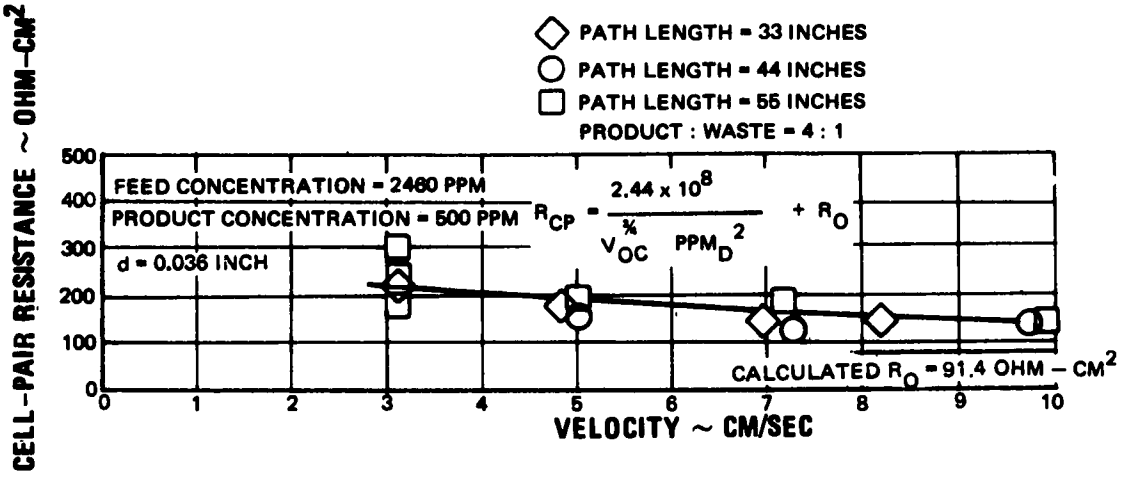

Figure 29 Cell-Pair Resistance Correlation. Data from SRI Report No. 6 to P&WA, Contract 14-01-0001-1262

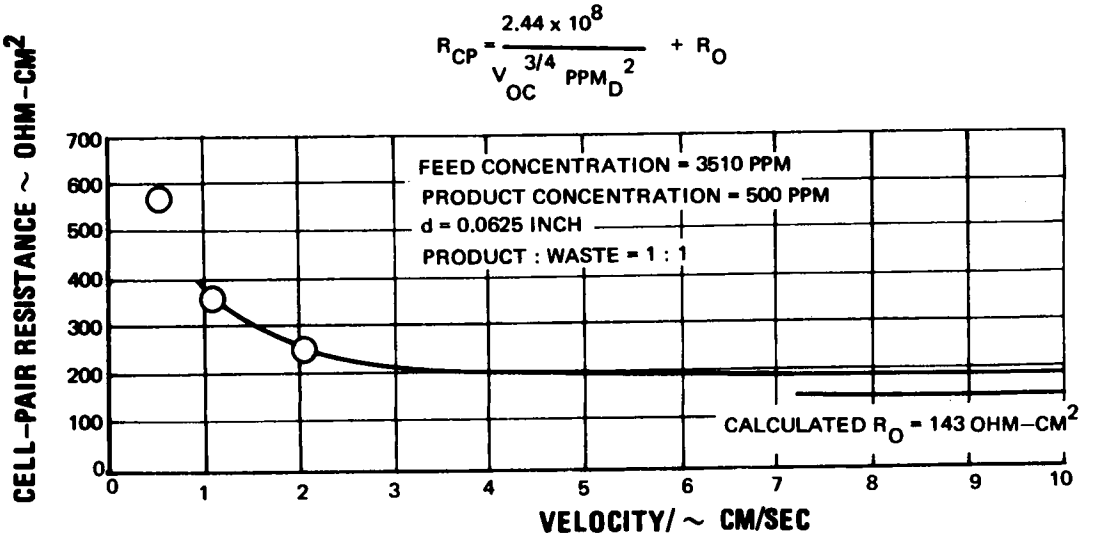

Figure 30 Cell-Pair Resistance Correlation. Data from SRI Report No. 4 to OSW, Contract 14-01-0001-698

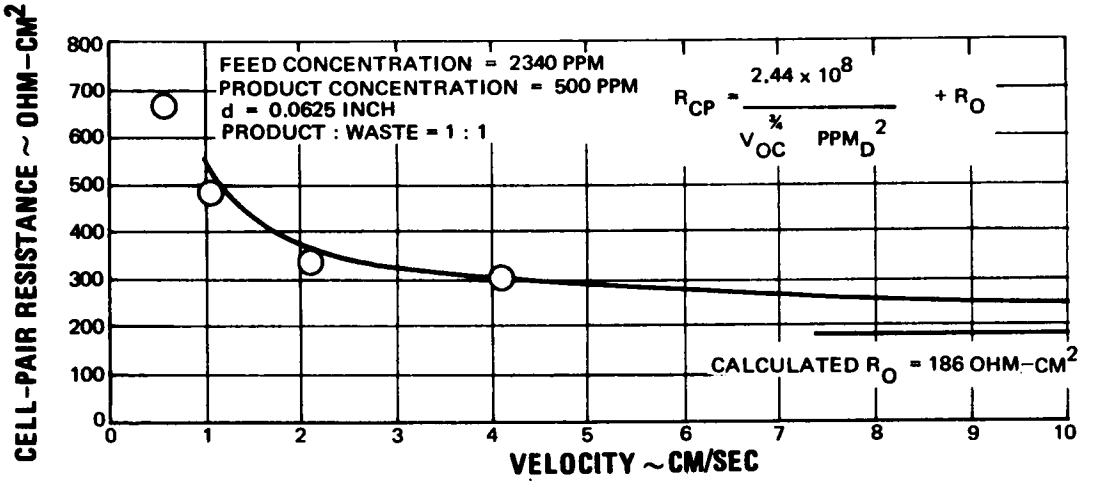

31 Cell-Pair Resistance Correlation. Data from SRI Report No. 4 to OSW, Contract 14-01-0001-698

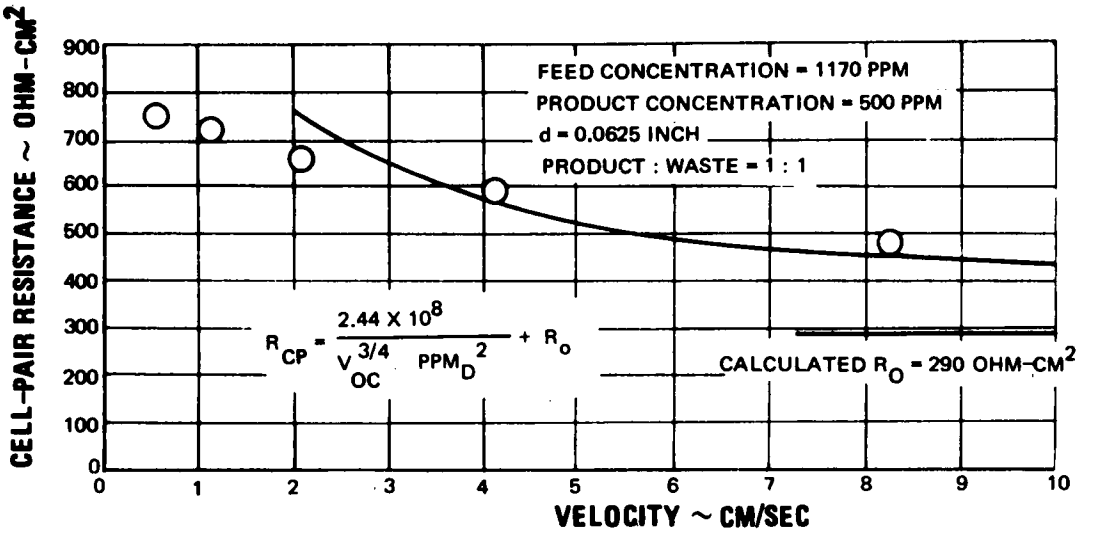

Figure 32 Cell-Pair Resistance Correlation. Data from SRI Report No. 4 to OSW, Contract 14-01-0001-1262

3. Stack Pressure Loss Correlation

The fluid pressure loss through the stack can be expressed as the sum of several component pressure losses as described in Section III. B. above.

$$\Delta P_{total} = \Delta P_{headers} + \Delta P_{manifolds} + \Delta P_{inlets\ and\ exits} + \Delta P_{channels}$$

Pressure loss through the spacer screen represents the largest portion of the total pressure loss and is the most difficult to predict. The correlation of these losses for the spacer-screen design selected for the pilot-plant stack is described here. In a well-designed stack, manifold and header losses should be insignificant and accurate calculation of these losses is not required.

a. Channel-inlet pressure loss is assumed to be the sum of a contraction loss, a wall friction loss and an expansion loss.

$$\Delta P_{inlet} = \Delta P_{contraction} + \Delta P_{friction} + \Delta P_{expansion} \qquad (49)$$

From fluid mechanics, these losses can be expressed as

$$\Delta P_{contraction} = K_c \frac{\rho v_I^2}{2g} \qquad (50)$$

$$\Delta P_{friction} = 4f \frac{L_I}{D_I} \frac{\rho v_I^2}{2g} \quad (51)$$

$$\Delta P_{expansion} = K_e \frac{\rho v_I^2}{2g} \quad (52)$$

where:

K_c and K_e = empirical coefficients, assumed equal to 1.0
ρ = fluid density
v_I = solution velocity in inlet passages
L_I = length of inlet passages
D_I = hydraulic diameter of inlet passages
f = skin friction coefficient in inlet passages
g = 32.2 ft/sec^2

Furthermore, skin friction in laminar flow, as is the case here, is inversely proportional to Reynolds number.

$$f = \frac{16}{R_e} \quad (53)$$

$$R_e = \frac{\rho v_I D_I}{\mu} \quad (54)$$

Where:

μ = dynamic viscosity of solution

For the specific case of water flowing through an inlet with fixed geometry, Equations (51), (53) and (54) can be combined to show that the friction pressure loss is directly proportional to the solution velocity.

$$\Delta P_{friction} = K_1 v_I \quad (55)$$

Likewise, from Equations (50) and (52) the inlet contraction and expansion losses are proportional to the square of velocity.

$$\Delta P_{\text{contraction and expansion}} = K_2 v_I^2 \tag{56}$$

Therefore, the total inlet-pressure loss can be expressed in the following form.

$$\Delta P_{\text{inlet}} = K_1 v_I + K_2 v_I^2 \tag{57}$$

For fixed spacer-screen dimensions, the solution velocity in the inlets is directly proportional to the open-channel velocity, and Equation (57) becomes

$$\Delta P_{\text{inlet}} = K_1' V_{oc} + K_2' v_{oc}^2 \tag{58}$$

This equation can be used to correlate the measured pressure loss shown in Figure 9 for the pilot-plant solution-inlet configuration. The correlation results in the following equation.

$$\Delta P_{\text{inlet}} = 0.077 v_{oc} + 0.0073 v_{oc}^2 \tag{59}$$

b. Channel pressure loss data can be correlated by using a relationship for flow through a porous material. From experiments it has been found that

$$\left(\frac{\Delta P}{L}\right)_{\text{channel}} = \alpha \mu v_{oc} + \beta \rho v_{oc}^2 \tag{60}$$

where the first term on the right represents viscous effects and the last term inertial effects similar to turbulence. The constants α and β are functions of the porosity and the pore texture of the material. At low velocities and very open pores the inertia term is generally small as compared to the viscous term.

When the pressure-loss data for the screen used in the pilot-plant design is correlated with Equation (60), the following expression results.

$$\left(\frac{\Delta P}{L}\right)_{\text{channel}} = 0.0096 v_{oc} + 0.0027 v_{oc}^2 \tag{61}$$

For the specific pilot-plant channel length of 33.5 inches, Equation (61) can be further reduced to

$$\Delta P_{\text{channel}} = 0.321 v_{oc} + 0.0904 v_{oc}^2 \tag{62}$$

c. Total spacer screen pressure loss is the sum of the pressure losses through the inlet, the channel and the exit.

$$\Delta P_{\text{spacer screen}} = 2\,\Delta P_{\text{inlet}} + \Delta P_{\text{channel}} \tag{63}$$

The substitution of Equations (59) and (62) into Equation (63) results in the final expression for spacer-screen pressure loss.

$$\Delta P_{\text{spacer screen}} = 0.475\, v_{oc} + 0.105\, v_{oc}^{2} \tag{64}$$

Where:

$\Delta P_{\text{spacer screen}}$ = pressure loss between inlet manifold and exit manifold, psi

v_{oc} = open-channel velocity (velocity with no screen in channel), in/sec

V. DESIGN AND CONSTRUCTION OF PILOT PLANT

This section describes the design and construction of the pilot-plant stack and system. The first part describes the study of stack-design concepts which led to the selection of the final stack design. This final stack design is then described, followed by a description of the stack construction. Finally, a description of the design and construction of the pilot-plant system is included.

A. Stack Design Configuration Studies

Many stack configurations were evaluated in selecting the design for the transport-depletion pilot-plant stack. Some design concepts were immediately discarded because of basically undesirable characteristics. Workable configurations were evaluated on the basis of a set of design criteria which are described below. The most promising basic configuration was studied in further detail until ultimately the best variation of this basic configuration was selected.

The design finally selected for development was a multiple-pass internally-manifolded plate-and-frame design. This design was rated good to excellent in all the major areas of concern. Its great operational flexibility led to its selection. This stack is capable of producing experimental data which can be used to determine if another alternate would be better suited for use in a commercial stack.

1. Major Design Criteria

Five criteria were used in evaluating the candidate designs. They are structural integrity, membrane utilization, hydrodynamic performance, electrical performance, and operational flexibility. A design rated poor in any area was dropped from further consideration. Selection of a final design was based on comparison of the remaining configurations, using these criteria.

a. Structural Integrity

A stack must be structurally sound. Configurations with inherently difficult sealing problems should be avoided. The fragile neutral membrane should be protected from any unnecessary stress. Sufficient electrical insulation should be incorporated to assure a minimum of external shorting of the stack. The clamping arrangement should be as flexible as possible to accommodate any unknown sealing problems.

b. Membrane Utilization

A design should be capable of a high percentage of membrane utilization when scaled up to commercial size. Where two designs are nearly identical in performance, superior membrane utilization is preferred.

c. Flow Distribution and Pressure Levels

The manifold system for a stack should be capable of uniform flow distribution to all cell pairs. Internal flowpaths should be devoid of low-velocity pockets where polarization can take place. Pressure levels should be kept below those levels where excessive leakage is likely to occur.

d. Electrical Performance

The stack should operate with close to minimum expenditure of electrical energy at any desired current density. Therefore, electrical resistance should be a minimum; electrical leakage through manifolds should be minimized; and it should be possible to operate with a variable product-to-waste ratio to evaluate the trade-off of current efficiency with stack resistance.

e. Operational Flexibility

A pilot plant should be capable of producing a relatively complete performance map. To achieve a reasonably complete performance map, certain features are desirable. These include: 1) independent electrode rinse compartments, 2) independent inlets for dilute and concentrate streams, 3) variable electrical field strength, 4) variable path length, width, and depth, and 5) minimum assembly and disassembly time.

2. Basic Design Configuration

Four basic types of configuration were considered. They include: plate and frame, immersed stack, helical stack, and spiral stack designs. Several variations of these basic configurations are possible. The basic configurations are described below, and their unique features are indicated.

a. Plate and Frame

The basic structure of a plate-and-frame design is that of a multilayered sandwich clamped between endplates. The endplates contain the electrodes. Between the endplates are multiple layers of cell pairs, each consisting of a neutral membrane, a cation membrane and two spacer-frame assemblies. The sandwich is held together by the bolts which squeeze the cell pairs between the endplates. Many variations of the basic plate-and-frame configuration are possible. Figures 33 through 38 show several such variations.

The four-stack module illustrated in Figure 37 is an example of a stack packaging concept. It consists of several duplicate stacks arranged around a central pylon which combines the functions of a structural support, electrode holder, and hydraulic connector unit. This arrangement could be adapted to any plate-and-frame concept. It is not particularly suited to the pilot-plant application, but may offer unique packaging advantages for use in large commercial-size plants.

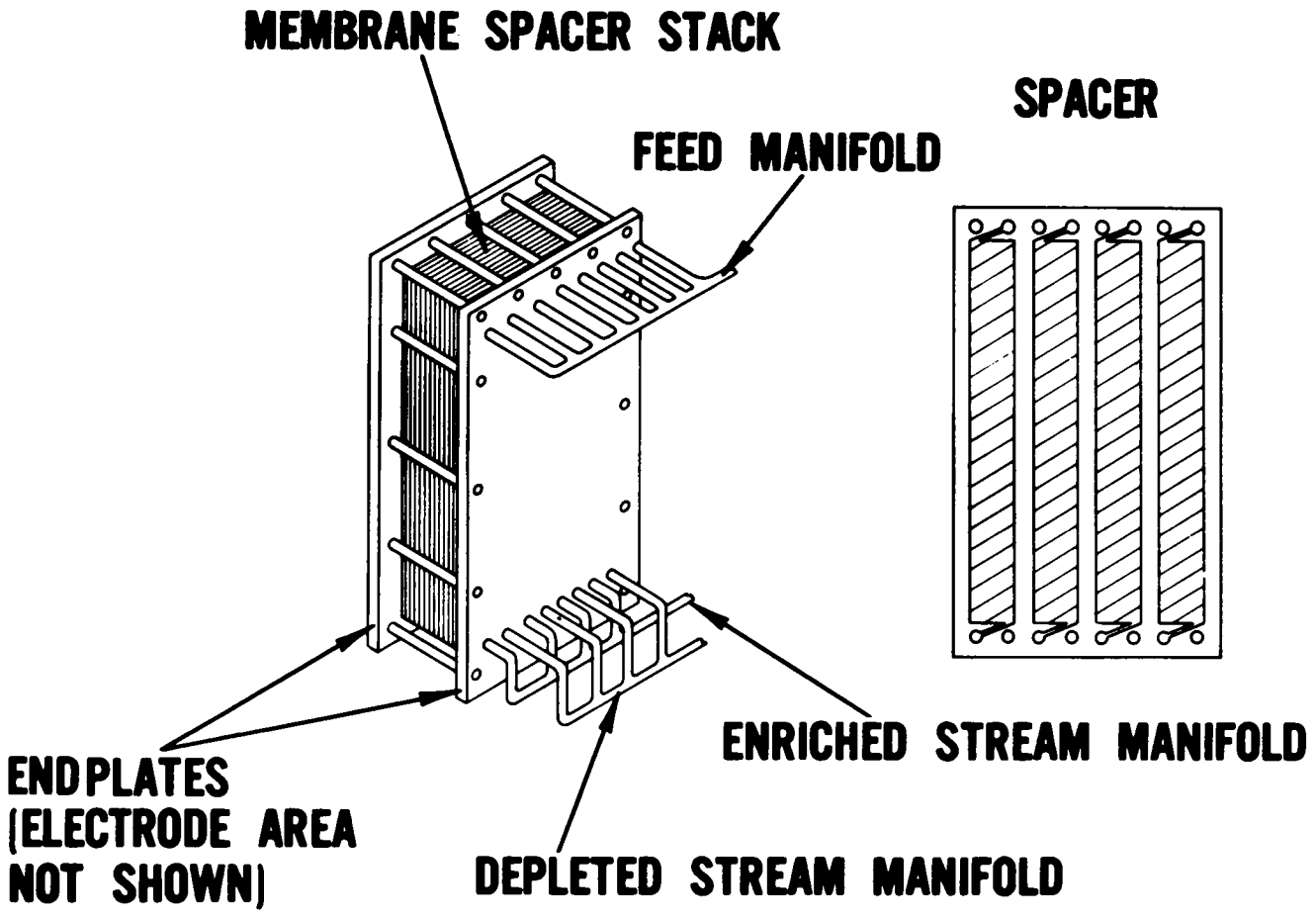

Figure 33 Four-Channel Rectangular Stack M-48434

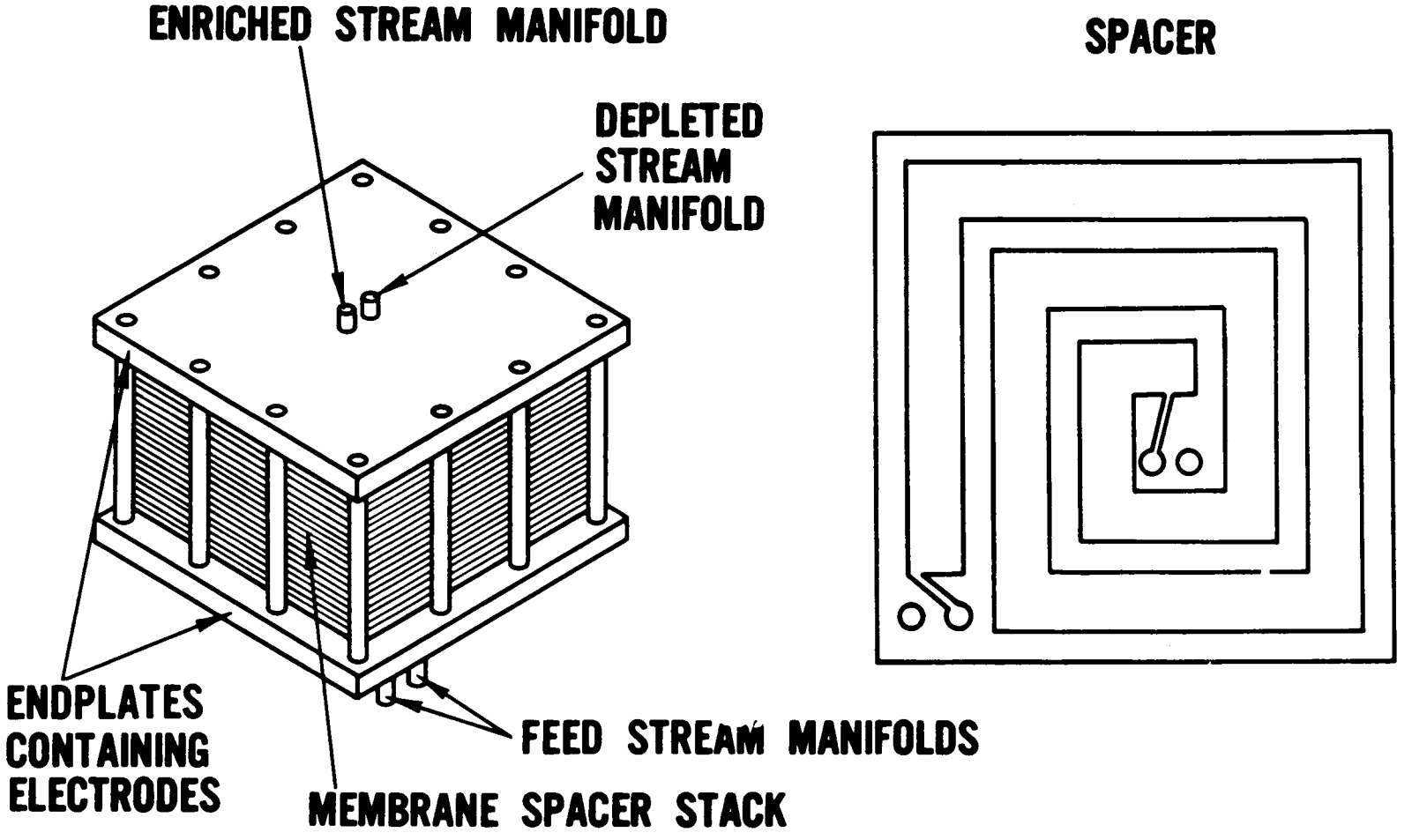

Figure 34 Square Spiral Stack M-48410

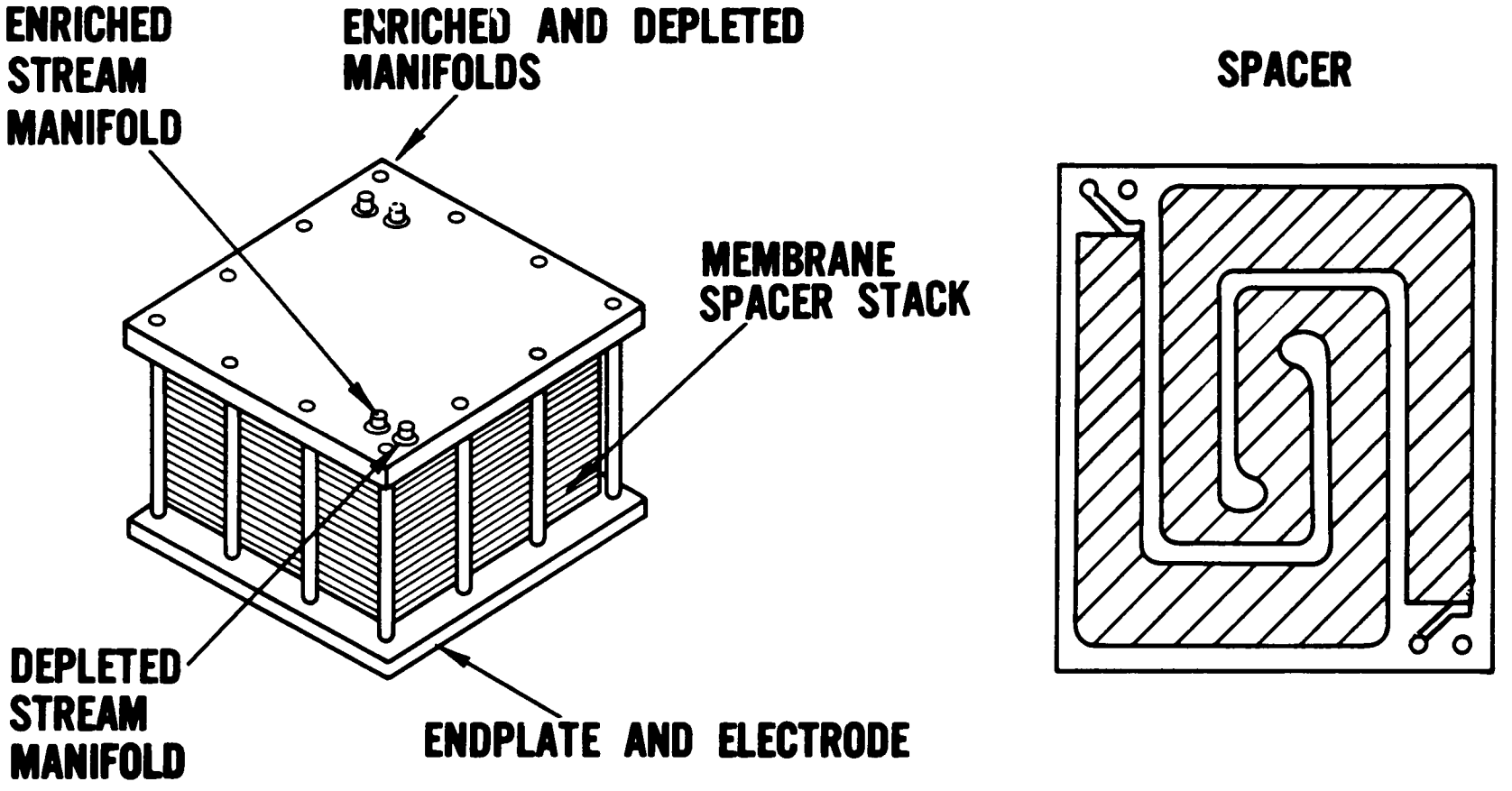

Figure 35 Spiral Flow Module M-48409

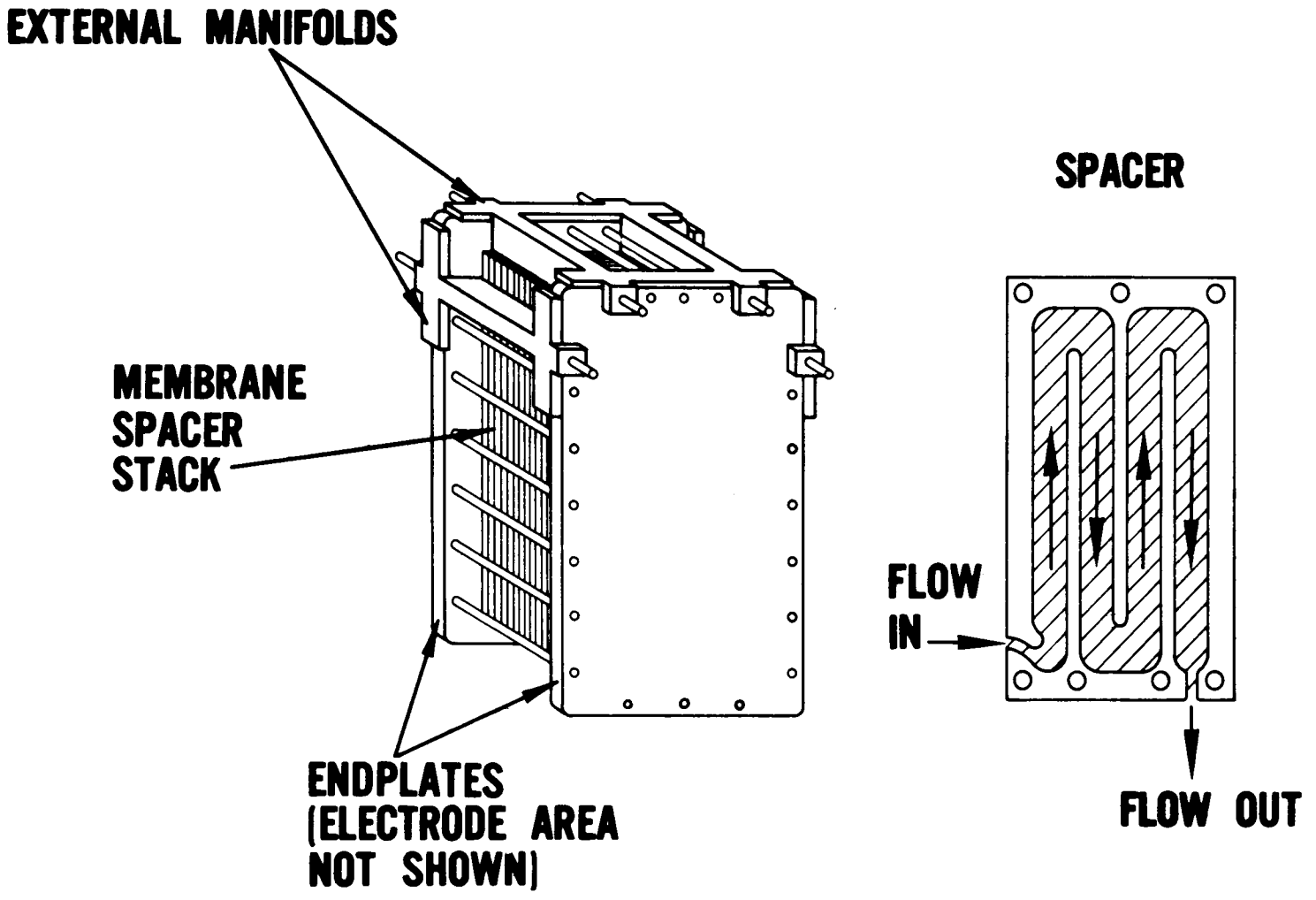

Figure 36 Externally-Manifolded Module M-48433

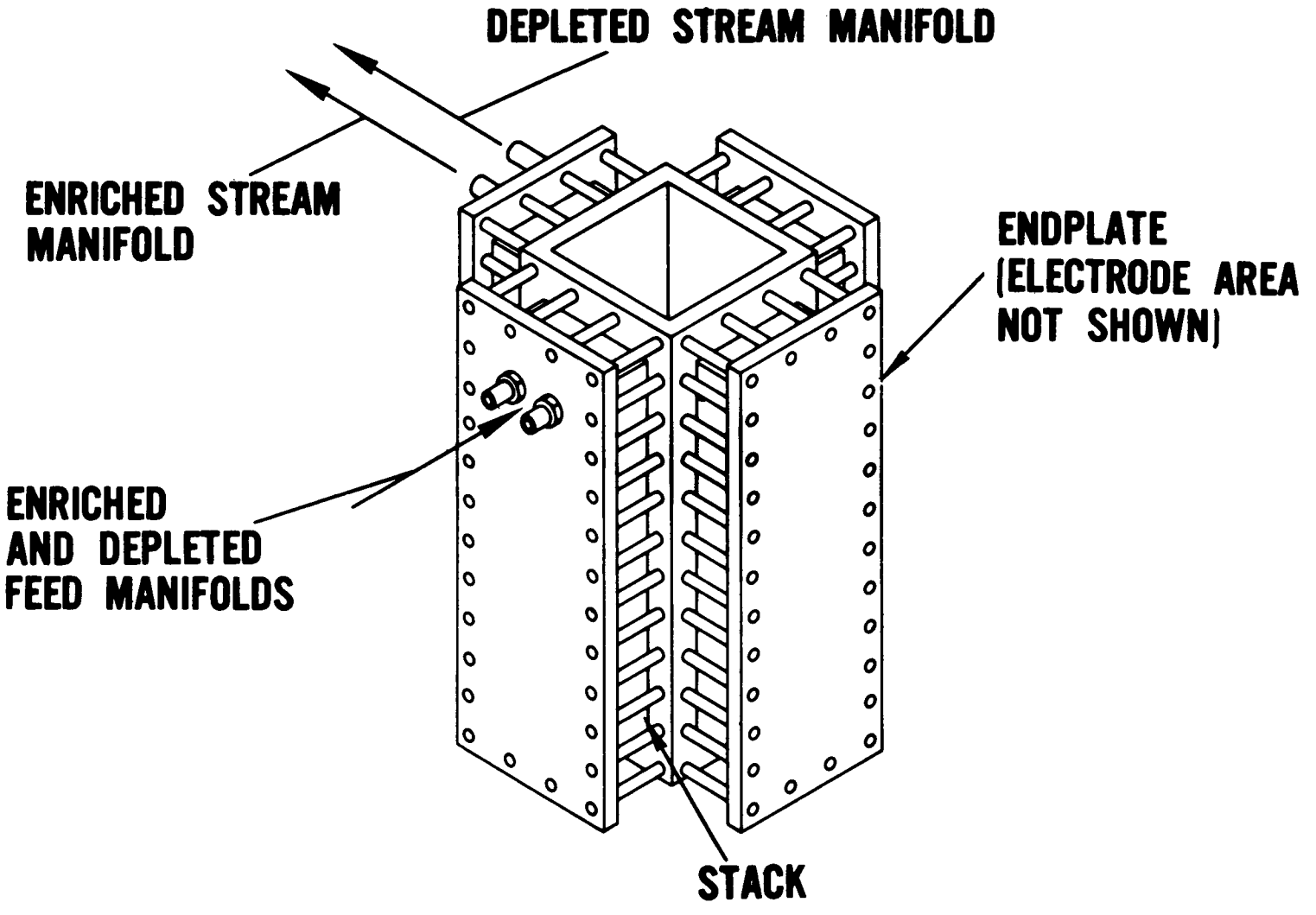

Figure 37 Four-Stack Module M-48411

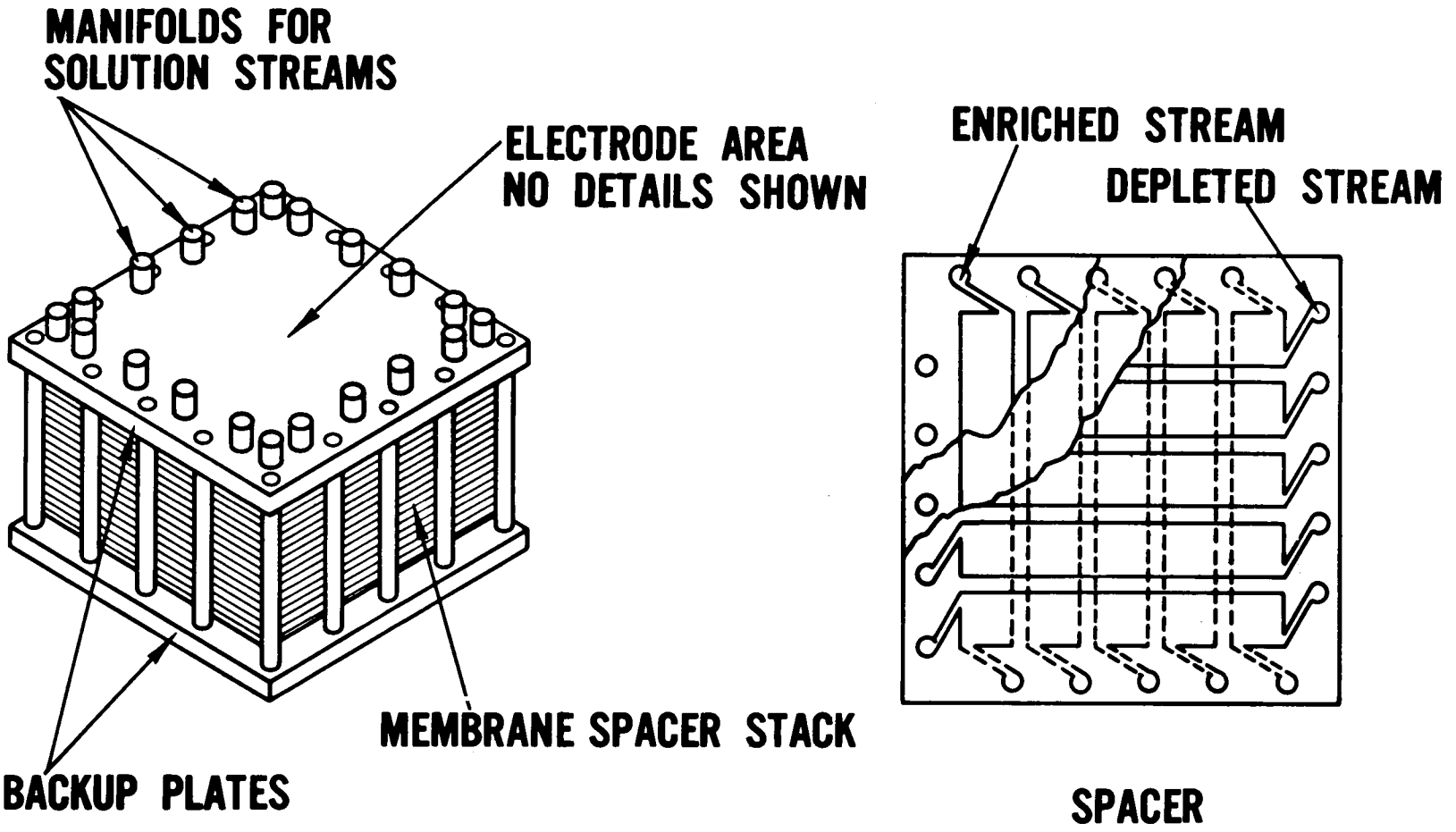

Figure 38 Cross-Flow Design M-48408

The plate-and-frame design was rated highest because of its simplicity, soundness, and relatively good electrical and hydrodynamic characteristics. Because of the wide variety of possible plate-and-frame configurations, Section V. A.3. below is devoted exclusively to discussions of these various designs. The variations differ in performance characteristics, but are all basically similar.

b. Immersed Stack

The stack of the immersed-stack design is contained in a specially-designed tank. The feed solution fills this tank and the product and concentrate solutions are extracted from the center of the stack. The unique feature of this design is the absence of internal inlet manifolds.

This configuration was conceived with the idea of reducing the risk of solution leakage out of the stack. By feeding solution into the stack as shown in Figure 39, the outward leakage of solution is stopped.

Several problems exist with this design. The most serious is the lack of control of the concentration of the concentrate stream feed. Both concentrate and product streams use the same feed source. Therefore it is not possible to recirculate the concentrate stream, or to evaluate the use of staging. A further problem is the relatively large current leakage possibility through the tank around the stack. Tolerances must be kept tight between the stack and tank to avoid large leakage currents.

c. Helical Stack

The helical stack, shown in Figure 40, was conceived as a method of reducing current leakage. Since manifolds do not extend directly between the electrodes, no current leakage would occur through them. The only leakage path is along the flow path.

The apparent advantage of reduced current leakage is reduced, however, by an increased stack resistance. All flow paths are inclined with respect to the current paths. Therefore the membrane and solution-compartment path appears longer electrically. This increase in resistance tends to negate the current efficiency advantage.

A second more serious disadvantage is inherent. Because of the symmetry of the flow paths, a constant current density would be present throughout the flow path. This is not desirable. In the previous configurations the increased resistance of the product stream at the tail end of the stack leads to a naturally-decreasing current-density profile which is helpful in relieving polarization problems. Such is not the case in a helical stack arrangement.

Design problems also exist. An adequate electrode-rinse system would have to be found, and a special clamping method would be needed to counteract the torsional forces produced by the helical spacers.

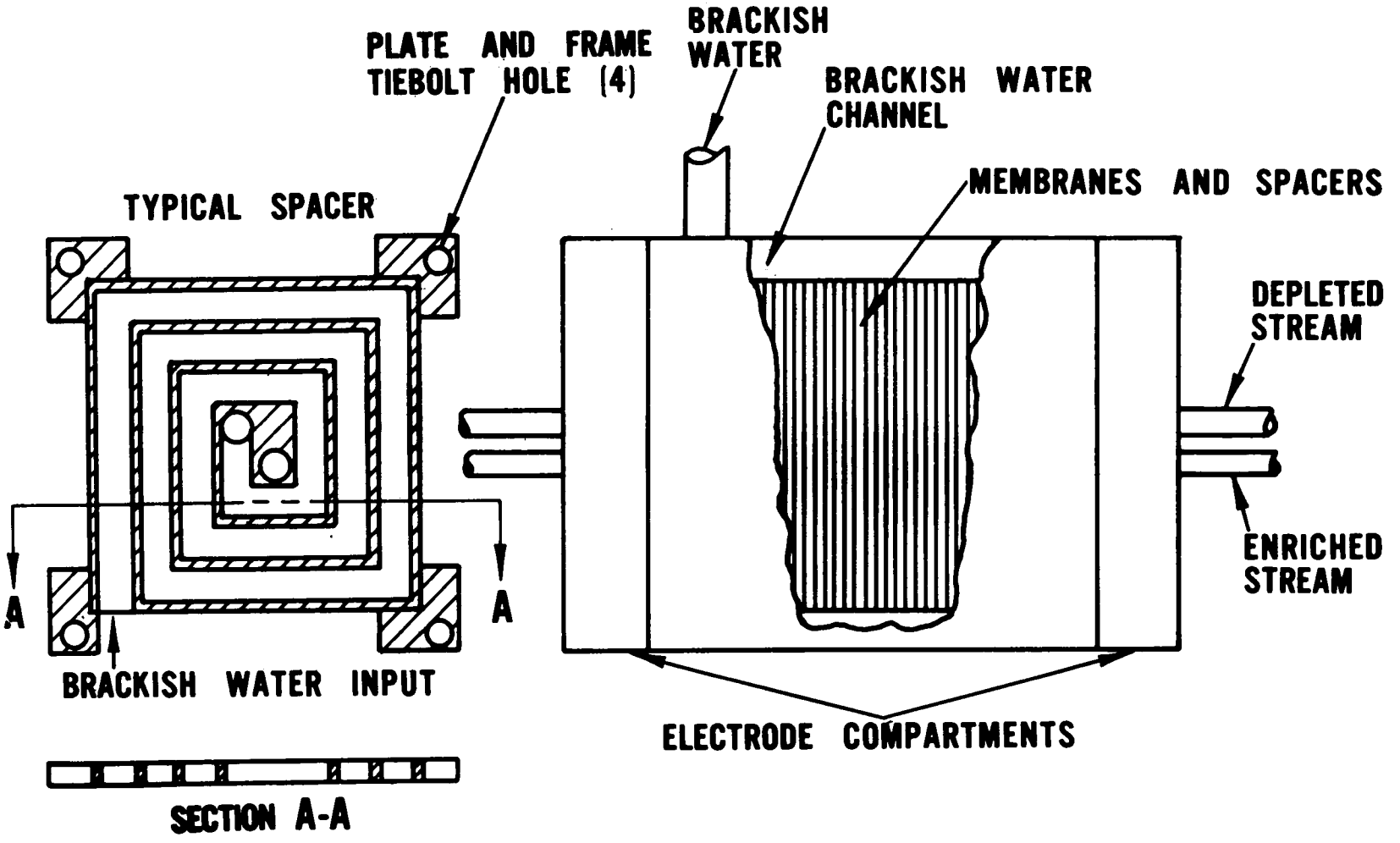

Figure 39 Immersed-Stack Configuration M-42838

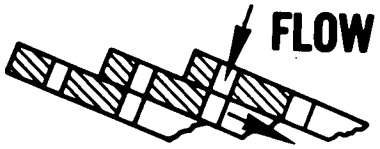

ELECTRODE COMPARTMENT NOT RESOLVED

FLOW ENTRANCE CROSS SECTION
THRU SPACER HOLES

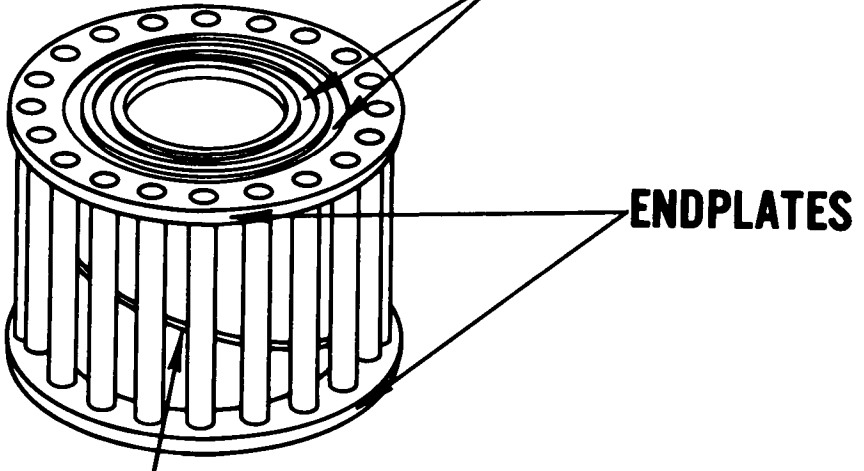

TYPICAL MEMBRANE CELL PAIR

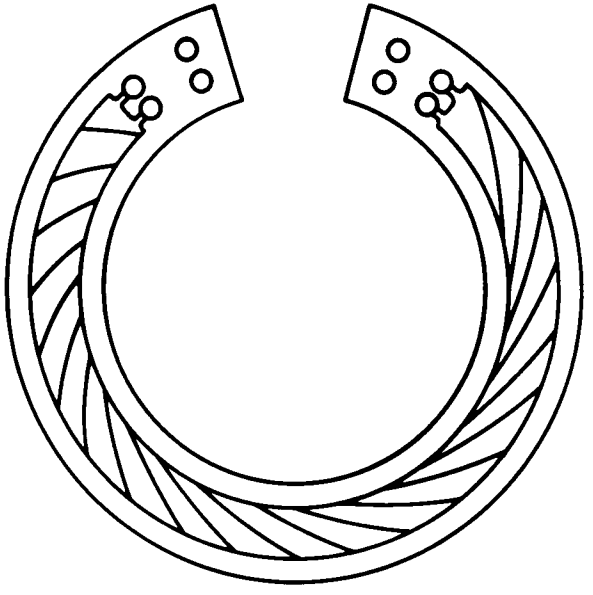

SPACER

Figure 40 Helical Stack M-48436

d. Spiral Stack

The spiral stack represents a novel approach to stack design. A preliminary sketch of this design concept is shown in Figure 41.

The electrode areas are not resolved, as it was decided that this design did not offer sufficient advantages to justify the intensive design work required to develop such a novel design.

The electrodes of a spiral stack are two concentric cylinders. The membranes and spacers spiral outward from inner electrode to outer electrode. Solutions are fed into the inner section, and product and concentrate outlets are located near the outer electrode shell. In this way a natural decrease in current density is achieved along the path from entrance to exit.

Two advantages of this design are the long natural path length and the inherent electrical safety feature offered by grounding the outer electrode. The solutions should flow outward from the inner electrode to obtain the natural decrease in current density as the path is traversed. A long path length is obtained in a relatively small volume with this design. The safety feature of this stack is readily apparent. The outer electrode can be grounded with the inner electrode receiving the total potential. The inner electrode is then safety-enclosed in the shell of the outer electrode.

These advantages do not seem to justify the development of such a stack at this time. First, a flexible spacer would be required and only flexible membranes could be used. Second, a way of manifolding the system would have to be found. Third, a method of scaling up this stack to commercial sizes without affecting path length would have to be determined. The expense and time required to resolve these problems, along with the marginal improvements in performance over other systems, were the major reasons for eliminating this concept from further consideration.

3. Plate-and-Frame Configuration

The plate-and-frame configuration was chosen for further study, based on evaluation of the four basic configurations. The next step in the design process was to determine the type of flow path to be used. Many variations of the flow path in a plate-and-frame design are possible, and some offer superior performance characteristics.

Consideration was given to the relative advantages and disadvantages of internal versus external manifolding. Figures 33 and 36 illustrate the differences. Slightly higher membrane utilization could be obtained by external manifolding. However, the possible sealing problems outweigh this advantage for a pilot-plant application. External manifolding was dropped from consideration because of the added sealing problem and because of the vulnerability of the ex-

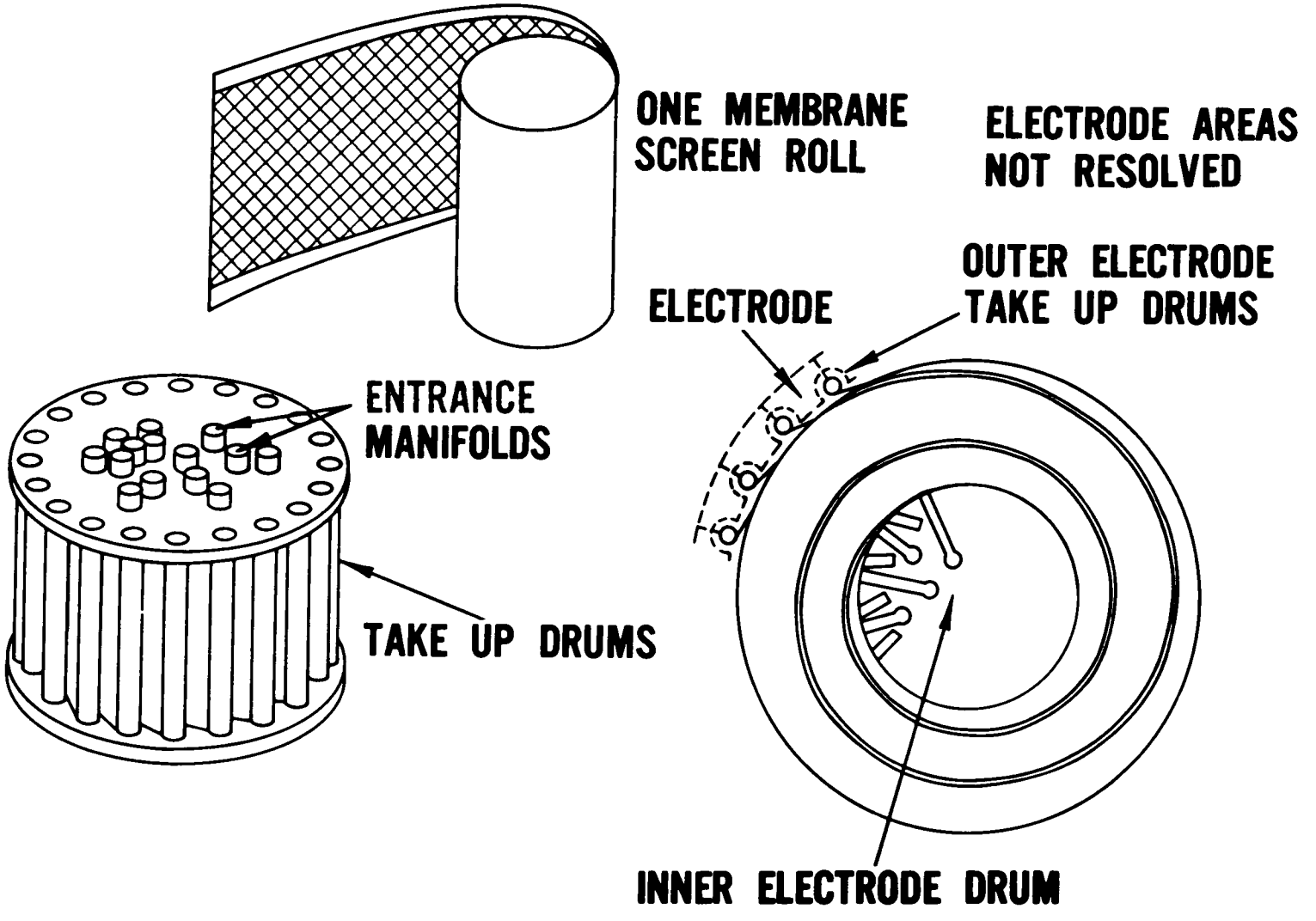

Figure 41 Spiral Immersed Stack M-48432

ternal manifolds to damage. In a commercial stack, however, external manifolding should be reevaluated since membrane utilization is potentially greater.

Several spacer-screen and spacer screen-stack geometries were studied. The design finally selected was the multiple-pass internally-manifolded linear-flow-path design shown in Figure 33 and at the left in Figure 43. The deciding factor in favor of this design was its superior operational flexibility. Its drawbacks are mainly due to the large number of inlets and exits. In a commercial design the number of inlets could be decreased, thus eliminating these drawbacks.

Two examples of torturous path designs are shown in Figures 34 and 35. This type of design allows a relatively long path to be incorporated in a given cell area. It could represent a possible flow-path design for a commercial stack, if it is demonstrated that long flow paths are necessary to good stack performance.

Figure 38 illustrates a cross-flow design. In this design, enriched streams flow in one direction, and depleted streams flow perpendicular to them. The only advantage is that the two streams are more fully separated at the manifold areas. Solution leakage paths between channels in the same spacer frame could easily develop in the multiple-pass cross-flow system. Pressure differentials could cause bulging of the membranes, since they are supported only at the cross-over points shown in the spacer-screen sketch.

Figures 42 and 43 show staggered stack configurations. The reason for considering these configurations is that they eliminate the direct manifold paths between the electrodes, and should therefore result in reduced current leakage. The disadvantage is, as in the case of the helical stack, a relatively-constant current-density profile. The prospective disadvantages of this current-density profile weighed heavily in the decision to discard this concept. The multiple-pass design could be assembled to approximate the staggered stack setup shown in Figure 42. Thus its performance could be determined with the multipass setup.

Figure 44 compares the multiple-pass spacer with a variable-width spacer. The variable-width spacer would produce a variation in solution velocity, thus changing boundary-layer characteristics along the path length. This design was seriously considered, but was finally dropped in favor of the multiple-pass design. The main reason for dropping this design was that the optimum channel width profile is not known. Extensive testing with the multiple-pass system could be used to determine such an optimum profile. Once an optimum velocity profile is determined, a spacer of variable path width capable of producing such a velocity profile could be designed.

When all the possible spacer configurations were evaluated it was decided that the multiple-pass spacer screen would be most advantageous for the pilot-plant design. At the same time, however, it is apparent that some of the other designs could offer improved performance over a narrower range of operating conditions, and could therefore represent excellent designs for a future commercial unit.

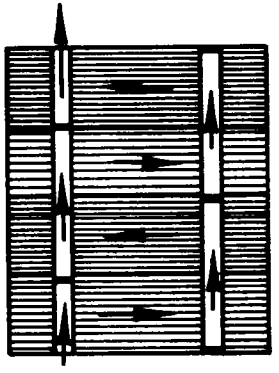

FLOW SCHEMATIC

4 PACKETS CONNECTED IN SERIES AS INDICATED, EACH PACKET COMPOSED OF 25 MEMBRANE PAIRS

SPACERS

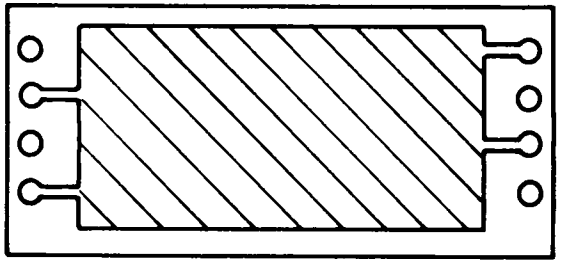

TYPE A

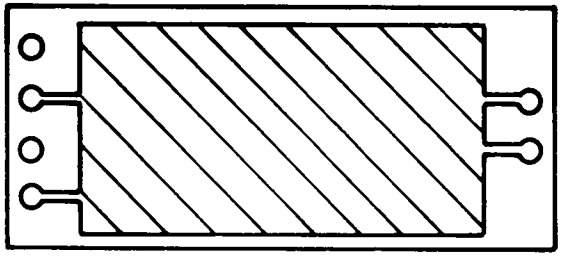

TYPE B

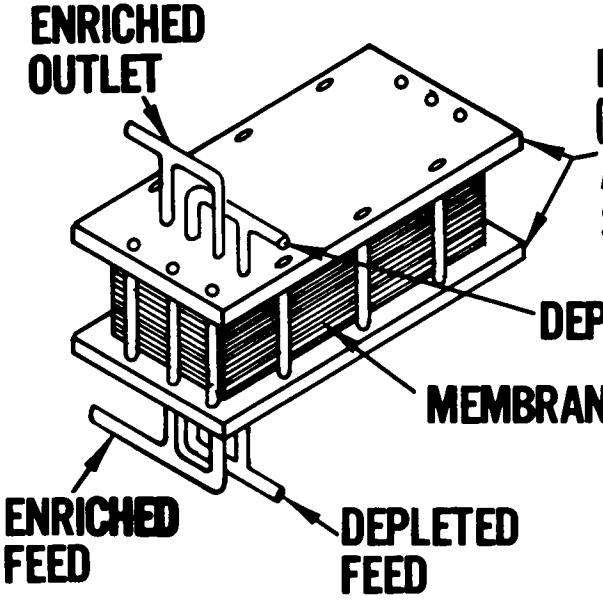

TYPE A FOR MEMBRANE PAIRS WITHIN A PACKET

TYPE B FOR USE BETWEEN PACKETS

Figure 42 Linear Stack Staggered M-48800

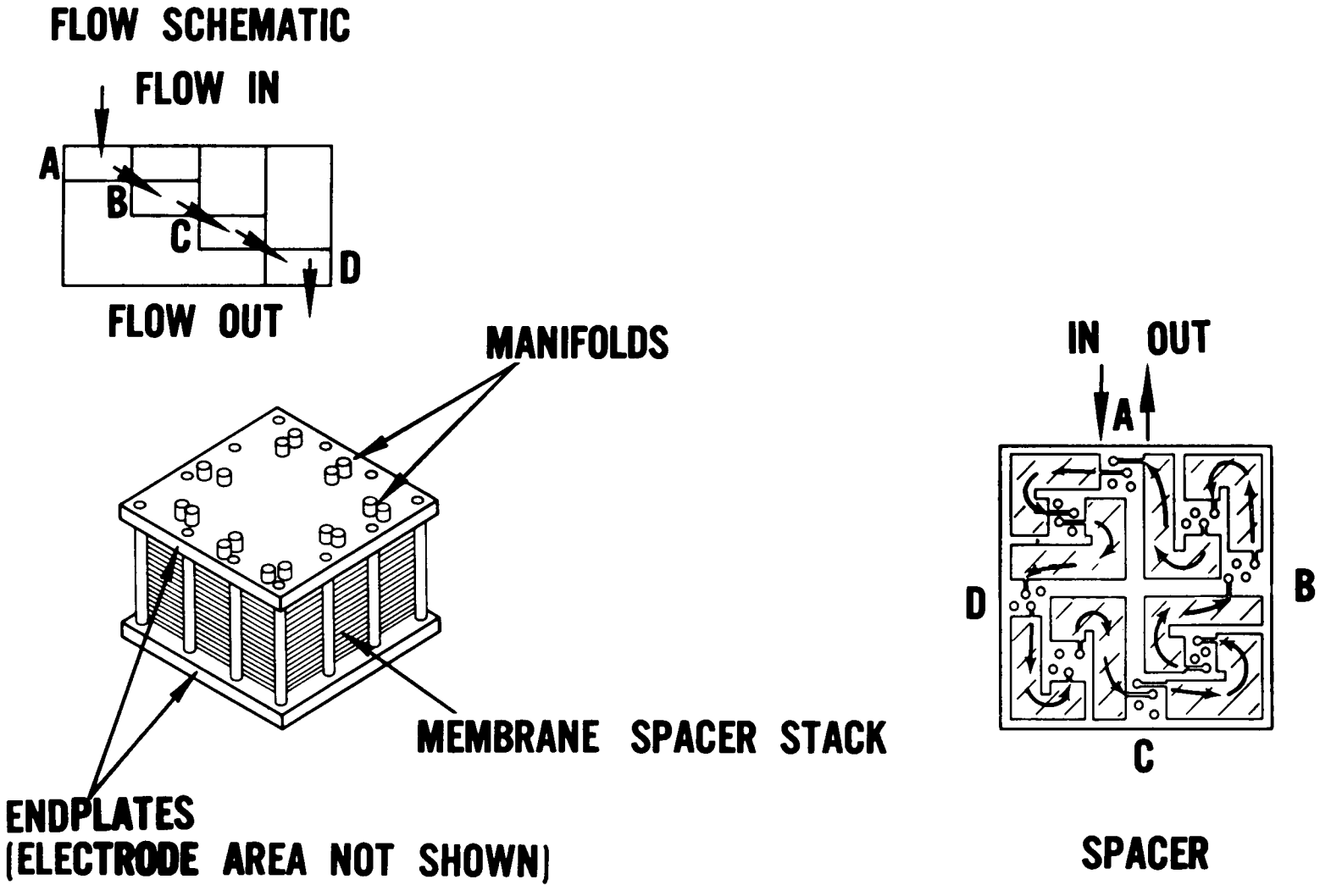

Figure 43 Square Stack Staggered M-48435

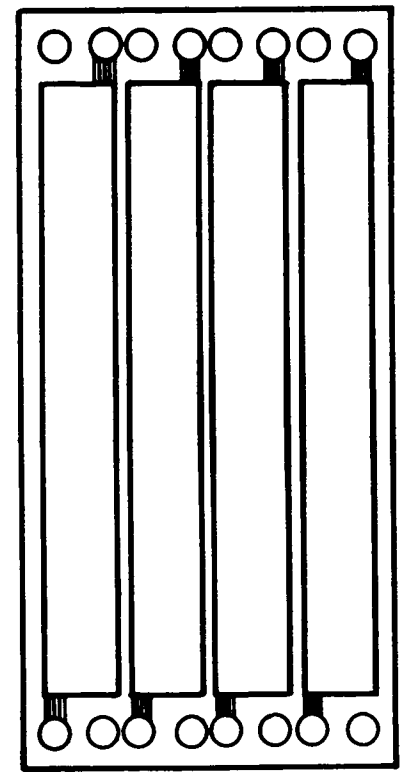

CONSTANT WIDTH
SEPARATE MANIFOLDS

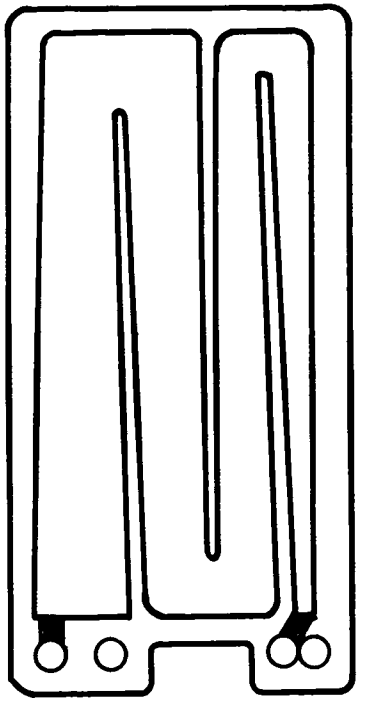

VARIABLE WIDTH
SINGLE CHANNEL

Figure 44 Typical Spacer Configurations M-48802

B. Final Design of Stack

The final design of the pilot-plant stack is a four-channel linear-flow-path plate-and-frame configuration. The design contains forty cell pairs with overall dimensions of 22 by 40 inches. Nominal membrane separation is 30 mils. The major geometric parameters and design-point performance estimates are shown in Table 3. Figure 45 shows the assembled stack and identifies the major components.

TABLE 3

Geometric and Design-Point Operating Parameters of Pilot-Plant Stack

Geometric Parameters

spacer-screen size	22 x 40 inches
number of channels	4
path length per channel	33.5 inches
total path length (series connections)	134 inches
channel depth	30 mils
channel width	4.5 inches
number of cell pairs in stack	40
manifold diameter	2.0 inches
channel inlet and exit tube inside dimensions	0.01 x 0.08 inch
channel inlet and exit tube length	0.5 inch
number of tubes per inlet	12
membrane utilization	68.5 %
endplate thickness	3 inches
number of clamping bars	12
clamping bar height	6.0 inches
clamping bar width	3.0 inches

Design-Point Operating Parameters

plant capacity	10,000 gpd
feed solution	3000 ppm NaCl
product solution	500 ppm NaCl
current density	23 ma/cm^2
total current	89.5 amps
estimated voltage	105 volts
estimated manifold leakage	2.3%
open channel flow velocity	4.95 inches/sec
stack pressure drop (series channel connections)	24 psi

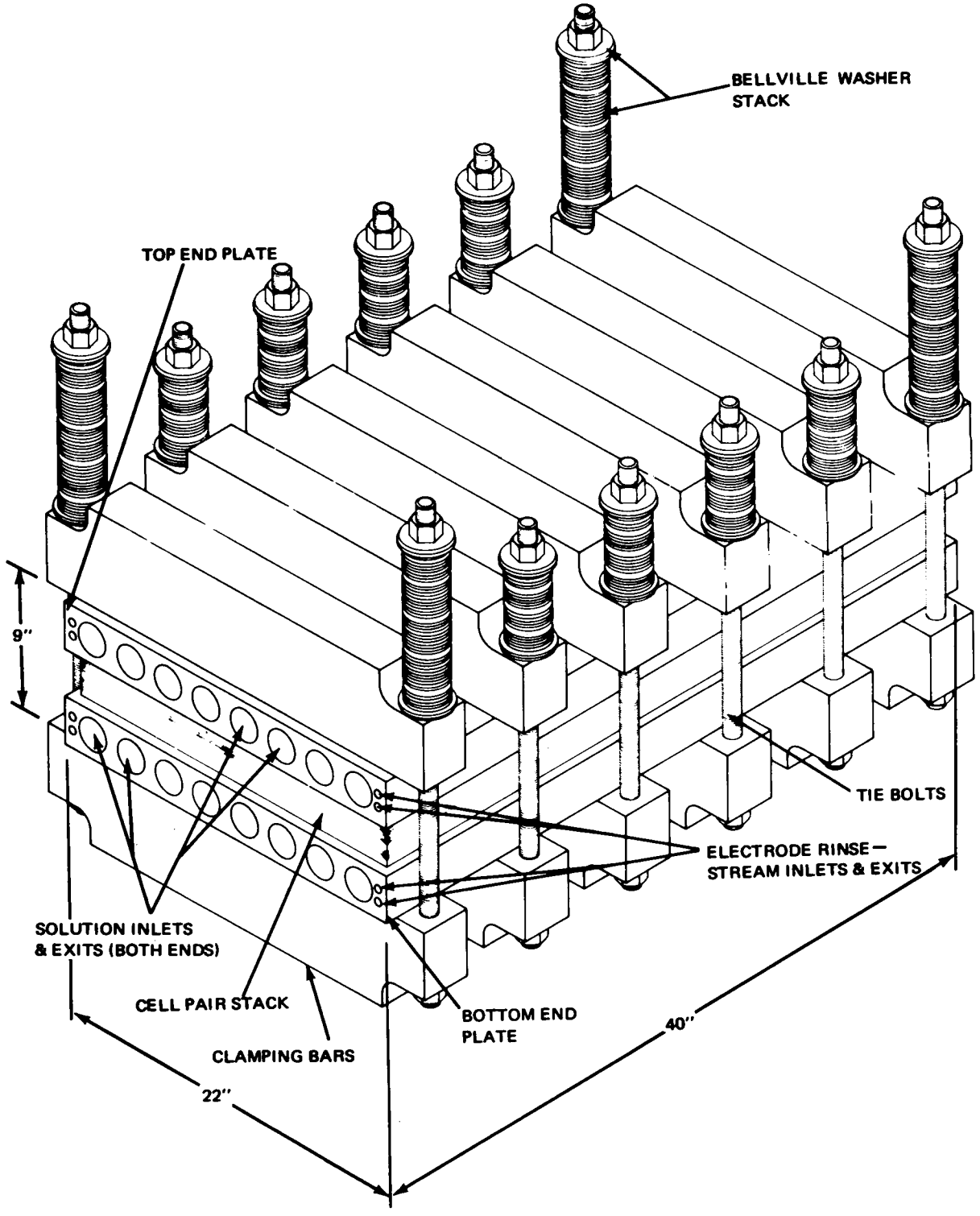

Figure 45 Assembled Pilot-Plant Stack

Each cell pair contains four independent solution channels with separate manifolding. Thus the forty-cell-pair stack actually consists of four independent single-channel stacks, each with its own set of electrodes and electrode-rinse streams. This arrangement provides great flexibility of operation and should permit the evaluation of the transport-depletion process over a wide range of operating parameters.

At the selected design point, the stack is capable of producing 10, 000 gpd of 500 ppm product water, from a 3000 ppm NaCl feed solution, using a current density between 20 and 25 ma/cm^2. This design point is based on a channnel velocity of 4.95 inches/sec with the four-channel stacks hydraulically connected in series. With the channel stacks connected in parallel, a 40,000 gpd flow rate is possible at the same solution channel velocity and a lower cut. Higher velocities, higher current densities, and series-parallel channel connnections are possible, and permit operation over a significant range of variables.

The review of transport-depletion process and performance data, discussed in Sections III. and IV., led to the decision to design the pilot-plant stack with an overall path length capability of between 100 and 200 inches, and a membrane spacing (channel depth) of 20 to 35 mils. A membrane spacing of 30 mils was selected after consultation with potential vendors and considering fabrication requirements. This spacing appears to be the thinnest practical size to fabricate and handle with reasonable success at this time. Further development could permit the fabrication of thinner spacers.

The overall cell pair dimensions of 22 x 40 inches were selected as a result of a survey of available membrane sizes. It is highly desirable that the stack permit the use of several different cation and neutral membranes. Table 4 is a summary of membrane data which shows the available sizes of several commercially available membranes. The final choice of stack dimensions, 22 x 40 inche is large enough to produce data applicable to a larger commercial-size stack, and also permits the use of two of the three neutral membranes and four of the five cation membranes listed in the table.

The selection of four channels represents a realistic trade-off between pressure loss and path length. Each of these parameters increases with increasing number of channels. Four channels in a 22 x 40-inch spacer permits operation at path lengths of 33.5, 67, 100.5, and 134 inches, by appropriate external manifold connections. Figure 46 schematically shows the external stack connections for these path lengths.

Prior to the selection of the final 40-cell-pair 22 by 40-inch design, a 37-cell-pair 19 by 58-inch stack with four channels was designed. Working drawings for this design were prepared. The maximum path length of 210 inches and increased stack length of 58 inches would have provided more realistic operational experience and data useful for scaling up the process to commercial-size designs. This design was finally rejected because it would have permitted the use of only one or two commercially-available cation membranes.

A description of the major components of the pilot-plant stack follows.

TABLE 4

Membrane Data Summary

Neutral Membranes

Vendor	Material	Max. Width, Inches	Comments
A. H. Thomas	regenerated cellulose	9	used as neutral membranes for the majority of SRI experiments
Union Carbide	regenerated cellulose, Zephyr Z	22	Wider sheets can be made by making a ½ inch overlap joint. This joint has a 10-20% bond and is twice the thickness of the base material.
DuPont	cellophane	46	very poor transport and structural properties

Electrodialysis Membranes

Vendor	Length, inches	Width, inches	Comments
Ionics	40	36	reinforced
Asahi Chemical	44	44	structurally weaker than reinforced membranes
Asahi Glass	25	25	no T. D. performance data
AMF	roll	44	no T. D. performance data
Ionac	120	40	anion membrane easily fouled

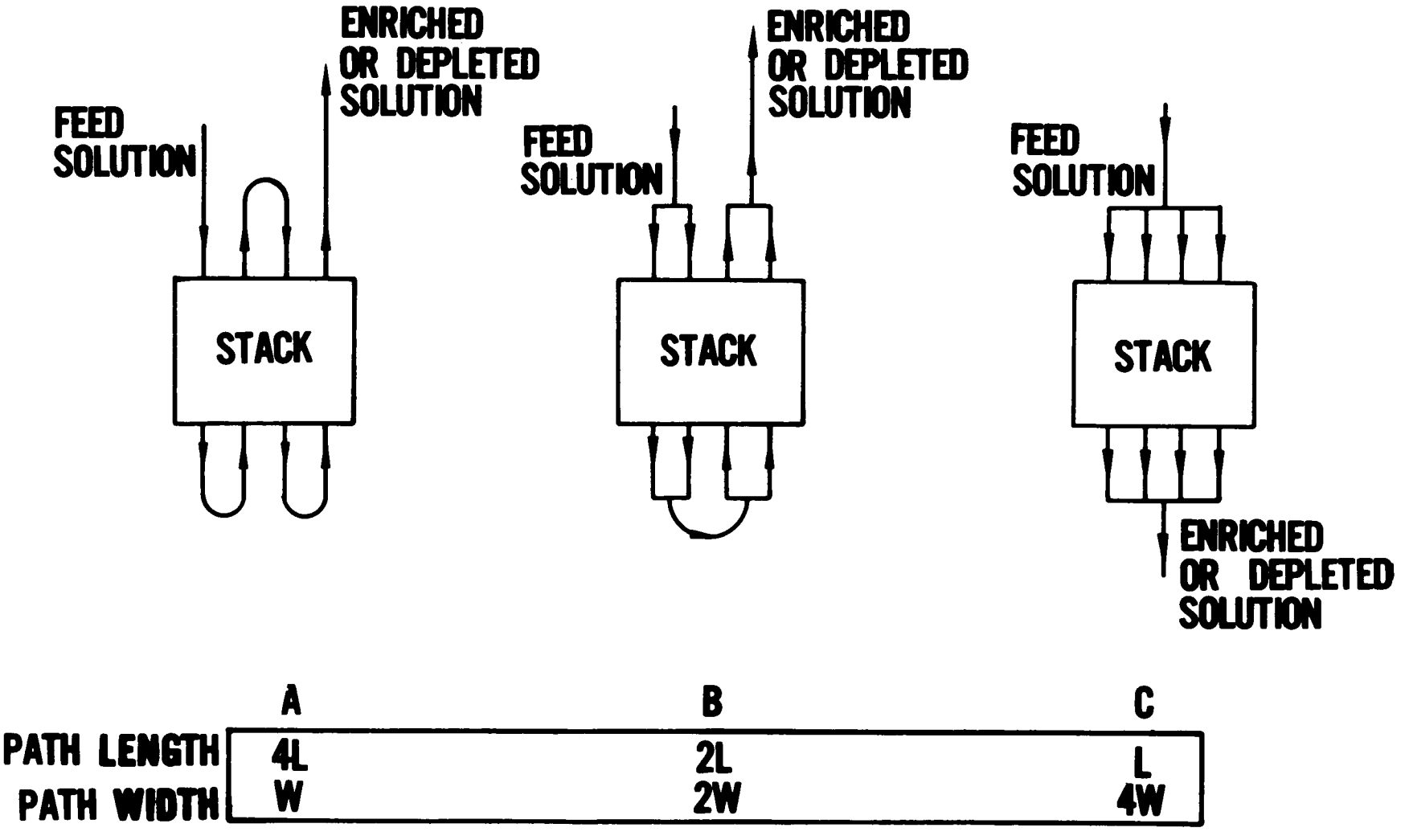

Figure 46 Alternate Stack Flow Arrangements M-42834

1. Spacer-Screen Assembly

The spacer-screen assembly is the heart of the transport-depletion stack. The spacer maintains uniform membrane separation and defines the solution flow paths. The integral turbulence-promotion screen supports the membranes and minimizes concentration polarization at the membrane surfaces. Figure 47 illustrates the plan form of the assembly. Each spacer screen contains two sets of manifolds, one for the concentrate streams and one for the dilute. Each spacer-screen assembly is rotationally symmetrical and may be used as either a dilute or concentrate compartment depending upon its orientation.

The solution inlet and exit configuration between the manifold holes and the solution channels is shown in Figure 48. This configuration consists of a spacer comb placed between the two outer frame sheets. The many teeth of the comb provide proper spacing and support to the outer frame sheets, while the slots between the comb teeth form rectangular solution flow tubes. This configuration prevents intercompartmental leakage by providing continuous support to both membranes. It limits electrical leakage through the manifolds while causing minimum flow resistance. Tests performed on open-groove inlet configurations showed a tendency for the membranes to flow into the inlet groove under the influence of the sealing forces, if the membrane were not fully supported in the inlet area. Several other inlet configurations considered for the design are shown in Figure 49.

The inlet area was made as large as possible under the restrictions imposed by structural integrity considerations. Evaluation of the hydrodynamic versus electrical performance trade-offs resulted in the conclusion that in a forty-cell-pair multiple-pass pilot-plant stack, pressure losses are a more serious problem then electrical leakage. A 0.5-inch minimum inlet length was chosen to assure good sealing at the inlet. Calculations show that electrical leakage is not unreasonably large at even the largest inlet areas that can be produced without seriously affecting the structural integrity of the inlets.

Figure 48 also shows the basic three-layer construction of the spacer frame and the method of attaching the turbulator screen to the spacer. The spacer frame is made of three 10-mil epoxy-impregnated Fiberglas sheets cemented together with an epoxy adhesive that is catalytically cured at room temperature. The epoxy-glass material used is a Panelyte grade 161, NEMA grade G-10 sheet stock, manufactured by Thiokol Chemical Corporation. Other similar materials could be used. The Vexar 15-PDS-129 polypropylene turbulator screen is integrally-bonded between the two outer frame sheets along the edges of the solution channels. This is accomplished by mechanically coining the edge of the screen to a thickness which fits into a groove formed by cutting back the center frame sheet along the edges of the solution channels.

2. Electrodes

There are eight electrodes in the stack. Each of the four channels has its own anode and cathode. All eight electrodes are made of 40-mil titanium sheet with a 1 to 2 mil mech-

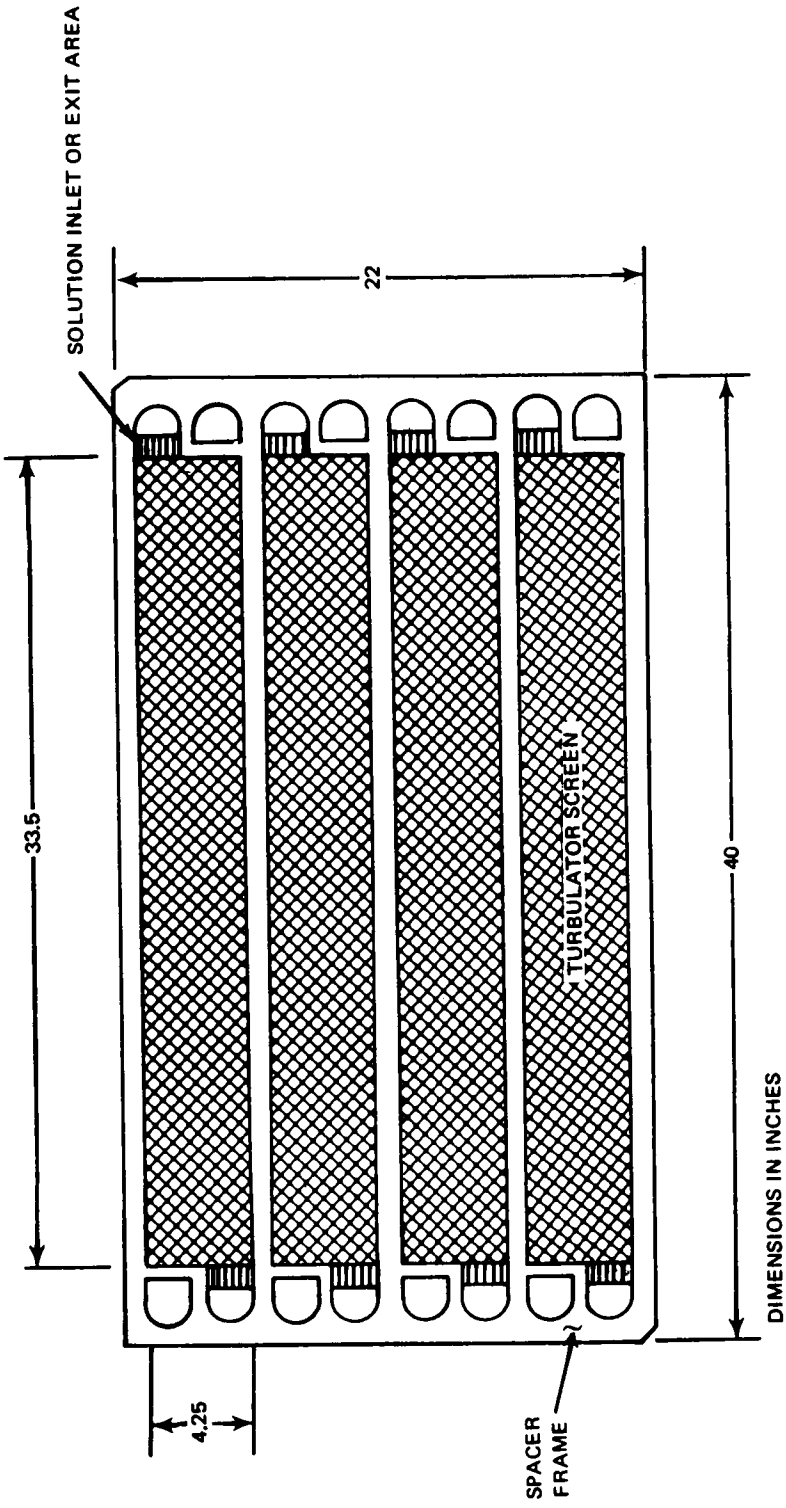

Figure 47 Plan View of Spacer Screen

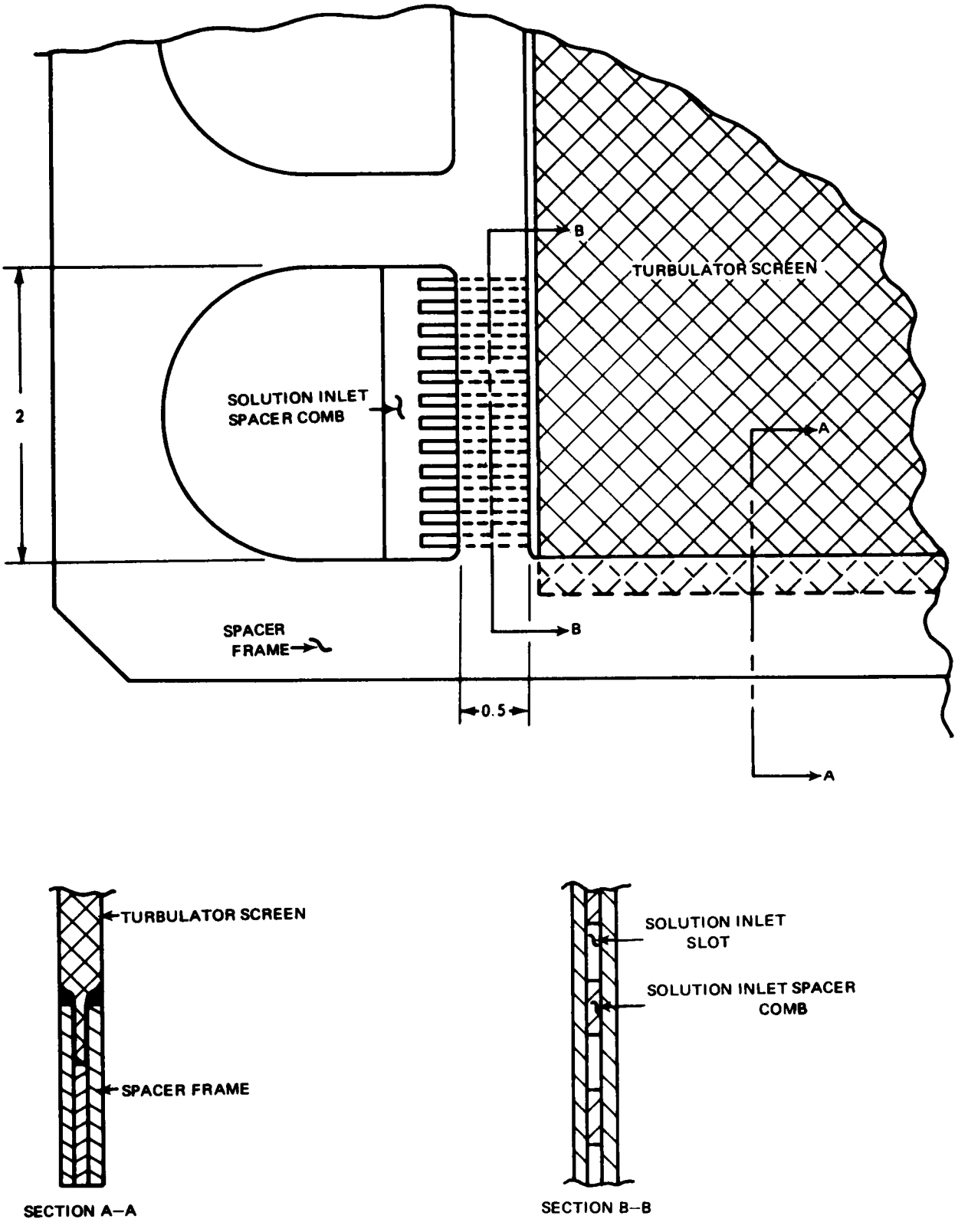

Figure 48 Details of Pilot-Plant Spacer Screen

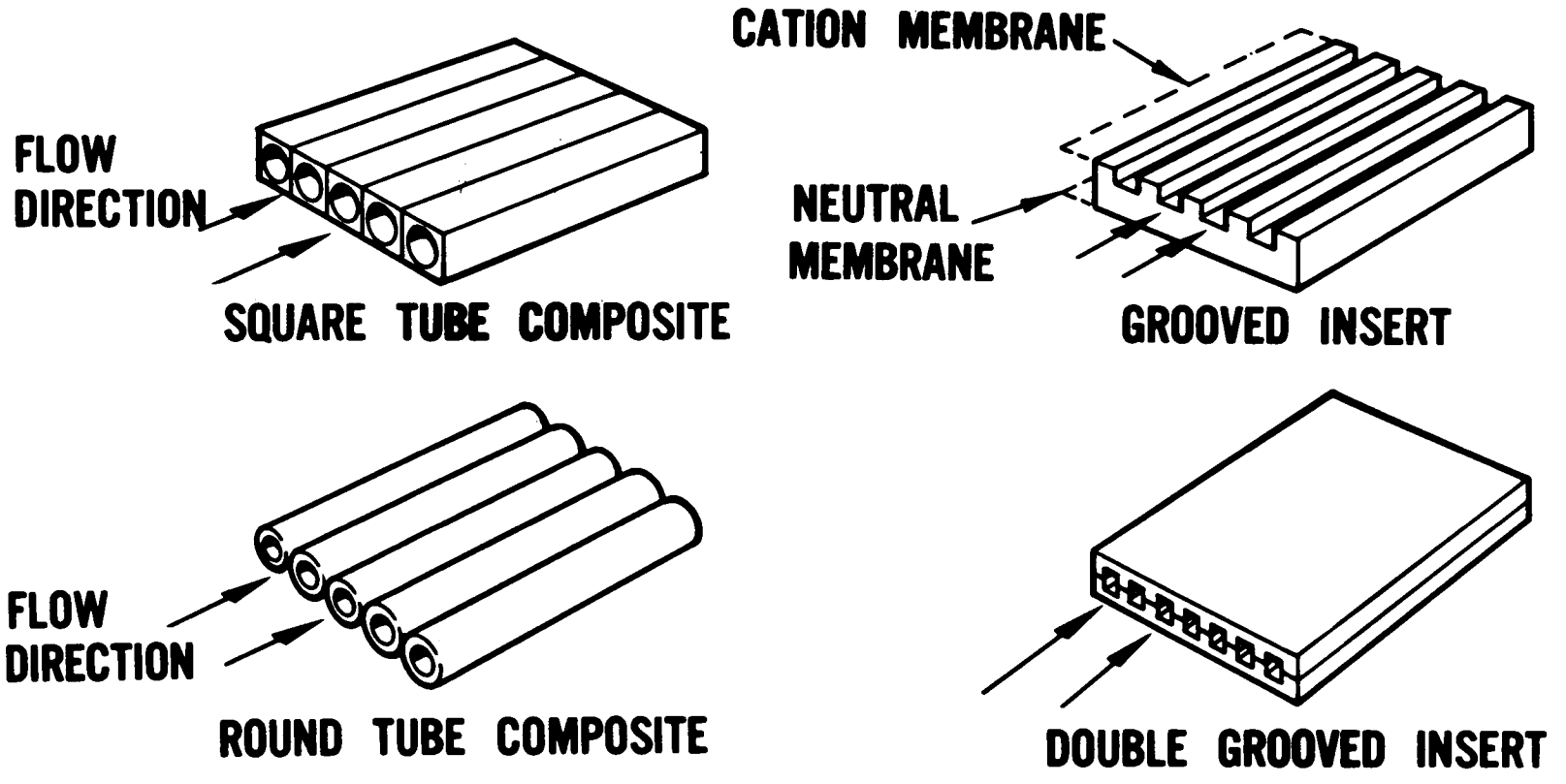

Figure 49 Channel Inlet Configurations M-48801

anically-bonded platinum surface on the solution side of the electrode. Englehard Industries series 5000 platinum coating was used and should provide long service life.

Platinized titanium was chosen for several reasons. Very low electrode over-potentials can be expected using a platinum electrode surface. The titanium provides a conductive backing for the platinum and is protected from corrosion by the natural protective oxide coating of titanium. Identical cathode and anode materials permit the operation of the stack with reversed current.

Electrical connections are made to the electrodes through a threaded titanium stud which is welded perpendicular to the back side of the titanium sheet. This stud passes through a hole in the endplate and protrudes from the outer side of the endplate.

3. Endplates

The endplates serve several important functions. They form a base for the semi-rigid clamping arrangement and permit the application of a uniform sealing pressure to the cell-pair stack. They provide external connections to the stack manifolding. They serve as a backing onto which the electrodes are bonded. They contain the electrode rinse stream manifolds and provide for visual inspection of the internal stack manifolding.

The endplates are fabricated from slabs of Westinghouse Micarta grade 221, three inches thick. This is a cotton-cloth-base phenolic material which fulfills all requirements necessary for successful performance of this component. Deterioration in a water or brine environment should be minimal since slabs of this material of a thickness of three inches are very impervious to water. Micarta is an excellent insulator and is relatively easy to machine. Machinability is important to permit the detailed maching operations required in fabricating this component.

All external connections to the concentrate and dilute stream manifolds are located on the ends of the endplate assembly. This design allows the clamping bars to be placed directly over the sealing surfaces of the solution-stream entrances and exits. Inspection holes are provided which allow direct visual inspection of the solution manifolds during the final stages of the stack assembly operation. These inspection holes are sealed with specially-designed plugs containing O-ring seals. The plugs are held in place by the outer clamping bars which apply the sealing load to the solution-stream inlets and outlets.

The electrode rinse stream manifolds are also contained in the endplates. Separate manifolds are used for each of the four channels. Holes evenly distributed across the width of the flowpath at the ends of the channels provide good flow distribution in the electrode compartments. The electrodes are bonded into recesses machined in the endplates to form a nominally flush surface with the sealing surface of the endplate. Eccobond 55 with catalyst 9, manufactured by Emmerson Cummings, Inc. was used for the bonding agent. The actual electrode rinse stream compartments are formed by 30-mil thick spacer-screen assemblies modified to eliminate the solution inlets and exits to the channels. These modified spacer-screen assemblies are sealed to the endplate sealing surfaces with a rubber gasket.

4. Clamping Arrangement and Stack Support

A semi-rigid arrangement of clamping bars and tie bolts was selected as the method of providing the sealing load to the stack. Six sets of independent clamp bars and tie rods are placed across the width (22 inches) of the stack. Each clamp bar is fabricated of 3 x 6-inch steel bar stock with a 24-inch center-to-center distance between tie rods. The tie rods consist of 1 inch x 8 NC threaded 100 KSI steel rods.

The clamp bars are larger than would be required in a commercial design because of the more severe sealing problems associated with the pilot-plant stack. First, relatively high solution pressures are needed to traverse the large number of inlets and exits associated with the use of four separate channels. Second, the high solution pressure combined with separate channels requires a rigid clamping arrangement to prevent intercompartmental leakage across the internal sealing surfaces between the channels. The dimensions of the tie bar were chosen so that the overall deflection at any sealing surface in the stack would be less than 0.005 inch when the internal solution pressure is 50 psi and the stack sealing pressure is 750 psi. This calculated deflection includes the deflection of the endplate in the 4.3-inch span between the clamp bars.

The semi-rigid clamping arrangement was selected after careful consideration of several alternate methods, including a one-piece egg-crate type design. The egg crate could either be cast in one piece or could be a welded and machined assembly. It was felt that the selected arrangement would offer more flexibility, should unanticipated sealing problems develop during pilot-plant operation. A commercial design would use a lighter and more sophisticated clamping arrangement.

The sealing force exerted by the clamp bars is measured by observing the deflection of an arrangement of Bellville spring washers placed at one end of each tie bolt. The selected Bellville washer is No. B2500-120 from Associated Spring. Its dimensions are 2.5 inches outside diameter, 1.25 inches inside diameter, 0.12 inch thick, and 0.18 inch uncompressed height. Each washer has a spring rate of 53,000 lb/inch and a load at maximum compression of 3200 lb. By assembling these washers in various series and parallel combinations, many combinations of spring rates and load capabilities of the washer stack are possible. To achieve a reasonable deflection at a 750 per sealing load, a stack of 80 washers (10 in series, 8 in parallel) are used on the four end tie bolts, and a 40 washer stack (10 in series, 4 in parallel) are used on the other eight tie bolts. The measured load on the clamp bar can be directly converted into the sealing pressure on the stack.

The assembled stack is supported in a horizontal position on a transportation stand equipped with casters. The horizontal position permits solution flow in either direction without the risk of becoming air bound. The anticipated high solution velocities should be sufficient to remove any air during startup. The movable support stand permits easy transport of the stack between the assembly area and the pilot-plant test system.

C. Stack Construction

This section describes the fabrication of the spacer-screen assemblies, the endplate subassemblies the preparation of the membranes and the final assembly of the stack.

1. Spacer-Screen Fabrication

Figure 50 shows a completed spacer-screen assembly. The spacer frame of this assembly is a sandwich layup of three 10-mil epoxy-glass sheets, bonded together using Eccobond No. 55 epoxy adhesive with room temperature curing catalyst No. 9. The turbulator screen is Vexar 15-PDS-129 polypropylene plastic netting which is mechanically bonded to the spacer frame.

The complete spacer screen assembly consists of fifteen separate components.

1) Two A-frames (SKN 44715) make up the outer layers of the three-layer spacer-frame sandwich.

2) One B-frame (SKN 44716), similar to the A-frame is used for the center layer of the three-layer spacer-frame sandwich.

3) Eight solution inlet spacer combs (SKN 44651) form the solution inlet and exit ports between the channels and the manifolds. These are shown installed in a completed spacer-screen assembly in Figure 51.

4) Four turbulator screens (SKN 46491) are required for each of the four channels in the spacer frame. These turbulator screens are mechanically coined along their long edges to a thickness less than 10 mils, to fit between the two B-frames along the edges of the channels.

Prior to the assembly of the complete spacer screen all necessary components were prepared. Special tooling was developed and fabricated to locate and cut out the manifold holes and the inlet areas for the solution inlet combs. All surfaces of the A and B-frames and the solution inlet combs to be bonded were abraded with No. 80 grit emery paper. The edges of the turbulator screens were mechanically coined using a specially-developed tool in a hydraulic press. Before assembly, all necessary parts were degreased, checked for proper fit, and laid out on clean plastic sheets.

The final assembly of the spacer screen started with the preparation of the epoxy adhesive. Epoxy was first applied with a roller to the bottom A-frame. This A-frame was then placed on a clean sheet of plastic which was in turn placed on a clean smooth and flat polyvinylchloride plate. The plastic sheet served as a parting agent for the epoxy adhesive. The B-frame was then positioned on the A-frame, airpockets were removed, and the surface was checked for irregularities. Excess epoxy was removed from the inlet areas and the solution inlet combs were installed. These solution inlet combs were bonded at their edges only to prevent epoxy

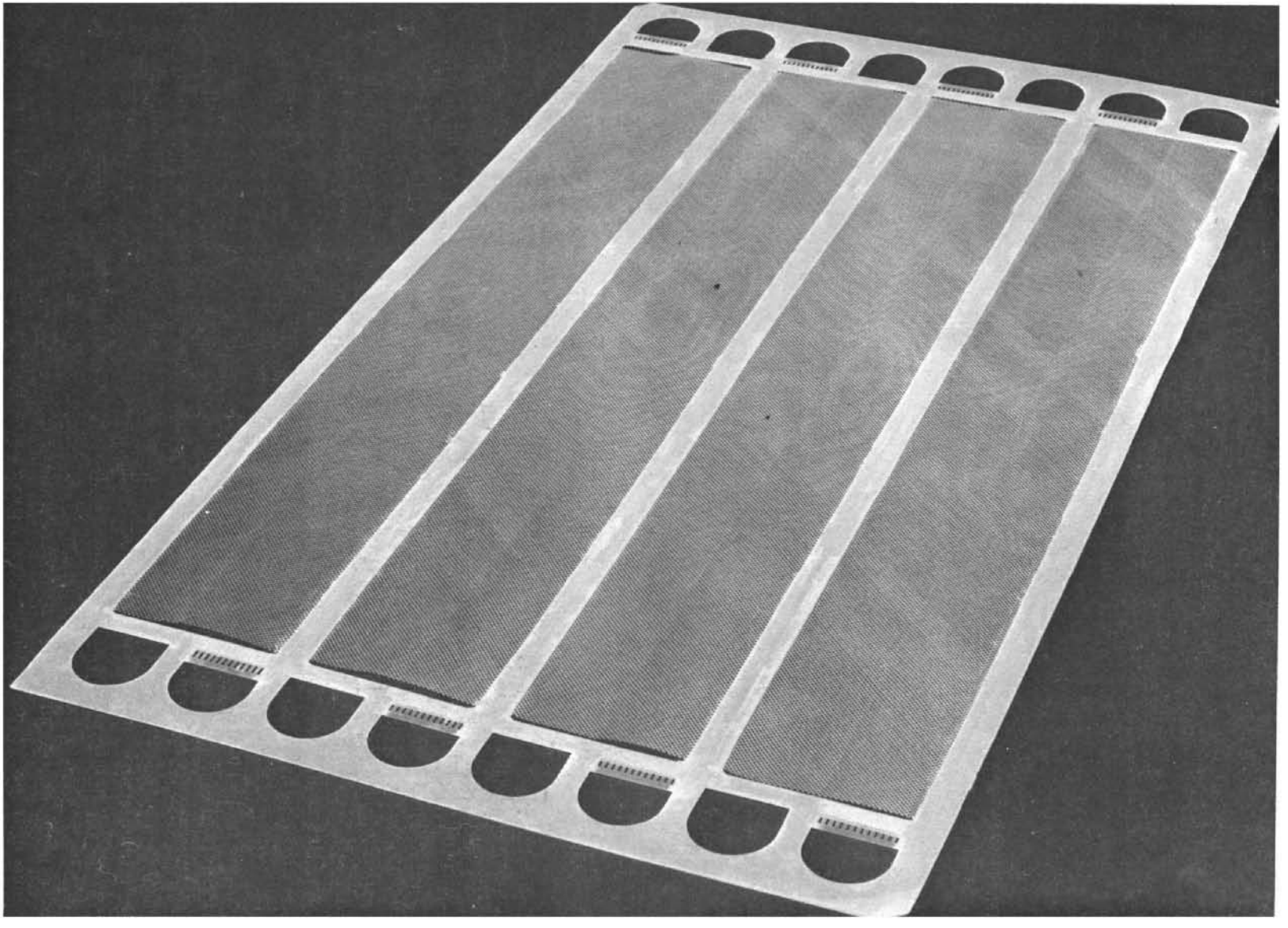

Figure 50 Pilot-Plant Spacer-Screen Assembly WO-21

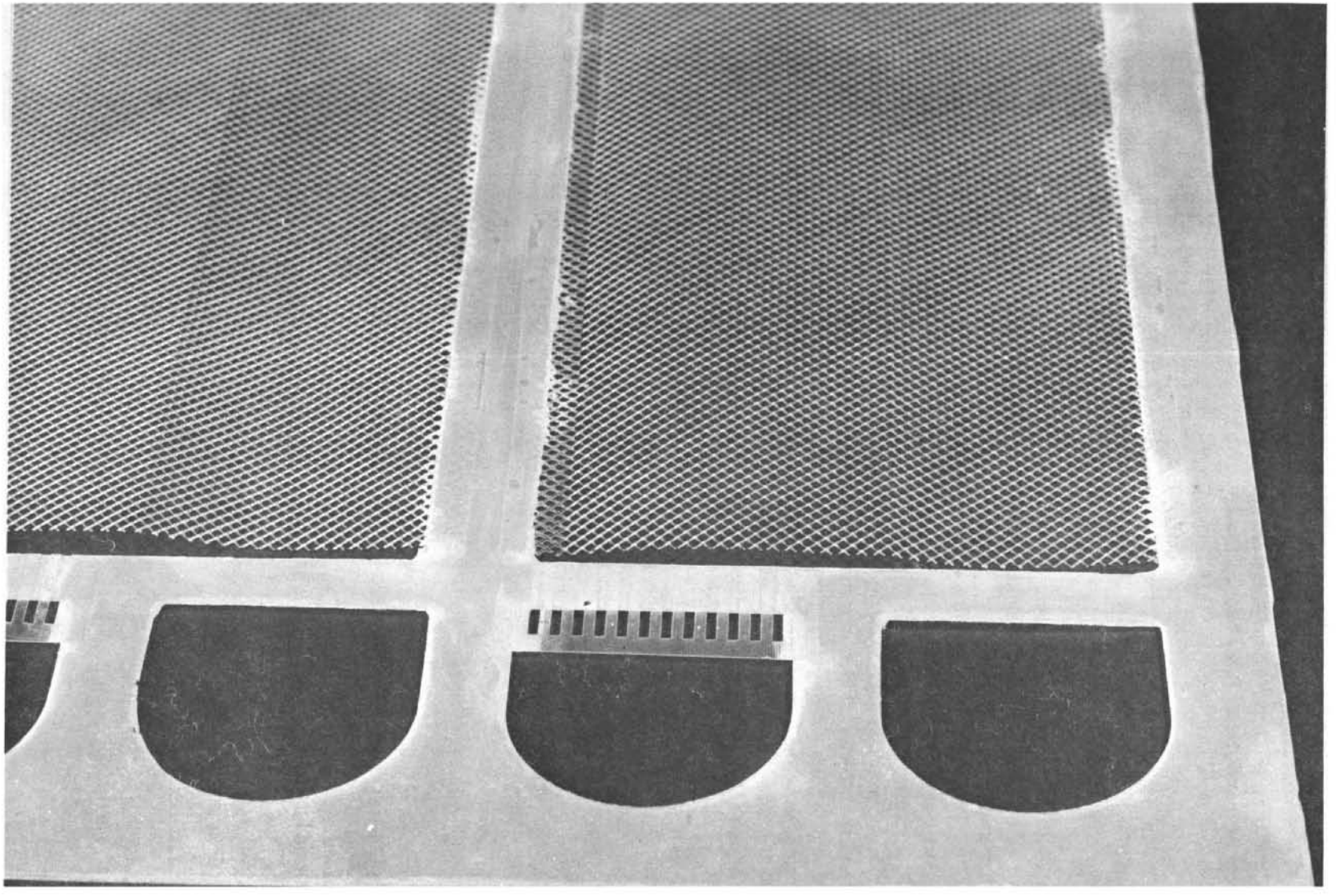

Figure 51 Manifold Details of Pilot-Plant Spacer Screen WO-23

from blocking the solution ports. The four turbulator screens were then positioned in the channels. A bead of epoxy was placed along the coined edge of the screen with a hypodermic needle and syringe. This epoxy bead was smoothed into the coined edge. Epoxy was next rolled onto the top A-frame and positioned on the B-frame. As before, air pockets were removed and the surface checked for irregularities. A clean sheet of plastic followed by a flat smooth PVC plate was squarely positioned on the assembly.

Pressure was applied with 300 lb of weight distributed over the top PVC plate. The assemblies were then allowed to cure for 24 hours at room temperature before final clean-up, inspection, and serial numbering.

The rinse-stream spacer screens were fabricated in the same manner except that no solution inlets or exits were included. Special B-frames were fabricated without cutouts for the solution inlet combs.

Four instrumented spacer-screen assemblies were constructed similar to the regular spacer-screen assemblies, but with the addition of voltage-measurement probes. Two voltage probes were installed in each channel and located as shown in Figure 52. Special A and B-frames were prepared which included external tabs for each probe. The 8-mil platinum wire probes were placed in slots cut in the B-frame and potted in place with epoxy adhesive. Electrical connections were made by soldering No. 18 silver wire to the probe in the area of the tabs.

2. Endplate Subassembly

Each endplate subassembly consisted of an endplate, four electrode assemblies, an electrode-rinse gasket and a rinse-stream spacer screen. The electrode assemblies were bonded into recesses in the endplates using Eccobond No. 55 epoxy adhesive with room temperature curing catalyst No. 9. Figure 53 shows the two endplates with some of the electrode assemblies installed. Two of the electrode assemblies in this figure are drawn backside up to show details of the electrode studs. These studs protrude through holes from the back side of the endplate.

The rinse-stream spacer screen was then installed. A neoprene gasket was used between the endplate and the spacer screen to fill surface irregularities in the endplate and assure a good rinse-stream seal. A gasket 60 mils thick was used in the five-cell-pair stack and a gasket 15 mils thick in the final forty-cell-pair stack. The change to the 15-mil thick gasket was made because excessive gasket extrusion was observed during the teardown of the five-cell-pair stack. The extruded gasket had partially blocked some of the rinse-stream inlet and exit ports. It was anticipated that the thinner gasket would reduce extrusion. The gasket material was bonded to both the endplate and the rinse-stream spacer screen with contact cement in both the five-cell-pair and the forty-cell-pair stacks.

3. Membrane Preparation

Both the Ionac MC-3142 cation membrane and the Union Carbide Zephyr Z neutral membranes were initially rough-cut to approximate dimensions while dry. The membranes were

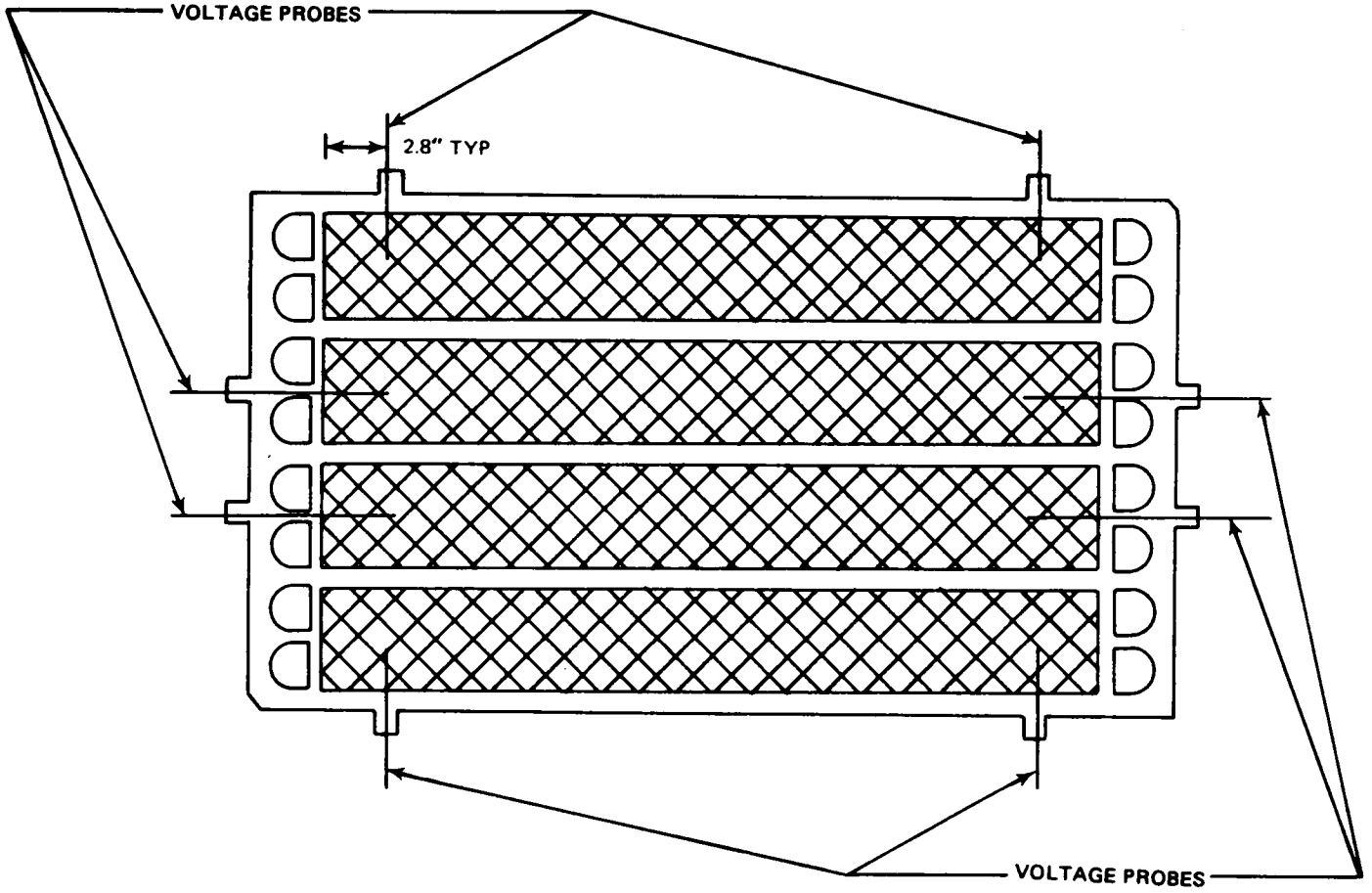

Figure 52 Probe Locations on Instrumented Spacer Screen

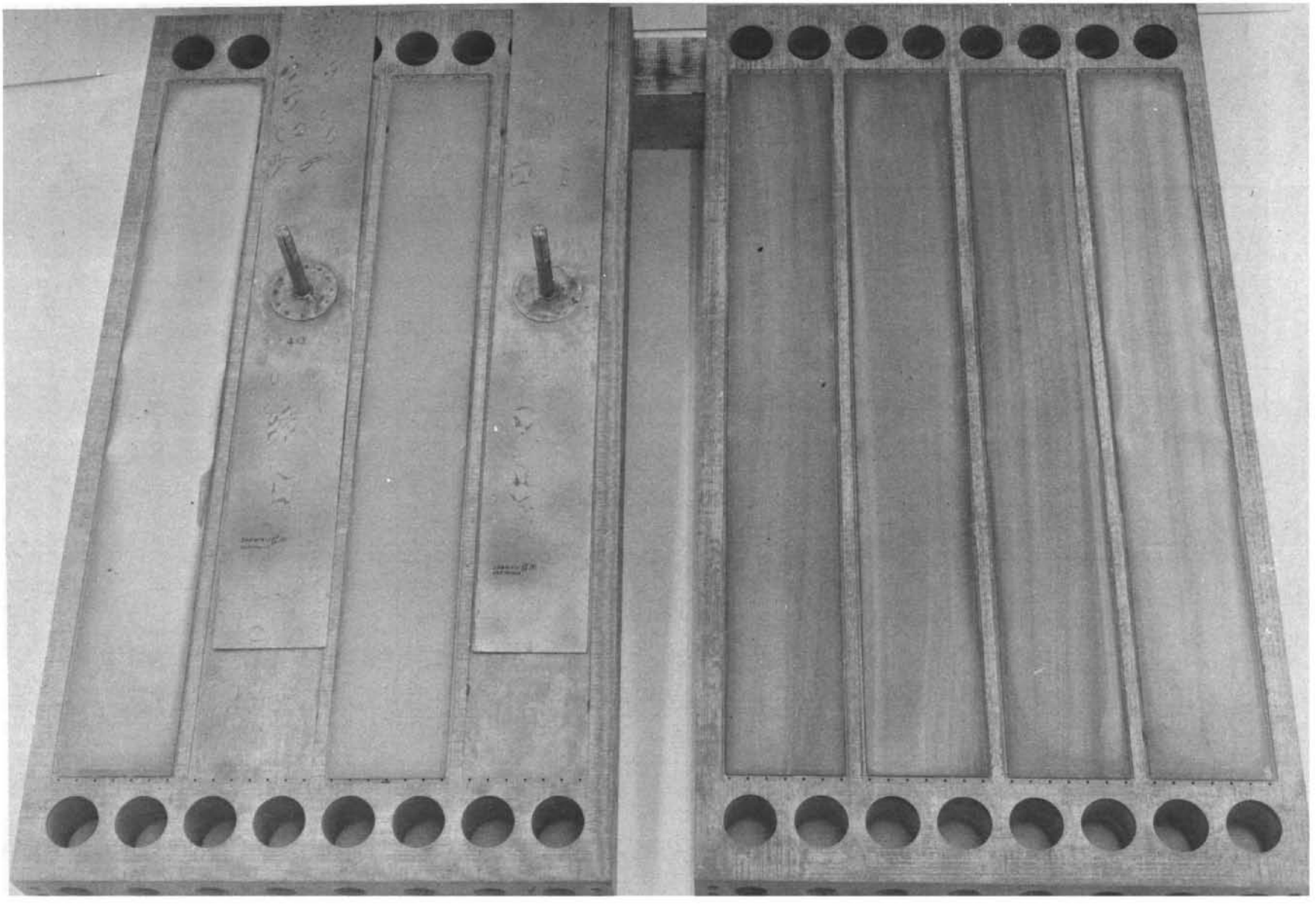

Figure 53 Endplate Assemblies of Pilot-Plant Stack AP-5664

then equilibrated in 3000 ppm NaCl solution for at least twenty-four hours before final cutting. All final cutting was accomplished while the membranes were wet and the membranes were kept wet until final stack assembly.

For the five-cell-pair stack, the membranes were finish-cut while in the salt solution. For the forty-cell-pair stack it was found that the membranes could be removed from the soak tank and finish-cut much faster and easier without drying out. After cutting to final size, the membranes were returned to the salt solution and stored until stack assembly.

4. Stack Assembly

The assembly of the cell-pair stack with the two endplates was accomplished in an assembly tank which was filled with a 3000 ppm NaCl solution to prevent the membranes from drying out. This assembly was then removed from the assembly tank, and positioned on the transportation stand where the clamp bars and associated hardware were installed and tightened up to seal the stack.

The first assembly step was to position the lower endplate subassembly, with inspection plugs installed, in the assembly tank on supports which protect the electrode studs from damage. Four alignment pins were then placed in specific manifold holes (two in each end) in the endplate sub-assembly. The alignment pins have a D-shaped cross section and were oriented to clear the solution inlet combs in the spacer screens.

The cell-pair stackup was initiated with a cation membrane placed over the alignment pins onto the rinse-stream spacer screen. Stackup continued with a spacer-screen assembly, a neutral membrane, and another spacer-screen assembly. Each suceeding spacer screen was reversed so that the first spacer screen became an enriching compartment, the second became a depleting compartment, etc., until the required number of cell pairs was achieved. Likewise, the membranes were alternated between cation and neutral membranes, with a cation membrane always following an enriching spacer screen, and a neutral membrane always following a depleting spacer screen. The specific membrane and spacer arrangements are shown schematically for the five-cell-pair and forty-cell-pair stacks in Figures 54 and 55, respectively. No instrumented spacer screens were used in the five-cell-pair stack. The four instrumented spacer screens installed in the forty-cell-pair stack were used as the 4th, 12th, 28th, and 36th enriching compartments, respectively. When the required number of cell pairs had been installed, a final cation membrane was added and the upper endplate subassembly was placed in position.

The five-cell-pair stack used a total of five neutral membranes, six cation membranes and 10 spacer-screen assemblies. The forty-cell-pair stack used forty neutral membranes, forty-one cation membranes, and eighty spacer-screen assemblies, four of which were instrumented.

Upon completion of the cell-pair stackup, the assembly was lifted out of the assembly tank and positioned on the lower clamp bars which had previously been positioned on the transportation stand. The four center upper clamp bars were then installed with tie bolts, guide washers, Belleville washers, and nuts and tightened to apply a light sealing load to the stack.

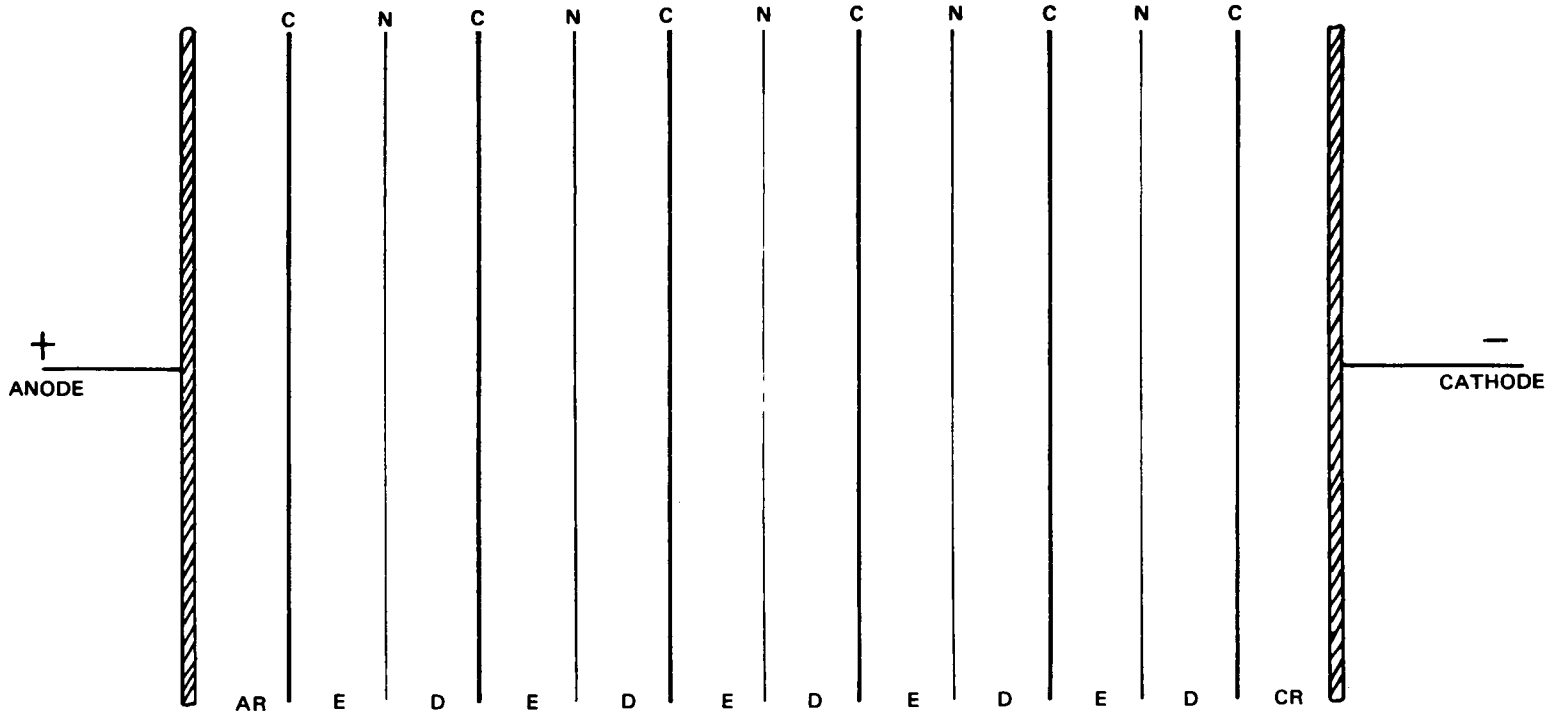

C – CATION MEMBRANE, IONAC MC-3142
N – NEUTRAL MEMBRANE, UCC ZEPHYR Z
E – ENRICHING COMPARTMENT (CONCENTRATE STREAM)
D – DEPLETING COMPARTMENT (PRODUCT STREAM)
AR – ANODE RINSE COMPARTMENT (BASE FEED)
CR – CATHODE RINSE COMPARTMENT (ACID FEED)

Figure 54 Arrangement of Membranes in Five-Cell-Pair Pilot-Plant Stack

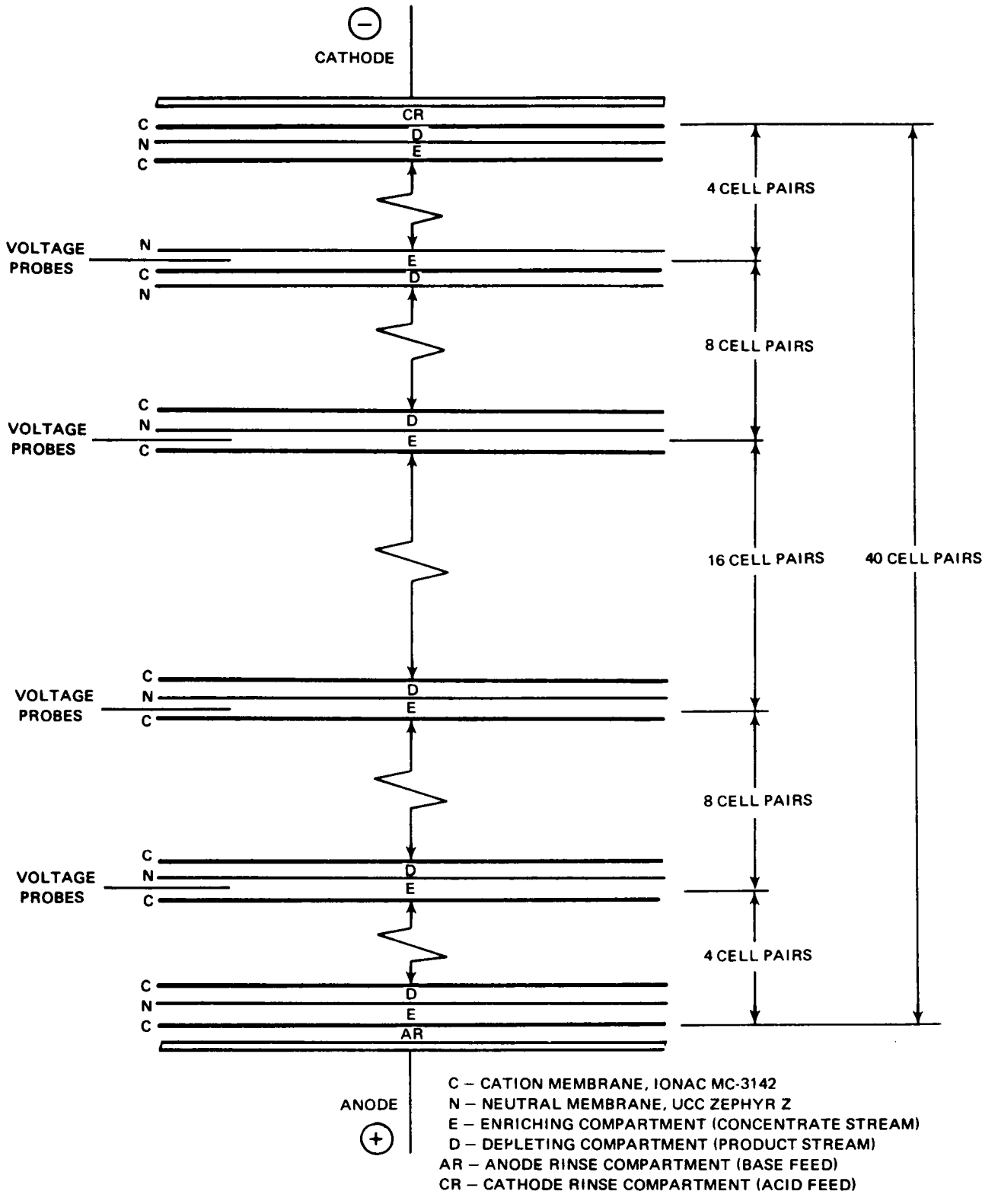

Figure 55 Arrangement of Membranes in Forty-Cell-Pair Pilot-Plant Stack

The alignment pins were removed and all internal manifolds checked for alignment and freedom from blockage. Following this, the inspection plugs, and the upper-end clamp bars and related hardware were installed. All tie rods were then tightened to about one-half the calculated deflection value of the Belleville washers at a 750 psi sealing load.

A 3000 ppm NaCl solution supply was connected through a sixteen-branch manifold arrangement so that all compartments were constantly filled with solution. The stack was allowed to set for at least 24 hours and then retightened to a maximum loading of 750 psi. A pressure check up to 50 psi was made, using the branch manifold arrangement to insure that all compartments were subjected to the same pressure.

D. Design and Construction of Pilot-Plant System

This section describes the design of the hydraulic and electrical systems of the pilot-plant and the physical arrangement of the various system components.

The hydraulic and electrical systems of the pilot plant were designed to provide a broad spectrum of operating capabilities to permit the evaluation of the transport-depletion process over a large number and range of variables. This design philosophy required both the selection of components capable of operating over a wide range of conditions and a piping system capable of several alternate operating modes.

1. Hydraulic System

The hydraulic system provided four separate feed streams to the stack. These were a product stream, a concentrate stream, an acid-rinse stream for the cathode compartments, and a base-rinse stream for the anode compartments. Each stream had its own feed tanks, pumps, filters, and flow-control valves.

Two general modes of operation were possible, a closed-loop mode and an open-loop mode. In the closed-loop mode, the product and concentrate solution feed streams were both supplied to the stack from a common feed tank. The product and concentrate exit streams from the stack were then returned to a common mixing tank which then supplied the common feed tank. In the open-loop mode, the product and concentrate streams were supplied from separate feed tanks and all stack exit streams were directed to a drain. The obvious advantage of the closed-loop operating mode is the capability of long pilot-plant operating times independent of the feed-tank capacities. This advantage is gained at the risk of building up contaminants in the feed solution over long periods of operation.

In either operating mode, the concentrate stream could be recirculated through the stack for feed-and-bleed operation, or run once through in a manner similar to the product stream. In all cases, the acid and base-rinse exit streams were sent directly to a drain with provisions for venting any gases generated in these two streams.

All solution feed streams employed the same basic methods for the control of flow rates and pressure levels. A pump bypass valve was located at each pump exit to return excess solution to the feed tank. A flow control valve was located in each solution exit stream from the stack to permit the control of back pressure in each stream. The bypass valves were used for setting approximate flow rates and pressure levels. The flow control valves provided fine flow-rate adjustments and set stack-exit pressure levels. The concentrate recirculation stream had a bypass valve and a flow-control valve located at the exit of the recirculation pump.

All bypass valves and the flow control valves for the product, concentrate, and concentrate recirculation streams were polyvinylchloride diaphragm-type valves. The flow control valves for the acid and base rinse streams were PVC needle valves. All other setup valves in the system used to establish the desired operating mode were PVC ball valves. All system flow lines were constructed of PVC pipe and fittings. In areas of permanent plumbing, Schedule 40 PVC pipe and solvent-welded joints were used. In the stack-header areas where plumbing changes were required to operate with different stack path lengths, Schedule 80 PVC pipe with threaded fittings were used.

The four solution streams were filtered before entering the stack, using Aircraft Porous Media PVC case filters with 10-micron cartridges. Four model ACS 1001 US AKH filters in parallel were used in both the product stream and the concentrate stream. Two model ACF 4463 US AKH filters in parallel were used in both the acid-rinse stream and the base-rinse stream.

Four cylindrical Tamco polyethylene solution tanks were used. Each electrode-rinse solution-feed tank had a capacity of 55 gallons. The two main feed tanks had a capacity of 550 gallons each. In the closed-loop operating mode, one 550-gallon tank was used as the concentrate source and the other 550-gallon tank as the product-feed tank. In the open-loop operating mode, both 550 gallon tanks were used as solution-feed tanks.

All five solution pumps were Aurora APCO A-series turbine pumps with 316 stainless-steel bodies and impellers. The product-feed, concentrate-feed, and concentrate-recirculation pumps were model 14A which had a rated capacity of 25 gpm at 54 psi and were driven by 2 HP motors. Model D4 pumps were used in the electrode-rinse streams. These had a rated capacity of 5 gpm at 54 psi and were driven by ¾ HP motors. All pump motors were capable of operation on an electrical supply of either 220 or 440 volts 3-phase AC.

Because the rated capacity of the pumps was over three times the capacity required for operation at design conditions, safety devices were employed to prevent damage to the stack and system if an overpressure condition were encountered. Two types of devices were used, pressure-relief valves, and pressure-cutoff switches. Pressure-relief valves were installed at the pump exits in all four feed streams. These relief valves could be adjusted to relieve at any pressure between 0 and 100 psi. If the flow capacity of the relief valve were exceeded, adjustable pressure-cutoff switches were installed in the four stack-inlet streams to shut down all pumps and the stack power supply. Any pressure-cutoff switch could shut down the entire system. A warning light on the control panel indicated which stream had initiated the shutdown.

Solution flow rates in the four feed streams and the concentrate recirculation stream were measured with Fisher & Porter glass-tube indicating flowrators with stainless-steel metering floats and fittings. The product and concentrate streams each used a high and a low flowmeter in parallel, with useful capacity ranges of 2.4 to 24 gpm and 0.95 to 9.5 gpm, respectively. Setup valves were provided so that either flowmeter could be used, depending on the flowmeter range desired. The concentrate-recirculation stream and the two electrode-rinse streams each used one flowmeter. The capacity range of the concentrate-recirculation stream was 2.4 to 24 gpm. The range covered by the electrode-rinse stream flowmeters was 0.12 to 1.2 gpm. All flowmeters had a linear percent scale and were calibrated before use.

System pressures were measured with helicoid bourdon-tube gages with K monel bourdon tubes. Pressure taps were located in the four solution streams to measure pressures at the stack inlet and exit, and between the four stack channels when required. These pressure taps could also be used to measure differential pressures between the various streams with U-tube manometers.

System temperatures were measured with chromel-alumel 1/8-inch diameter sheathed thermocouples with sealed junctions. These thermocouples were installed in the same general location as the pressure taps. Temperature readout during the pilot-plant tests was accomplished with a Brown model 156 indicating potentiometer.

Conductivity cells for measuring solution concentrations were located in the product and concentrate streams at the stack inlets and exits, and between the four stack channels. This equipment was manufactured by Beckman Instruments, Inc. A model R 14 Solu Bridge Indicator incorporating an AC wheatstone-bridge circuit with manual temperature compensation and a solid-state amplifier was used. The stated accuracy was within 1 subdivision of scale (usually less than 1 percent). All conductivity cells were screw-in type with Type 316 stainless-steel housings and flush platinized gold-plated nickel electrodes. Five cells had a cell constant of 20/cm for a range of 0 to 10,000 micromhos. Seven cells had a cell constant of 40/cm for a range of 0 to 20,000 micromhos. Connections between the cells and the indicator was accomplished through a Shallcross 2-pole 12-position nonshorting switch with gold-plated contacts.

Sampling valves were located at the stack inlet and exit in all four streams, and between the four stack channels in the product and concentrate streams. These valves could be used to collect solution samples for subsequent chemical analysis or conductivity measurement with a dip-type cell.

2. Electrical System

The electrical system included the stack power supply, the control circuits for the power supply and pump motors, and the electrical instrumentation.

The power supply was basically a magnetic amplifier consisting of a transformer, a saturable-core reactor, and a rectifier bridge. It required a 440-volt 3-phase AC input and had a maximum output of 200 amperes at 300 volts DC. The magnetic-amplifier design was selected

primarily because of its stable and continuously-variable output over a very wide range. Its maximum power output of 60 KW was over six times the estimated design-point requirement of the stack. This excess capacity permitted operation at many combinations of stack current and voltage at lesser power levels.

The design used a 60-KW 440/222-volt 3-phase transformer. The input to the transformer was controlled by a 75-KVA 440-volt 3-phase saturable-core reactor with a 75-volt DC 2.7-ampere control winding. Power to the control winding was supplied by a 120-volt AC power-stat with a variable output from 0 to 120 volts AC 12 amperes which was connected to a single-phase full-wave rectifier bridge rated at 10 amperes, 400 volts DC. An adjustable resistor was installed between the rectifier-bridge output and the control windings which could be used to adjust the available turn-down of the power supply. Both the transformer and the saturable-core reactor were manufactured by Davis Electric Company.

The output of the transformer was rectified by a 3-phase full-wave bridge rectifier with a rated output of 330 volts DC at 200 amperes. The rectifier and heat-sink assembly was manufactured by International Rectifier Company. Polarity of the rectifier output could be reversed by a DPDT reversing switch installed between the rectifier and the pilot-plant stack.

The power-supply voltage to the stack was measured with a Weston DC voltmeter with an accuracy of 1 percent. This is a dual-range meter with ranges of 0-150 and 0-300 volts DC.

Total stack current was measured with a Weston dual-range ammeter coupled with a calibrated Tel-Labs Inc. Shunt with an accuracy of 0.05 percent. The two ranges permit readings at 0-100 or 0-200 amperes DC. Individual stack electrode currents were measured with four Weston DC ammeters rated at 2 percent accuracy. Two of the meters had ranges of 0-100 amperes and the other two 0-50 amperes.

Power to the five pumps and the power supply was controlled by push-button switches through relays associated with the pressure-cutoff-switch circuits. The switches, pilot lights and warning lights were located on the control bench. In case of shutdown due to an over-pressure condition, a reset button on the control bench had to be activated to restore all relays to their normal position before restarting the system. Switches to control four solution-mixing motors installed in the four solution supply tanks were also located on the control bench.

A voltage-probe panel was located on the control bench for measuring stack voltages with the platinum probes in the instrumented spacer screens. The panel contained thirty-two jacks connected to the eight probes in each of the four instrumented spacer screens.

3. Pilot-Plant Arrangement

The components of the pilot-plant system were organized into three major modules, a control bench, power supply, and stack transportation stand. These three modules and the four solution supply tanks were arranged in an area 12 by 14 feet in a manner which permitted easy plumbing and electrical connections. The modules and their relative arrangement can best be described by referring to a series of photographs taken at various stages of construction.

Figure 56 shows the solution supply tanks mounted on their support tanks. Also apparent in this figure is the intentional incline in the support stands which aids in draining the tanks. Sufficient space between the tanks was provided so that the plumbing could be accomplished during construction, and all setup valves were accessible during pilot-plant operation. Figure 57 shows an overall layout of the area with the partially-completed modules located in their correct positions. The power supply was placed next to the control bench for ease of electrical hookup and the stack transportation stand was centrally located for ease of plumbing. Figure 57 also shows the five pumps positioned along the bottom shelf of the control bench. Figure 58 shows a rear view of the control bench with some of the PVC piping in place. It may be noted that the plumbing between the tanks and control bench is confined to as small an area as practical to provide adequate floor space around the stack and its transportation stand. The solution supply filters are also visible in this figure. The filters for the product and concentrate streams were suspended on overhead supports for two principle reasons, 1) this location became the high point in the system and bleed valves were located at the top of the filter banks for air removal, and 2) this location was free of obstructions, yet easily accessible for changing filter elements. The rinse stream filters were positioned for accessibility and plumbing convenience.

Figure 59 shows the power supply component layout. The saturable-core reactor generates considerable heat, so that the area over this component was kept open. A cooling fan was built into this unit to blow cooling air upward through the core. The rectifier was mounted high on the power-supply wall over the relatively efficient transformer. The rectifier heat sink was positioned vertically to encourage convective-heat transfer for most efficient diode cooling. Figure 60 shows the completed power supply with protective screens installed and the polarity-reversing switch on the left.

Two views of the front of the completed control bench are shown in Figures 61 and 62. Pressure gages were located overhead, flowmeters and control valves on the left, and electrical meters and control switches for the pumps and power supply on the right side.

Two typical installations of the stack are shown in Figures 63, 64 and 65. Figure 63 shows the 5-cell-pair stack installation with all solution channels connected for parallel flow. Figures 64 and 65 show each end of the 40-cell-pair stack with the solution channels connected in the series-parallel arrangement. These two installations demonstrate the flexibility of the overhead manifold arrangement shown in these two figures.

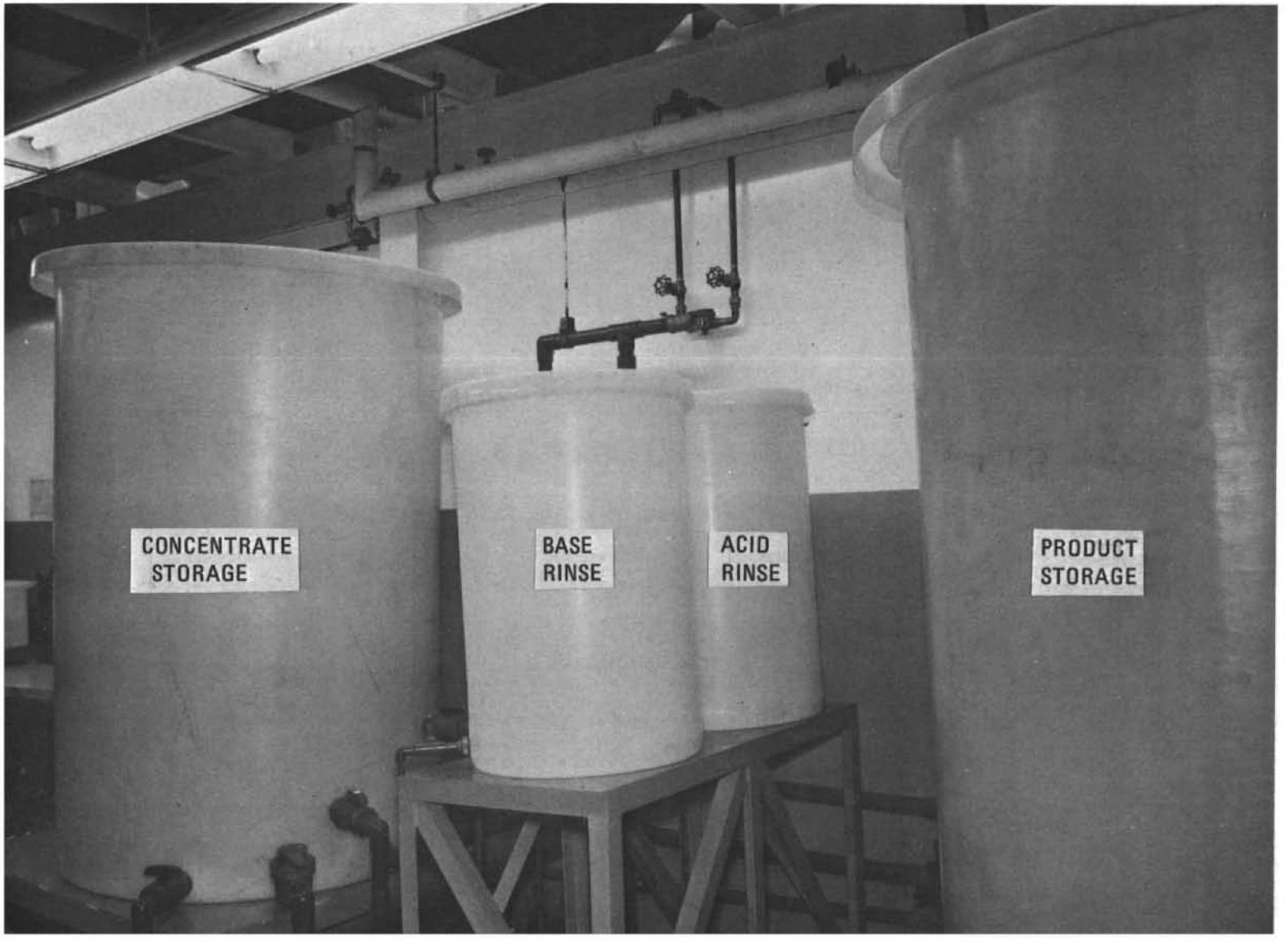

Figure 56 Pilot-Plant Solution Supply Tanks X-29014

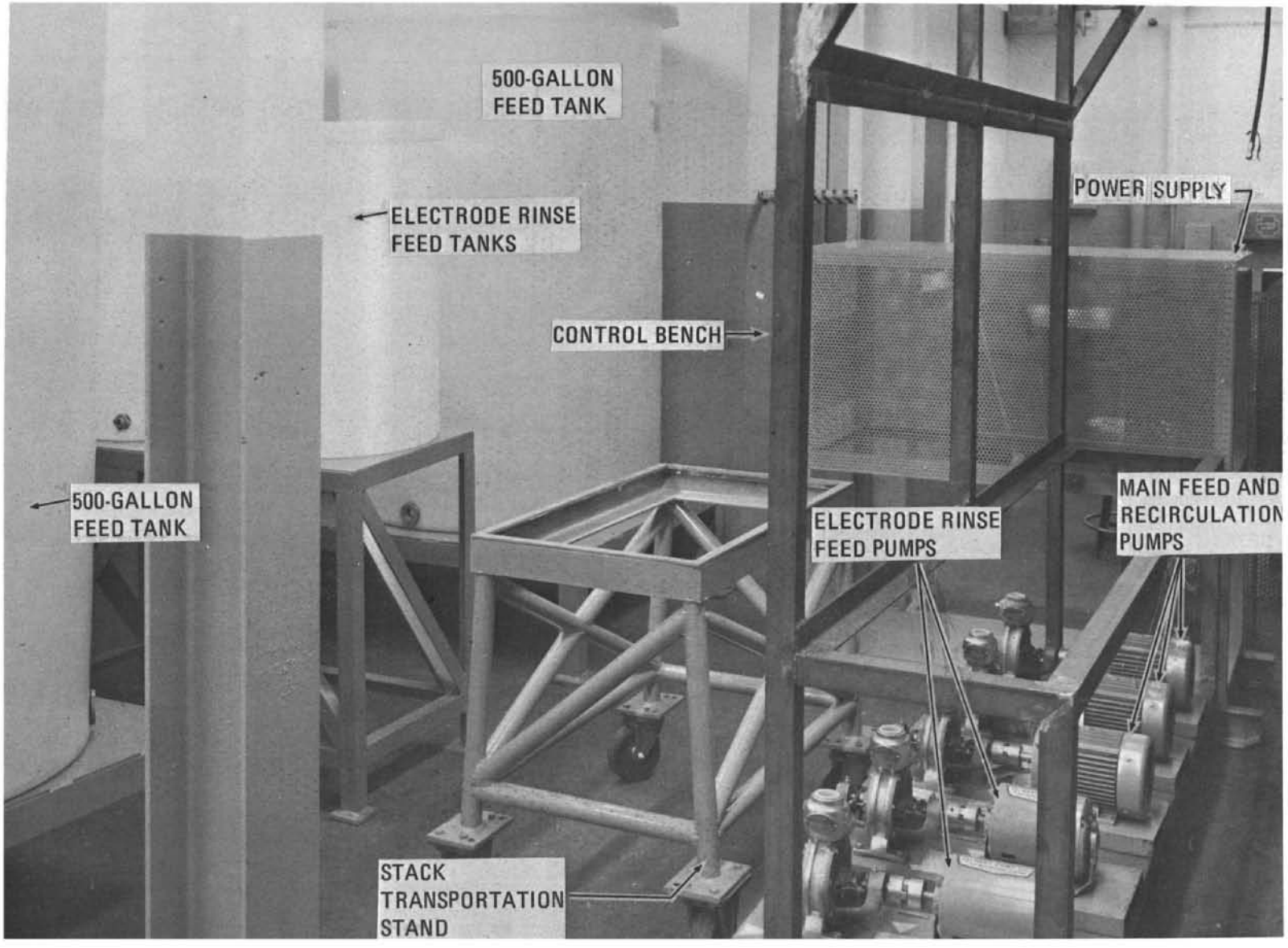

Figure 57 Transport-Depletion Pilot Plant XP-85479

Figure 58 Operator's Stand of Pilot-Plant System X-29229

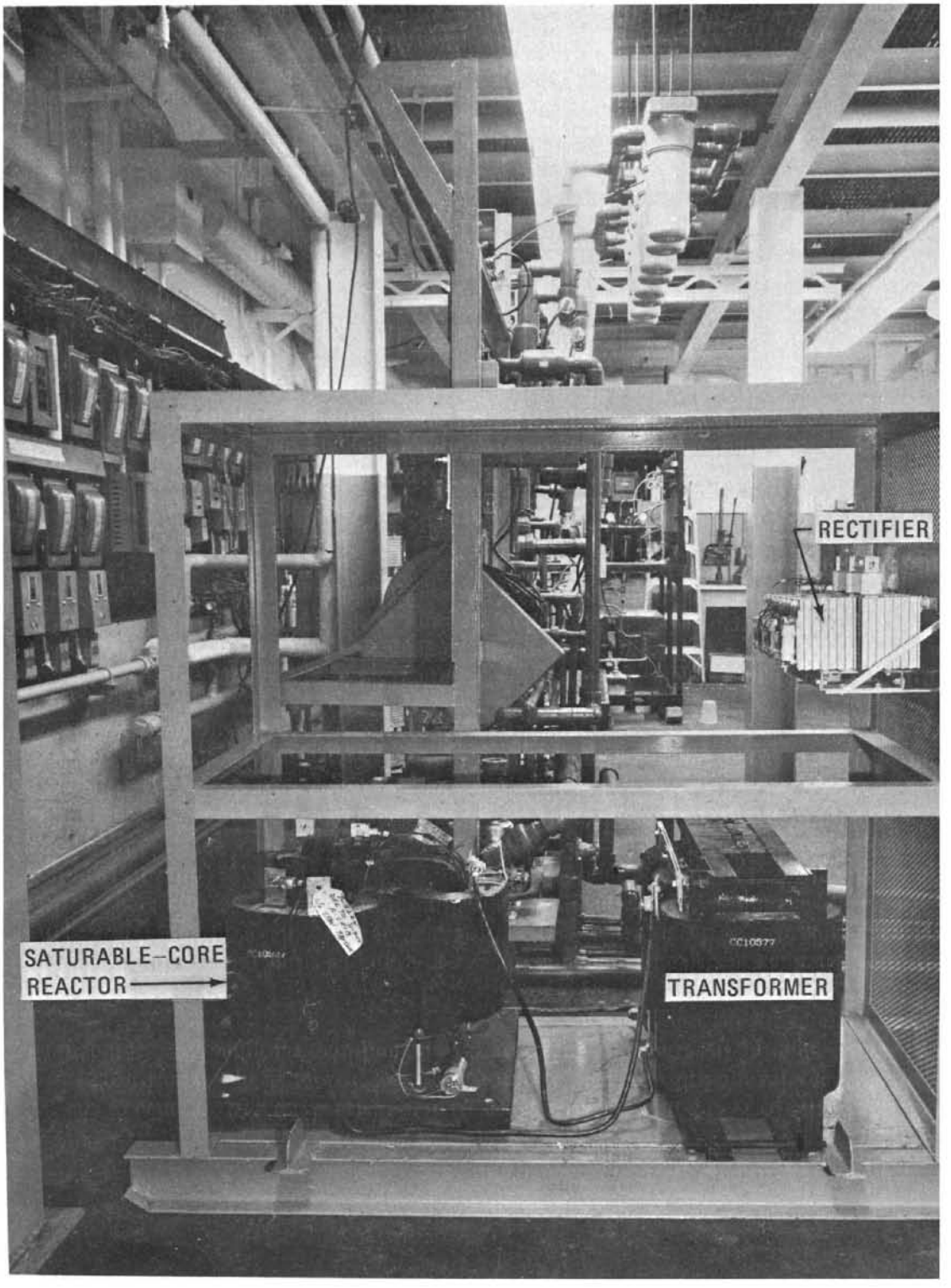

Figure 59 Power-Supply Arrangement X-29230

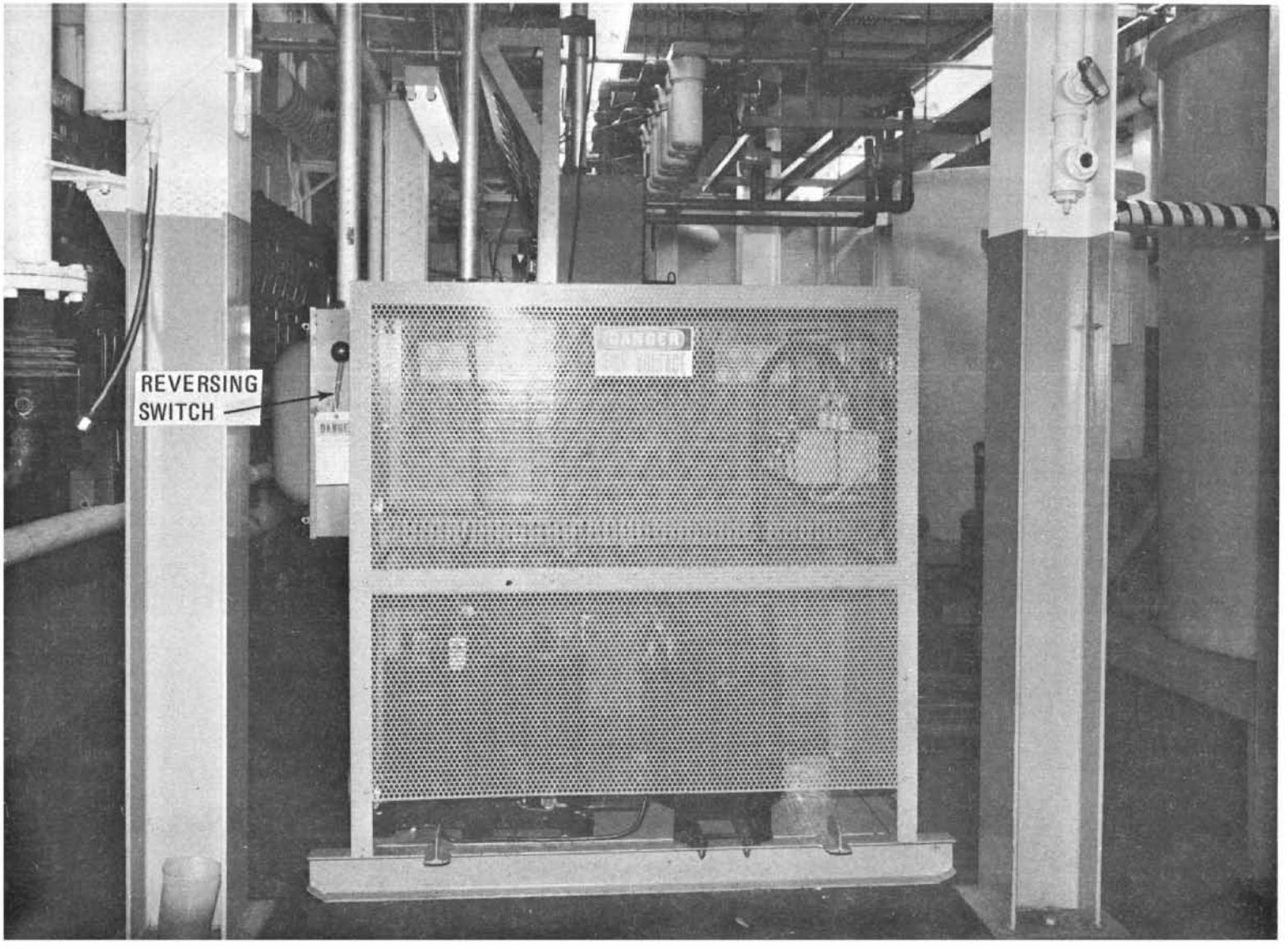

Figure 60 Completed Power Supply X-29439

Figure 61 Pilot-Plant Control Bench X-29437

Figure 62 Pilot-Plant Control Bench X-29438

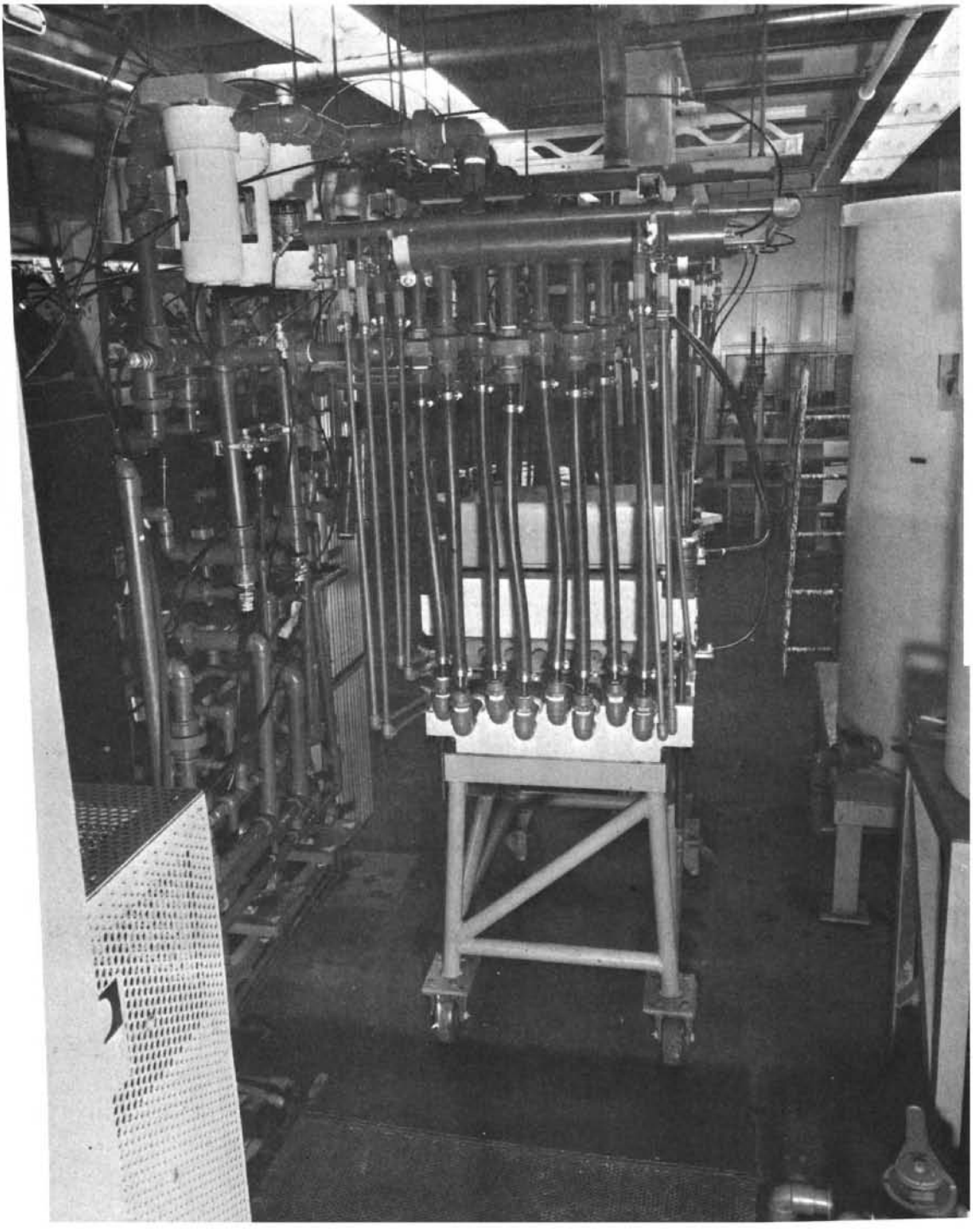

Figure 63 Installation of Five-Cell-Pair Stack XP-90728

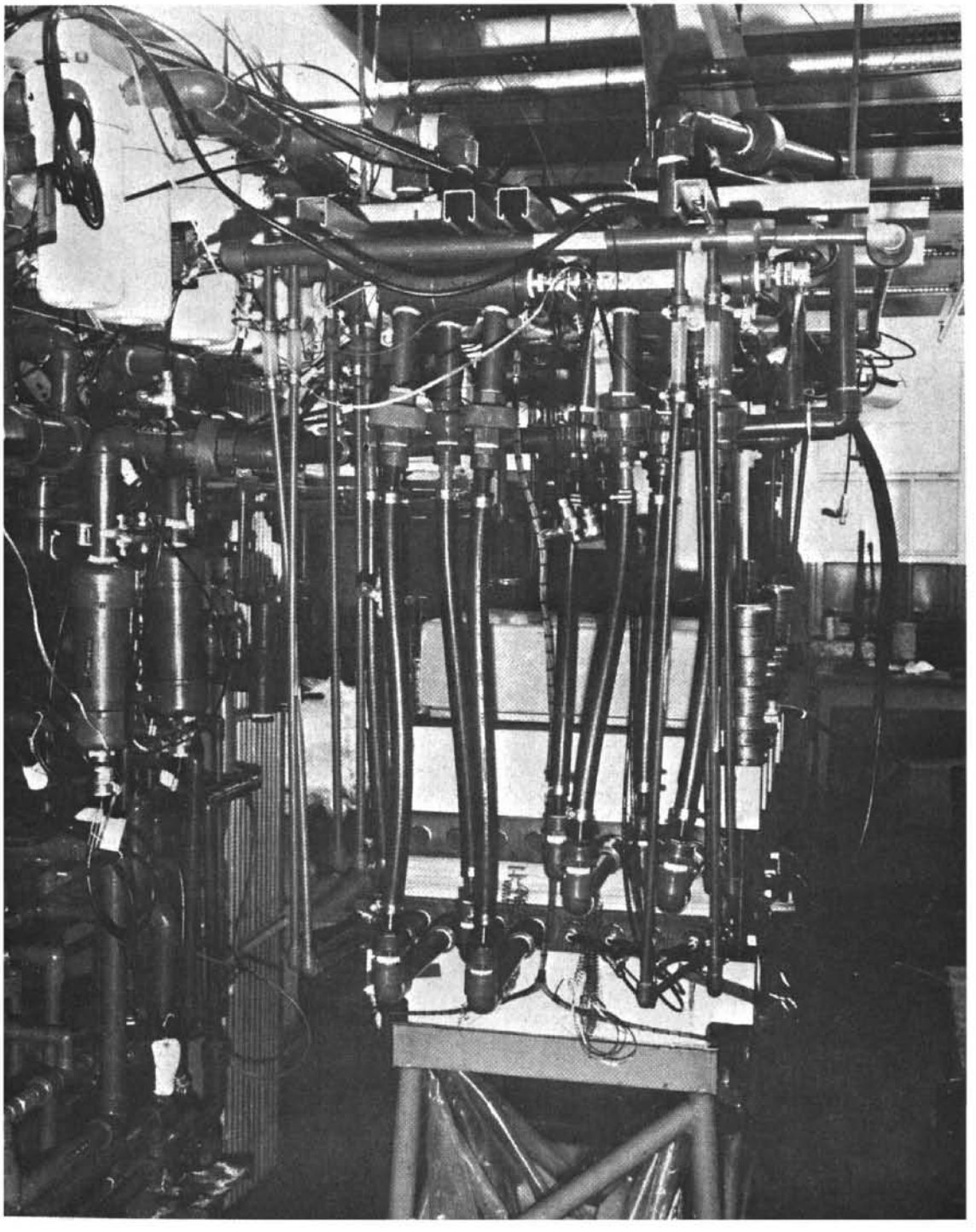

Figure 64 Installation of Forty-Cell-Pair Stack X-30298

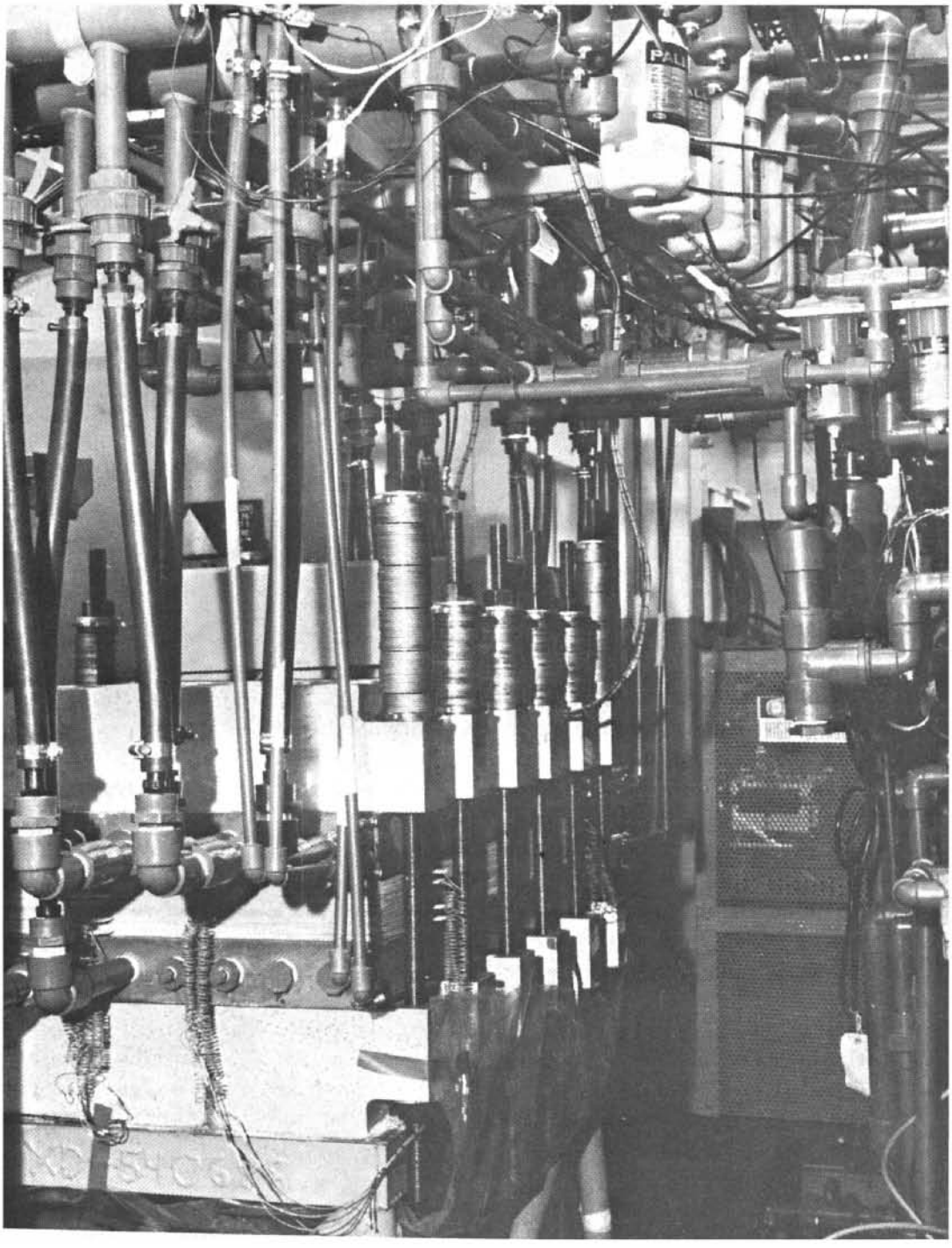

Figure 65 Installation of Forty-Cell-Pair Stack X-30297

VI. PILOT–PLANT OPERATION

A number of pilot-plant test runs were made to demonstrate the general capability of the pilot plant for evaluating the transport-depletion process. Runs were made using two different stack assemblies, a five-cell-pair stack, and a forty-cell-pair stack. General operating procedures were developed during the initial runs of the five-cell-pair stack. These procedures were then followed for all subsequent pilot-plant operation with only minor deviations.

A. Tests of Five-Cell-Pair Stack

The objective of the five-cell-pair stack tests was to conduct a system shakedown and to demonstrate the general capability of the stack design before completing fabrication of the spacer-screens for the forty-cell-pair stack assembly. Stack connections, system leaks, and instrumentation were checked and corrected as required. All five-cell-pair stack tests were limited to single-pass non-recirculation open-loop operation. That is, headers were used to provide parallel flow through both the product and concentrate streams, both 550-gallon storage tanks were used for solution feed and all exit streams from the stack were dumped to drain. The parallel-flow arrangement provided an effective path length of 33.5 inches through the stack.

Figure 66 is a flow schematic of the pilot-plant system. Referring to this schematic, the five-cell-pair stack installation was operated with the following setup valves closed: valves numbers 2, 8, 9, 10, 12, 16, 18, 22, 25, 28, 29, 31, 34, 35, 40, 42, and 43 for product and concentrate stream flow rates less than 9.5 gpm. All other system valves were open. With the above conditions set, the four feed pumps were simultaneously started. During this startup period, pressure gages were constantly monitored to detect and prevent large pressure differentials between streams. The bypass and flow-control valves in each stream were alternately adjusted to increase the flow rates and pressure levels to the desired conditions for the test being run. Once the desired conditions were set, system bleeds were opened as required to remove trapped air from the system. After bleeding, the flow rates and pressure levels were again checked and adjusted as required. When stable steady-state conditions were reached, a hydraulic reading was taken. This included readings of flow rates, pressures, temperatures. Conductivity-cell readings and solution samples were taken for later titration analysis.

With the powerstat set at zero, the power supply was turned on and allowed to warm up. The desired current density was then set by adjusting the powerstat. The five-cell-pair stack was run for at least five minutes at each condition before recording data. At each test condition readings were taken of flow rate, pressure, temperature, conductivity, stack current and voltage, and individual electrode currents. Also solution samples were taken.

Pilot-plant shutdown was accomplished in the following manner. The powerstat was set at zero and the power supply was shut off. Flow rates were maintained for at least three additional minutes to flush out gases from the rinse streams and to assure that all product and concentrate compartments were filled with the 3000-ppm NaCl feed solution. All pumps were then shut off simultaneously and all valves were closed.

Figure 66 Flow Schematic for Transport-Depletion Pilot Plant

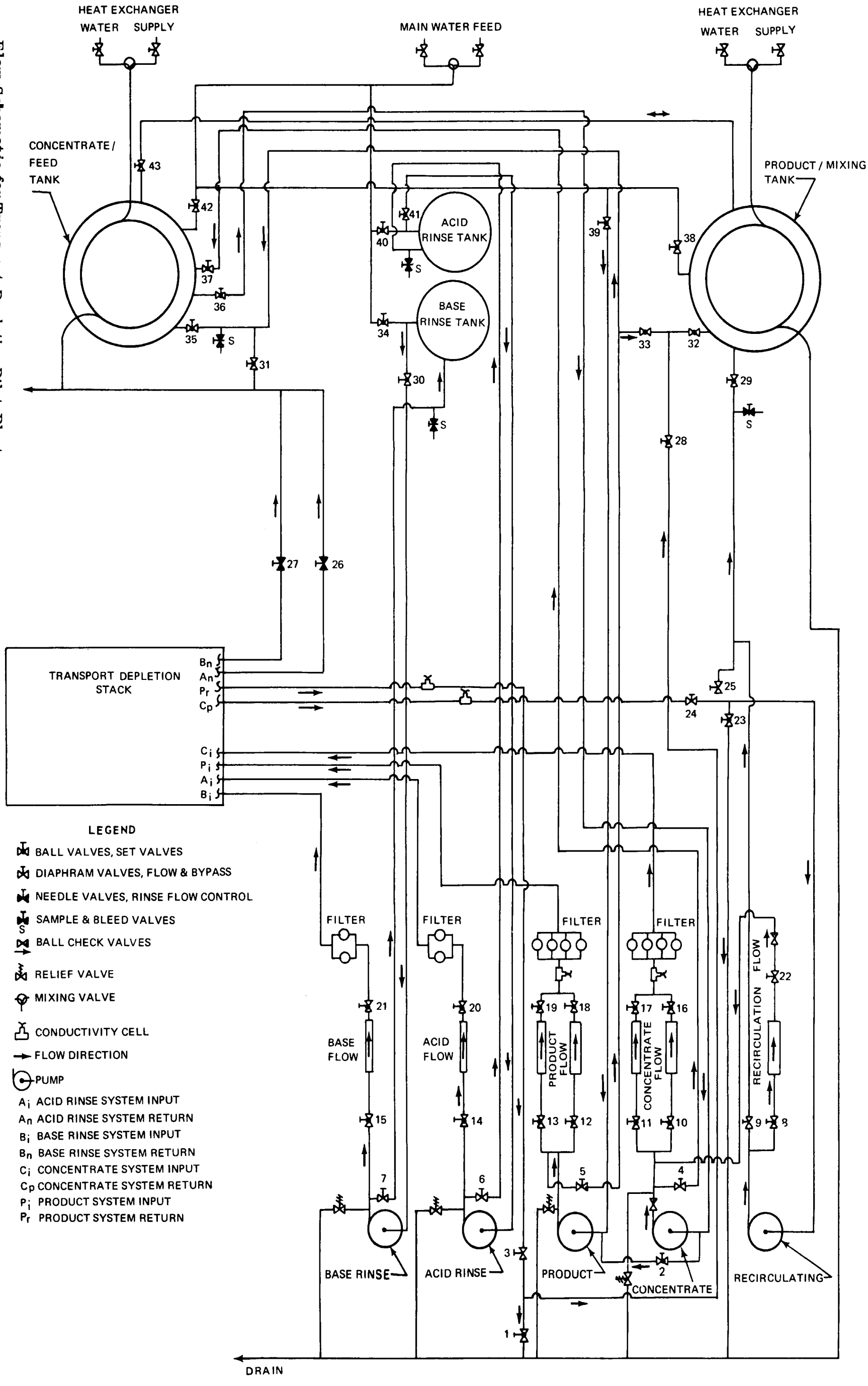

B. Tests of Forty-Cell-Pair Stack

The objective of the forty-cell-pair stack tests was to demonstrate the performance of the pilot-plant system with the full-size stack assembly, and to generate an initial performance map for use in evaluating the transport-depletion process and in developing more-detailed future test programs for the pilot plant.

The forty-cell-pair stack tests were run using the closed-loop operating mode with one 550-gallon storage tank used as the solution feed and the second as a solution mixing tank for the return streams from the stack. The stack was run with both concentrate-stream recirculation and non-reciruclation. For the non-recirculation runs, the following valves (refer to Figure 66) were closed before pilot-plant startup: valves numbers 1, 8, 9, 22, 23, 31, 34, 39 and 40. For the runs with concentrate-stream recirculation, valves numbers 1, 23, 25, 31, 33, 34, 39, and 40 were closed before startup. Also, in all cases valves numbers 10, 12, 16 and 18 were closed if the desired product and concentrate flow rates were less than 9.5 gpm, and valves numbers 11, 13, 17, and 19 were closed for flow rates greater than 9.5 gpm.

Three different path lengths were tested. The series manifold arrangement resulted in the longest path length of 134 inches, the series-parallel arrangement provided a path length of 67 inches and the parallel arrangement provided the same path length of 33.5 inches as the five-cell-pair stack. Bleed valves were located at the top of each manifold which also doubled as solution-sample valves.

The system startup procedure was generally the same as that used for operation of the five-cell-pair stack. All bypass and flow control valves were opened prior to startup for operation with concentrate recirculation, and all but the recirculation bypass and flow control valves were opened when no recirculation was desired. All other hydraulic and electrical procedures were the same as for the five-cell-pair stack.

For the forty-cell-pair stack tests, data was recorded after at least six minutes of stable operation. Stable operation was considered to be achieved when stable exit conductivity readings were observed. The recorded data included flowrates, pressures, temperatures, conductivities, power supply current and voltage, and individual stack electrode currents. Also voltage-probe measurements were made using the probes in the instrumented spacer-screens. Figure 67 shows the probe locations and probe numbering system on the jack panel.

Voltage readings were taken between the two probes in one channel, for example, between probes 1 and 2. Then between probes in different cells, for example, between probes 1 and 9, 1 and 17, and 1 and 25. Similar readings were taken for all the other channels. For the tests of 34-inch path length, the method of recording probe voltage was partially changed. The initial readings were recorded in the same manner, but the second set was taken for example between 1 and 25, 1 and 9, 9 and 17, and 17 and 25.

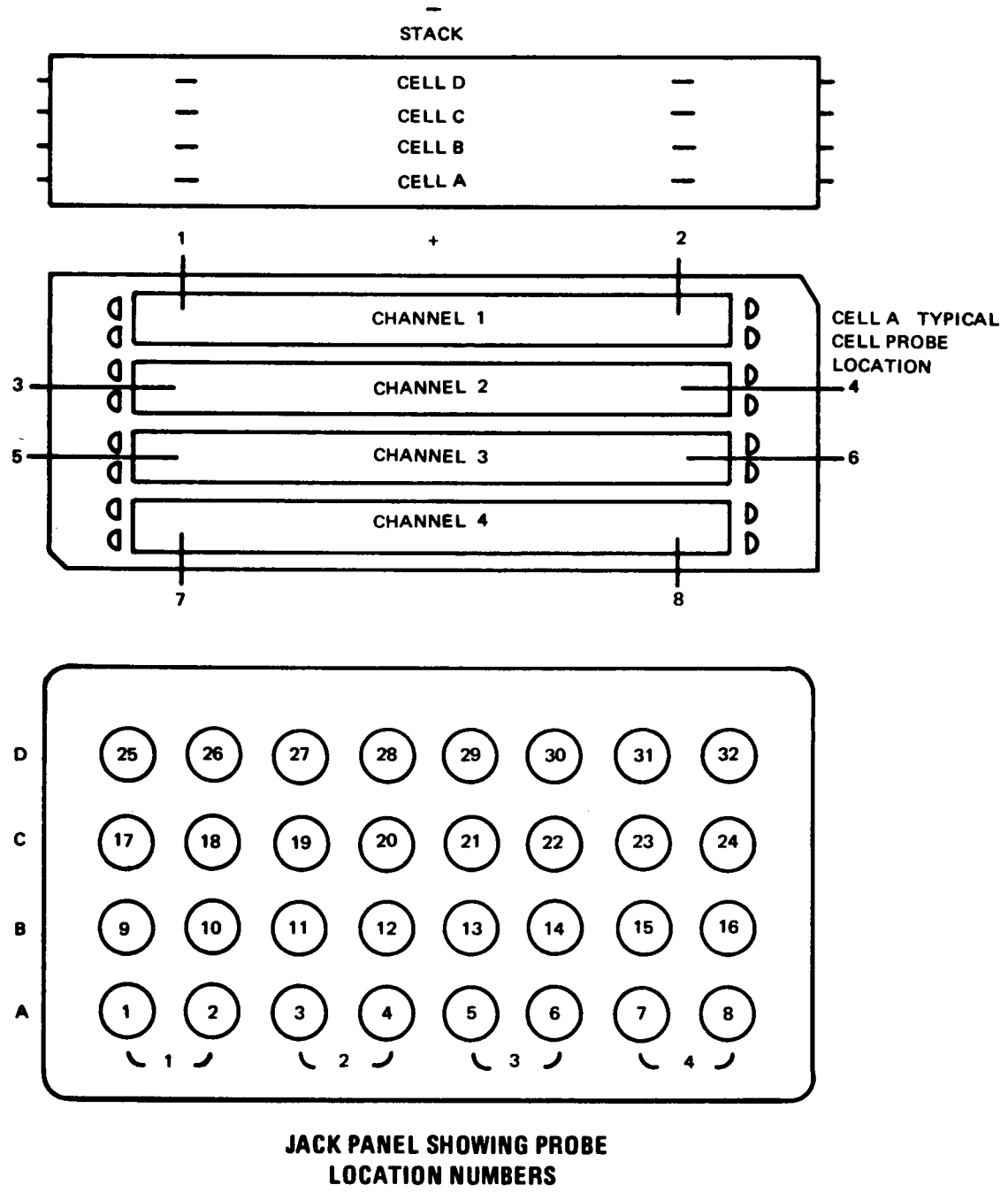

Figure 67 Voltage Probe Instrumentation

VII. ANALYSIS OF PILOT–PLANT DATA

The data obtained from the pilot-plant tests described in Section VI was analyzed to determine the performance characteristics of the stack. The results of this analysis are described below.

A. Test Results of Five-Cell-Pair Stack

A total of six runs were made using the five-cell-pair stack assembly. These runs and the parameters that were varied are listed in Table 5. Each run encompassed operation at several current densities up to 40 ma/cm^2, as shown in Table 5.

The assembly and operation of the five-cell-pair stack was an additional requirement that was added to the program after the design of the pilot-plant system had been fixed. Therefore only a limited range of variables could be explored because of the gross mismatch between the excess capacity of the pilot-plant system and the one-eighth size stack assembly. The data generated during these tests is subject to considerable variation due to the difficulty of controlling the pilot-plant systems at the low flow rates required by the small stack.

The tests satisfactorily met the intended objective of providing a preliminary evaluation of the pilot-plant-stack design and performance characteristics, before assembling the forty-cell-pair stack. The tests also provided an opportunity to shake down the system before testing the larger stack assembly. The results of the five-cell-pair stack evaluations are summarized as follows:

TABLE 5

Test Conditions for Five-Cell-Pair Stack

Run No.	Path Length, inches	Product-to-Waste Ratio	Channel Velocity, inches/sec[1]	Current Density, ma/cm^2
1	33.5	1/1	4.64	5,10,15,20
2	33.5	1/1	4.72	5,10,15,20,25, 30,35
3	33.5	1/1	4.07	5,15,25,35,40
4	33.5	1/1	4.73	20,40
*5	33.5	1/1	4.73	5,10,15,20,25,30 35,40,20
7	33.5	1/1	7.50	20
	33.5	1/1	7.93	30,40

[1]System design did not encompass the operation of a five-cell-pair stack. Therefore the control modes were too coarse to accurately maintain a specific velocity. These velocities represent an average for the conditions of the test.

*For this test, the concentration of the product-stream feed was 1200 ppm NaCl and that of the concentrate-stream feed was 4000 ppm NaCl. In all other runs the concentration of both product and concentrate-stream feeds was 3000 ppm NaCl.

1) The stack design operates satisfactorily and produces demineralized product water by the transport-depletion process.

2) Stack pressure drop at the design channel velocity was found to be typically between 5 and 6 psi per channel, although values up to 8 psi were observed. Considerable variations in pressure and a degree of flow instability were observed.

3) The channel velocity which results in a pressure drop of 12.5 psi per channel (50 psi with all channels in series) was measured and was about 7.5 inches per second (19 cm/sec).

4) Figures 68 through 83 illustrate the demineralization performance obtained with the five-cell-pair stack. Current efficiencies above 25 ma/cm^2 ranged between 36 and 63 percent (efficiencies as high as 70 percent were calculated at lower current densities, but are subject to calculation uncertainties because of the small cuts involved). These efficiencies were calculated using product solution concentration values determined by volumetric analysis of samples using the Volhard method. This method gave good agreement between calculated efficiencies based on the product-stream conditions and the efficiencies based on the concentrate-stream conditions. Solution concentrations were also determined from conductivity measurements, however, these values were very inconsistent and not always repeatable. Also, the conductivity data imply that considerably more salt is transferred to the concentrate streams than is removed from the product stream. Because of the unreliability of the conductivity measurements, Volhard titration of solution samples was used in all succeeding test runs.

5) The measured electrical currents in the four solution channels were not always equal to each other, as would be expected with the four channels connected in parallel. The apparent cause of this was unequal solution flow rates in the electrode-rinse streams caused by blockage. This condition was partially corrected by back-flushing the rinse-stream compartments in the stack. Run 3 was made at about 75 percent of design channel velocity, with the four channel currents nearly equal. Figure 74 shows that current efficiencies for this run were between 55 and 70 percent with 60 percent being a good indication of the current efficiency capability of the five-cell-pair stack at a reasonable current density. In the other runs, unequal currents in the four channels resulted in lower current efficiencies (36 to 50 percent above 25 ma/cm^2) than normally expected.

6) Subsequent teardown of the five-cell-pair stack revealed that several of the solution inlet and exit holes to the electrode-rinse compartments were partially blocked by extrusion of the rubber gasket between the endplate and the rinse-stream spacer screen. Also several electrode rinse-stream inlet passages in the endplate contained small chips of polyvinylchloride which apparently caused partial blockage of flow to the rinse compartments. The location of the PVC chips and rubber extrusion blockage correlate well with the channels which exhibited high resistance during the test runs. Also noted during teardown was a tendency of the cation membranes to adhere to the spacers in some areas. This adherence was so severe in

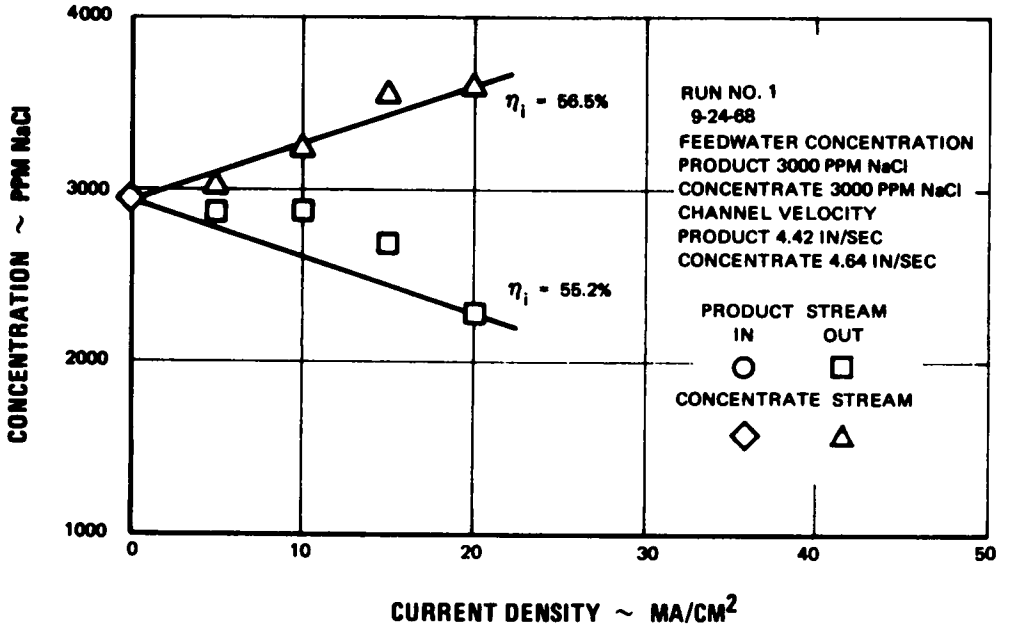

Figure 68 Five-Cell-Pair Stack Titration Data. Concentration vs Current Density. Run No. 1

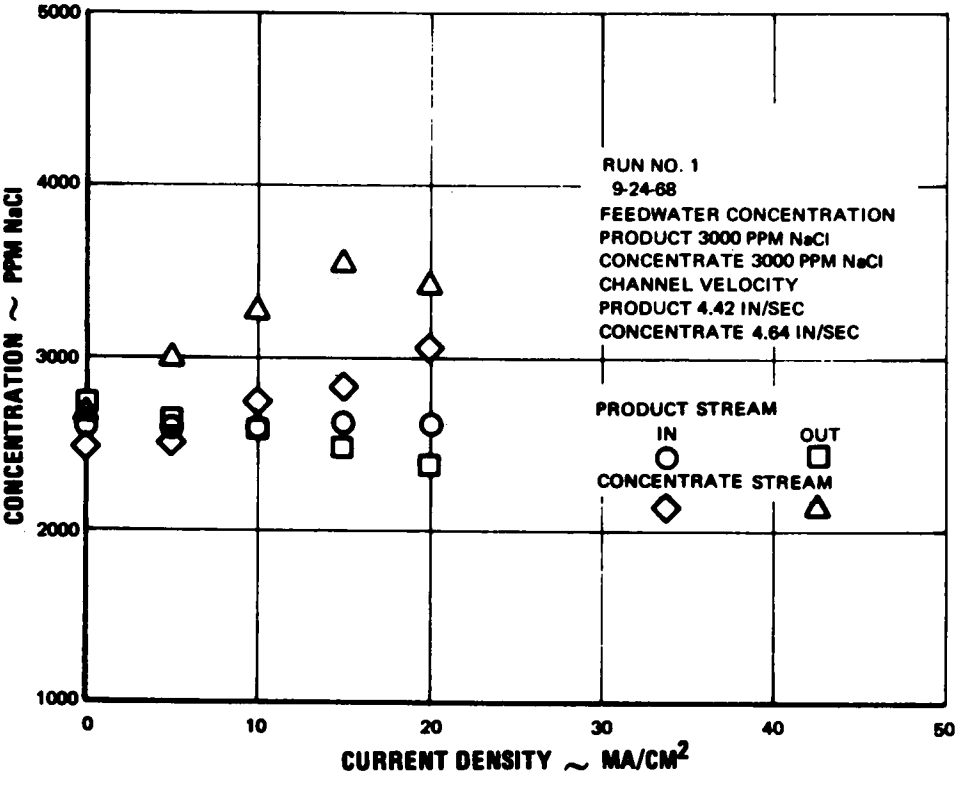

Figure 69 Five-Cell-Pair Stack Conductivity Data. Concentration vs Current Density. Run No. 1

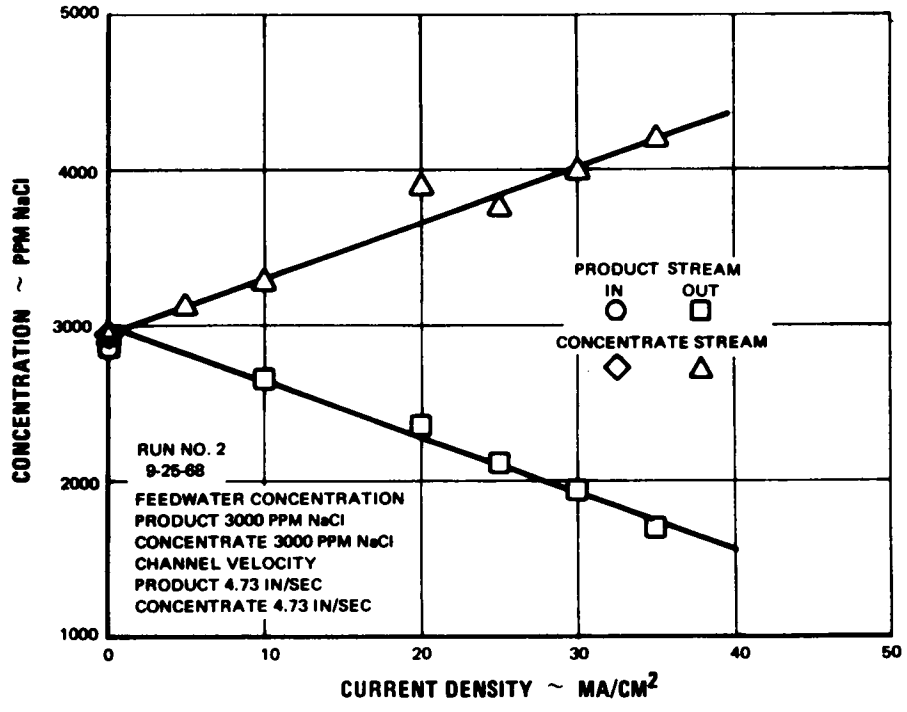

Figure 70 Five-Cell-Pair Stack Titration Data. Concentration vs Current Data. Run No. 2

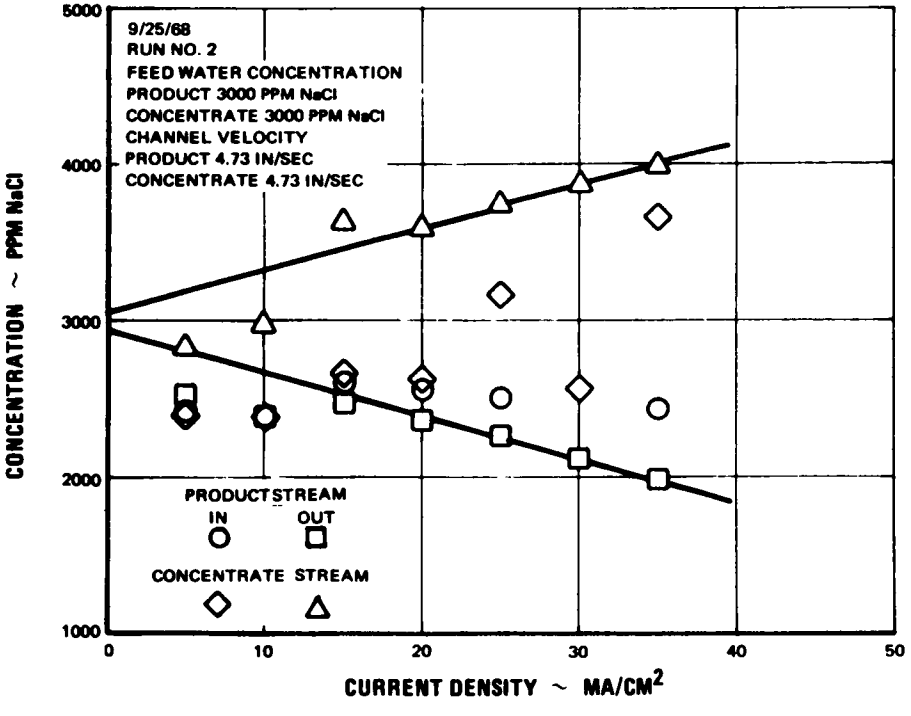

Figure 71 Five-Cell-Pair Stack Conductivity Data. Concentration vs Current Density. Run No. 2

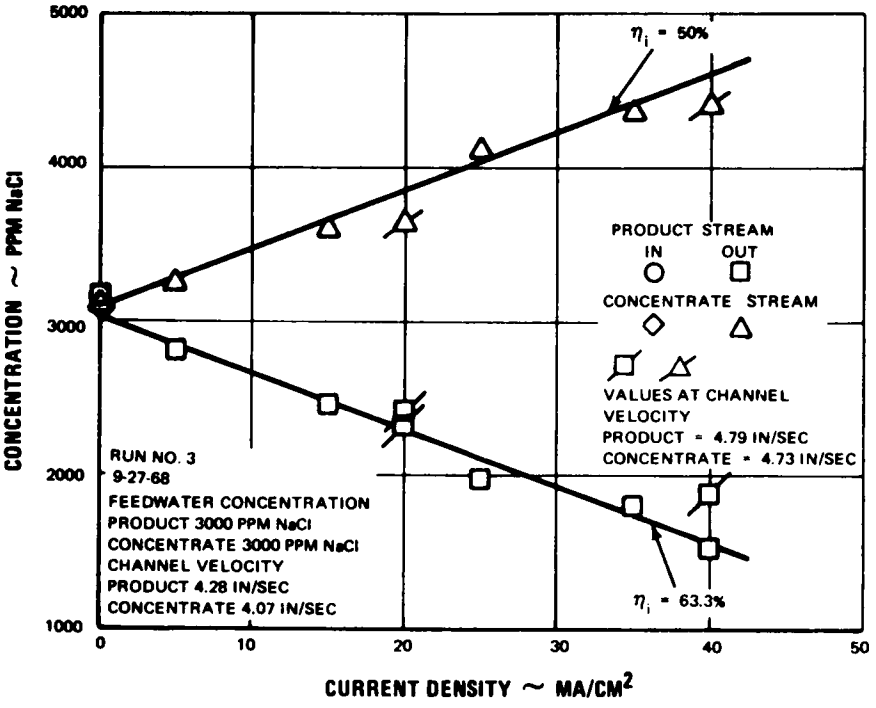

Figure 72 Five-Cell-Pair Stack Titration Data. Concentration vs Current Density. Run No. 3

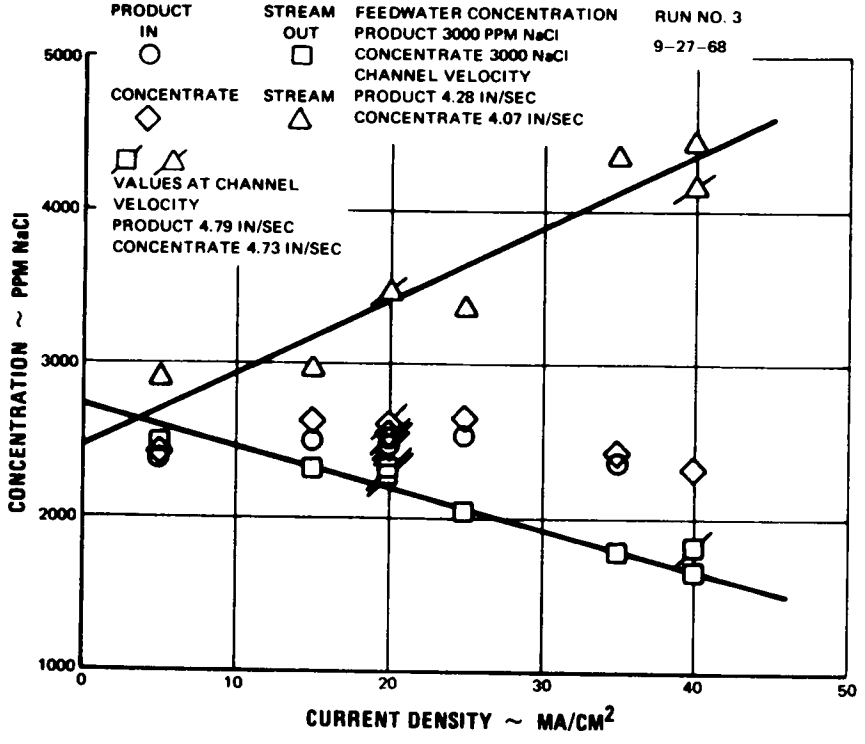

Figure 73 Five-Cell-Pair Stack Conductivity Data. Concentration vs Current Density. Run No. 3

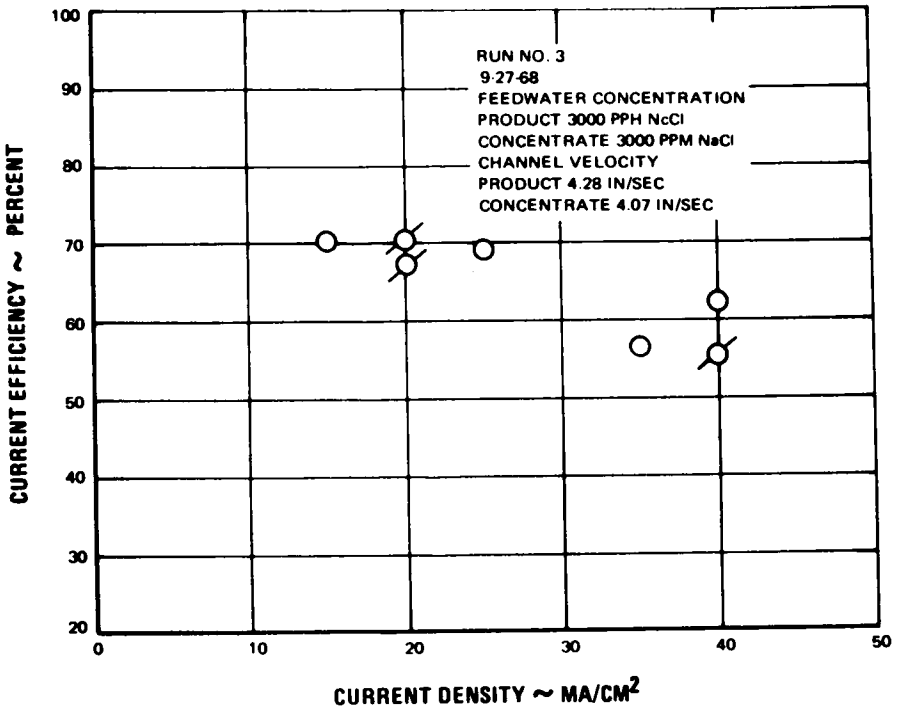

Figure 74 Five-Cell-Pair Stack Product-Stream Titration Results. Current Efficiency vs Current Density. Run No. 3

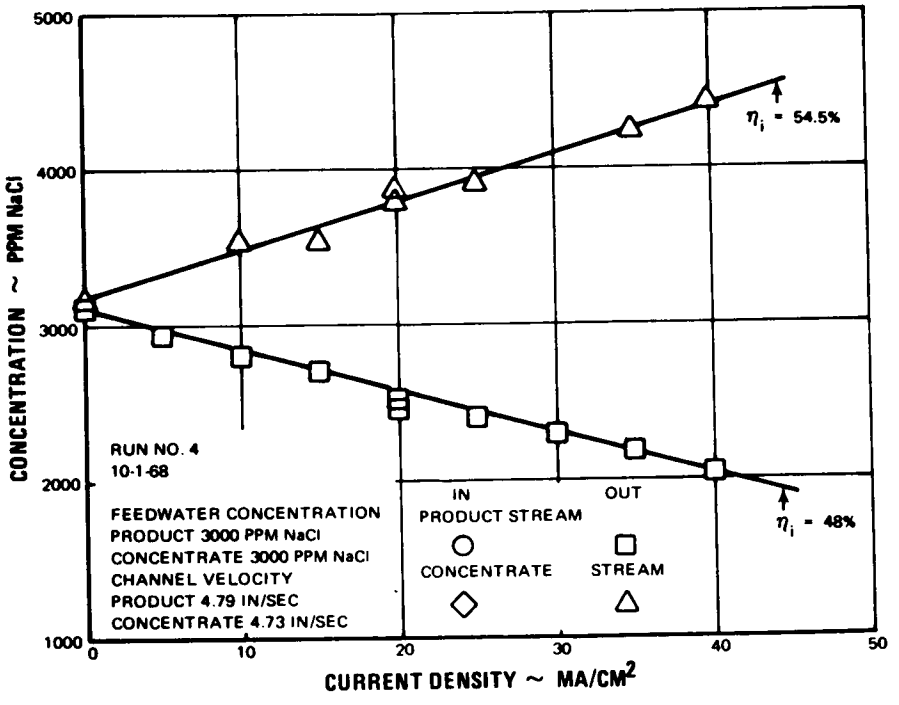

Figure 75 Five-Cell-Pair Titration Data. Concentration vs Current Density. Run No. 4

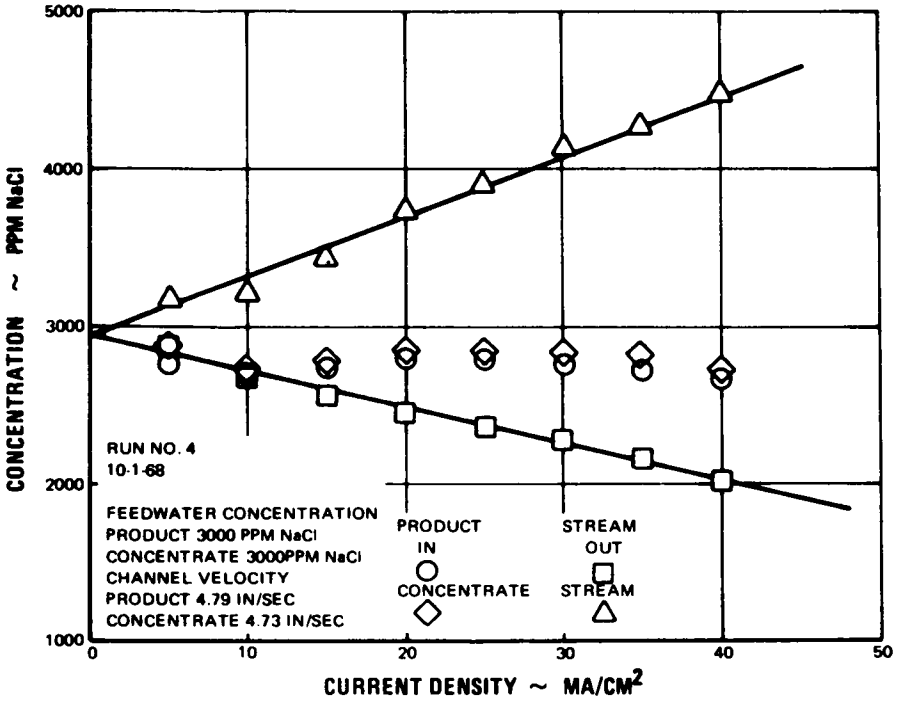

Figure 76 Five-Cell-Pair Stack Conductivity Data. Concentration vs Current Density. Run No. 4

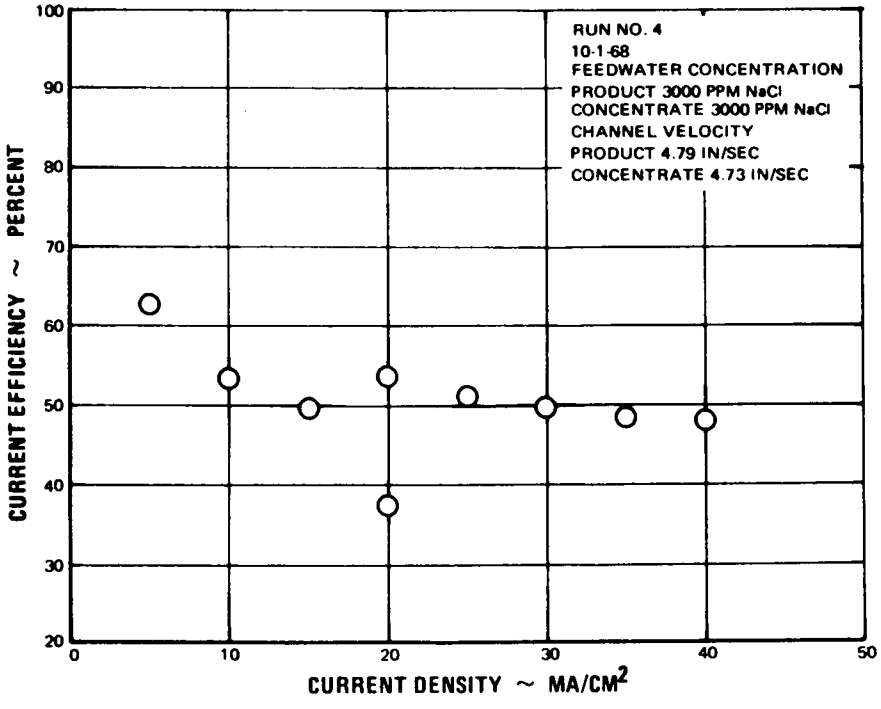

Figure 77 Five-Cell-Pair Stack Product-Stream Titration Results. Current Efficiency vs Current Density. Run No. 4

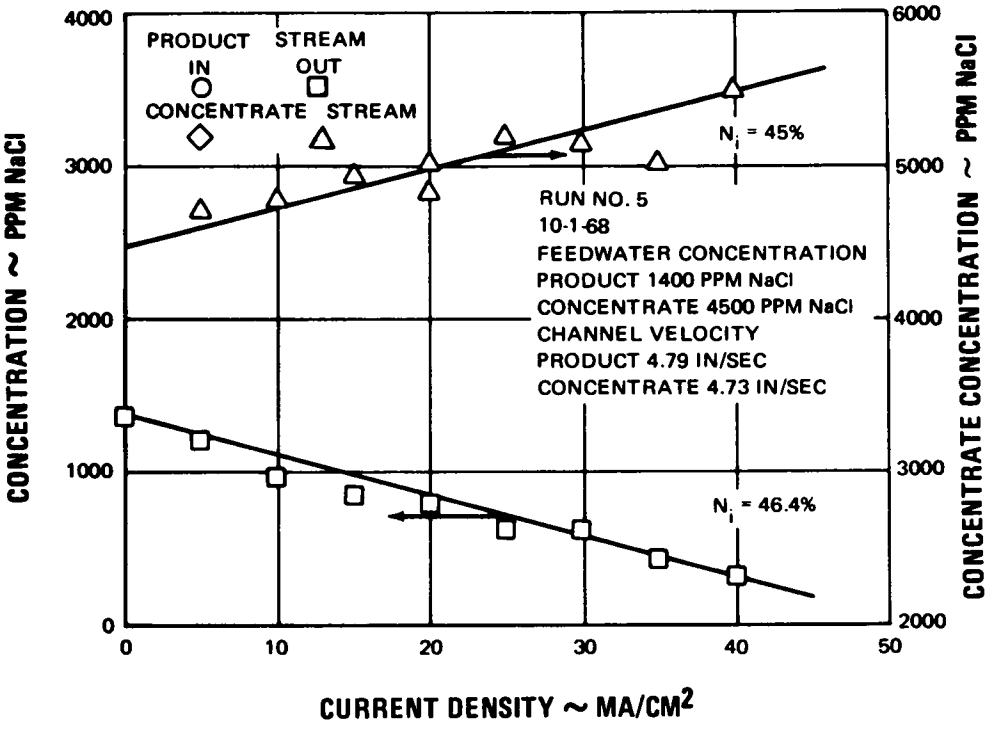

Figure 78 Five-Cell-Pair Stack Titration Data. Concentration vs Current Density. Run No. 5

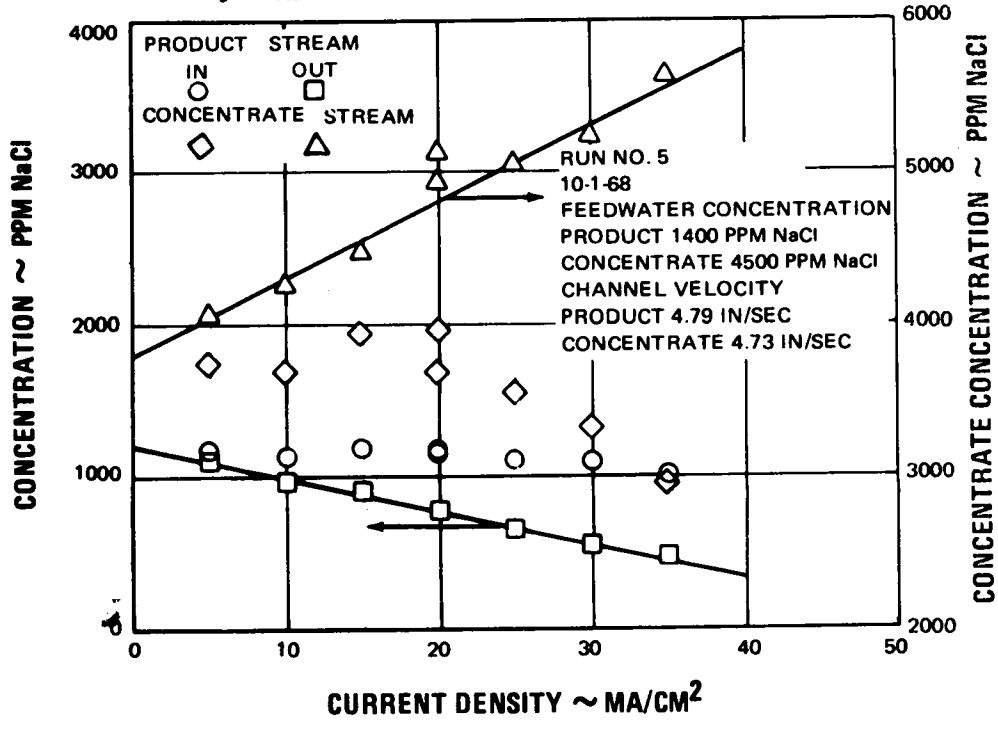

Figure 79 Five-Cell-Pair Stack Conductivity Data. Concentration vs Current Density. Run No. 5

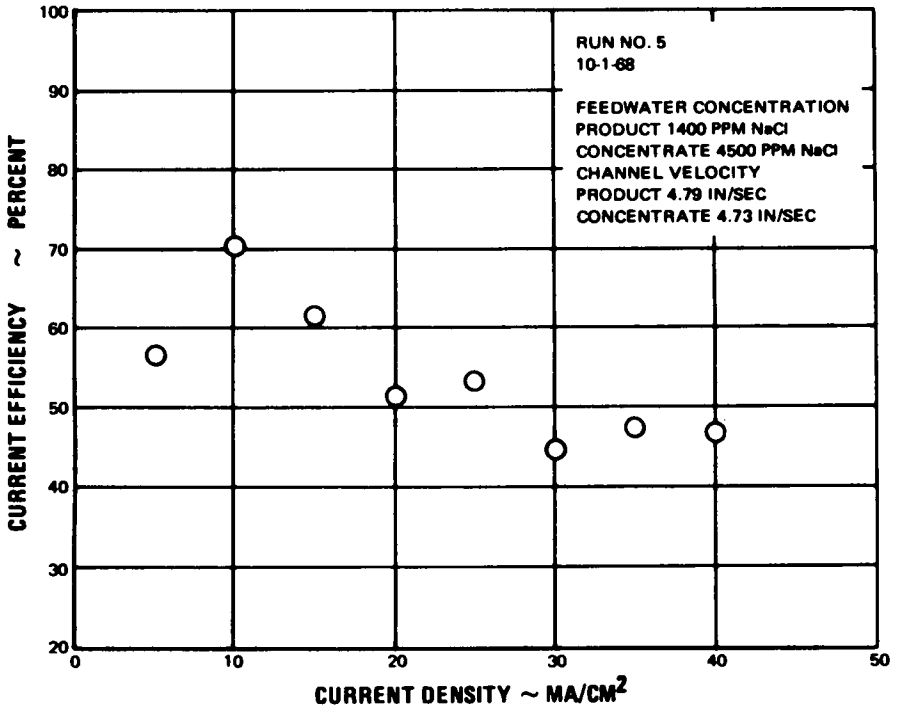

Figure 80 Five-Cell-Pair Stack Product-Stream Titration Results. Current Efficiency vs Current Density. Run No. 5

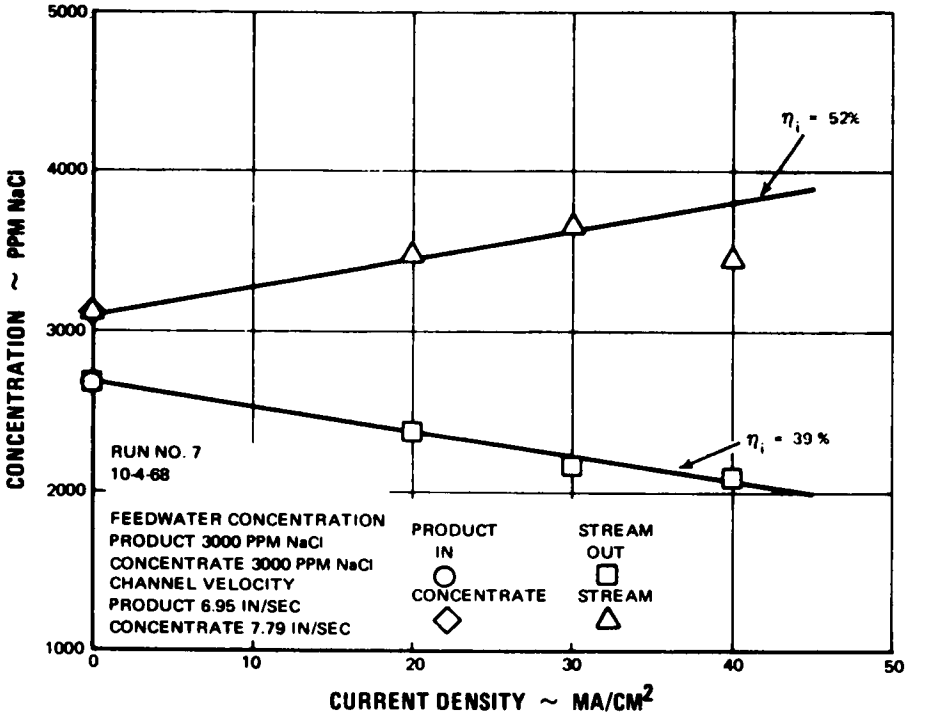

Figure 81 Five-Cell-Pair Stack Titration Data. Concentration vs Current Density. Run No. 7

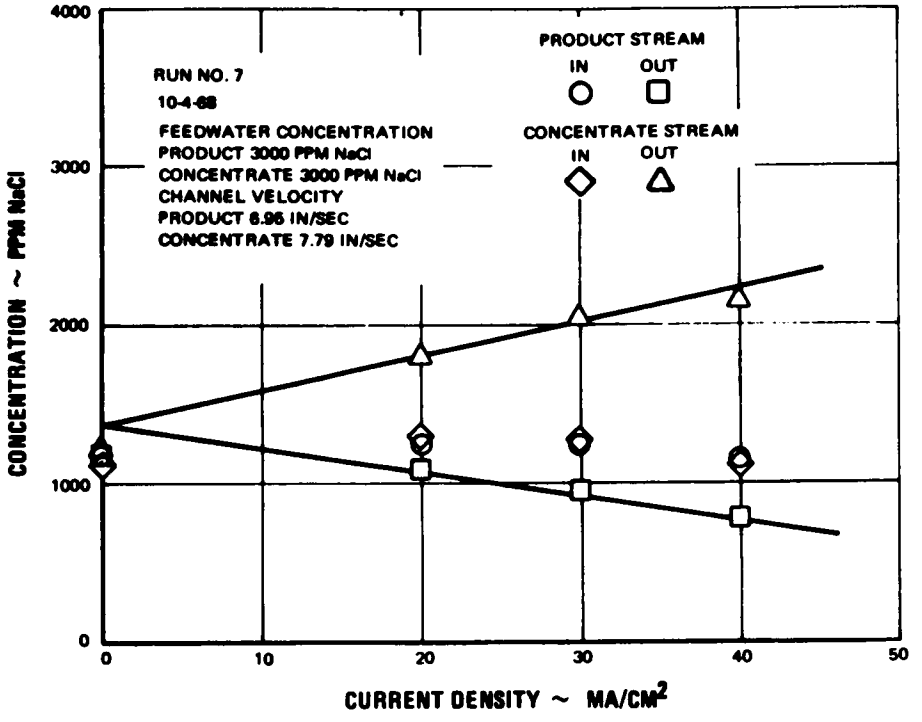

Figure 82 Five-Cell-Pair Stack Conductivity Data. Concentration vs Current Density. Run No. 7

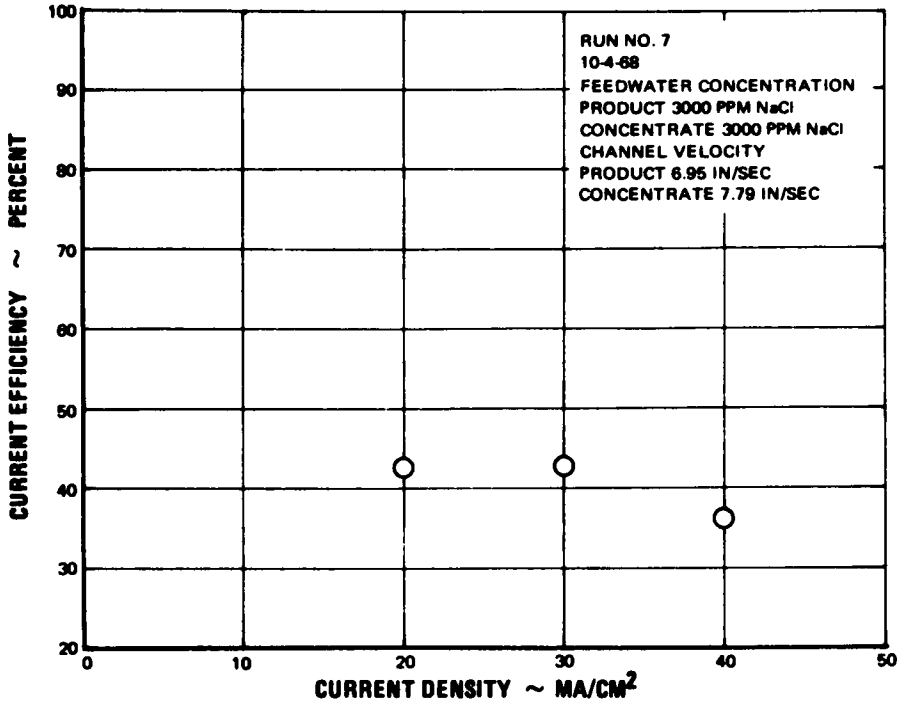

Figure 83 Five-Cell-Pair Stack Product-Stream Titration Results. Current Efficiency vs Current Density. Run No. 7

several areas that separation removed sufficient resin material from the cation membrane to expose the cloth backing and preclude their reuse. No similar adhesion was noted between the neutral membranes and spacers and they appeared to be quite reusable.

7) Several small changes to the stack were made as a result of the five-cell-pair tests and subsequent teardown and inspection. To preclude gasket extrusion from blocking the rinse-stream inlets and exits, the 60-mil thick rubber gasket was replaced with a 15-mil rubber gasket in the forty-cell-pair stack assembly. Also the new gasket was relieved (cut back) about 60 mils in the areas of the rinse-stream ports. The rinse stream inlet and exit ports in the endplates were enlarged from 0.093-inch to 0.129-inch diameter to lessen the possibility of small solid particles blocking flow through the rinse-stream compartments. The enlarged holes should also reduce the pressure drop in these streams and improve the removal of gases generated at the electrodes.

B. Test Results of Forty-Cell-Pair Stack

1. Test Program

Table 6 outlines the test program accomplished on the forty-cell-pair stack. The test program was designed to determine the effects on stack performance of variations in path length,

TABLE 6

Test Program Forty-Cell-Pair Stack

Run No.	Path Length, Inches	Product-to-Waste Ratio	Channel Velocity, Inches/Sec	Stack Capacity, gpd	Current Density, ma/cm^2
1	134	4/1	2.0	4,030	5, 10, 12.5
2	134	4/1	3.0	6,100	5, 10, 15
3	134	4/1	3.9	7,840	5, 10, 15, 20, 25
4	134	4/1	4.95	10,000	5, 15, 20, 25, 30
5	134	4/1	5.75	11,650	5, 10, 15, 20, 25,
6	134	4/1	4.95	10,000	*
7	134	4/1	4.95	10,000	*
8	134	1/1	5.0	10,010	10, 20, 30
9	134	8/1	5.0	10,010	10, 20, 30
10	134	12/1	5.0	10,010	10, 20, 30
11	67	4/1	3.0	12,100	20, 30, 35
12	67	4/1	4.0	16,100	30, 40, 50
13	67	4/1	5.0	20,300	10, 20, 30, 40, 5(
14	67	4/1	5.0	20,300	*
15	67	4/1	5.0	20,300	*
16	67	1/1	5.0	20,300	30, 40, 50
17	67	8/1	5.0	20,100	30, 40, 50
18	67	12/1	5.0	20,300	30, 40, 50
19	33.5	4/1	2.0	16,250	15, 20, 25
20	33.5	4/1	3.0	24,200	30, 40, 50
21	33.5	4/1	3.6	28,800	30, 40, 50
22	33.5	4/1	3.6	28,800	*
23	33.5	4/1	3.6	28,800	*
24	33.5	1/1	3.6	28,800	30, 40, 50
25	33.5	8/1	3.6	28,800	30, 40, 50
26	33.5	12/1	3.6	28,800	30, 40, 50

*Runs 6, 14 and 22 were intended to evaluate the effect of unbalanced pressures between the product and concentrate streams, the product-stream pressure being greater. Runs 7, 15, and 23 were intended to evaluate the effect of unbalanced pressures between the product and concentrate streams, the concentrate-stream pressure being greater. Significant pressure differences between the two streams could not be established.

Note: All runs were made using a nominal 3000 ppm NaCl feed solution.

channel velocity, product-to-waste ratio, current density, and pressure differentials between the product and concentrate streams.

Three different path lengths (134, 67 and 33.5 inches) were run by making appropriate series or parallel connections between the four channels. The first set of runs was made with a stack header arrangement which provided series flow of the product and concentrate streams through the four channels, creating an effective path length of 134 inches. The second set of runs was made with a path length of 67 inches. This path length was created by a header arrangement which provided parallel flow of the product and concentrate streams through the first two channels and the second two channels with series flow between these two sets of channels. The last set of runs was made with headers which connected all four channels in the product and concentrate streams in parallel, to provide a path length of 33.5 inches.

In all cases the electrode-rinse stream headers were arranged to provide parallel solution flow through the electrode compartments. This was done primarily to minimize the possibility of electrode reaction products, such as gases and pH shifts, from causing excessive electrode compartment resistance or interfering with the performance of the repeating-cell pairs.

Five different channel velocities were run with the 134-inch path length and three channel velocities with each of the other two path lengths.

Most of the runs were made with a product-to-waste flow-rate of 4 to 1. In addition, runs were made at one velocity for each path length with product-to-waste ratios of 1/1, 8/1, and 12/1.

At least three different current densities were included in each run to provide a total of over 69 steady-state data points from the tests. The maximum current density of 50 ma/cm^2 results from the power supply maximum current rating of 200 amperes. Higher current densities could be obtained by disconnecting and blocking off one or more channels in the stack.

Attempts were made to operate the stack with unequal pressure levels between the product and concentrate channels. This attempt was discontinued when it was discovered that no significant pressure differential could be established when equal channel velocities were maintained. This result is believed to be caused by movement of the membranes towards the channel having the lower pressure level. The resultant reduced flow area in the lower pressure channel causes an increased pressure loss in this channel, which in turn requires a higher inlet pressure level to maintain the same flow rate.

The maximum stack capacity tested was 28 800 gpd. This represents the pressure head/flow rate capacity of the main feed pumps. Higher capacities could be achieved by plumbing modifications designed to reduce the back pressure downstream of the stack.

2. Demineralization Performance

Figures 84 through 117 show the demineralization performance results listed in the order of the run numbers as shown in Table 6. The data from each run with the two longer path

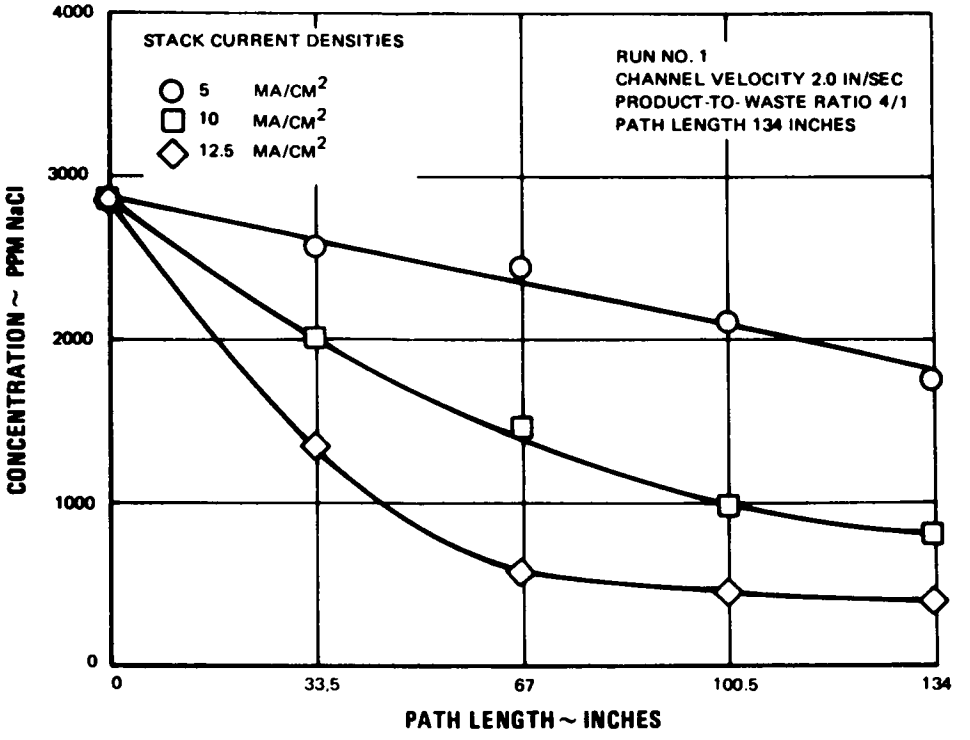

Figure 84 Forty-Cell-Pair Stack. Concentration vs Path Length. Run No. 1

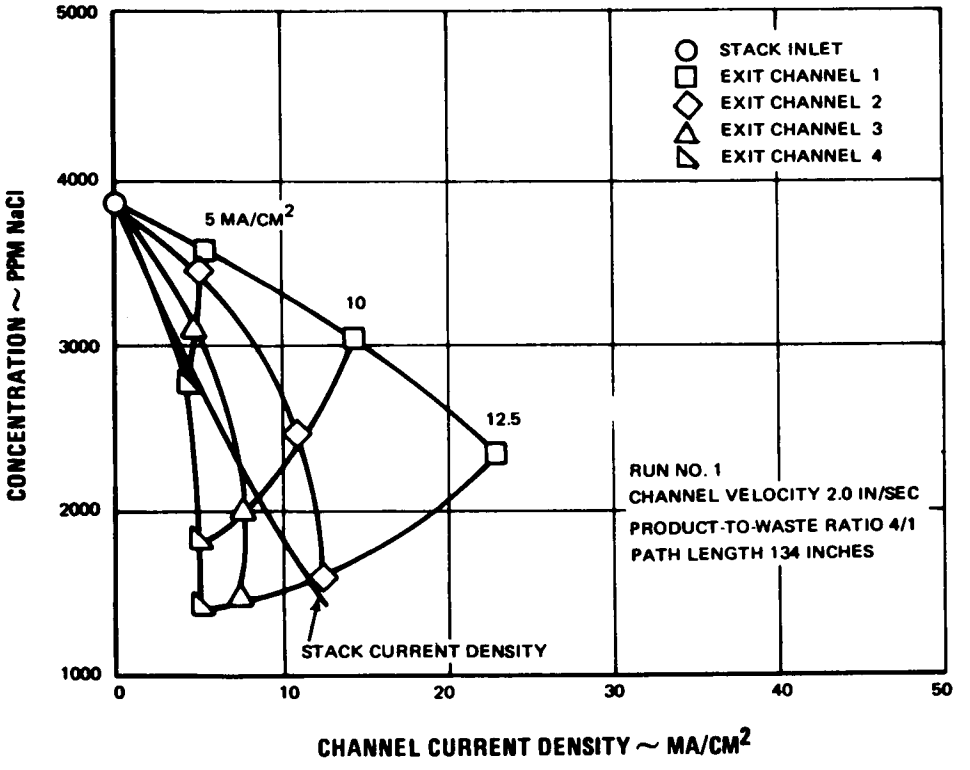

Figure 85 Forty-Cell-Pair Stack. Concentration vs Current Density. Run No. 1

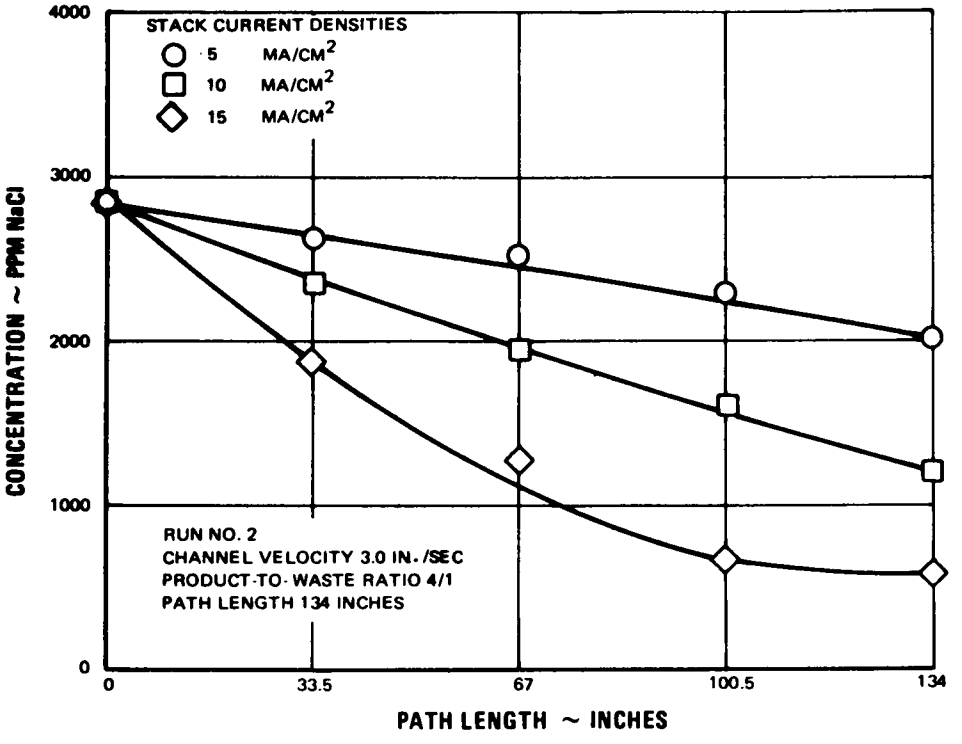

Figure 86 Forty-Cell-Pair Stack. Concentration vs Path Length. Run No. 2

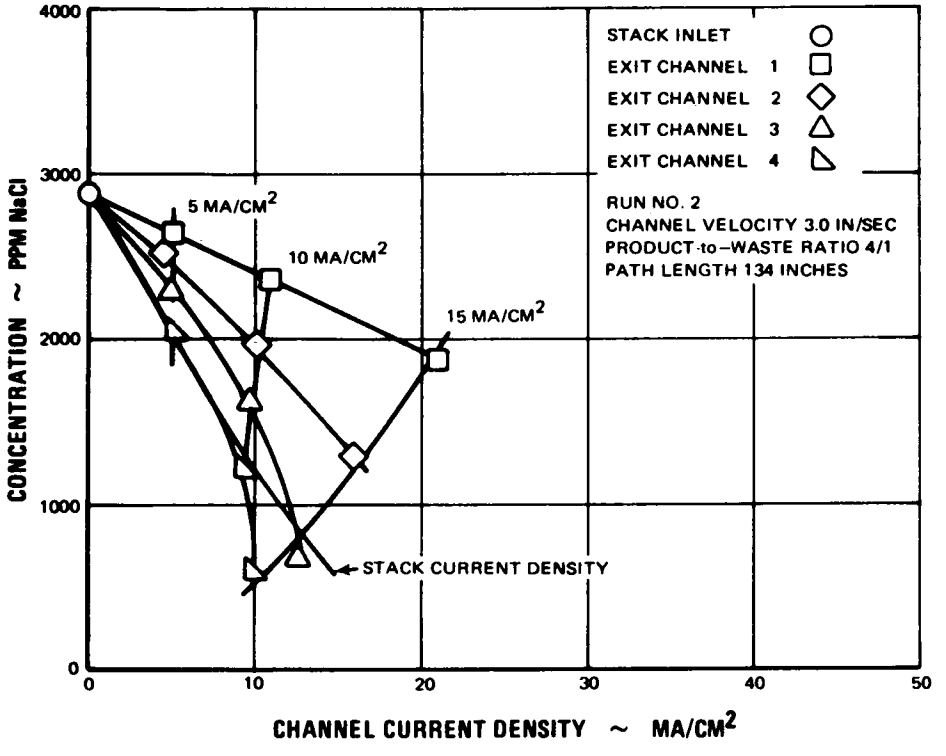

Figure 87 Forty-Cell-Pair Stack. Concentration vs Current Density. Run No. 2

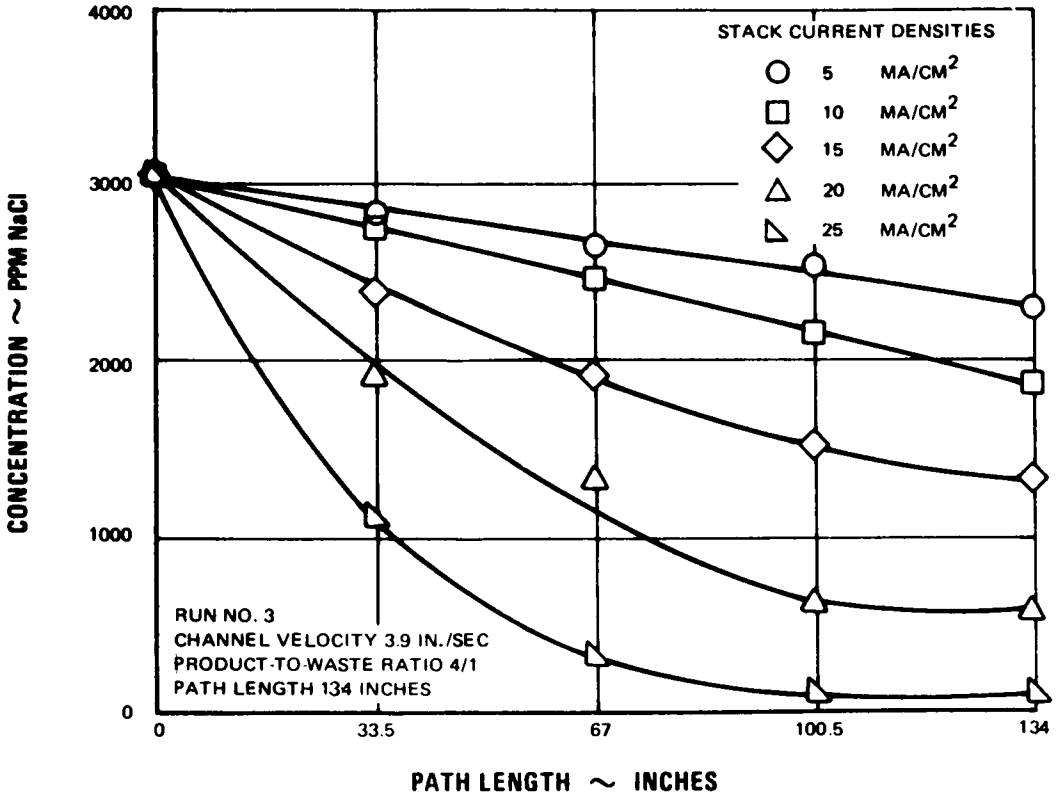

Figure 88 Forty-Cell-Pair Stack. Concentration vs Path Length. Run No. 3

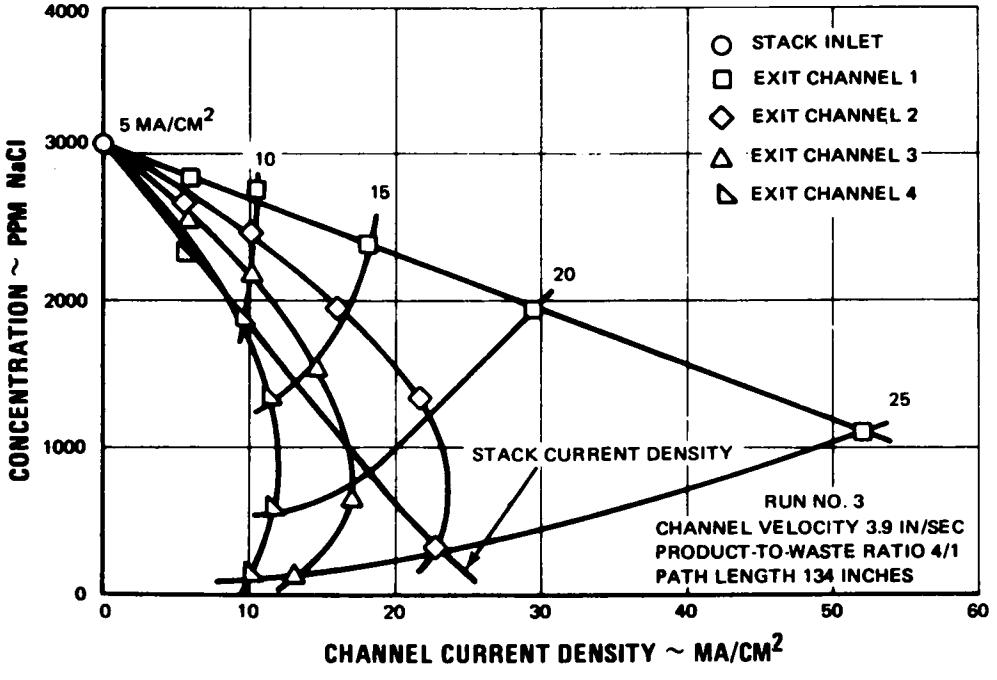

Figure 89 Forty-Cell-Pair Stack. Concentration vs Current Density. Run No. 3

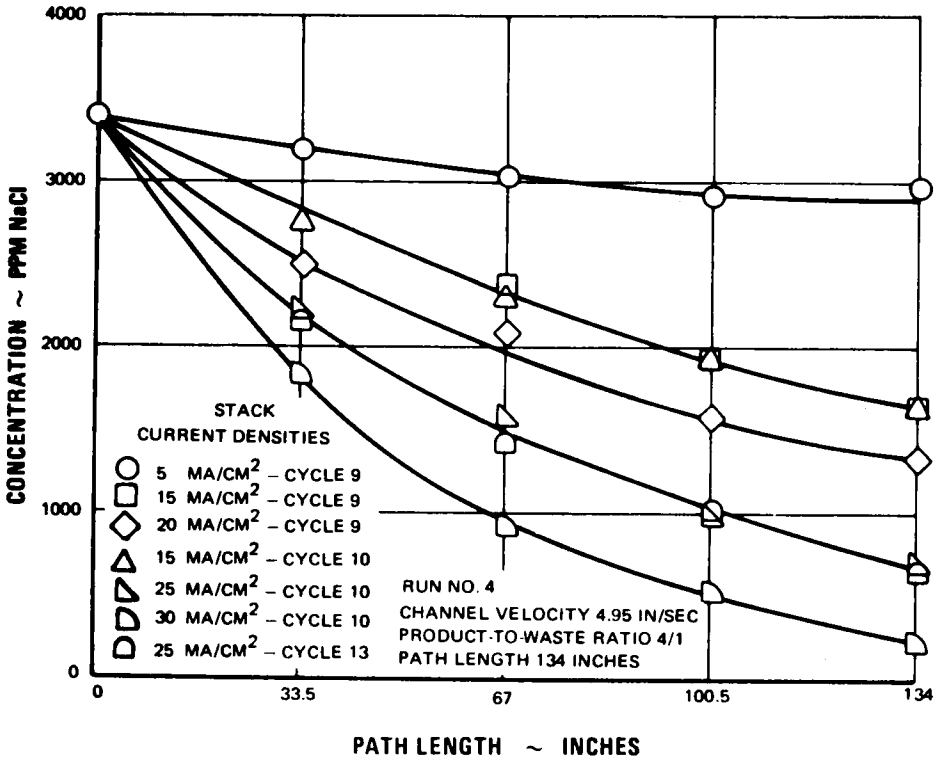

Figure 90 Forty-Cell-Pair Stack. Concentration vs Path Length. Run No. 4

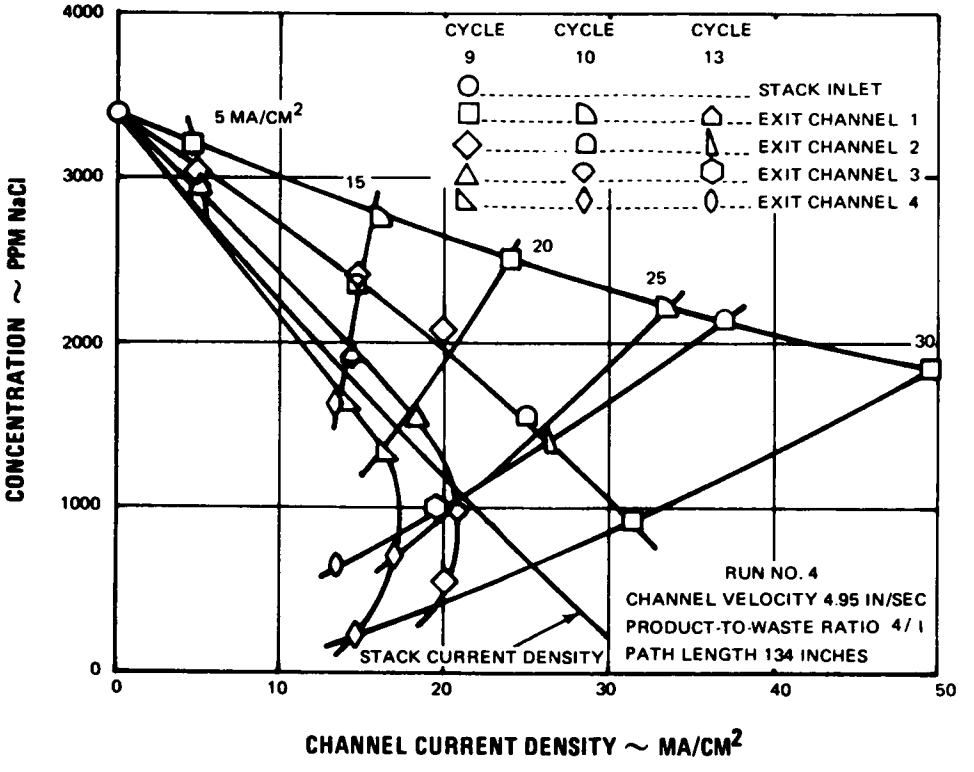

Figure 91 Forty-Cell-Pair Stack. Concentration vs Current Density. Run No. 4

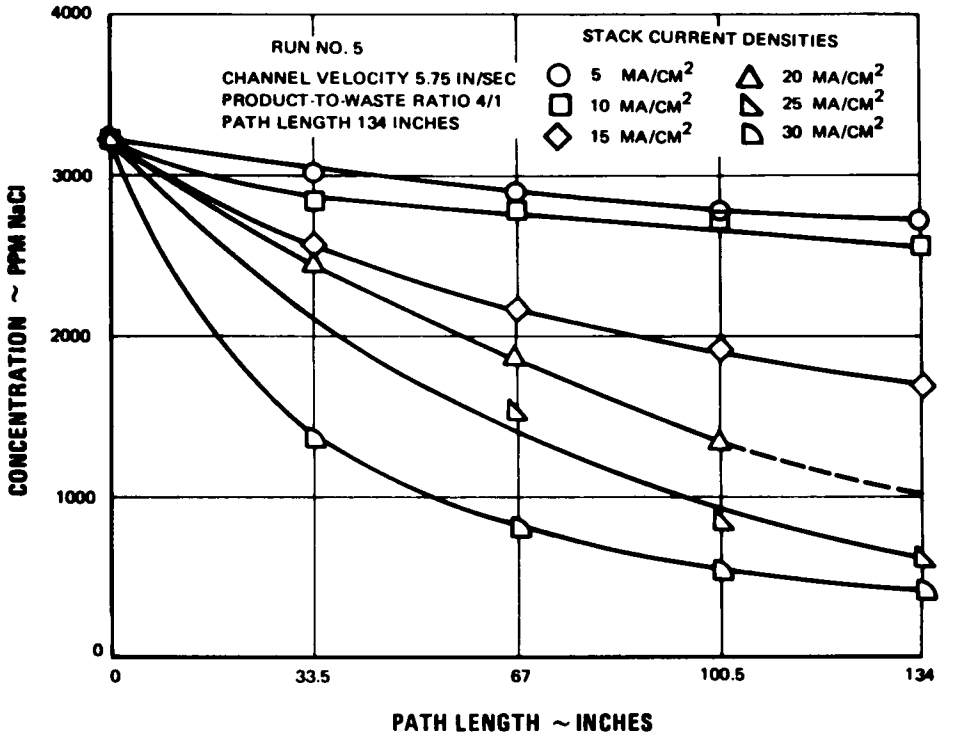

Figure 92 Forty-Cell-Pair Stack. Concentration vs Path Length. Run No. 5

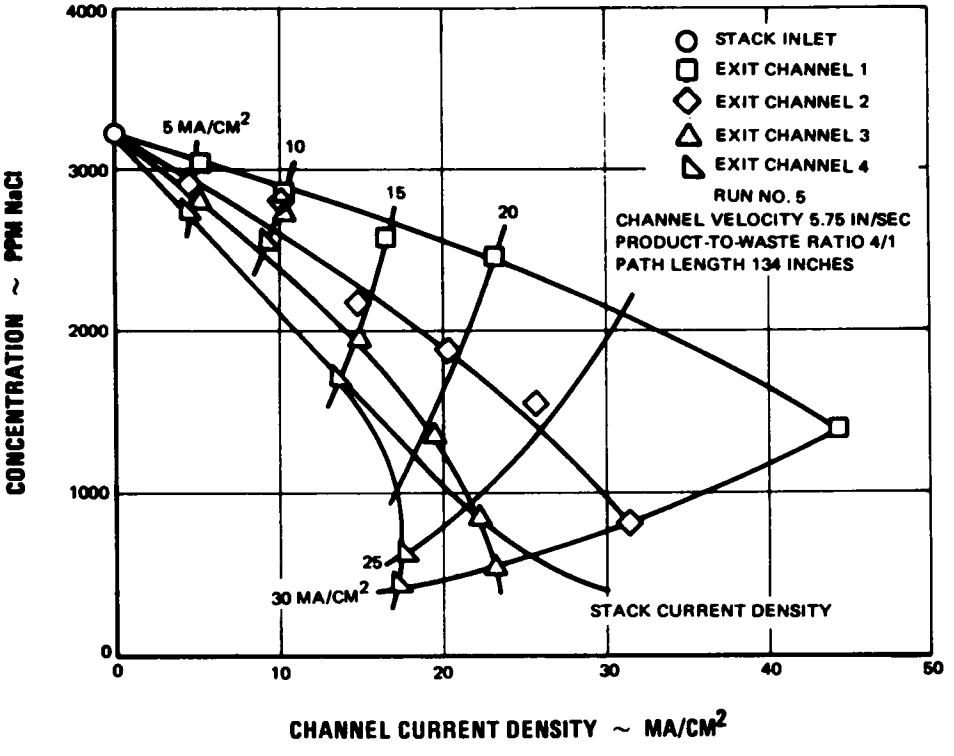

Figure 93 Forty-Cell-Pair Stack. Concentration vs Current Density. Run No. 5

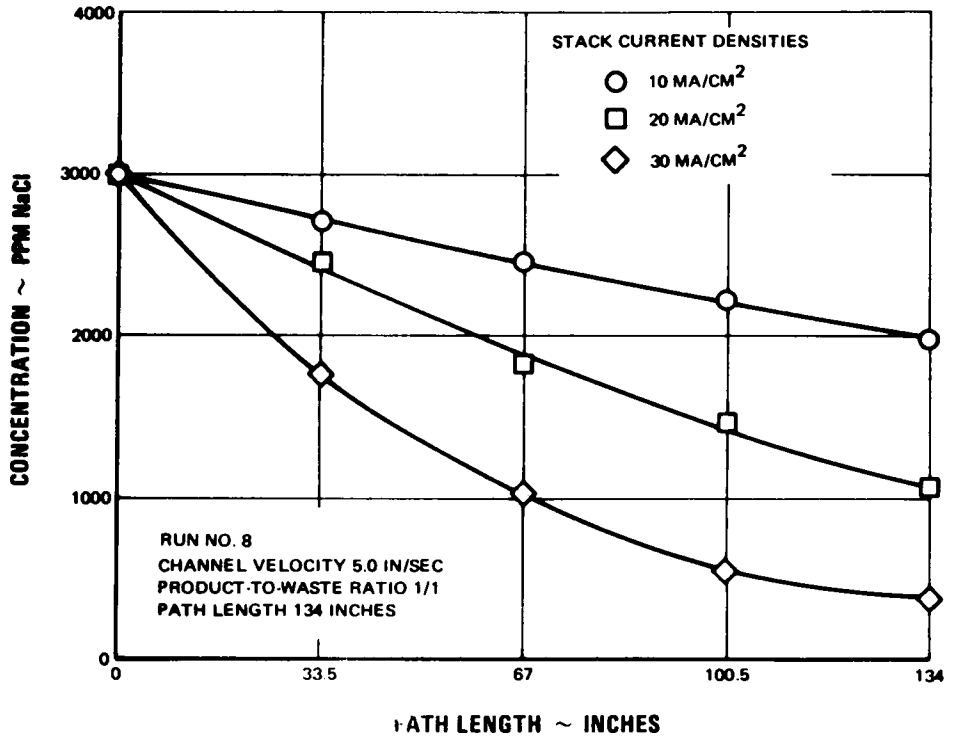

Figure 94 Forty-Cell-Pair Stack. Concentration vs Path Length. Run No. 8

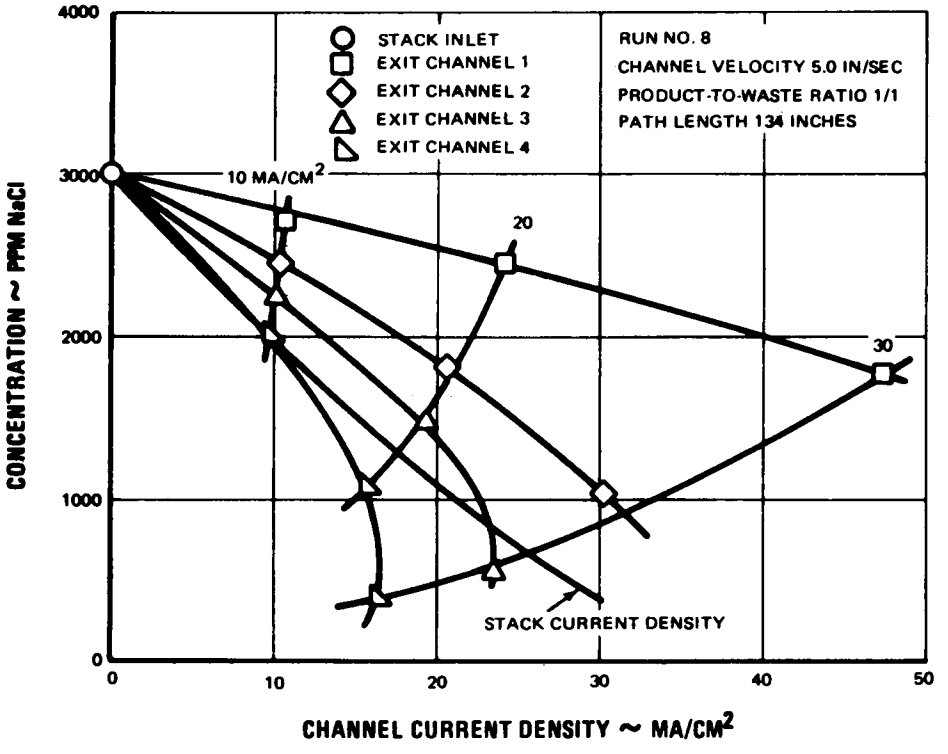

Figure 95 Forty-Cell-Pair Stack. Concentration vs Current Density. Run No. 8

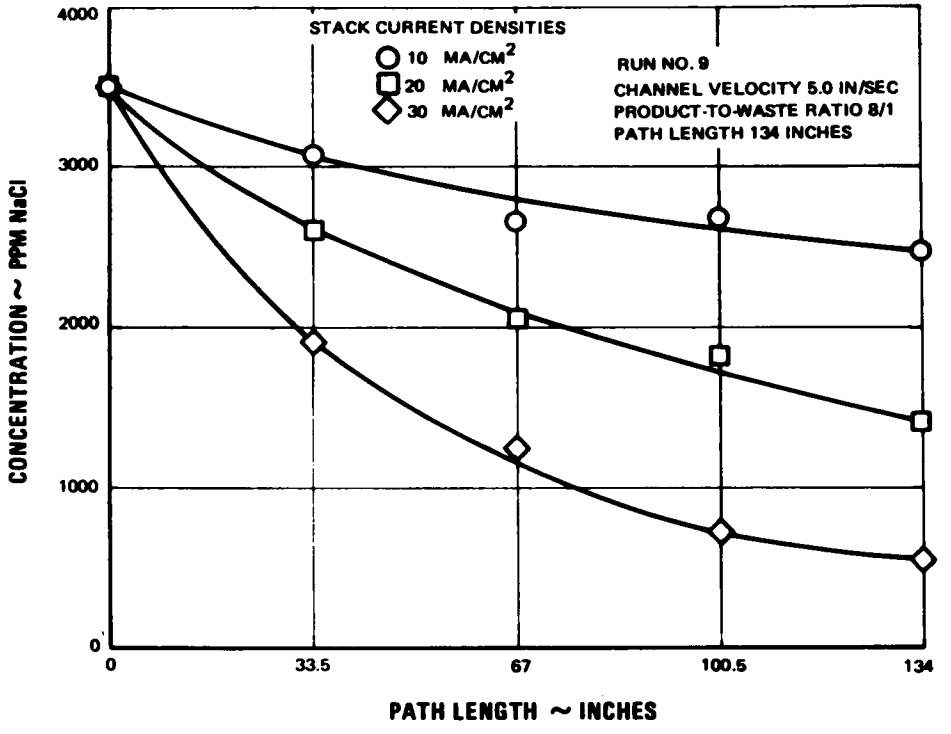

Figure 96 Forty-Cell-Pair Stack. Concentration vs Path Length. Run No. 9

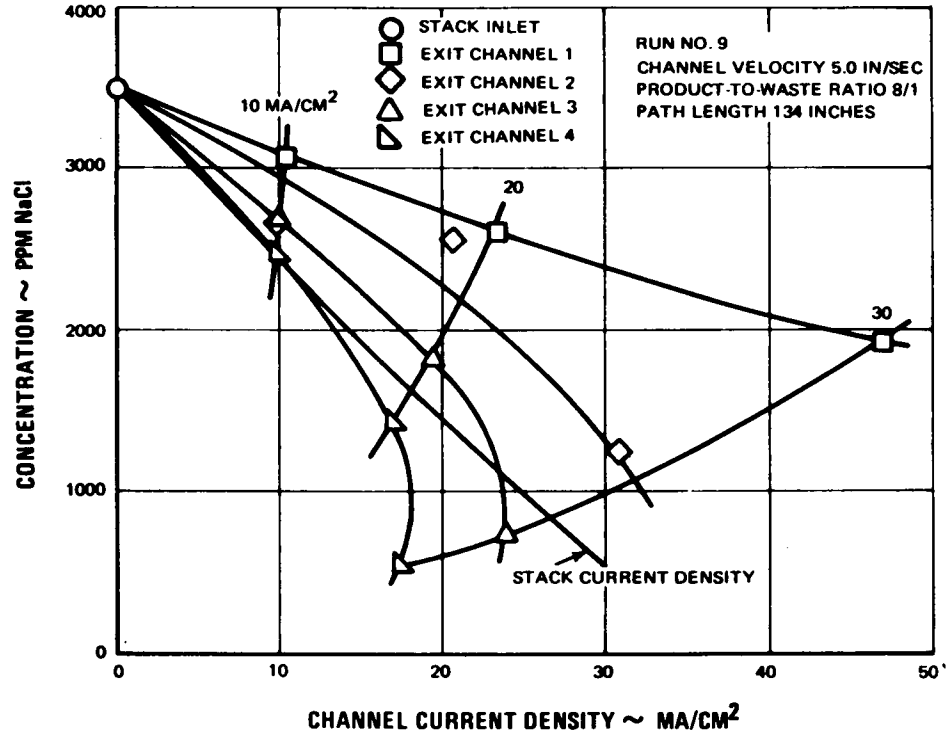

Figure 97 Forty-Cell-Pair Stack. Concentration vs Current Density. Run No. 9

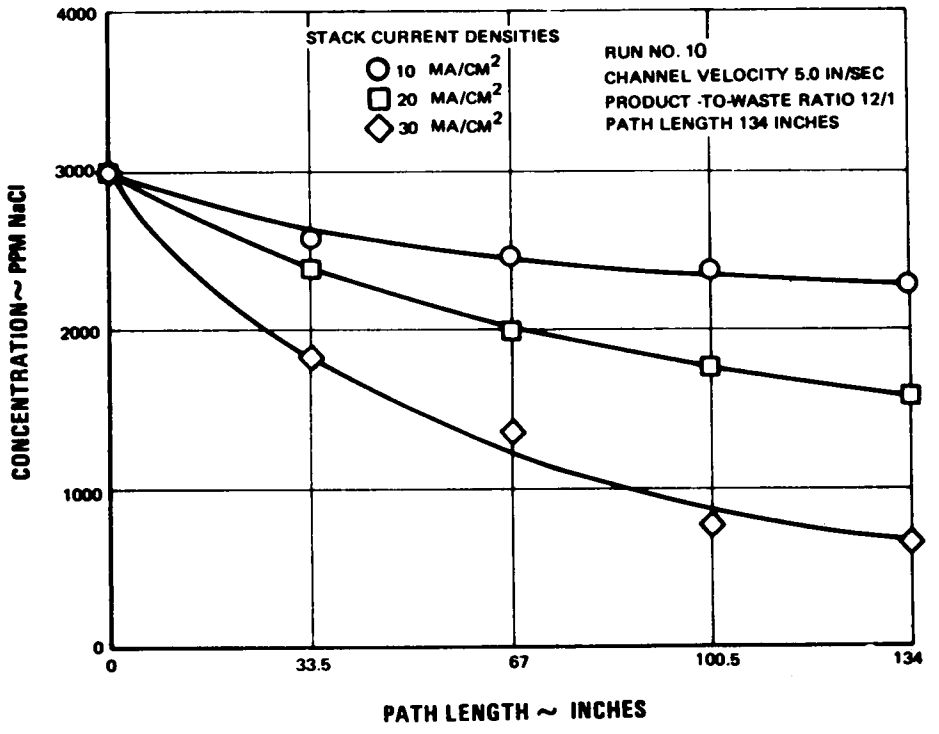

Figure 98 Forty-Cell-Pair Stack. Concentration vs Path Length. Run No. 10

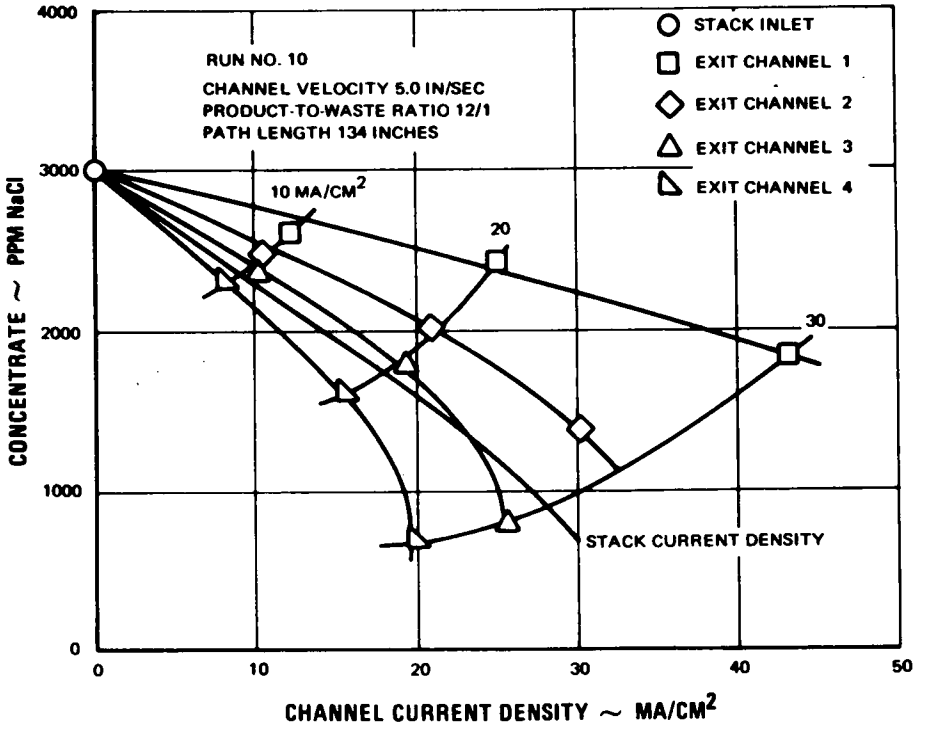

Figure 99 Forty-Cell-Pair Stack. Concentration vs Current Density. Run No. 10

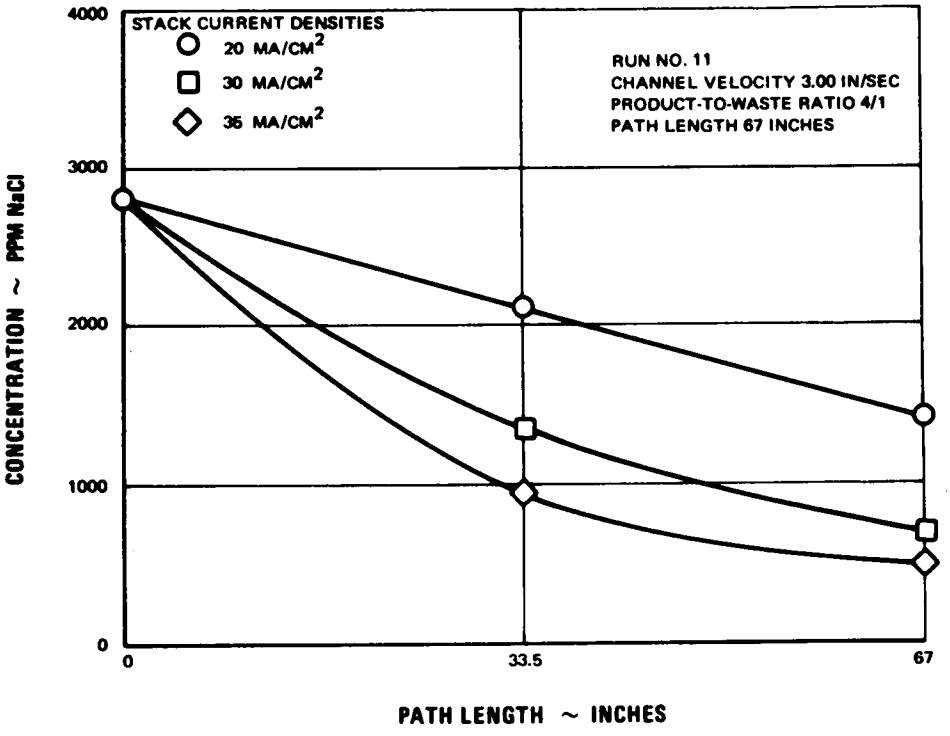

Figure 100 Forty-Cell-Pair Stack. Concentration vs Path Length. Run No. 11

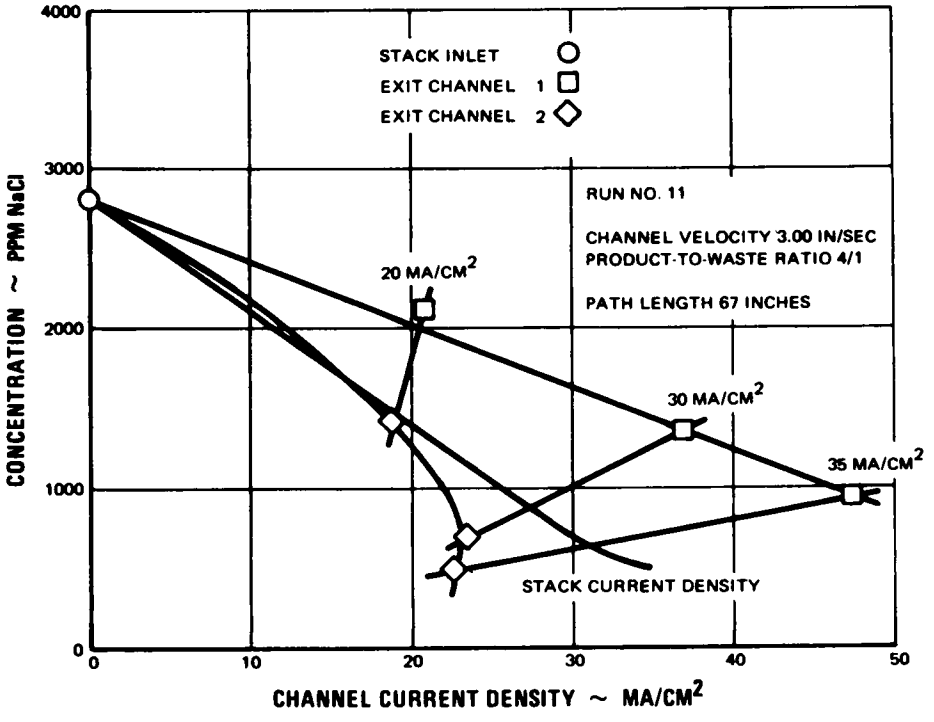

Figure 101 Forty-Cell-Pair Stack. Concentration vs Current Density. Run No. 11

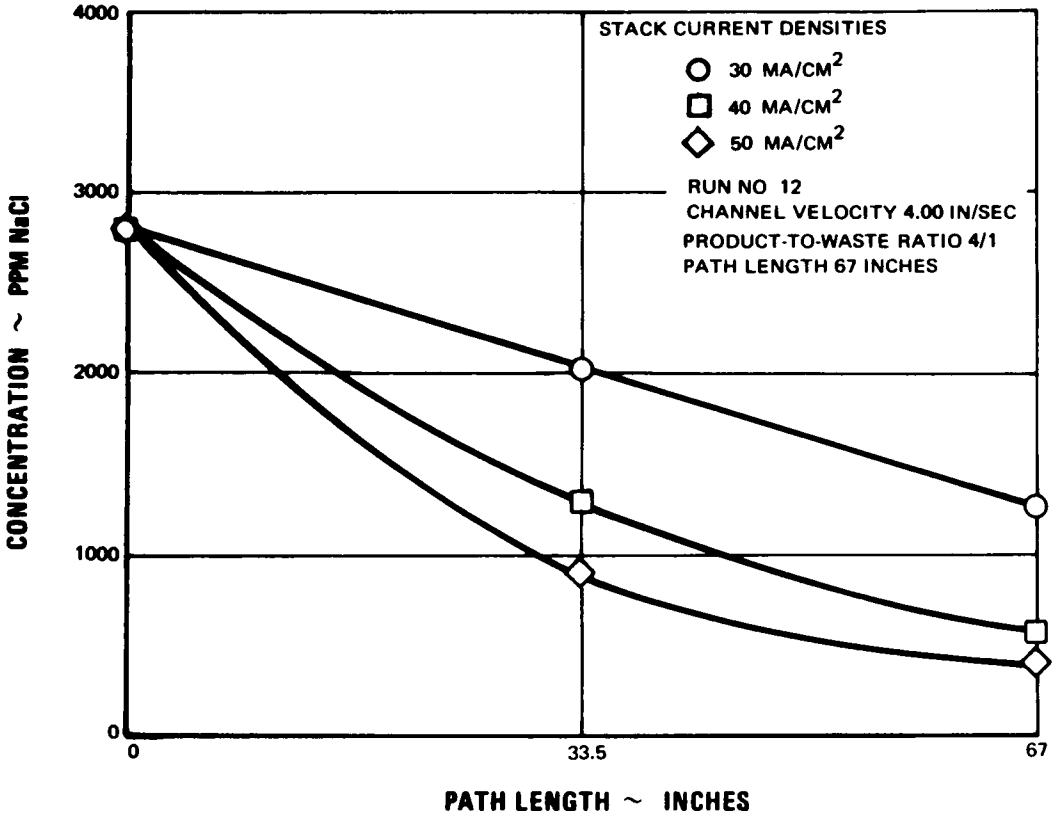

Figure 102 Forty-Cell-Pair Stack. Concentration vs Path Length. Run No. 12

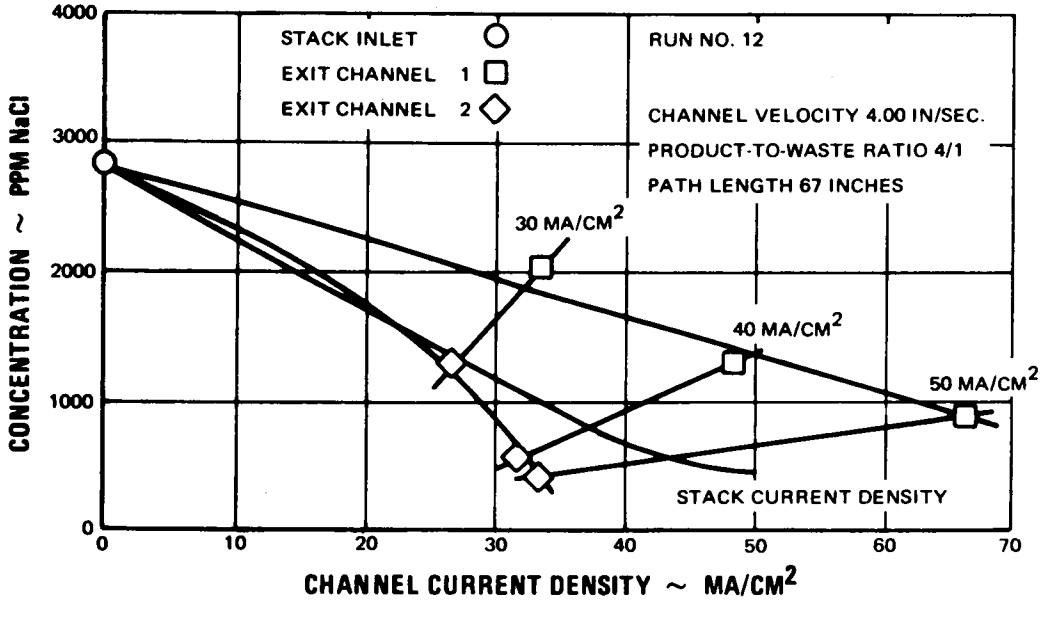

Figure 103 Forty-Cell-Pair Stack. Concentration vs Current Density. Run No. 12

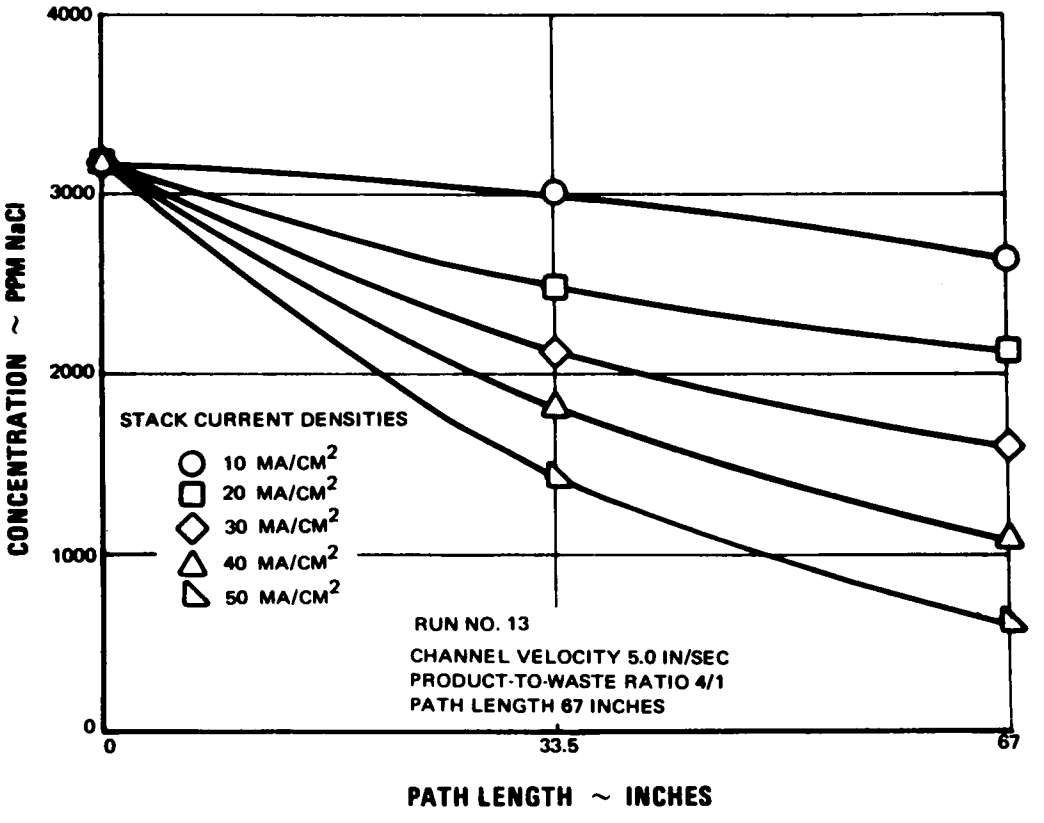

Figure 104 Forty-Cell-Pair Stack. Concentration vs Path Length. Run No. 13

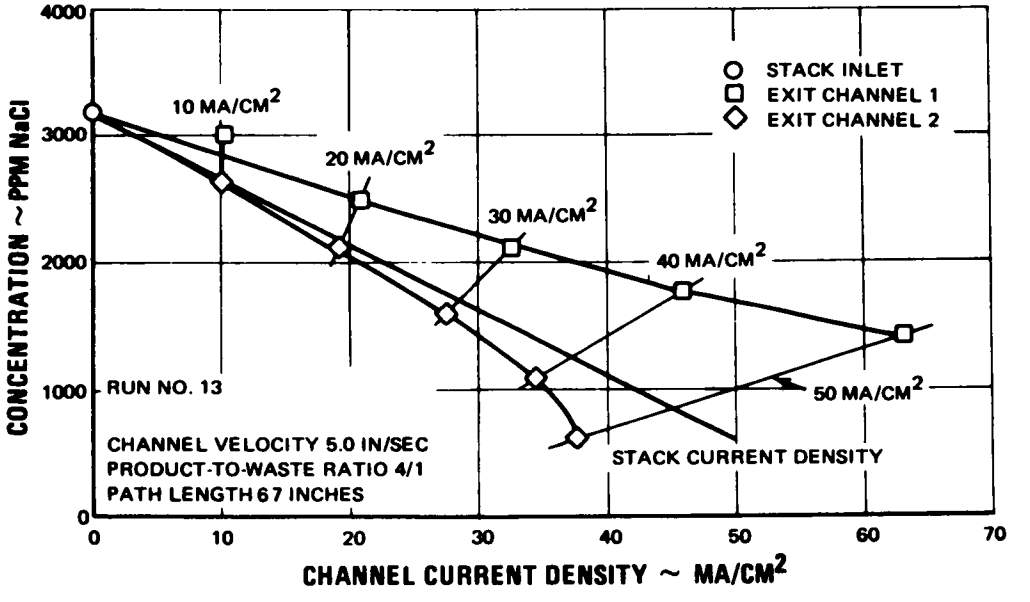

Figure 105 Forty-Cell-Pair Stack. Concentration vs Current Density. Run No. 13

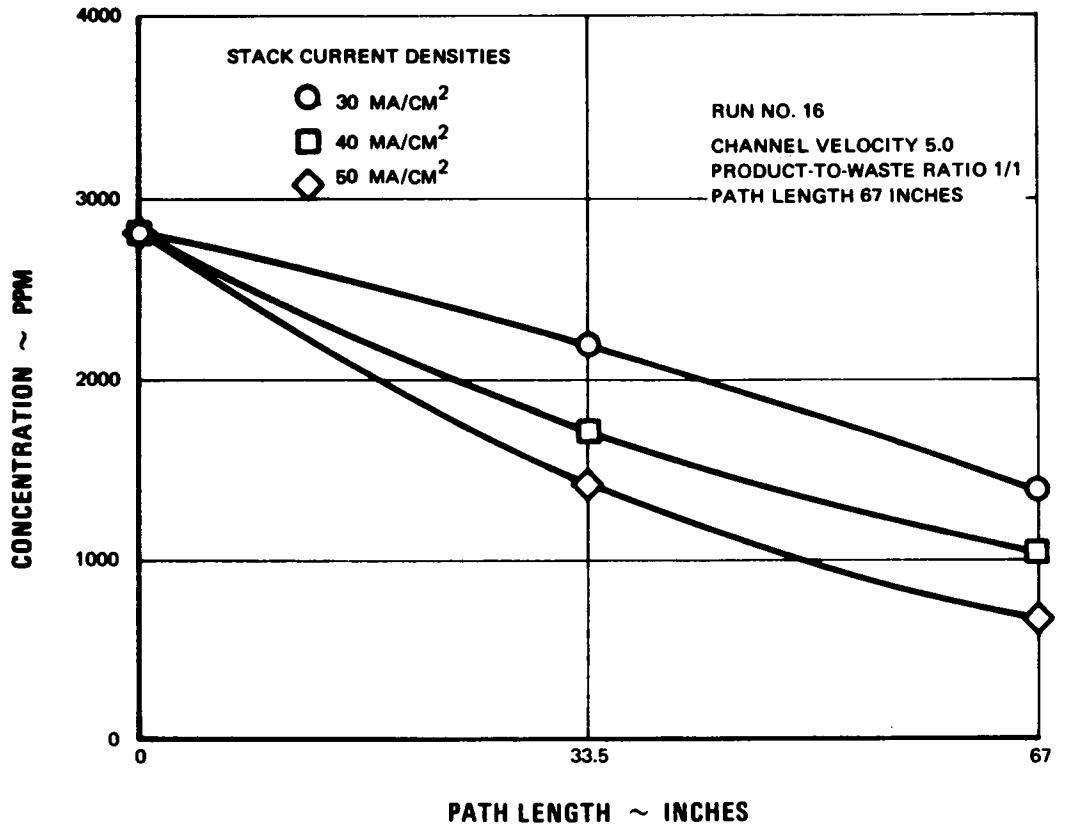

Figure 106 Forty-Cell-Pair Stack. Concentration vs Path Length. Run No. 16

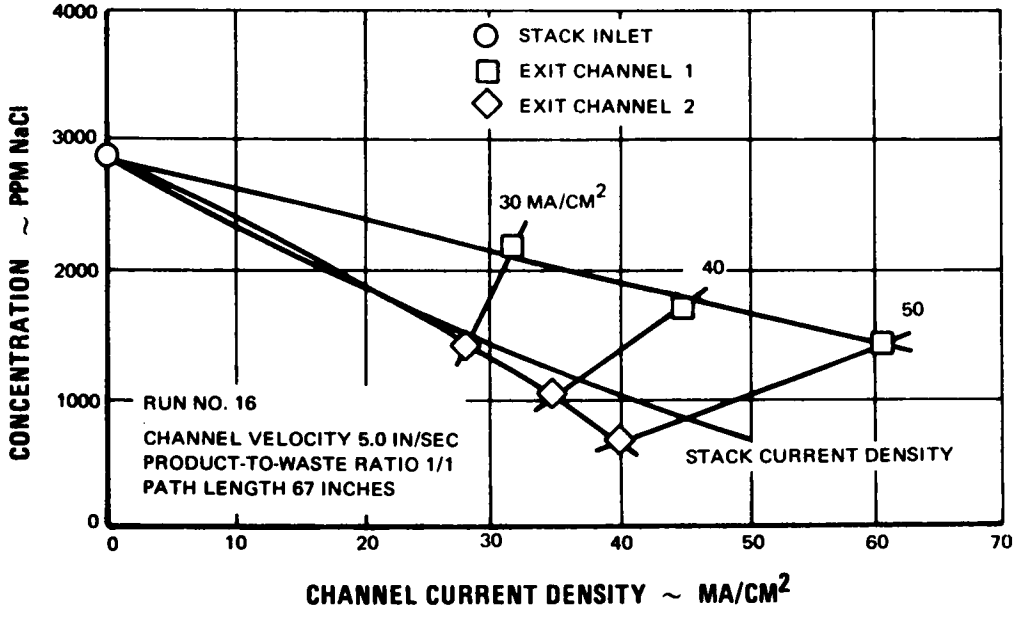

Figure 107 Forty-Cell-Pair Stack. Concentration vs Current Density. Run No. 16

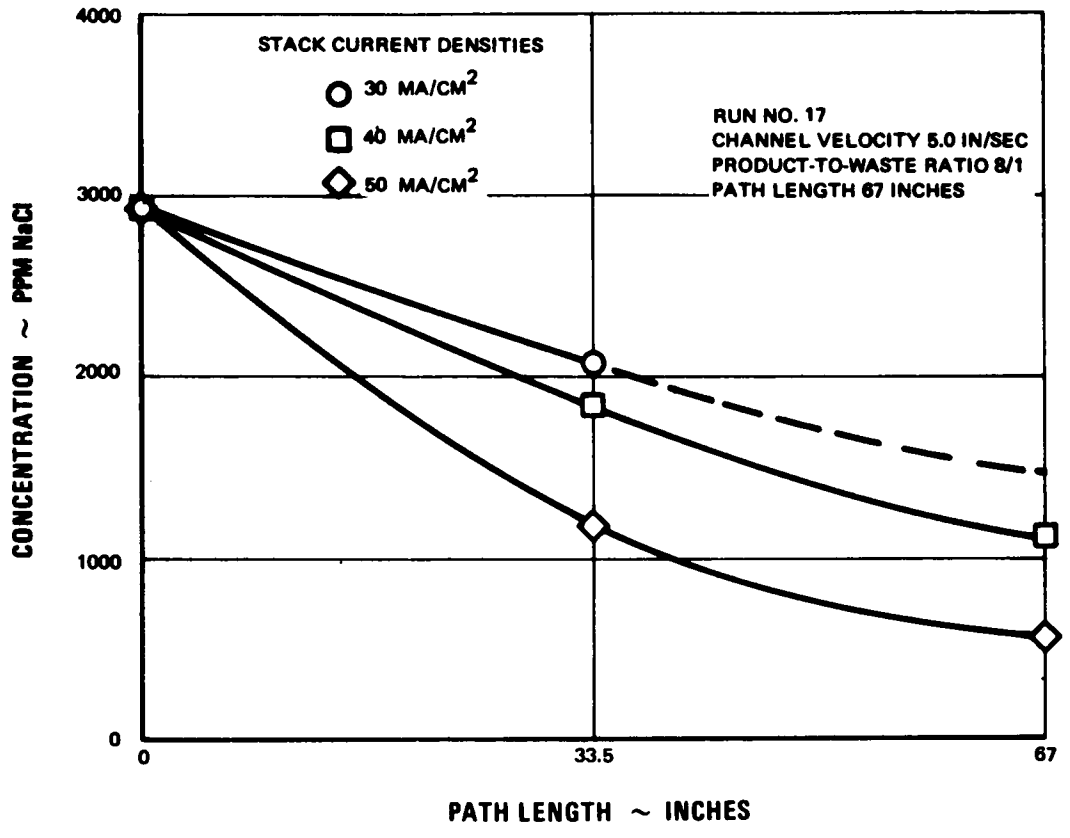

Figure 108 Forty-Cell-Pair Stack. Concentration vs Path Length. Run No. 17

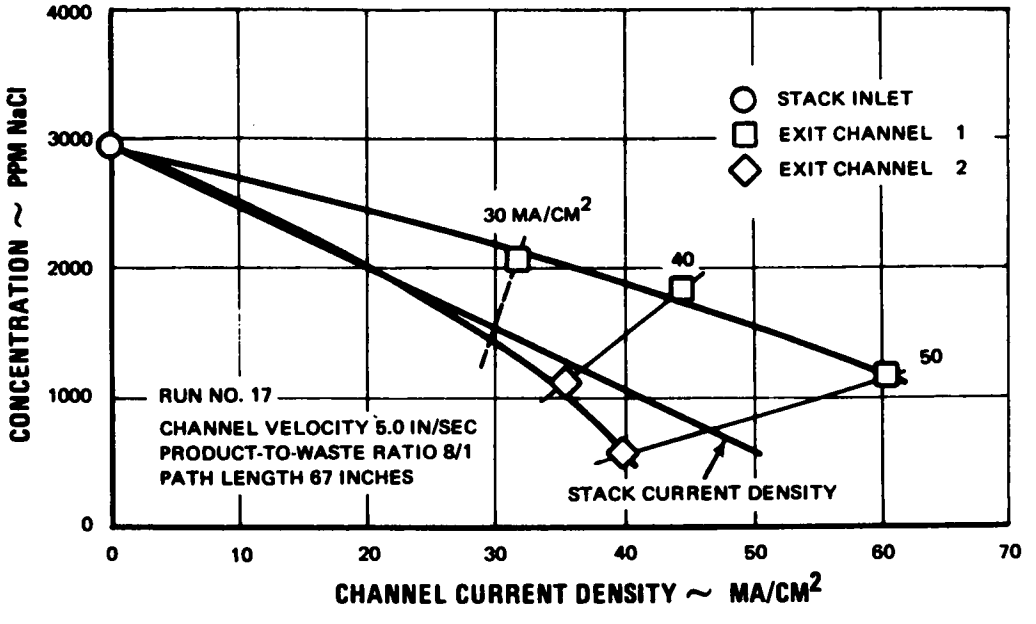

Figure 109 Forty-Cell-Pair Stack. Concentration vs Current Density. Run No. 17

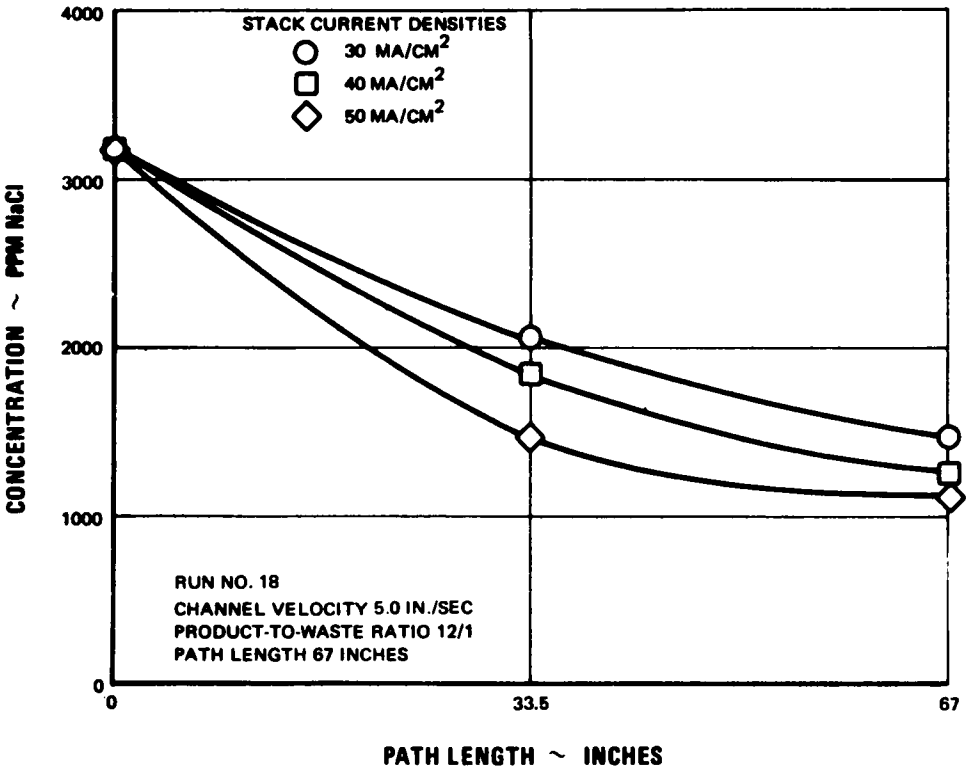

Figure 110 Forty-Cell-Pair Stack. Concentration vs Path Length. Run No. 18

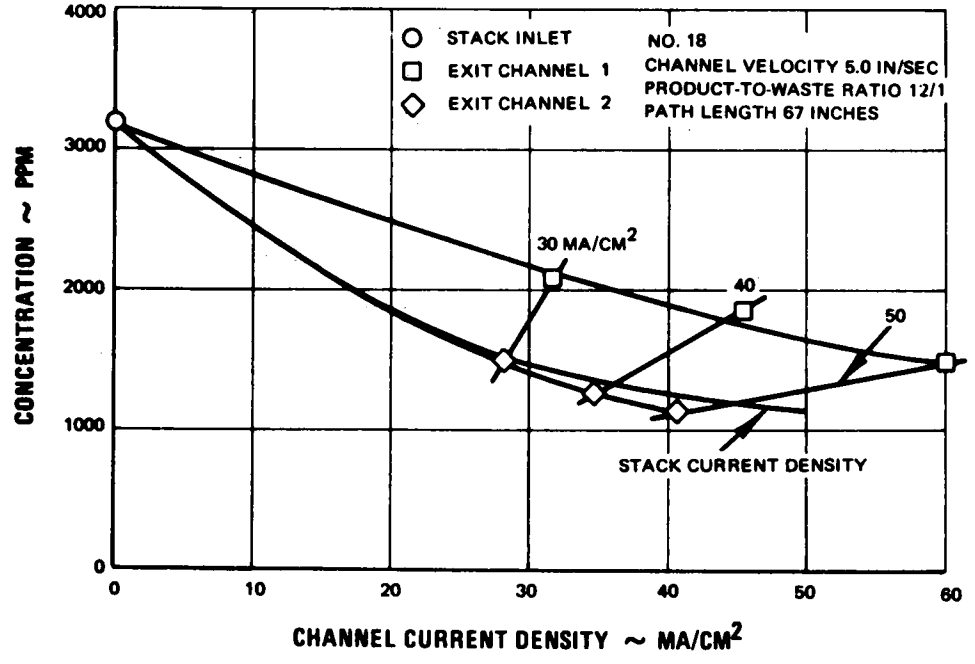

Figure 111 Forty-Cell-Pair Stack. Concentration vs Current Density. Run No. 18

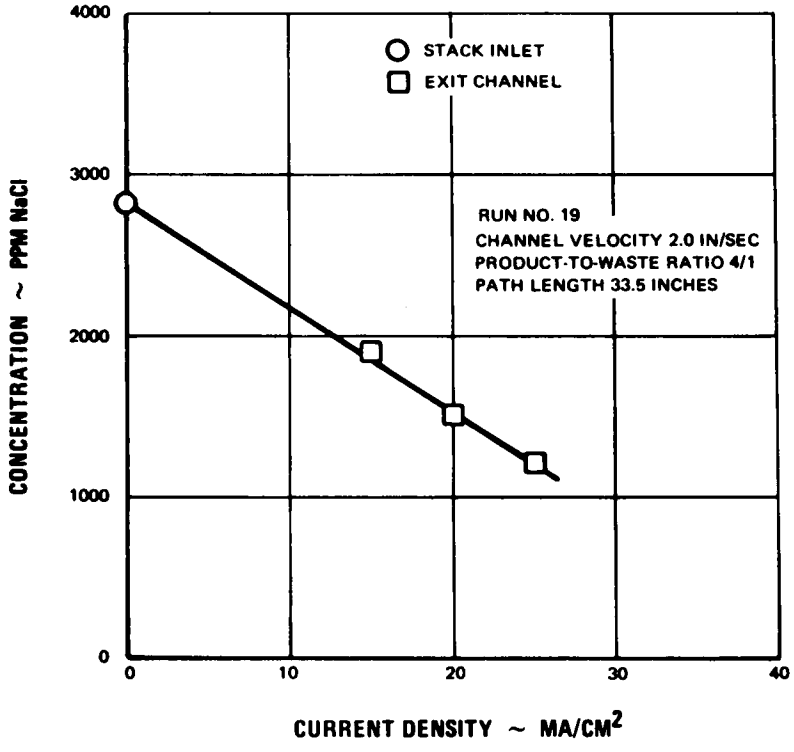

Figure 112 Forty-Cell-Pair Stack. Concentration vs Current Density. Run No. 19

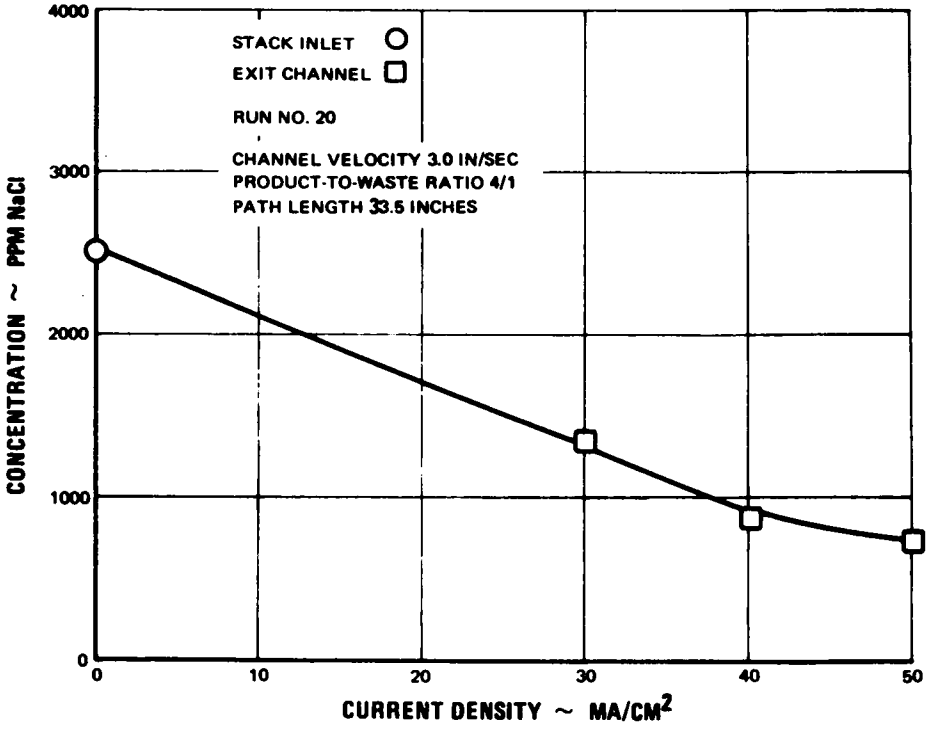

Figure 113 Forty-Cell-Pair Stack. Concentration vs Current Density. Run no No. 20

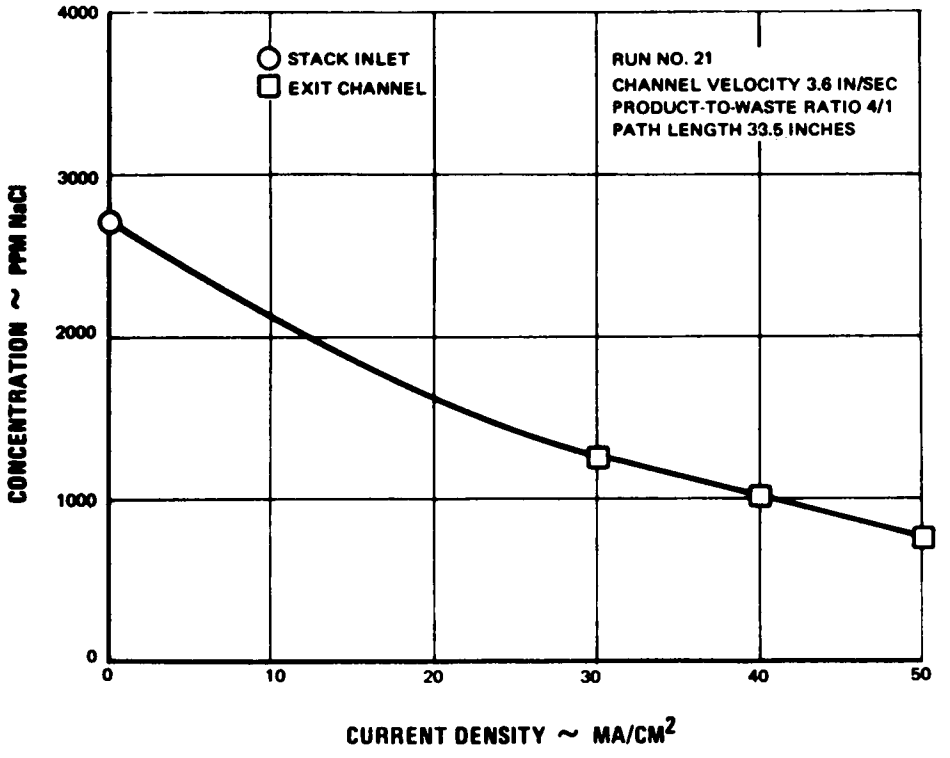

Figure 114 Forty-Cell-Pair Stack. Concentration vs Current Density. Run No. 21

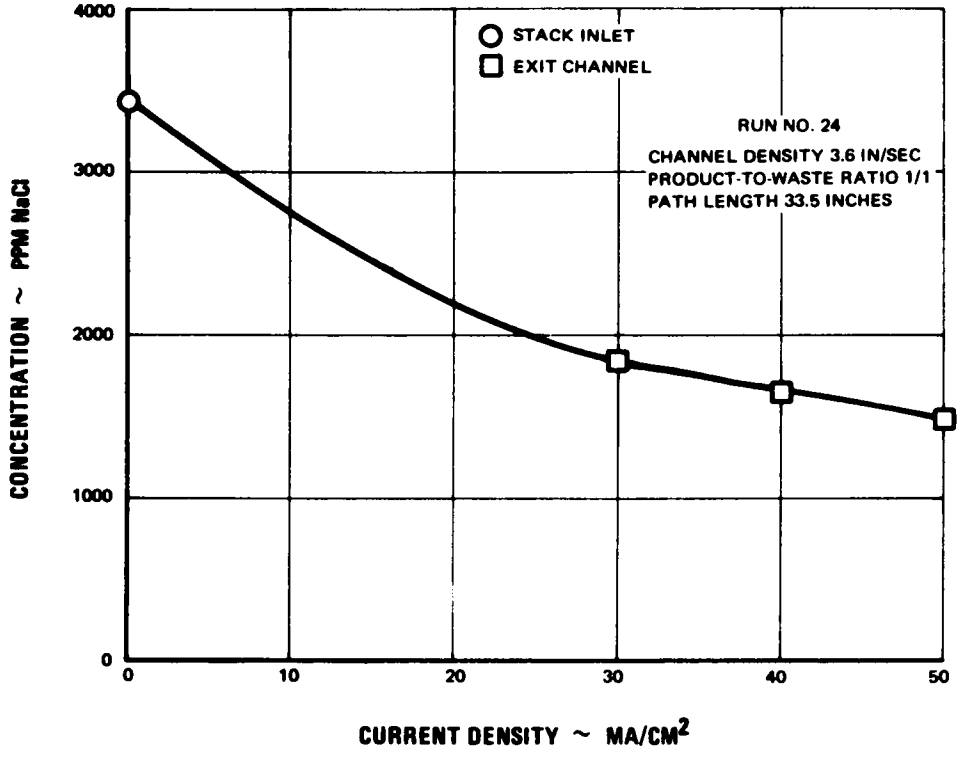

Figure 115 Forty-Cell-Pair Stack. Concentration vs Current Density. Run No. 24

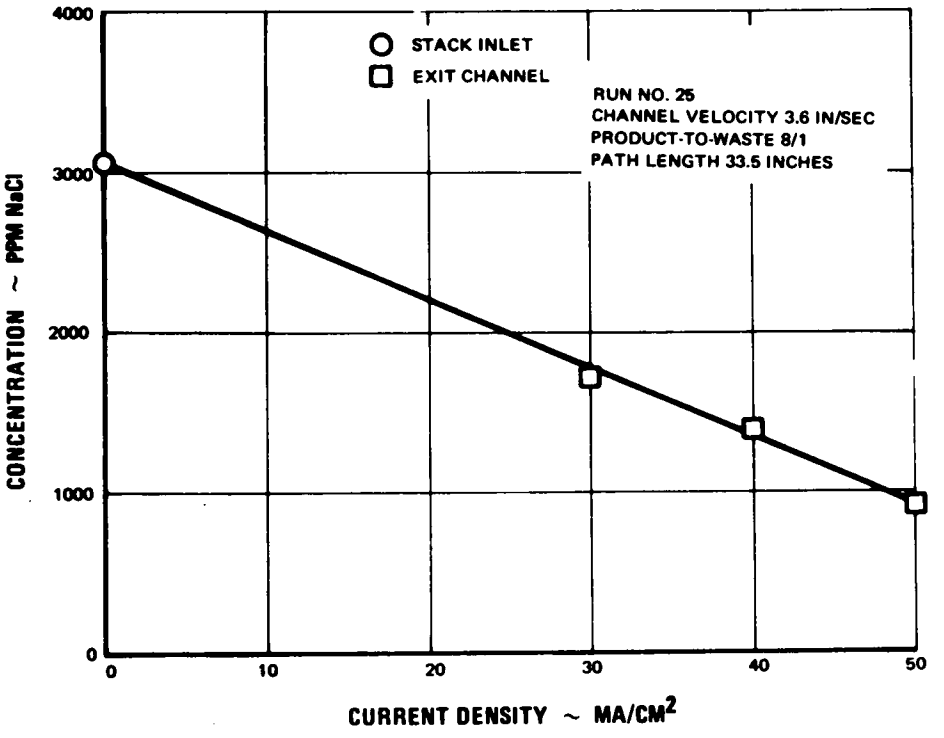

Figure 116 Forty-Cell-Pair Stack. Concentration vs Current Density. Run No. 25

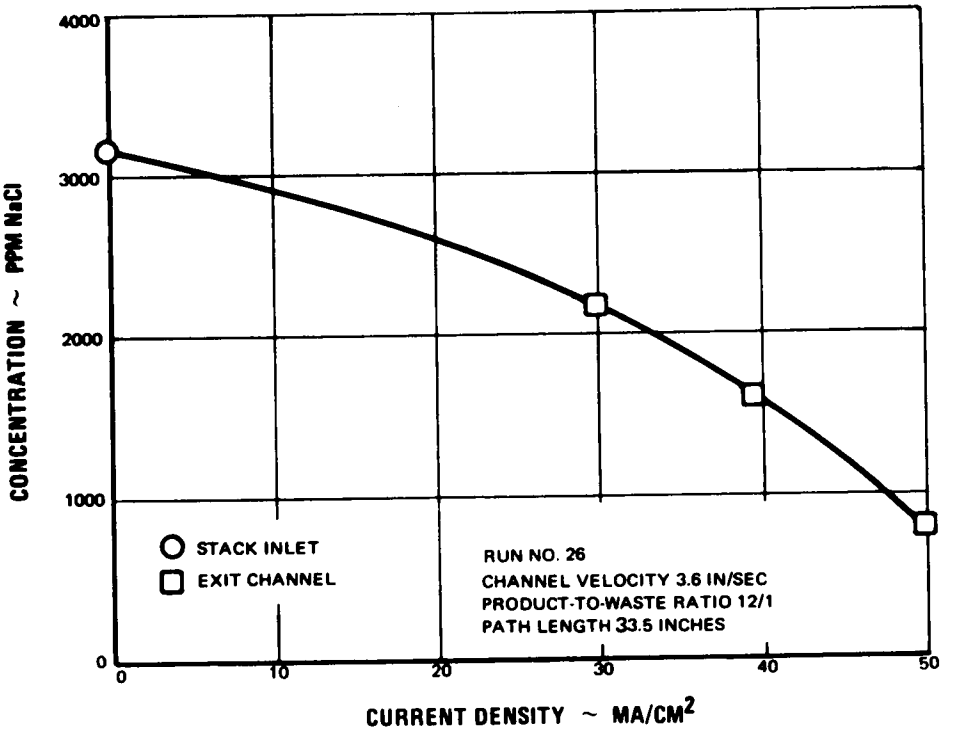

Figure 117 Forty-Cell-Pair Stack. Concentration vs Current Density. Run No. 26

lengths (134 and 67 inches) was plotted in two ways, concentration versus path length and concentration versus channel current density. The data from the runs using the shortest path length (33.5 inches) was plotted as concentration versus stack current density The data from the longer path lengths provide a good indication of the rate of demineralization and distribution of current density along the path length of the stack. As would be expected, the higher current densities and longer cuts occur at the beginning of the path length where the product stream concentration is the highest.

Seven of the twenty runs produced product-water concentrations below 500 ppm. Some nine of the remaining thirteen runs should have resulted in a product-water concentration below 500 ppm if a higher current density had been used. In most cases a current density above 50 ma/cm^2 would have been necessary, which is beyond the rated current capacity of the power supply. The remaining four runs appear to have been limited to a higher product-water concentration, either because of a high product-to-waste ratio (Run No. 18) or too short a path length (Runs No. 20, 21, and 24).

Run No. 4 at the design value of channel velocity, 4.95 in/sec, produced a product-water concentration of 230 ppm with a stack current density of 30 ma/cm^2. If the stack current density line in Figure 91 is adjusted to a feed-water concentration of 3000 ppm (the design value), it appears that a stack current density of 23 ma/cm^2 (the design value) would have produced a product-water concentration of 500 ppm (the design value).

The lowest product-water concentration was produced during Run No. 3 at a channel velocity of 3.9 in/sec and a stack current density of 25 ma/cm^2. This run resulted in a product-water concentration of 120 ppm which is close to the mineral content (about 80 ppm) of the water used to prepare the 3000 ppm NaCl feed solution.

3. Current Efficiency Performance

Figures 118 through 123 present the stack current efficiencies obtained during the runs. These results are plotted versus stack current density for convenience.

Figures 118, 120 and 122 show the effect of channel velocity on current efficiency for the three path lengths. These curves indicate that current efficiency increases with increasing channel velocity. This observation is still true when points at approximately the same product water concentration are compared. The trend is less obvious for the runs with the 33.5-inch path length, but even here, a careful extrapolation of the curves to higher current densities corresponding to a lower product-water concentration, justifies the same conclusion. In general, the results from the runs with 33.5-inch path length are less consistent and less explainable than the other runs. This may be due to unequal flow, cuts and current efficiencies in each of the four parallel-connected channels.

The effect of product-to-waste flow-rate ratio on current efficiency is shown in Figures 119, 121 and 123. The results from the runs with 134-inch path length are as might be expected, particularly at the higher current density (lower product-water concentration) where in-

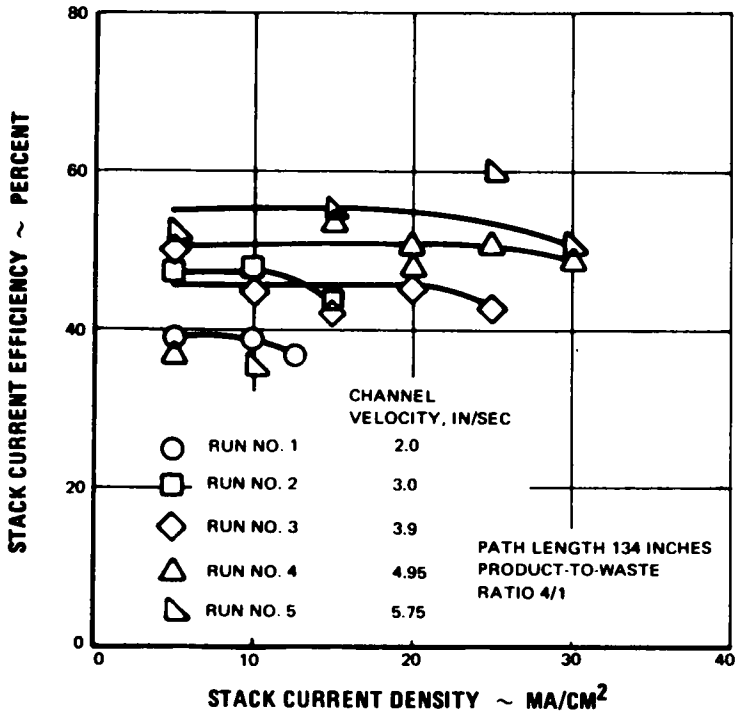

Figure 118 Forty-Cell-Pair Stack. Effect of Channel Velocity on Current Efficiency. Path Length 134 Inches

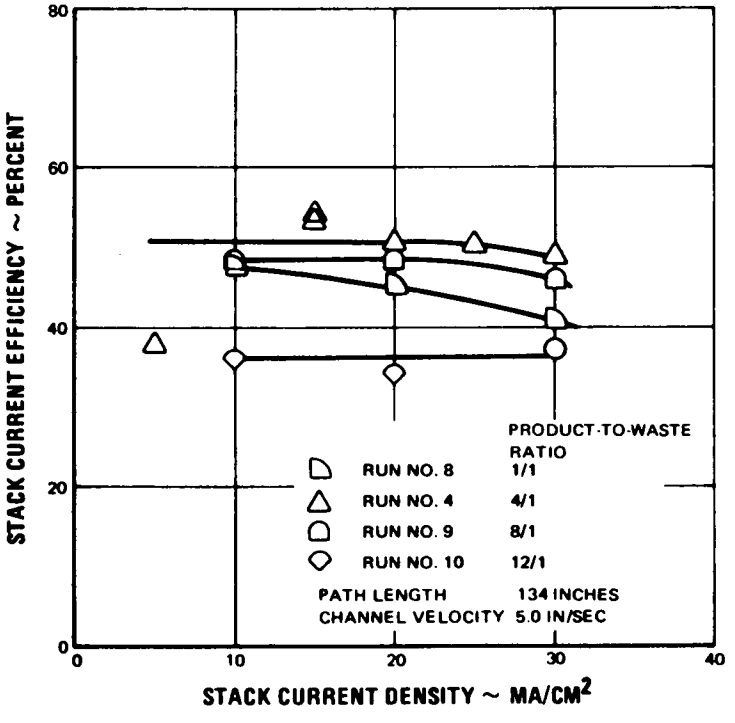

Figure 119 Forty-Cell-Pair Stack. Effect of Recirculation Rate on Current Efficiency. Path Length 134 Inches

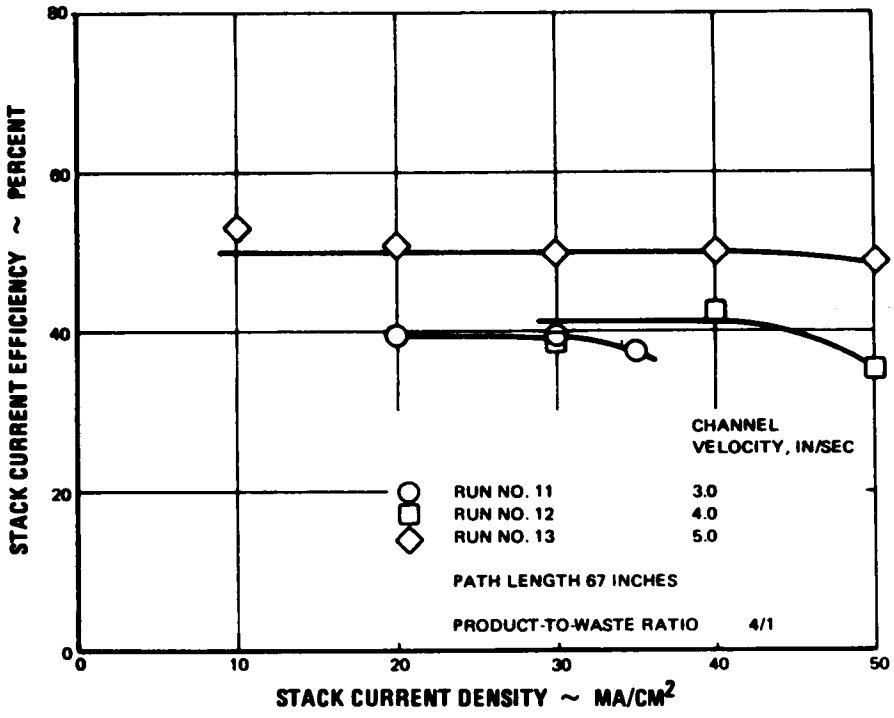

Figure 120 Forty-Cell-Pair Stack. Effect of Channel Velocity on Current Efficiency. Path Length 67 Inches

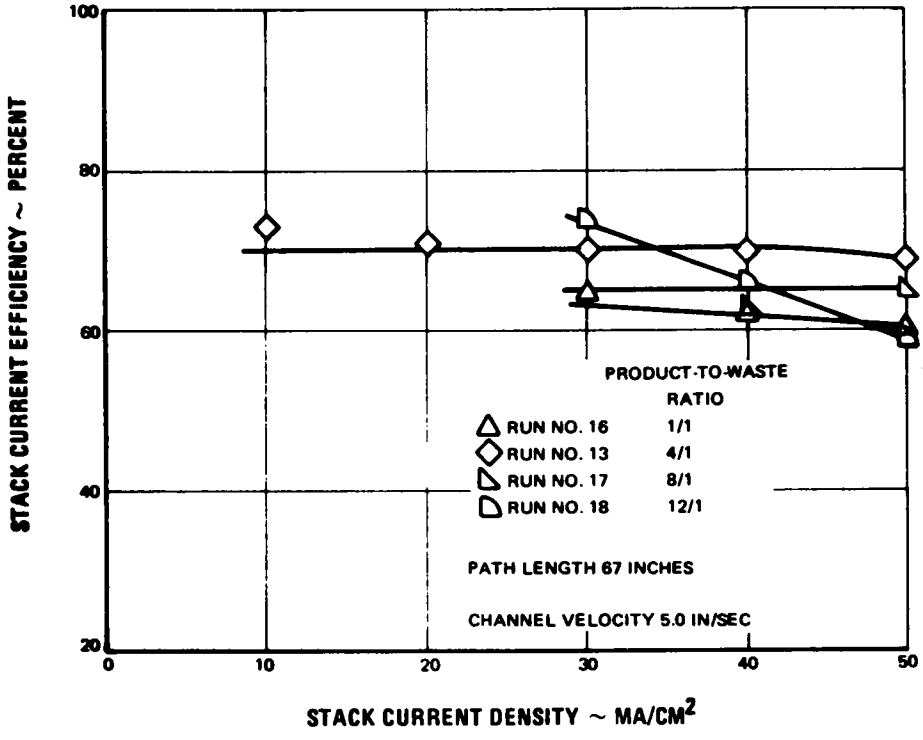

Figure 121 Forty-Cell-Pair Stack. Effect of Recirculation Rate on Current Efficiency. Path Length 67 Inches

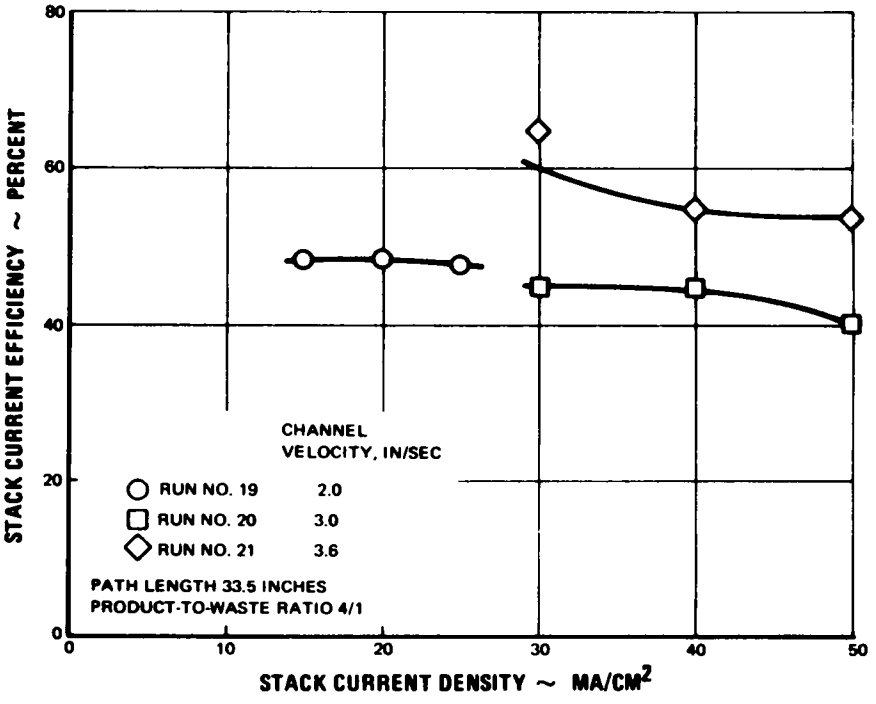

Figure 122 Forty-Cell-Pair Stack. Effect of Channel Velocity on Current Efficiency. Path Length 33.5 Inches

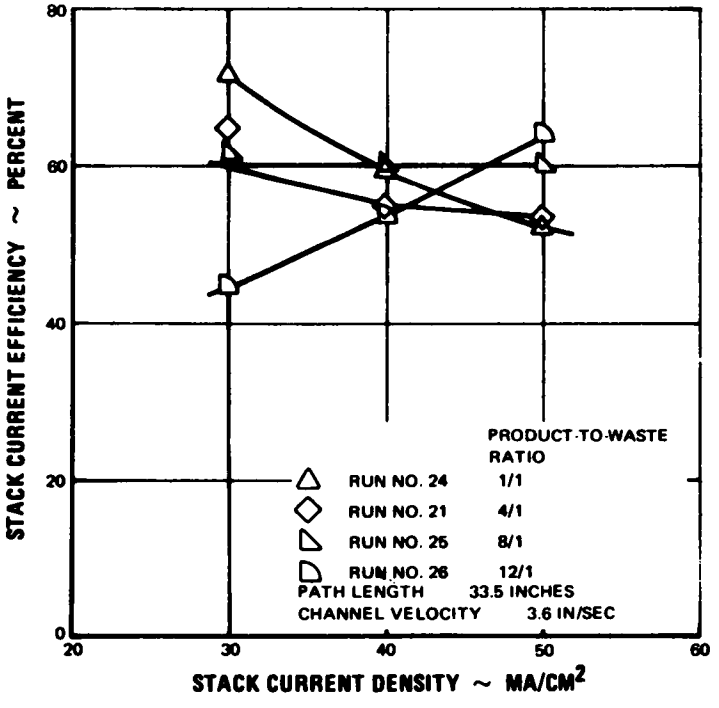

Figure 123 Forty-Cell-Pair Stack. Effect of Recirculation Rate on Current Efficiency. Path Length 33.5 Inches

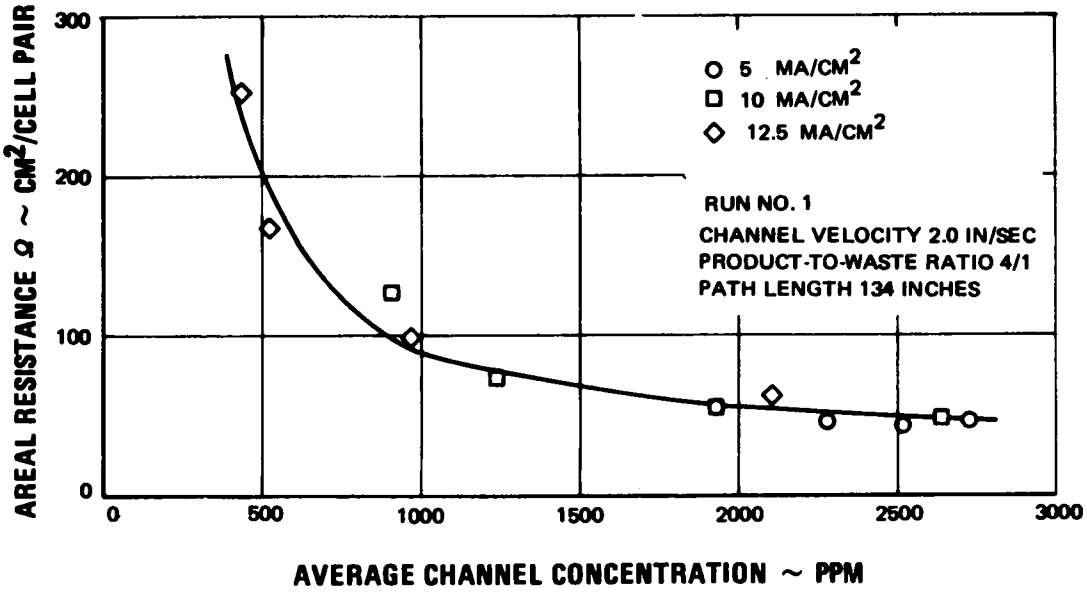

Figure 124 Forty-Cell-Pair Stack. Resistance vs Average Concentration. Run No. 1

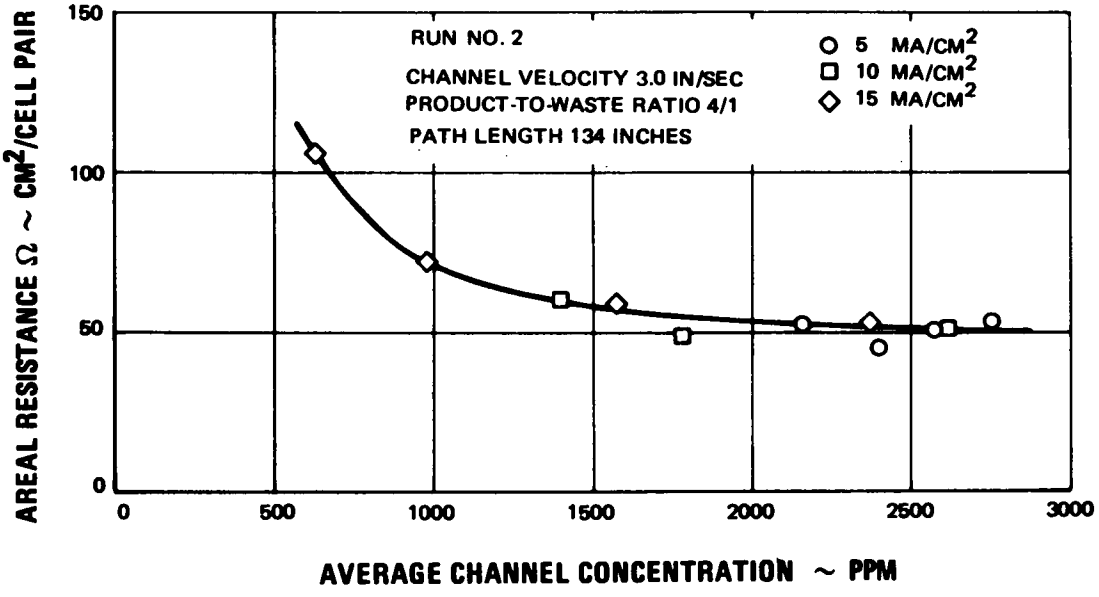

Figure 125 Forty-Cell-Pair Stack. Resistance vs Average Concentration. Run No. 2

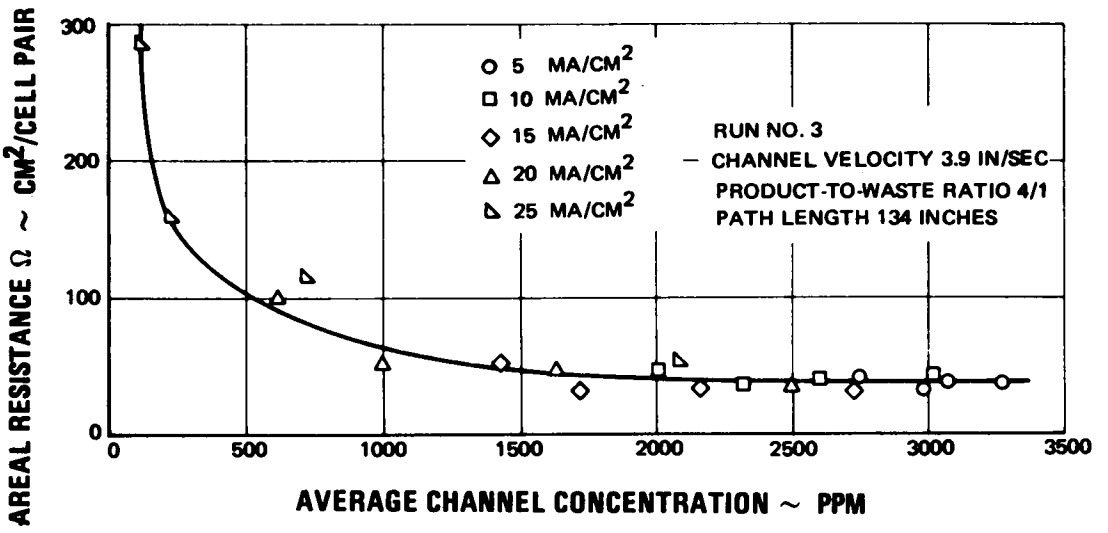

Figure 126 Forty-Cell-Pair Stack. Resistance vs Average Concentration. Run No. 3

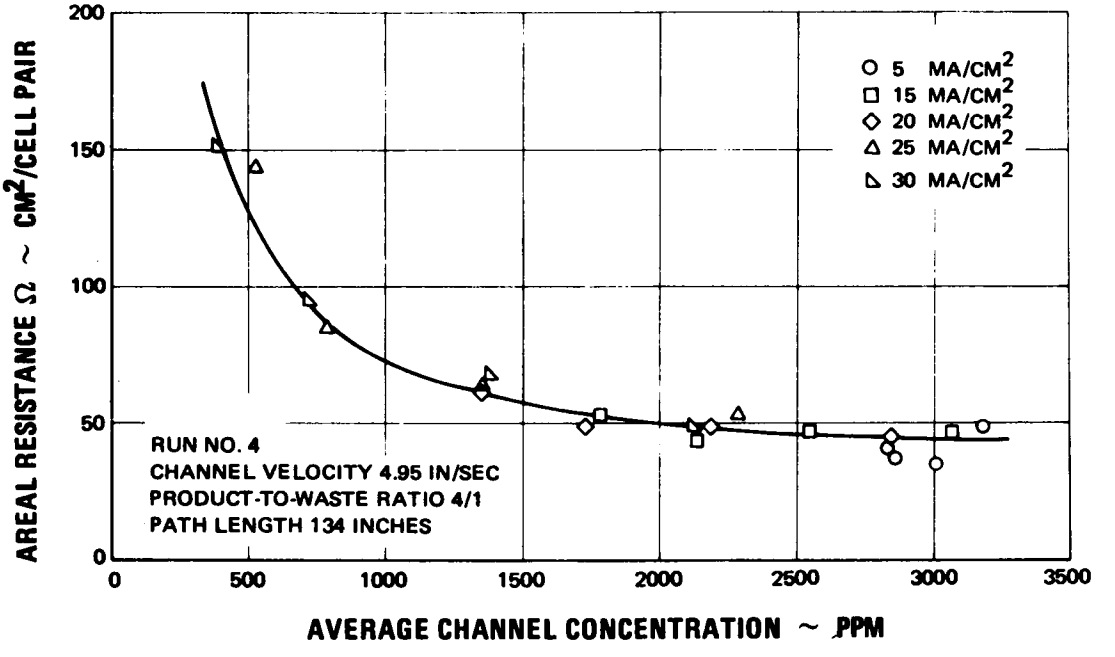

Figure 127 Forty-Cell-Pair Stack. Resistance vs Average Concentration. Run No. 4

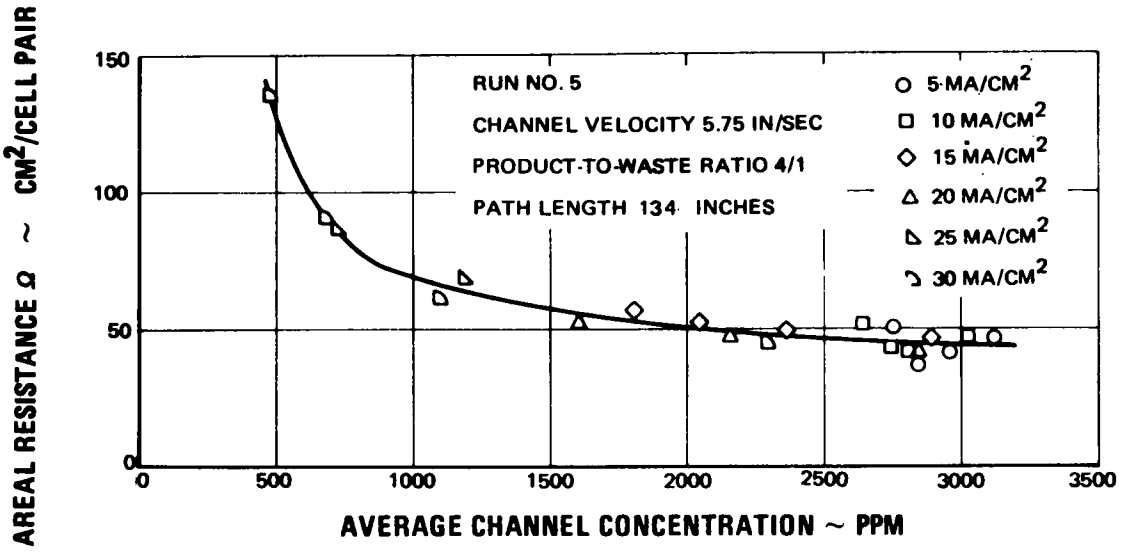

Figure 128 Forty-Cell-Pair Stack. Resistance vs Average Concentration. Run No. 5

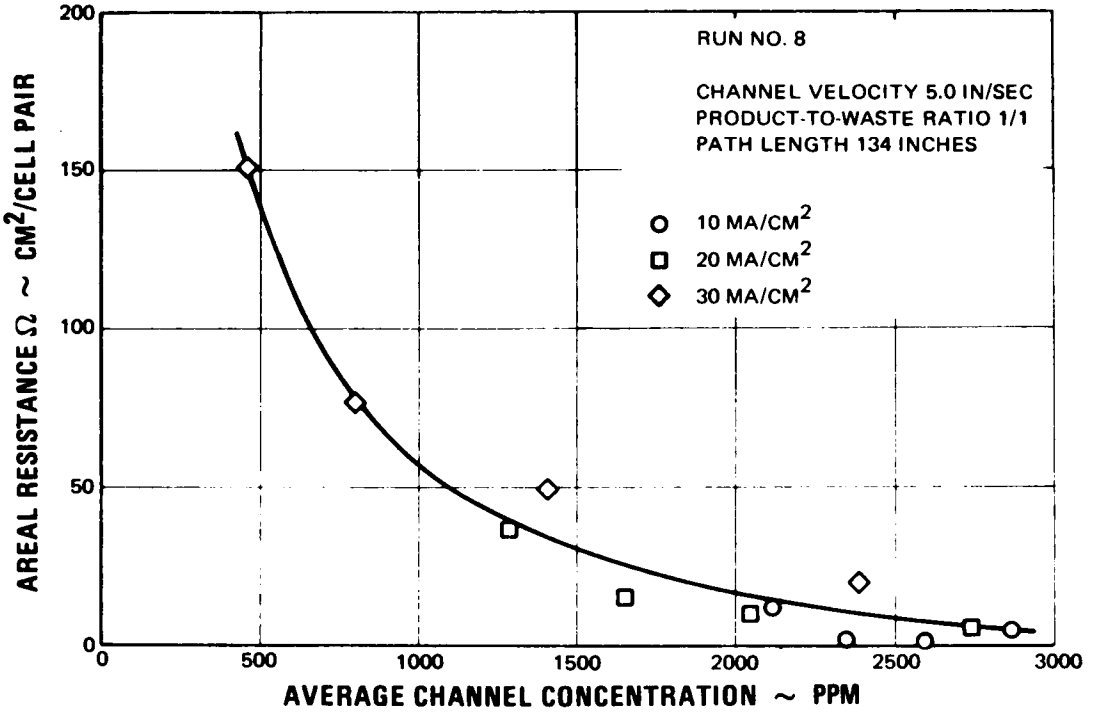

Figure 129 Forty-Cell-Pair Stack. Resistance vs Average Concentration. Run No. 8

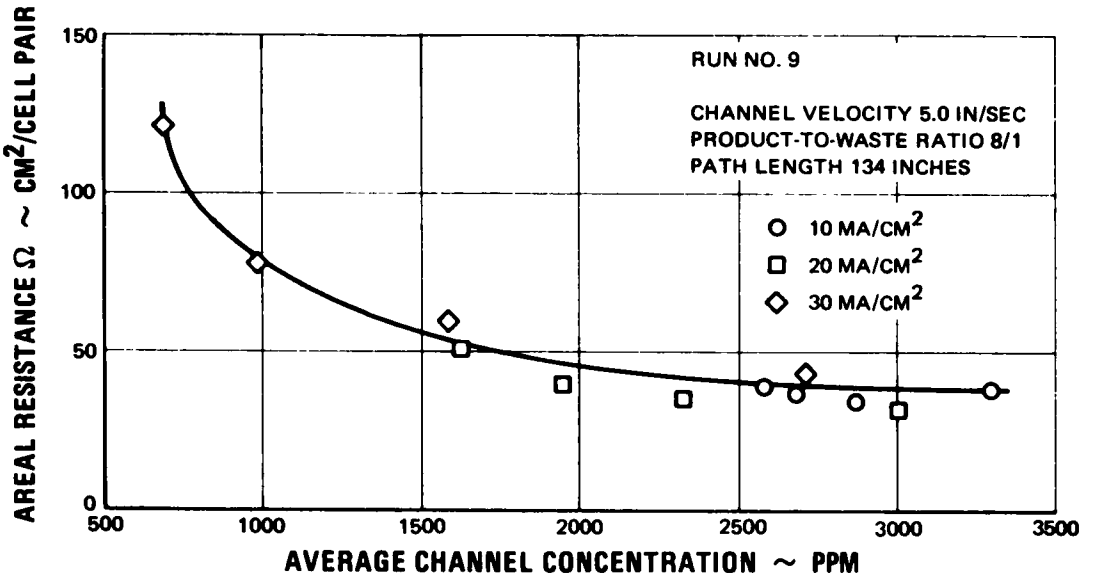

Figure 130 Forty-Cell-Pair Stack. Resistance vs Average Concentration. Run No. 9

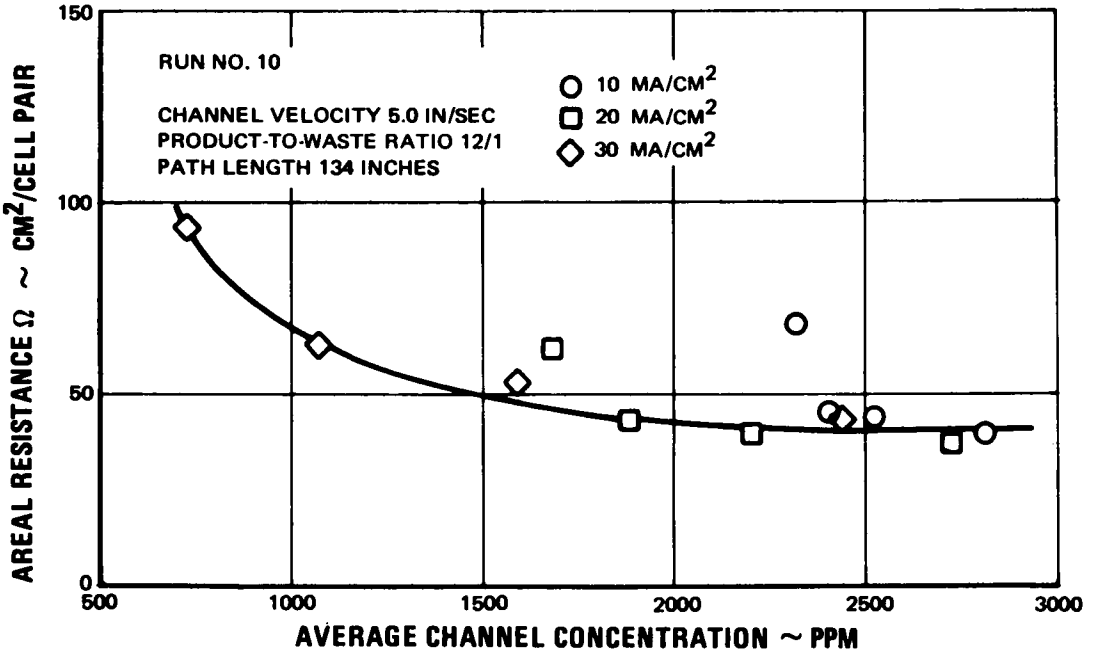

Figure 131 Forty-Cell-Pair Stack. Resistance vs Average Concentration. Run No. 11

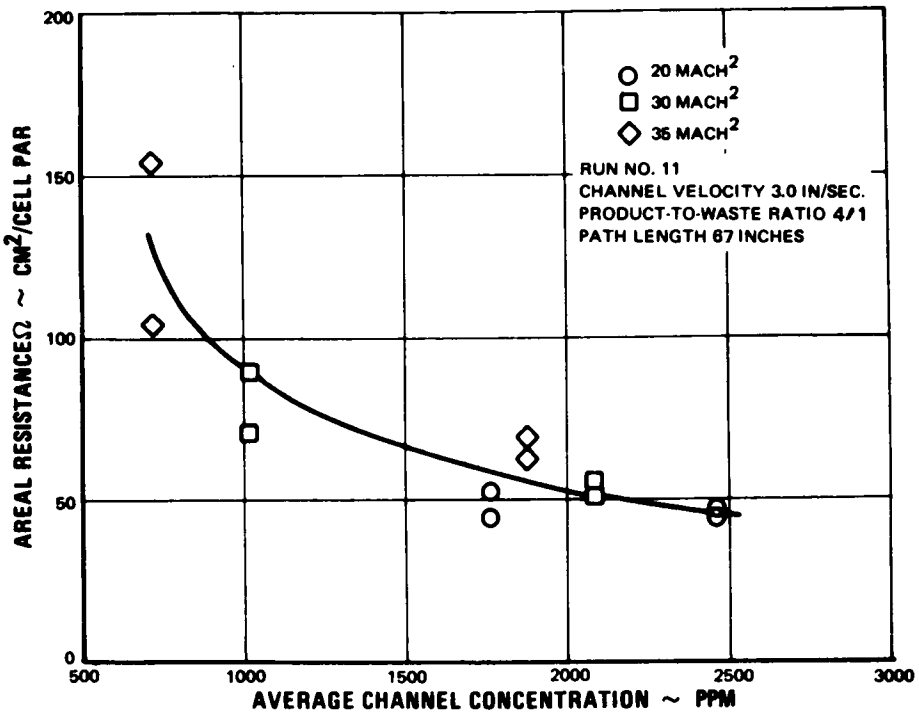

Figure 132 Forty-Cell-Pair Stack. Resistance vs Average Concentration. Run No. 11

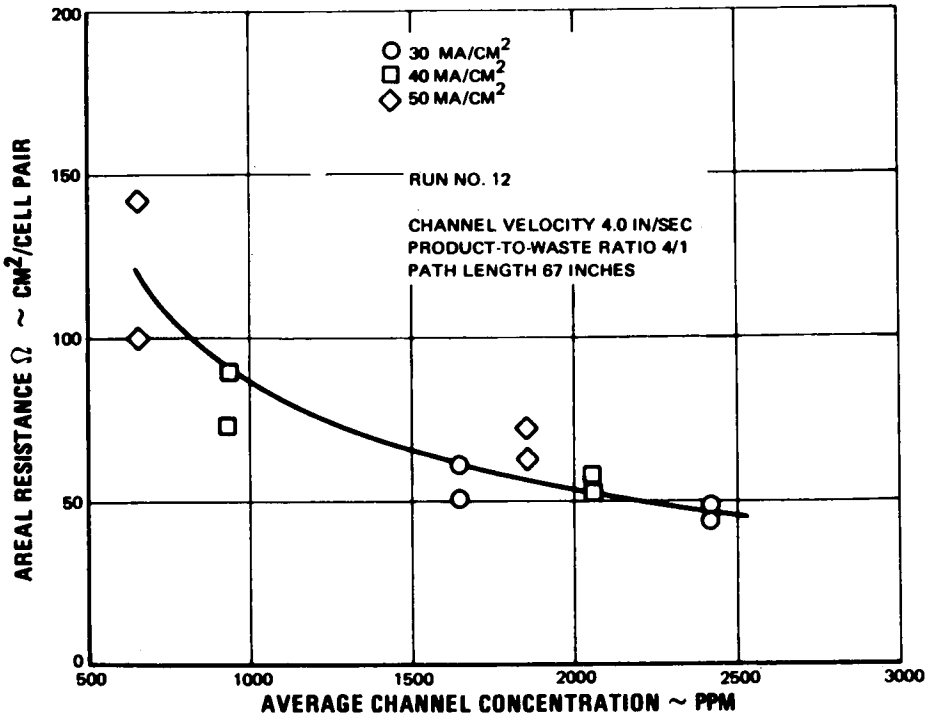

Figure 133 Forty-Cell-Pair Stack. Resistance vs Average Concentration. Run No. 12

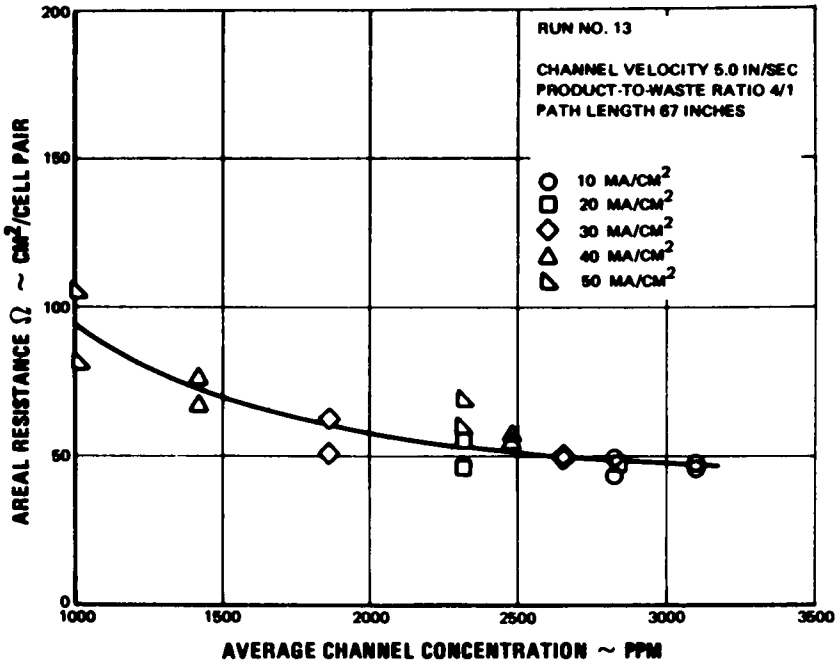

Figure 134 Forty-Cell-Pair Stack. Resistance vs Average Concentration. Run No. 13

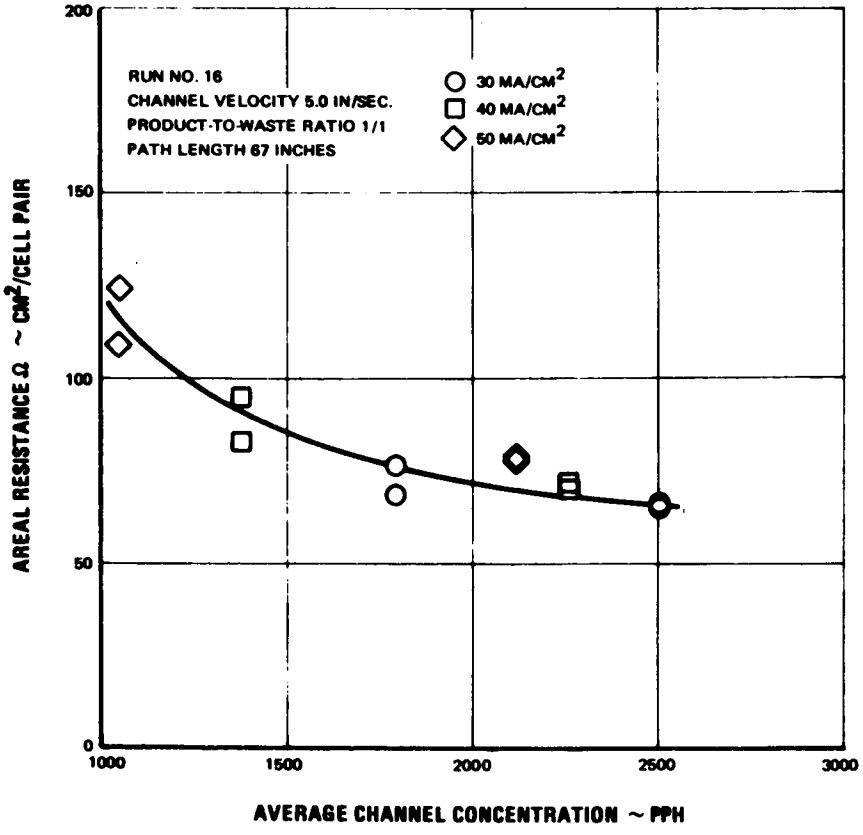

Figure 135 Forty-Cell-Pair Stack. Resistance vs Average Concentration. Run No. 16

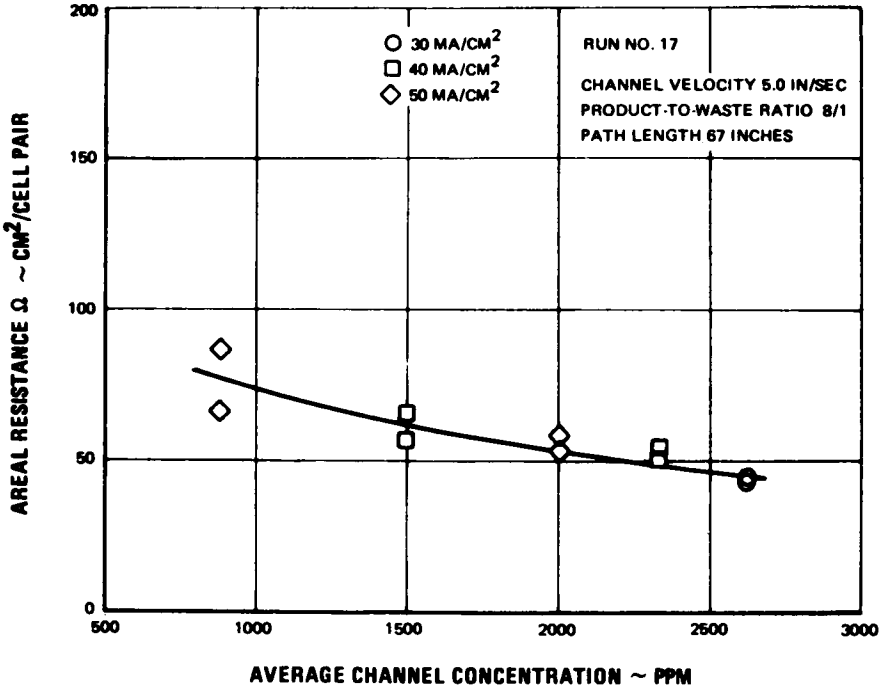

Figure 136 Forty-Cell-Pair Stack. Resistance vs Average Concentration. Run No. 17

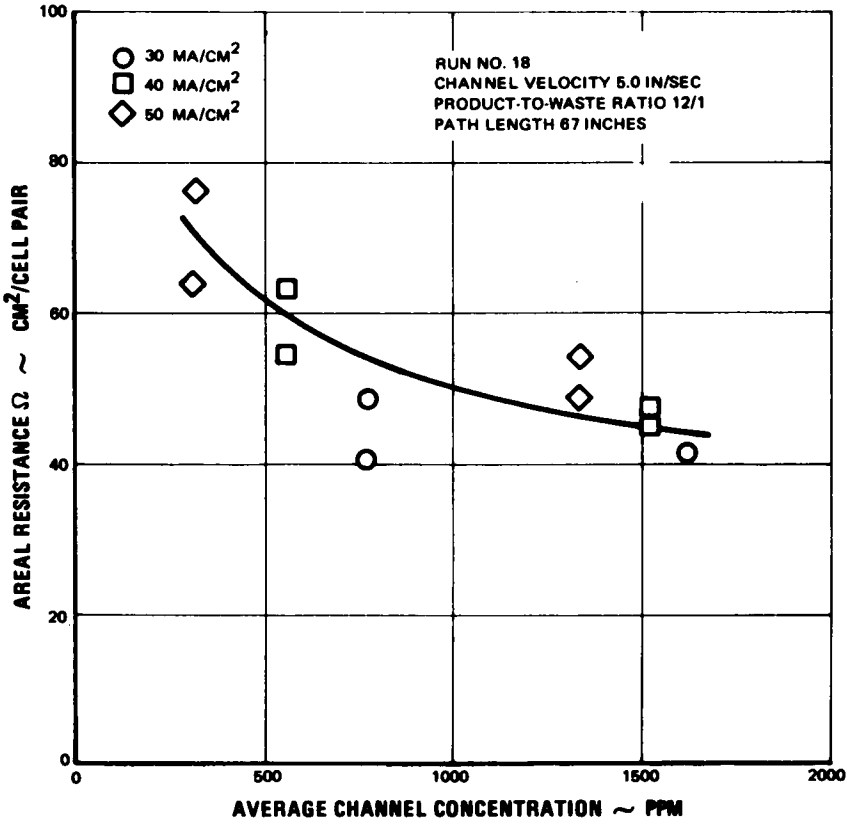

Figure 137 Forty-Cell-Pair Stack. Resistance vs Average Concentration. Run No. 18

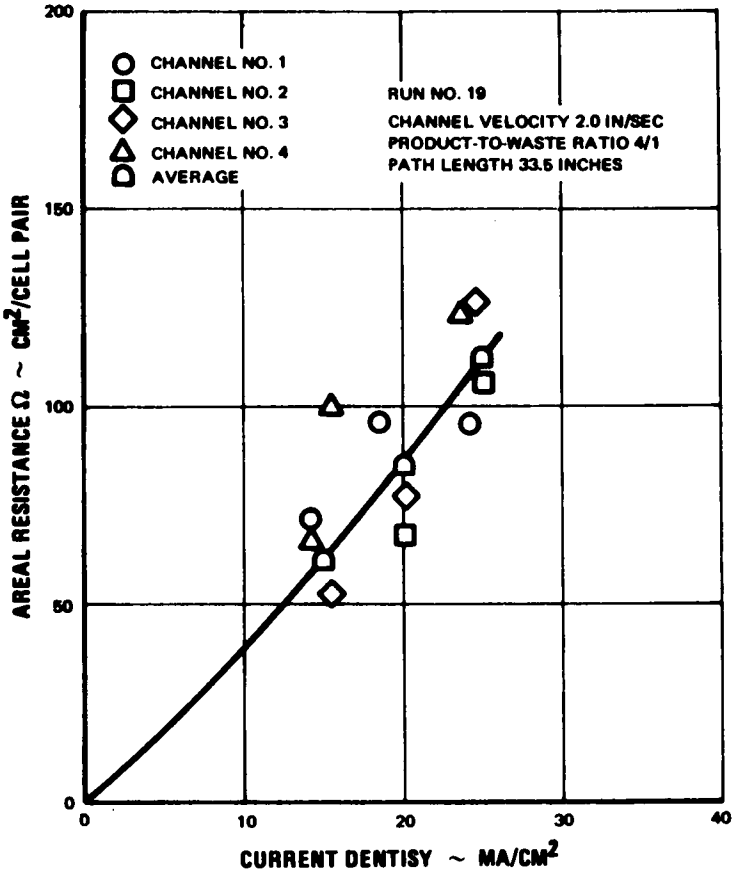

Figure 138 Forty-Cell-Pair Stack. Areal Resistance vs Current Density. Run No. 19

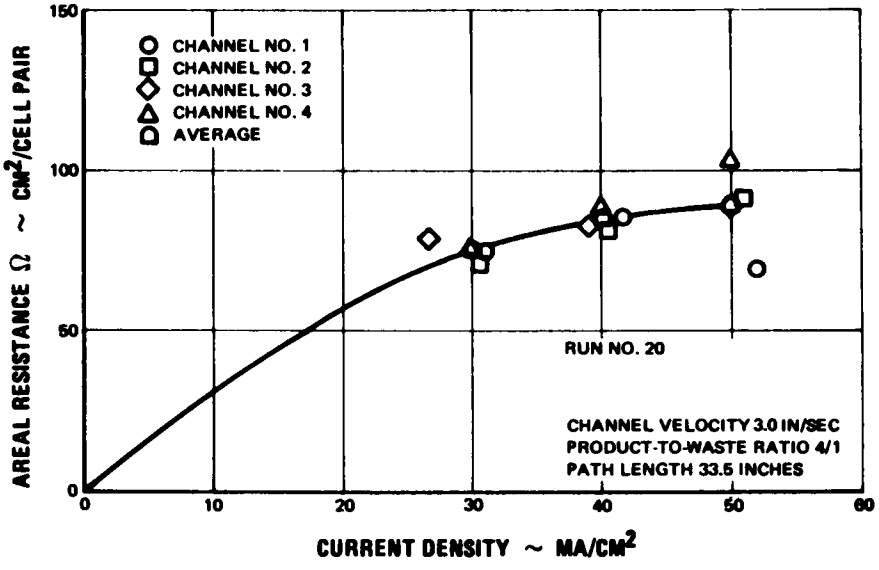

Figure 139 Forty-Cell-Pair Stack. Areal Resistance vs Current Density. Run No. 20

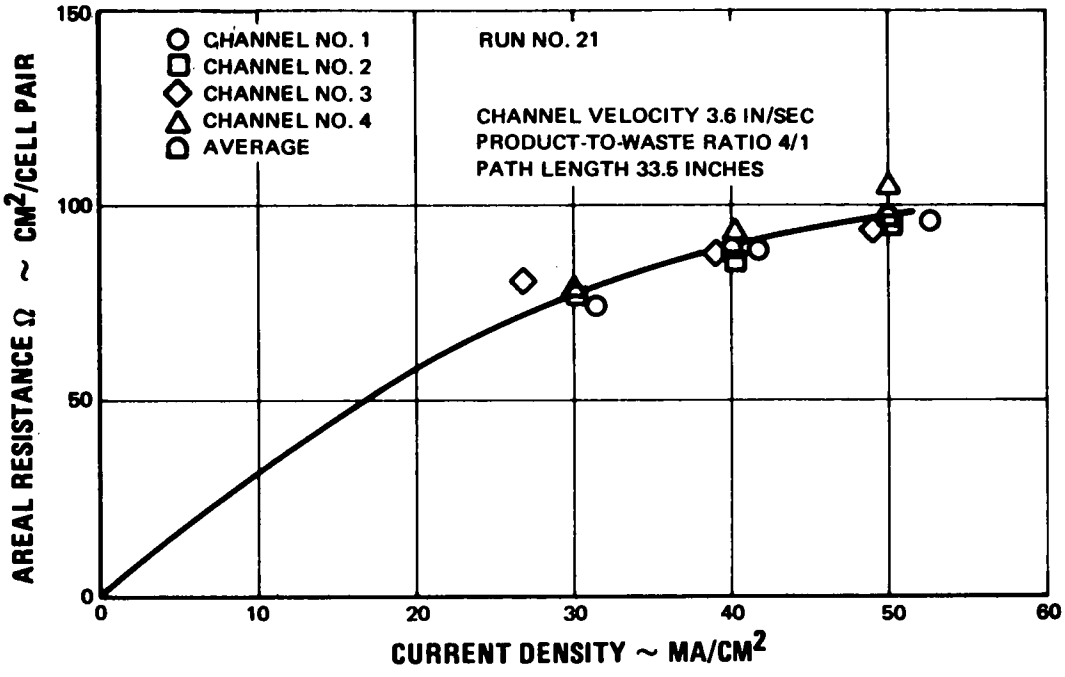

Figure 140 Forty-Cell-Pair Stack. Areal Resistance vs Current Density. Run No. 21

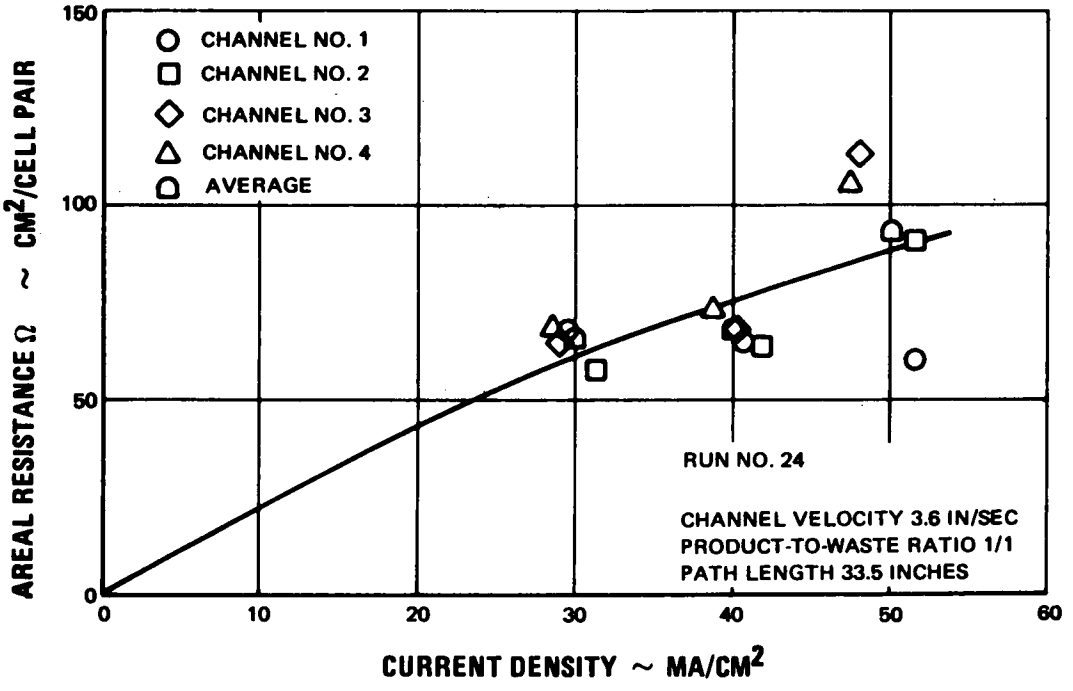

Figure 141 Forty-Cell-Pair Stack. Areal Resistance vs Current Density. Run No. 24

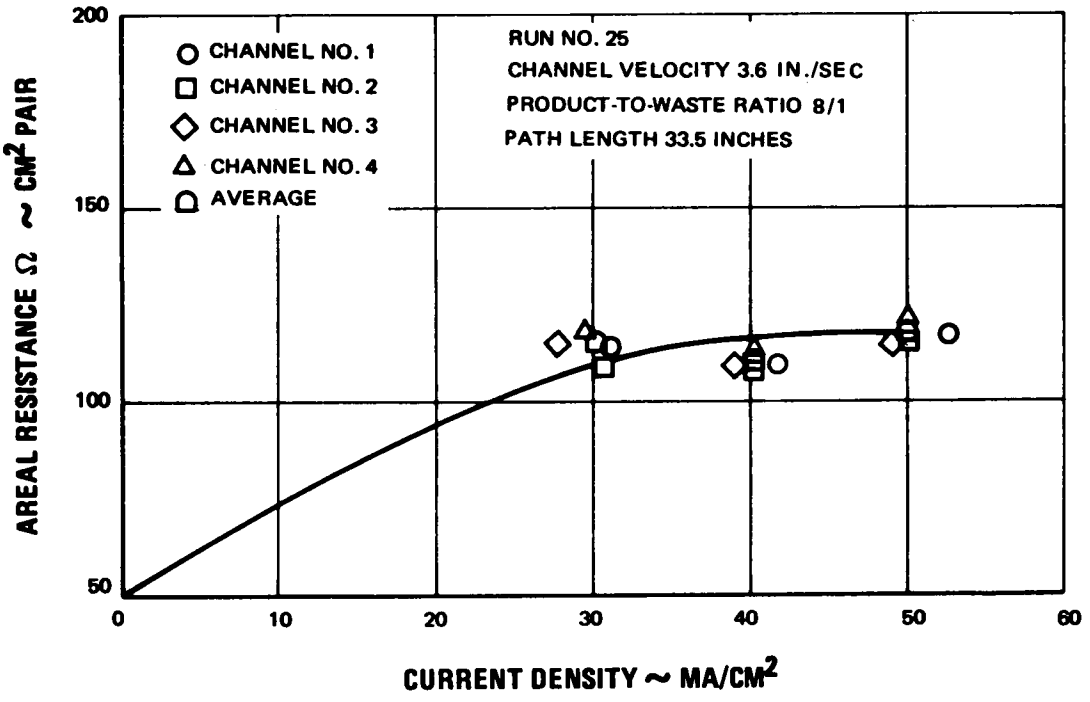

Figure 142 Forty-Cell-Pair Stack. Areal Resistance vs Current Density. Run No. 25

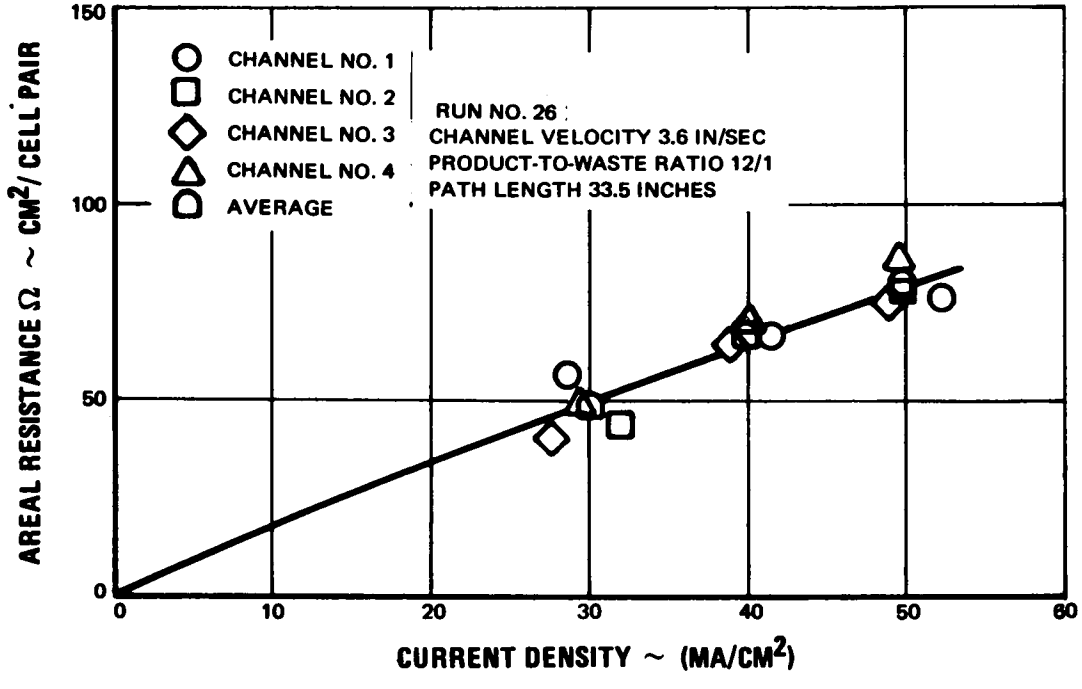

Figure 143 Forty-Cell-Pair Stack. Areal Resistance vs Current Density. Run No. 26

creasing the product-to-waste ratio results in lowering the current efficiency. This is what would be expected due to increasing back diffusion through the neutral membrane as the concentration difference across this membrane is increased. This trend is also observed in Figure 121 for the runs with 67-inch path length at the highest current density tested, although the data from Run No. 16 at a product-to-waste ratio of 1/1 is out of line for no obvious reason. Again the data from the runs at a path length of 33.5 inches is unexplainably not consistent with this trend.

4. Electrical Performance

Repeating cell-pair areal resistance data for all runs is presented in Figures 124 through 143. The data for the runs using the 134-inch and 67-inch path lengths has been plotted versus the numerical average of the product-stream inlet and exit concentrations for each channel. The figures show that this gives a reasonably good correlation of the data, particularly for the runs with 134-inch path length. The resistance data for the 33.5-inch path length has been plotted versus stack current density for convenience. Product-stream concentration data for these runs can be obtained from Figures 112 through 117. These curves (Figures 138 through 143) also show the variation in cell-pair resistance between the four channels when operating at the same current density.

Cell-pair resistance above an average concentration of about 2000 ppm is about the same for all channel velocities tested at the same product-to-waste ratio. At lower average concentrations, high channel velocities effectively suppress the increase in cell-pair resistance as compared to the resistance increase observed at low channel velocities. This result is consistent with the predicted effect of channel velocity on the depleted-stream boundary-layer resistance. The data generally show that cell-pair resistance decreases as the product-to-waste ratio is increased at the same channel velocity. This effect is more noticeable at lower average channel concentrations which correspond to higher current densities and higher cuts. Under these conditions, the concentration of the concentrate stream is considerably increased at high product-to-waste ratios, which lowers the bulk solution resistance of this stream.

It should be noted that the data for the runs with a 67-inch path length is not as well represented by a single line as is the 134-inch path length data. For these runs at higher current densities and larger cuts per channel, current density may have a significant effect on cell-pair resistance. Also for larger cuts per channel, it may no longer be sufficient to use a simple average of the product-stream inlet and exit concentrations, since the solution resistance is not a linear function of its concentration, and the exit end of the channel may therefore have a dominant effect on resistance.

5. Hydraulic Performance

Figure 144 is a plot of stack pressure loss versus channel velocity for the runs using the 134-inch path length. The pressure loss per channel is equal to one-fourth of the values shown in this figure. An extrapolation of this curve to higher velocities indicates that a channel velocity of about seven inches per second (18 cm/sec) could be achieved at a total stack-pressure loss of 50 psi. However, since a finite stack exit pressure is required for stable flow control, this

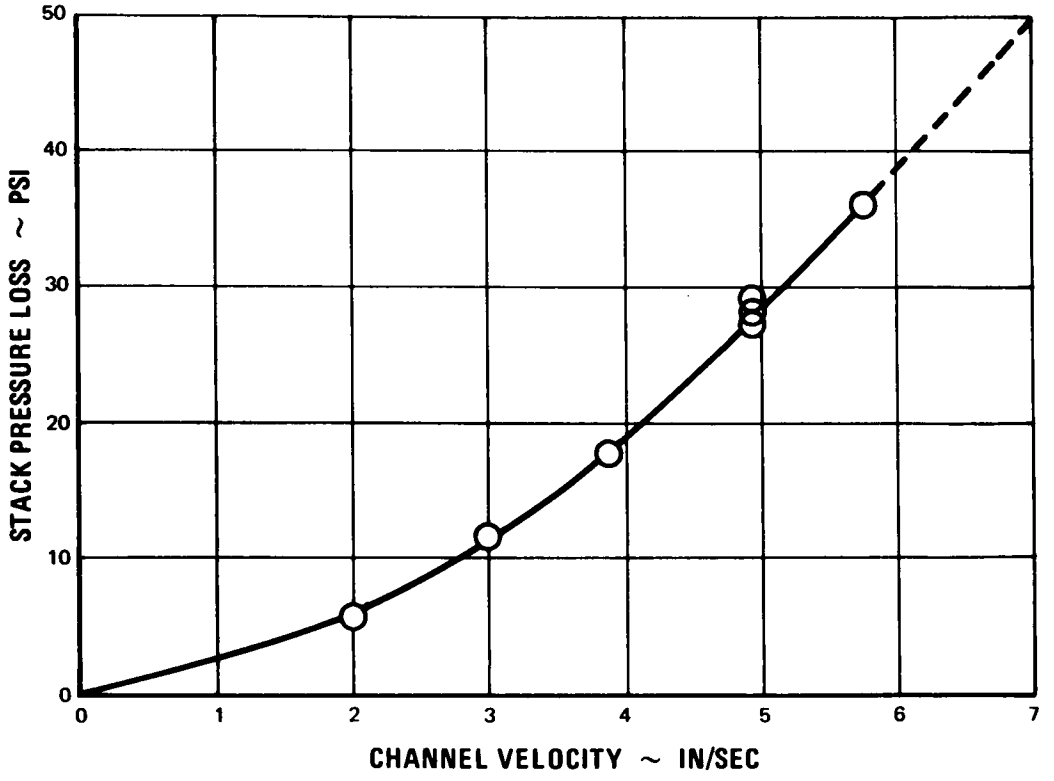

Figure 144 Forty-Cell-Pair Stack. Stack Pressure Loss vs Channel Velocity. Path Length 134 Inches

channel velocity cannot in fact be achieved without exceeding the design pressure of 50 psi at the stack inlet. With the present pilot-plant piping arrangement, a channel velocity of 5.75 inches/sec was achieved with an inlet pressure of 58 psi and a back pressure of 21.5 psi. Suitable modifications to the piping system can probably reduce this back pressure significantly.

6. Post-Test Disassembly

Following the completion of the forty-cell-pair stack test program, the stack was disassembled and the components inspected. As in the case of the five-cell-pair stack, many of the cation membranes adhered to the spacer screens in the area between the channels and were damaged when separated.

The rubber gasket between the top endplate and the rinse-stream spacer screen had extruded out (or blown) into a concentrate-stream internal manifold in one area. This occurred between the cathode compartment in the fourth channel and the concentrate-stream exit manifold from this channel, when the stack is connected in the 134-inch and 67-inch path length configurations. It is believed that this blowout occurred early in the test program, during Run No. 4, and was caused by an excessive static pressure difference across this 3/8-inch wide section of the rubber gasket. While establishing the flow conditions for Run No. 4 and before applying power to the stack, the acid rinse-stream inlet pressure was permitted to climb to a level which imposed a 16 psi pressure differential across the gasket. A significant pH shift was noted in the solution

return tank and the system was subsequently drained and flushed out. During all runs after this occurrence, system pressures were carefully monitored and controlled to always maintain the concentrate-stream pressure in this manifold equal to or greater than the acid rinse-stream inlet pressure. No pH shift or evidence of intercompartmental leakage was noted after this occurrence. However, it cannot be positively determined that some leakage did not occur in subsequent runs. It is possible that leakage may be partly responsible for the current efficiencies in some runs being lower (40 to 50 percent) than were expected.

Several cation membranes had black and green stains around the channel inlets and sealing edges. Also some of the neutral membranes were stained with a blue-green deposit in the area of the fourth channel.

VIII. TEST BED DESIGN AND COST STUDY

Design specifications and cost estimates were developed by Pratt & Whitney Aircraft and Stone and Webster Engineering Corporation, Boston, for a transport-depletion test-bed plant with a minimum capacity of 100,000 gallons per day. Pratt & Whitney Aircraft defined the transport-depletion stack design, the interface requirements and costs. Stone and Webster Engineering Corporation prepared a plant layout, process schematic and description, and in vestment and operating costs. The test-bed plant had a design capacity of 500,000 gpd, which is the direct result of selecting a commercial-size stack design of this capacity.

A. Ground Rules

The primary ground rules used in this study are listed in Table 7. In addition, raw-water pre-treatment to remove all iron in excess of 0.05 ppm and all manganese in excess of 0.05 ppm before entering the transport-depletion stacks was assumed. Also, feedwater filtration equivale to that produced by a filter of 10-micron pore size was assumed in order to prevent the possibil of inlet-plugging in stacks. The stack performance and staging requirements were based on a feedwater quality of 2500 ppm NaCl entering the first stage, since no transport-depletion performance data was available for operation on brackish waters similar to those listed in Table 8.

B. Plant Description

1. Commercial-Stack Description

Figure 145 shows a three-view drawing of the selected commercial-size stack. Dimensions of the major components and major specifications are listed in Table 9. This is a single-pass stack capable of desalting brackish water of between 1000 and 1500 ppm NaCl. Additional stages were added as required to treat waters of higher salt concentration. Two identical stages were required to desalt the 2500 ppm feedwater assumed for the test-bed plant design.

A single-pass (no turns) channel was considered desirable to avoid problems with the distribution of flow velocity. The path length of 60 inches is sufficient to desalt a 1000 to 1500 ppm solution at 20 ma/cm^2 using a 30-mil spacing and a 6 in/sec channel velocity. A design current density of 20 ma/cm^2 was selected on the basis of a preliminary systems analysis study. The 30-mil cell spacing represents a state-of-the-art minimum for present-day electrodialysis stacks and is the same spacing used in the pilot-plant stack. The selection of a channel velocity of 6 in/sec (15 cm/sec) is somewhat arbitrary. Bench-scale tests indicate that this velocity may be sufficient to achieve a minimum resistance value, although additional pilot-plant tests would be desirable to better define the velocity-resistance relationship.

The spacer-screen is illustrated in Figure 146. Its construction is based on the technology developed for the pilot-plant stack. The channel width of 36 inches was chosen to permit the use of most commercially-available cation membranes. Sixteen one-inch square manifolds are located at each end. This permits eight solution inlets across the 36-inch channel width,

TABLE 7

Basis of Design and Economic Criteria for
Transport-Depletion Desalination Study
of 0.5, 1.0, 5.0 and 10.0 mgd Plants

Basis of Design and Estimates

assumed plant location	near Colorado Springs, Colorado
type of building construction	enclosed
foundation conditions	soil bearing - 3,500 psi, sand, gravel or decomposed rock
plant life	30 years
battery limits	property limits
raw-water supply	intake pipe of adequate size delivering delivering constant stream of water at 2 psi gage pressure at property limits
product-water discharge	delivery pipe to property limits delivering product water at 2 psi gage pressure
raw-water quality	(see Table 8)
product-water quality	500 ppm TDS with only post-treatment chlorination permitted
raw-water temperature	70°F
on-site raw-water storage	minimum
on-site product-water storage	none
type of plant control function	central control room or panel
seismetic factor	none

Economic Criteria Used in Study

land costs	$1,000 per acre
plant life	30 years
interest rate for construction interest	3.25 percent per annum
construction period	
a. .5 MGD plant	6 months
b. 1.0 MGD plant	8 months
c. 5.0 MGD plant	10 months
d. 10.0 MGD plant	12 months
owner type	municipality or other tax exempt
fixed charge rate	5.27 percent per annum
insurance costs	included in fixed charge rate
electrical energy costs	7 mils per kw/hr
membrane service life	3 years

Economic Criteria Used in Study (continued)

membrane costs	
a. cation	$0.80/sq. ft.
b. neutral	$0.20/sq. ft.
plant capacity factor	90 percent (330 days per year)
start-up period	90 days
start-up costs	equivalent to 90 days of on-stream operating costs
payroll burden	15 percent of direct salaries
general administrative (overhead)	30 percent of direct salaries
chemical costs	from June 26, 1967 issue of Oil Paint and Drug Reporter
brine disposal costs per 1,000 gal. product water	
a. 1.0 MGD plant	$.030
b. 5.0 MGD plant	$.028
c. 10.0 MGD plant	$.025

personnel costs, annual direct wages

plant superintendent	$13,200
plant engineer	12,000
plant chemist	10,000
plant assistant chemist	7,000
shift supervisor	10,000
plant operators	8,000
maintenance supervisor	11,000
electrical maintenance	8,000
mechanical maintenance	8,000
membrane replacement	7,000
instrument technician	9,000
clerk steno	5,000
time keeper	4,000
storekeeper	7,000
janitor	5,000
laborer	5,000

maintenance schedule	6 month meantime between overhaul for any stack

TABLE 8

Chemical Composition of Three Test Waters
For Use on Transport-Depletion Studies

Water Type/Ion ppm	Webster, S.D.	Dell City, Tex.	Dalpra Farm, Colorado
sodium (Na)	81	227	886
magnesium (Mg)	79	151	72
calcium (Ca)	216	372	118
chloride (Cl)	20	335	131
sulfate (SO_4)	718	1,343	1,943
bicarbonate (HCO_3)	355	215	473
hardness (as $CaCo_3$)	864	1,553	590
iron (Fe)	2	-	2
manganese (Mn)	1	1	1
potassium (K)	-	-	16
fluoride (F)	1	2	-
nitrate (NO_3)	-	48	6
silica (SiO)	20	-	-
boron (B)	-	-	-
phosphate (PO_4)	-	-	-
COD	8	-	-
total dissolved solids (TDS)	1,490	2,693	3,648
pH	7.2		7.6

TABLE 9

Transport-Depletion Commercial-Stack Design

design concept	single-pass stack with split-manifolds
capacity	500,000 gpd
height	66 inches
width (spacer-screen)	40 inches
overall depth	33 inches (approximate)
path length	60 inches
path width	36 inches
spacer-screen thickness	30 mils
membrane utilization (38-inch membrane width)	86 percent
number of cell pairs	200
weight	5000 lbs. (approximate)
voltage	620 volts (typical)
current	290 amperes (typical)
power	180 KW (typical)
current leakage	< 5 percent
pressure loss	< 20 psi

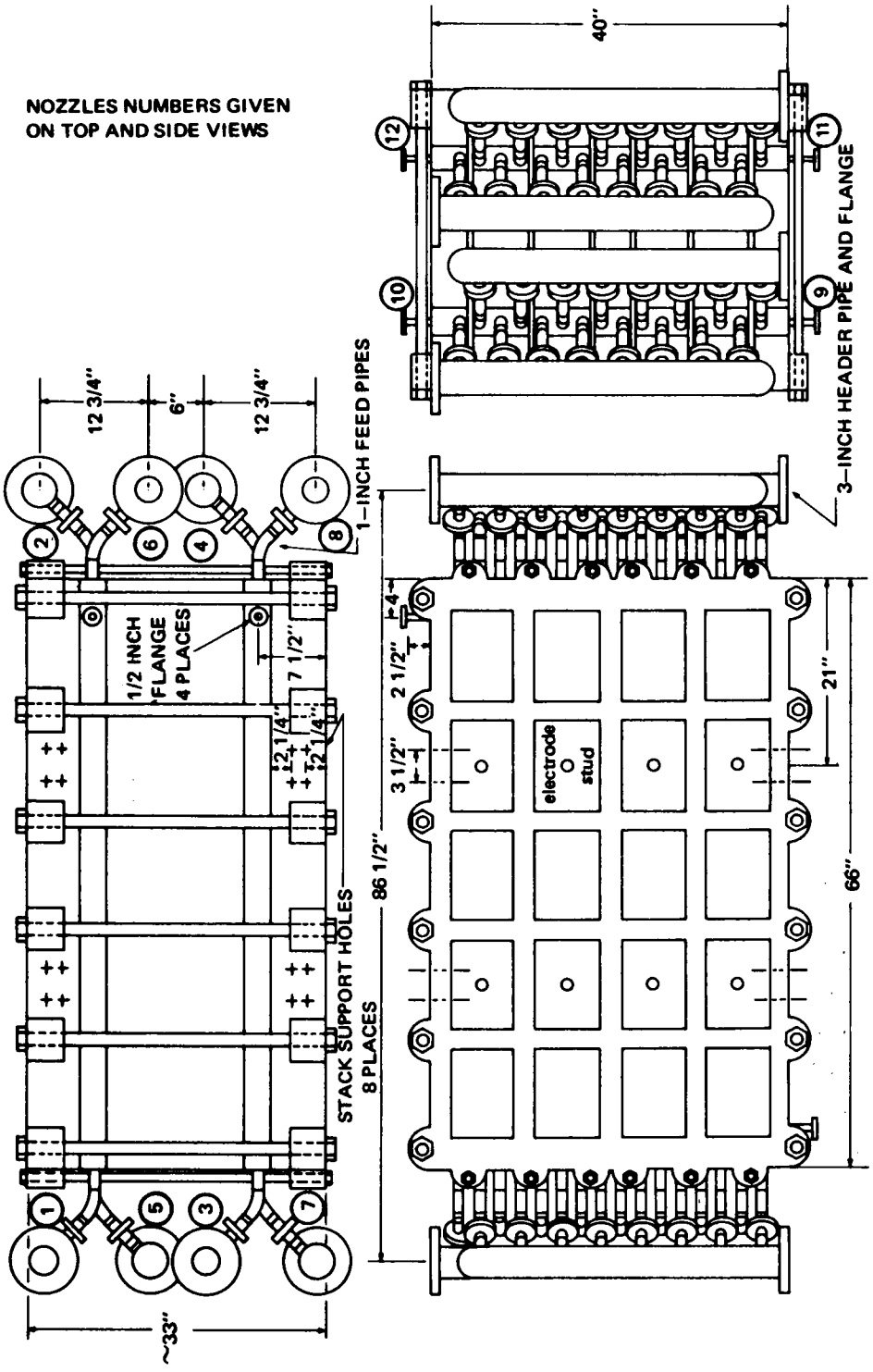

Figure 145 Test-Bed Stack

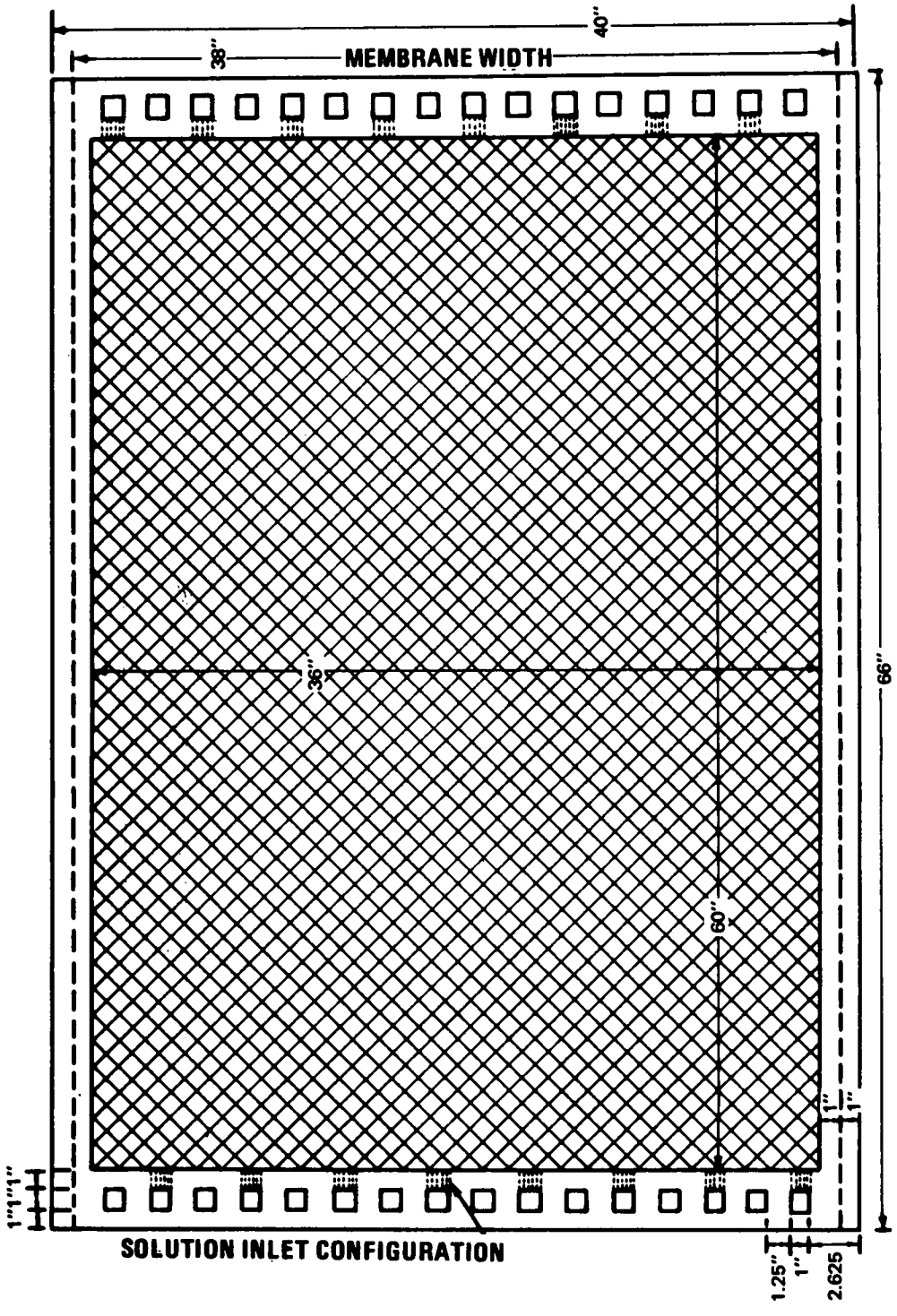

Figure 146 Spacer Screen for Commercial Stack

which provides a reasonable flow velocity distribution. The one-inch length of the inlets represents a balance between electrical resistance and pressure-loss characteristics.

A stack of 200 cell pairs was selected from two primary considerations. The first is stack capacity (500,000 gpd for 200 cell pairs). This is a rather large capacity for a single stack, but it could be reduced by decreasing either the width or the number of cell pairs if a smaller unit is desired. The second consideration is a trade-off between electrode-compartment power losses which are constant irrespective of the number of cell pairs, and manifold current leakage and pressure losses which increase as a function of cell-pair numbers. To achieve the maximum number of cell pairs with acceptably-low manifold current leakage and pressure-loss values, a split manifold arrangment was used. The stack is divided into two 100-cell-pair stacks by a solid (no manifold holes) spacer-screen in the center. Solution is fed to each 100-cell-pair stack by separate headers connected through each endplate. This arrangement can be seen in Figure 145 where nozzles numbers 1 and 5 are the product and concentrate-stream inlets, respectively, of one set of 100 cell pairs, and nozzles numbers 3 and 7 are the product and concentration-stream inlets, respectively, of the other set of 100 cell pairs. Likewise, the product and concentrate-exit streams are nozzles numbers 2 and 6, respectively, for the first set of 100 cell pairs, and 4 and 8 for the second set of 100 cell pairs.

The advantages of the split manifold arrangement in reducing manifold-current leakage can be seen in Figure 147, where a comparison is made between manifold current in an uninterrupted manifold (upper figure) and a split manifold (lower figure). The split-manifold arrangement permits twice as many cell pairs between a set of electrodes with no increase in manifold-current leakage.

2. Two-Stage Stack System for Test-Bed Plant

The test-bed plant requires two stages to demineralize 2500 ppm NaCl feedwater to 500 ppm product water. Each stage is mechanically identical to the commercial-size transport-depletion stack previously described. Table 10 lists the salt concentration and type in each solution stream entering and leaving the stacks.

A concentrate/recirculation ratio is used which produces four gallons of product water for every gallon of waste water that must be disposed of. This is an arbitrary choice. The optimum choice of product-to-waste flow rate ratio depends upon a trade-off between the cost of waste disposal and the incremental increase in operating costs associated with a higher product-to-waste ratio.

Table 11 lists the estimated power requirements for each stage. The maximum value specified represents those conditions which might exist at the end of useful life of a stack assembly, just before teardown and overhaul.

3. Test-Bed Plant Description

Figure 148 is a layout of the 500,000 gpd test-bed-plant, showing the location of all major components. A process flow diagram for this plant is shown in Figure 149 and an equipment

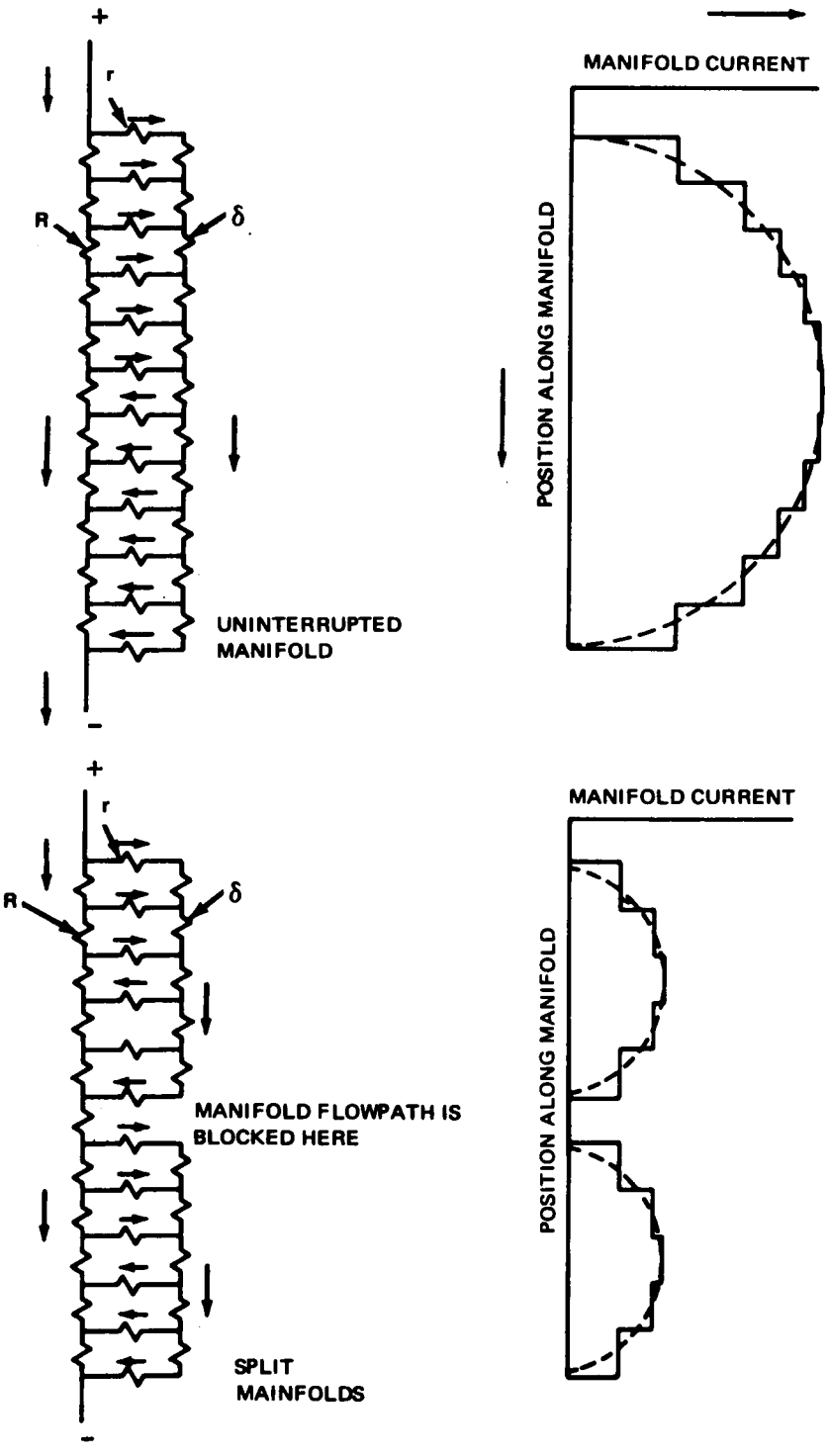

Figure 147 Advantages of Split Manifolds

TABLE 10

Solution Concentrations for Two-Stage Transport-Depletion System Operating on 2500 ppm NaCl Feedwater

Service	Solution Salt Concentration, ppm type	
	Stage I	Stage II
product inlet	2500 (NaCl)	1120 (NaCl)
product outlet	1120 (NaCl)	500 (NaCl)
concentrate inlet	8500 (NaCl)	9880 (NaCl)
concentrate outlet	9880 (NaCl)	10,500 (NaCl)
anode rinse inlet	8500(NaCl) + 3370 (NaOH)	8500(NaCl) + 1700(NaOH)
anode rinse outlet	(8500 NaCl)	8500(NaCl)
cathode rinse inlet	8500(NaCl) + 3070(HCl)	8500(NaCl) + 1550(HCl)
cathode rinse outlet	13,420(NaCl)	10,990(NaCl)

TABLE 11

Power Requirements for Two-Stage Transport-Depletion Systems

	Stage I		Stage II	
	Nominal	Max.	Nominal	Max.
voltage	585	700	690	830
current, amperes	461	510	232	250
power, KW	270	360	160	210

list is provided in Table 12. An electrical one-line diagram of the plant is shown in Figure 150.

Well water is received at 2 psi gage pressure and pumped to the top of an aeration tank (T-1), which removes carbon dioxide and oxidizes the irons in the raw water. The aeration step reduces the consumption and cost of hydrated lime used for chemical treatment. Water trickles through the aeration tank, flows by gravity into a clarifier (J-1) where it is treated and mixed with hydrated lime, aluminum sulphate and chlorinated. The clarifier effluent water flows into a pair of automatic valveless or monovalve gravity anthracite filters (J-2A and B).

The filtered water is retained in a treated water surge tank (T-2), where sufficient hydrochloric acid is injected and mixed with the water to control pH and stablize the water chemically.

The treated water is pumped through Solka-Floc precoat-type polishing filters (J-3A and B). The crystal-clear water is fed into the two-stage transport-depletion system (J-4 A and B) in four separate streams, product, concentrate, anode rinse, and cathode rinse. The potable water from the stacks is fed into a surge tank (T-3). The concentrated waste water is directed into a waste-water sump (J-5). The rinse water from both anode and cathode streams is fed into a separator (T-4) where generated hydrogen and oxygen are vented to atmosphere and the liquid is directed into the waste-water sump.

The waste-water sump is provided with a submerged weir which favors the deposition of solid suspension and is pumped out for disposal by means of a sludge pump (P-4). The skimming weir takes care of the clear saline water which is also pumped for disposal.

Potable water is drawn off from the elevated surge tank (T-3) which delivers the water at the required 2 psia gage pressure. For a full-scale plant, the surge tank would be set at grade and the potable water pumped to delivery pressure.

The only spare equipment for the test-bed plant is that which operates on an intermittent extended cycle, such as the Solka-Floc precoat-polishing filters. The monovalve gravity filter backwash cycle is 5 to 10 minutes, therefore, both filters are in normal use. The test-bed unit does not include any spare pumps. For larger plants, the pumps are spared or multiple partial-capacity units are provided to avoid 100 percent shutdown due to maintainenance.

Due to the complexity of piping surrounding the transport-depletion stacks, a separate flow diagram, Figure 151, is provided to show the controls as well as the piping arrangement.

The flow quantities for each plant capacity that was studied, including the test-bed plant, are shown on a material balance sheet identified as Table 13. The flows in gpm and pressure in psi gage shown on the flow diagram Figure 149, refer to the test-bed plant size.

MARK	DESCRIPTION	CHKD	COMM	APPD	DATE
A	ORIGINAL ISSUE				

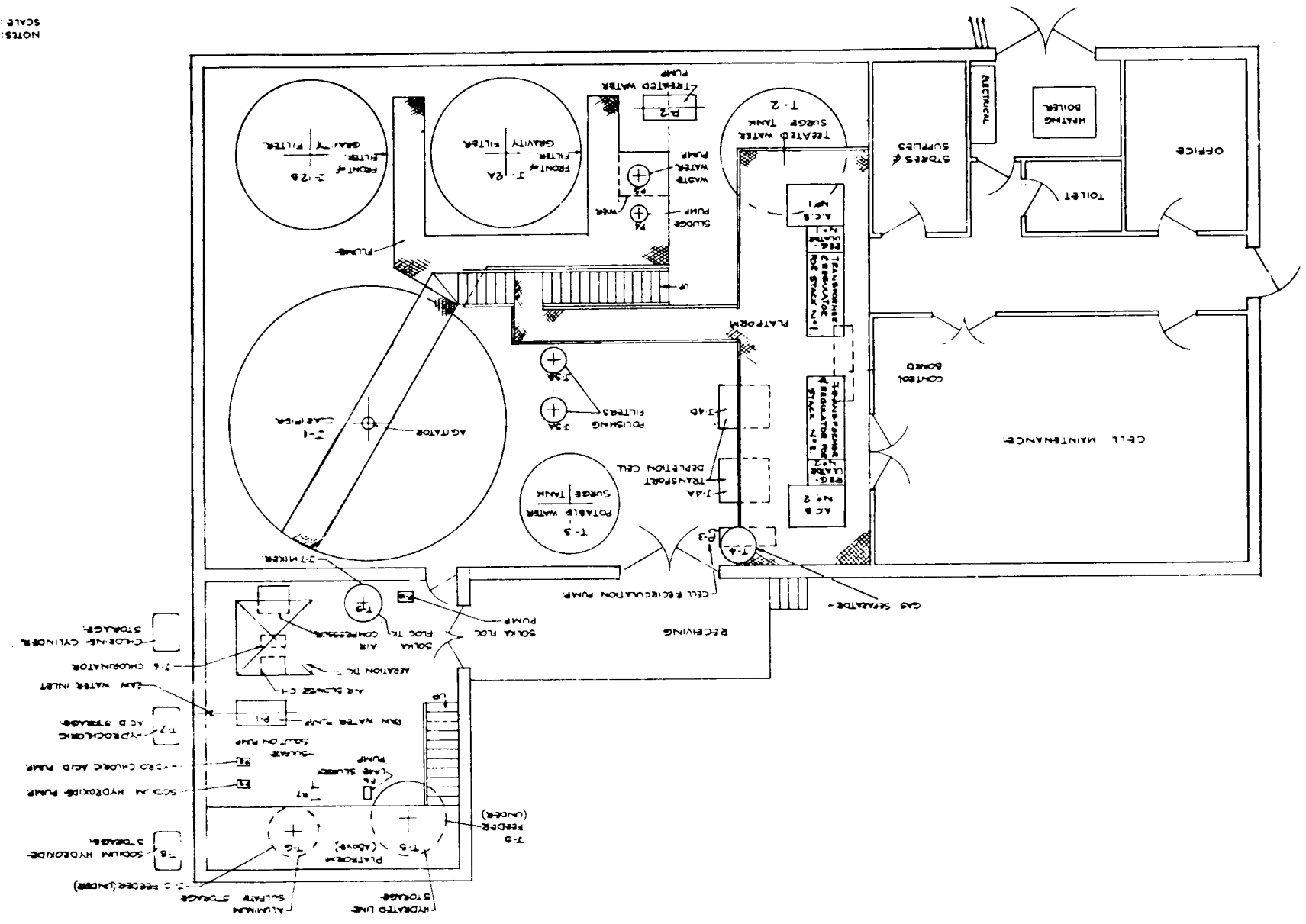

NOTES:
SCALE: 1/4"-1'-0"

Figure 148

7-5-66

500,000 GALS PER DAY TEST BED
TRANSPORT DEPLETION DESALINATION
PLANT
PRATT & WHITNEY AIRCRAFT DIVISION
UNITED AIRCRAFT CORPORATION
STONE & WEBSTER ENGINEERING CORPORATION
BOSTON, MASS.

DRAWING NUMBER 11650-FM-1A

11650-FM-1A.

TABLE 12

Equipment List for 500,000 GPD Test-Bed Plant Study
(Stone & Webster Engineering Corporation table)

Tanks and Bins

Item No.	Service	Type	Capacity, Gal.	Diam. Ft-In.	Height. Ft-In.	Pressure, Psi Gage	Temp. °F	Shell Material	Remarks
T-1	aeration tank	vert. square		6-0x6-0	9-0	atm	70	Wood	tank filled with redwood slats
T-2	treated-water surge tank	vert. cyl.	6,000	10-0	10-0	atm	70	C.S.	AWWA standard and lined with a coating of Plastic No. 7155
T-3	potable-water surge tank	vert. cyl.	3,500	8-0	10-0	atm	70	C.S.	lined with a coating of Plasite No. 7155
T-4	gas separator	vert. cyl.	15 (liq.)	12" pipe	4-4	atm	75	C.S.	
T-5	hydrated-lime storage bin	vert. cyl.	6 tons	6-0	10-0	atm	70	C.S.	conical bottom
T-6	aluminum-sulfate storage bin	vert. cyl.	(for large plants)			atm	70	C.S.	concial bottom and rubber-lined
T-7	hydrochloric-acid storage tank	horiz. cyl.	42			atm	70	C.S.	rubber-lined
T-8	sodium-hydroxide storage tank	horiz. cyl.	42			atm	70	PVC	
T-9	Solka-Floc slurry tank	vert. cyl.	200	3-0	5-0	atm	150	C.S.	

Miscellaneous Equipment

Item No.	Service	Type	Capacity, Gpm	Diam. Ft-In.	Height. Ft-In.	Material	Remarks
J-1	clarifier	vertical	500	22-0	20-0	C.S.	
J-2A/B	monovalve gravity filters	vertical	250	12-0	10-0	C.S.	
J-3A/B	polishing filters	vertical	500	2-0	10-0	C.S.	internal filter elements
J-4A/B	transport-depletion units	2 stage		3-0x3-6x7-6 each			membrane stacks
J-5	waste water and sludge sump		3,600 cu. ft.		5-0 (shallow end) 6-6 (deep end)	Concrete	5'-0" wide by 36'-0" long appr with inlet and outlet weirs. Settling area 5'-0" x 30'-0".
J-6	chlorinator	vertical	5.0				package unit
J-7	hydrated-lime screw conveyor		(for large plants)				
J-8	aluminum-sulfate screw conveyor		(for large plants)				

Item No.	Service	Description
J-9	hydrated-lime feeder	motor-driven gravimetric rotary-type feeder, complete with 50-gal. dissolver, agitator, and 50-cu. ft. extension hopper
J-10	aluminum-sulfate feeder	motor-driven gravimetric rotary-type feeder, complete with 50-gal. dissolver, agitator, and 50-cu. ft. extension hopper
J-11	clamp-on mixer	1/3 hp driver with 4'-6" S.S. shaft and propeller 110v - 1 hp - 60 cy

Pumps and Blowers

Item No.	Service	Type	Design Conditions: Capacity, gpm	Diff. Pressure, psi	Head, ft.	Material	Driver	Hp	Remarks
P-1	raw-water pump	cent.	520	23	53	C.I.	motor	10	
P-2	treated-water pump	cent.	520	98	230	C.I.	motor	40	
P-3	cell recirculation pump	cent.	290	72	170	epoxy resin	motor	20	
P-4	sludge pump	vert. cent.	10	12	30	high-silicon iron	motor	1	
P-5	waste-water pump	vert. cent.	100	12	30	high-silicon iron	motor	2	
P-6	hydrated-lime slurry pump	cent.	10	22	50	Worthite	motor	1	furnish with feeder
P-7	aluminum-sulfate pump	metering	12 gph	22		Worthite	motor	1/2	furnish with feeder
P-8	hydrochloric-acid pump	duplex diaphragm	1.5 gph	67		high-silicon iron	motor	1/2	
P-9	sodium-hydroxide pump	metering	1.0 gph	67		Ni-Cr-Mo	motor	1/2	
P-10	Solka-Floc slurry pump	cent	20	30	70	C.I.		1	
C-1	air blower		1,000 cfm	2		C.I.	motor	15	
C-2	air compressor	oil-free	30 acfm	100		C.I.	motor	10	incl. air dryer

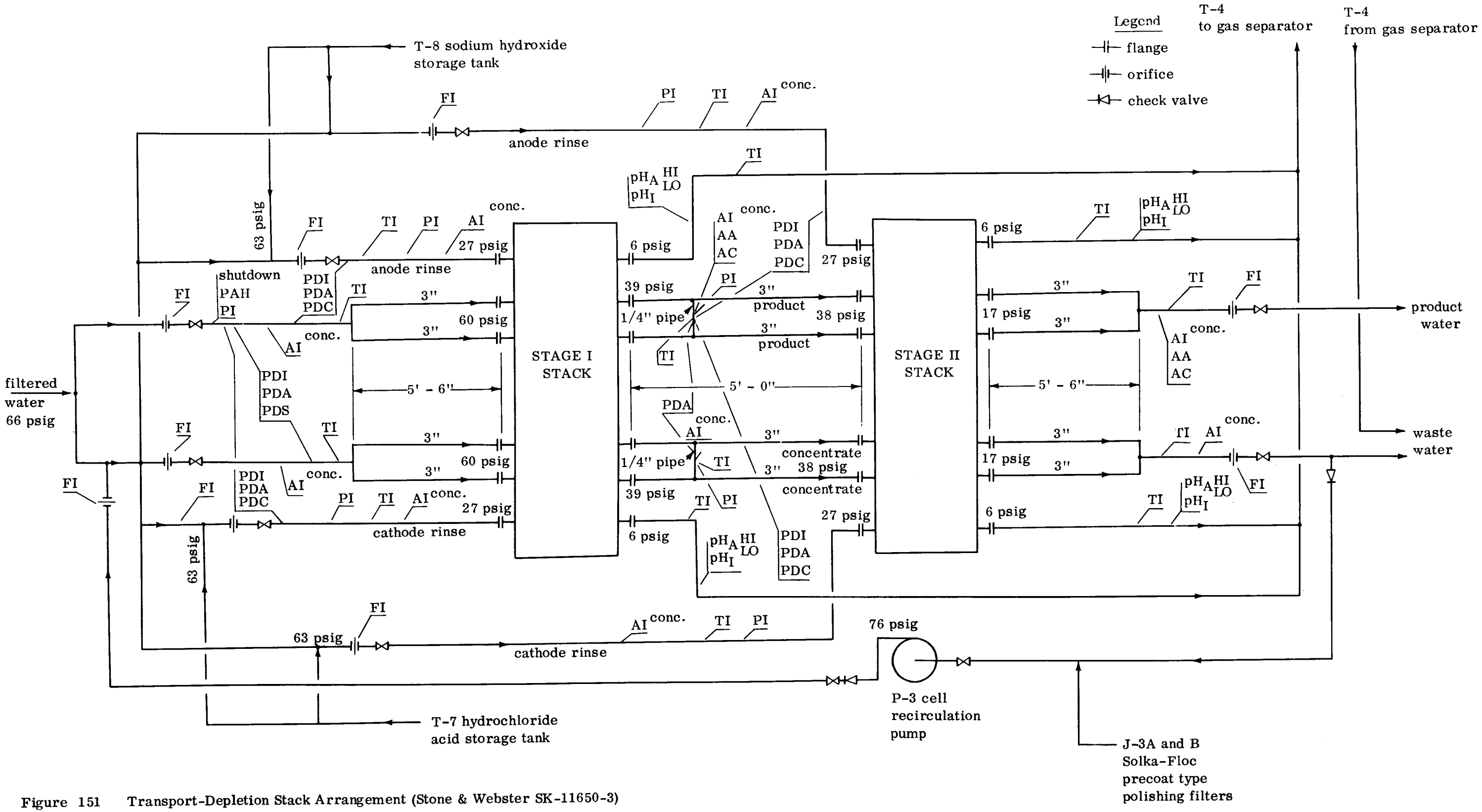

Figure 151 Transport-Depletion Stack Arrangement (Stone & Webster SK-11650-3)

TABLE 13

Transport-Depletion Process Material Balance
(Stone & Webster Engineering Corporation table)

			Plant Size											
			Test Bed 500,000 gpd			1×10^6 gpd			5×10^6 gpd			10×10^6 gpd		
No.	Stream	Fluid	Flow 1000 lb/hr	Press. psig	Temp °F	Flow 1000 lb/hr	Press. psig	Temp. °F	Flow 1000 lb/hr	Press. psig	Temp. °F	Flow 1000 lb/hr	Press. psig	Temp. °F
1	feed	water (w)	235.5	25	70	471.0			2,355			4,710		
2	clarified	w	233.3	6"H_2O	70	466.6			2,333			4,666		
3	*overflow	w	1.7	grav.	70	3.4			17			34		
4	*sludge	suspension	2.2	12	70	4.4			22			44		
5	*filter backwash	suspension	13.0	grav.	70	26.0			130			260		
6	*filter blowdown	suspension	1.3	85/10	70	2.6			13			26		
7	cell recirculation	w	131.5	76	75	263.0			1,315			2,630		
8	concentrate	w	173.5	***	75	347.0			1,735			3,470		
9	anode rinse	w	0.9	***	75	1.8			9			18		
10	cathode rinse	w	0.9	***	75	1.8			9			18		
11	product	w	173.5	17	75	347.0			1,735			3,470		
12	waste	w	42.0	17	75	84.0			420			840		
13	rinse waste	w	1.8	6	75	3.6			18			36		
14	*sludge waste	suspension	16.5	grav.	70	33.0			165			330		
15	treated sludge	suspension	1.6	10	70	3.2			16			32		
16	treated waste	w	42.2	10	70	84.4			422			844		
17	hydrated lime	5% slurry	2.5	22	70	5.0			25			50		
18	aluminum sulfate	5% solution	0.09	22	70	0.18			0.9			1.8		
19	chlorine	0.3% solution	0.14	5	70	0.28			1.4			2.8		
20	chlorine	0.3% solution	0.07	5	70	0.14			0.7			1.4		
21	chlorine	0.3% solution	0.07	22	70	0.14			0.7			1.4		
22	acid (31.5% HCl)	liquid (l)	0.0116	67	70	0.0232			0.116			0.232		
23	acid (31.5% HCl)	l	0.0066	67	70	0.0132			0.066			0.132		
24	acid (31.5% HCl)	l	0.005	3	70	0.01			0.05			0.1		
25	caustic (50% NaOH)	l	0.0046	67	70	0.0092			0.05			0.092		
26	feed aeration	air	1000 cfm	2	70	2000 cfm			10,000 cfm			20,000 cfm		
27	*lime aeration	air	neg.	2	70	neg.			neg.			neg.		
28	air supply	air	1000 cfm	2	70	2000 cfm			10,000 cfm			20,000 cfm		
29	filtered water	w	2.73	100	70	5.46			27.3			54.6		
30	filtered water	w	2.5	100	70	5.0			25			50		
31	filtered water	w	0.23	100	70	0.46			2.3			4.6		
32	dilution	w	0/131.5	25	70	0/263			0/1,315			0/2,630		
33	93% hydrated lime	powder	0.125	atm.	70	0.25			1.25			2.5		
34	aluminum sulfate	granular	0.009	atm.	70	0.018			0.09			0.18		
35	chlorine concentrate	l	0.0002	5	70	0.0004			0.002			0.004		
36	**spec. recirc.	w	0/173.5	17	75	0/347			0/1,735			0/3,470		
37	vent gas	$H_2 + O_2$	0.001	atm.	75	0.002			0.01			0.02		
38	*Solka-Floc	1/2% slurry	10	30	70	20			100			200		

*Intermittent flow
**Startup and balance line - 0/131.5 indicates range of flow (normal flow = 0)
***Refer to Figure 151

C. Cost Estimates for Test-Bed Plant

1. Investment Costs

An estimate of the investment costs for the 500,000 gpd test-bed plant is provided in Table 14. A detailed breakdown of both construction costs and owners costs is provided which shows that the total investment cost for this plant would be $1,401,700.

2. Operating Costs

Annual operating costs for the test-bed plant are shown in Table 15. The cost of water from this plant is estimated as $1.81 per 1000 gallons of potable water produced.

Table 16 lists the staff requirements and salaries that were assumed for the test-bed cost estimate, as well as for the larger commercial-size plants.

TABLE 14

Estimate of Investment Costs for 0.5 MGD
Transport-Depletion Desalination Plant
(Stone & Webster Engineering Corporation table)

CONSTRUCTION COSTS

Direct Costs	Material Costs	Labor Costs	Total Costs
site development	$ 500	$ 2,000	$ 2,500
raw-water intake structures	-	not included	-
plant buildings (including foundations, structures and painting)	135,000	92,000	227,000
raw-water storage	-	not included	-
raw-water treatment	86,700	5,300	92,000
raw-water pumps and strainers	700	200	900
chemical-feed equipment	19,800	2,700	22,500
treated-water pumps, filters, tanks and other equipment	5,500	500	6,000
transport-depletion cells, recirculation pumps and degasifier equipment	199,500	10,500	210,000
piping and covering	48,500	51,900	100,400
instrumentation (including pH control and air compressor	22,500	4,500	27,000
electrical equipment and wiring	96,400	18,600	115,000
product-water chlorination	4,000	300	4,300
product-water storage	4,000	300	4,300
waste water and sludge disposal equipment (not including brine)	6,100	400	6,500
total direct costs	$629,200	$189,200	$818,400
Distributable Costs			
office at works	$ 8,100	$ 40,000	$ 48,100
construction equipment, supplies and temporary construction	21,000	2,000	23,000
federal and state taxes, payroll burden and other distributables	-	48,000	48,000
total distributables	$ 29,100	$ 90,000	$119,100
TOTAL CONSTRUCTION COSTS	$658,300	$279,200	$937,500
Indirect Costs			
engineering and design	$ 78,700	$ 72,500	$151,200
allowance for indeterminants	33,000	28,300	61,300
fee	64,000	-	64,000
total indirect costs	$175,700	$100,800	$276,500
total construction			$1,214,000
OWNERS COST			
land			$ 500
interest during construction @ 3.25% of total construction and indirect costs			19,750
spare parts inventory (includes one spare stack)			102,800
machine tools and laboratory supplies			6,000
furniture and furnishings			2,000
start-up labor and materials			53,650
miscellaneous (including legal, travel and public relations)			3,000
total owners costs			$187,700
TOTAL INVESTMENT COSTS			$1,401,700
ESTIMATED CONSTRUCTION PERIOD			6 months

TABLE 15

Estimate of Annual Operating Costs for
0.5 MGD Transport-Depletion Desalination Plant
(Stone & Webster Engineering Corporation table)

FIXED OPERATING COSTS	
fixed charges on investment @ 5.27 percent + 0.25 percent for insurance	$ 77,370
operating labor	61,000
maintenance labor	15,000
general and administrative (overhead) including payroll burden	34,200
total fixed operating costs	$187,570
VARIABLE OPERATING COSTS	
membrane replacement	$ 2,560
maintenance supplies @ 0.5 percent of investment	7,100
chemical supplies	56,990
electrical energy @ $.007 per kwhr	37,500
brine disposal @ $.03 per 1,000 gal.	1,180
total variable operating costs	$105,330
TOTAL ANNUAL OPERATING COSTS	$292,900
UNIT PRODUCTION COSTS PER 1,000 GALLONS	$1.81

TABLE 16

Staff REquirements for Transport-
Depletion Desalination Plants
(Stone & Webster Engineering Corporation table)

Plant Size, MGD	0.5	1.0	5.0	10.0
Staff Position				
plant superintendent		1	1	1
plant engineer	1			1
plant chemist			1	1
assistant chemist	1	1		1
shift supervisor			4	4
shift operators	4	4	4	4
maintenance supervisor @ 11,000			1	1
mechanical maintenance @ 8,000	1	1	1	1
electrical maintenance @ 8,000			1	1
membrane replacement @ 7,000	1	1	2	2
instrument technician (pneumatic)				1
instrument technician (electrical)			1	1
clerk-steno	1	1	2	2
timekeeper				1
storekeeper				1
janitor	1	1	1	1
laborer				
totals	10	10	19	24
annual salary costs	$ 76,000	$ 77,200	$160,200	$200,200
payroll burden @ 15%	11,400	11,580	24,030	30,030
administrative & overhead @ 30%	22,800	23,160	48,060	60,060
total labor costs	$110,200	$111,940	$232,290	$290,290

IX. COMMERCIAL-PLANT PARAMETRIC COST ANALYSIS

A. Ground Rules and Methods

A parametric cost study was performed by Pratt & Whitney Aircraft to determine the effect of various changes in design and performance conditions on the cost of product water produced by commercial plants of 1, 5 and 10 mgd capacity. This study is based on the commercial-stack design described in Section VIII and the ground rules listed in Table 7.

Stone & Webster Engineering Corporation prepared a series of projected investment and operating costs for commercial plants of 1, 5 and 10 MGD capacity. These cost estimates were based on the same ground rules and process schematic that were used for the test-bed plant study described in Section VIII.

The costs estimated by Stone & Webster are considered the most realistic possible at the time of the study and can be used to normalize the parametric results generated by Pratt & Whitney. Accordingly, the results of the parametric study are presented as "relative" product-water cost versus the particular variable of interest.

B. Parametric Cost Study Results

The parametric cost study is based on a mathematical analysis that was subsequently programmed for high-speed digital-computer use. A logic flow chart showing the cost-estimating procedure is presented in Figure 152.

The plant parameters that were varied are:

plant capacity	1, 5 and 10 mgd
feedwater quality	1500, 2500 and 3500 ppm NaCl
average plant current density	10 to 34 ma/cm^2

The results of the parametric study are shown in Figures 153 through 161. Figures 153, 154 and 155 show the effect of feedwater quality on product-water cost for plant capacities of 1, 5 and 10 mgd respectively. As might be expected, the cost of water is almost directly proportional to the amount of demineralization required. Also, the optimum current density decreases with decreasing feedwater salt concentration, ranging from about 23 ma/cm^2 at 3500 ppm to about 12 ma/cm^2 at 1500 ppm.

Figures 156 through 161 show the effect of plant capacity on product-water cost for feedwater salinities of 3500, 2500, and 1500 ppm NaCl. An examination of Figures 157, 159 and 161 shows that the cost of product water decreases asymmptotically to some limiting value as plant capacity is increased. It also appears that the limiting value is nearly reached at a plant capacity of 10 mgd. The optimum current density is quite insensitive to plant capacity and is primarily a function of feedwater quality.

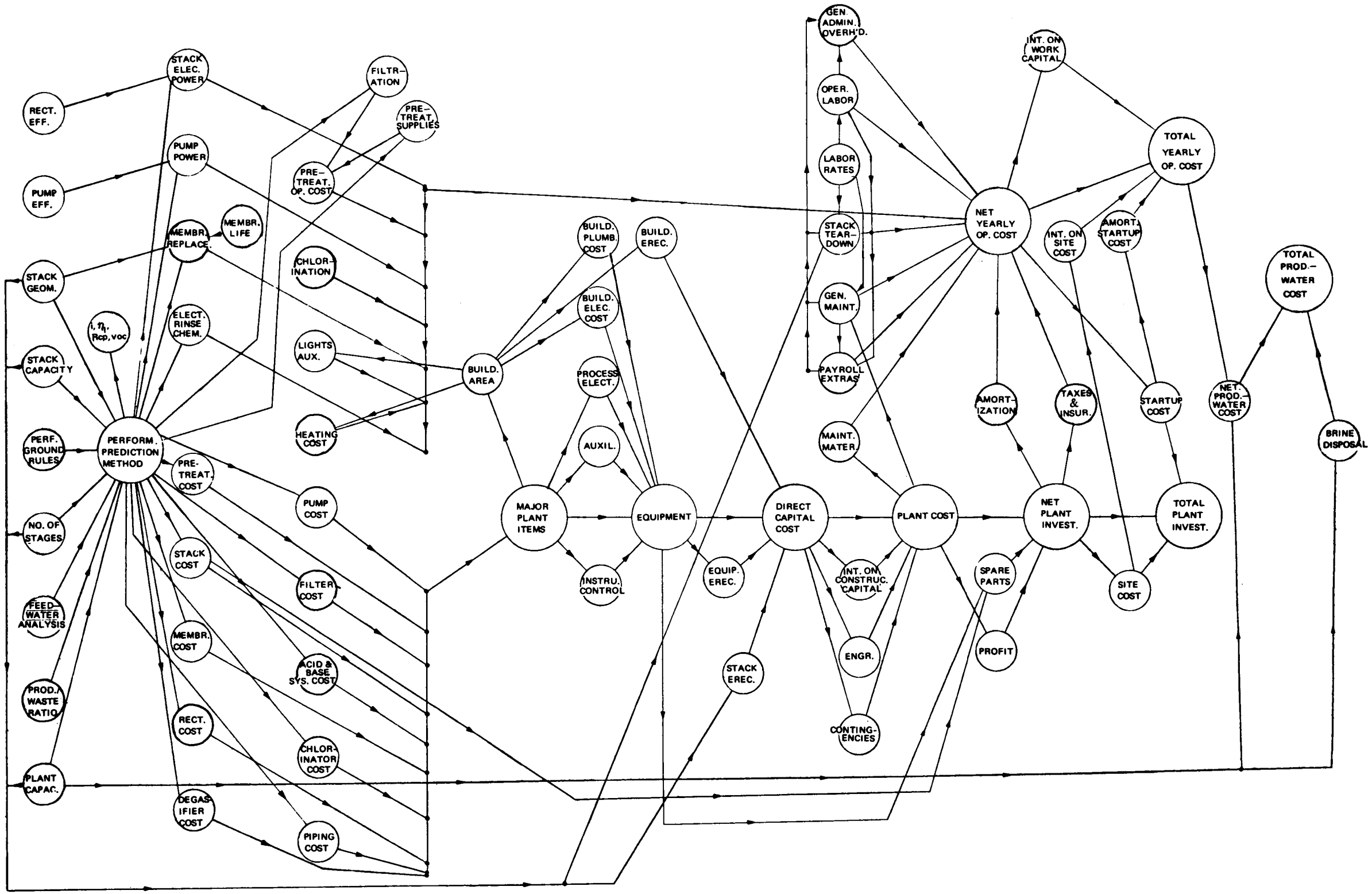

Figure 152 Water Cost Estimating Procedure

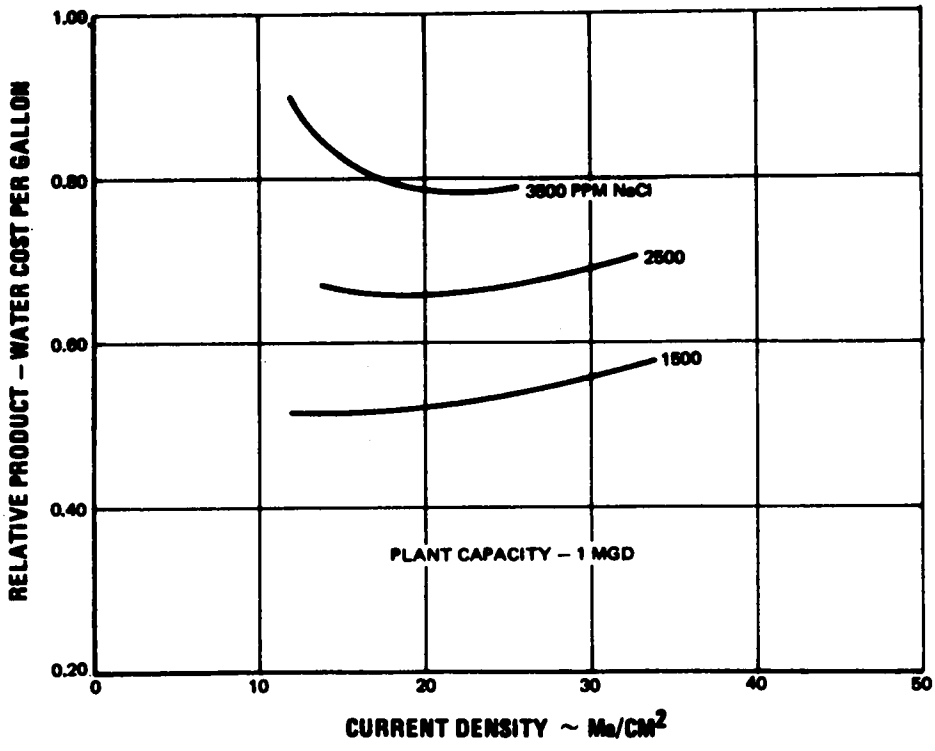

Figure 153 Product-Water Cost vs Current Density. Plant Capacity 1 MGD

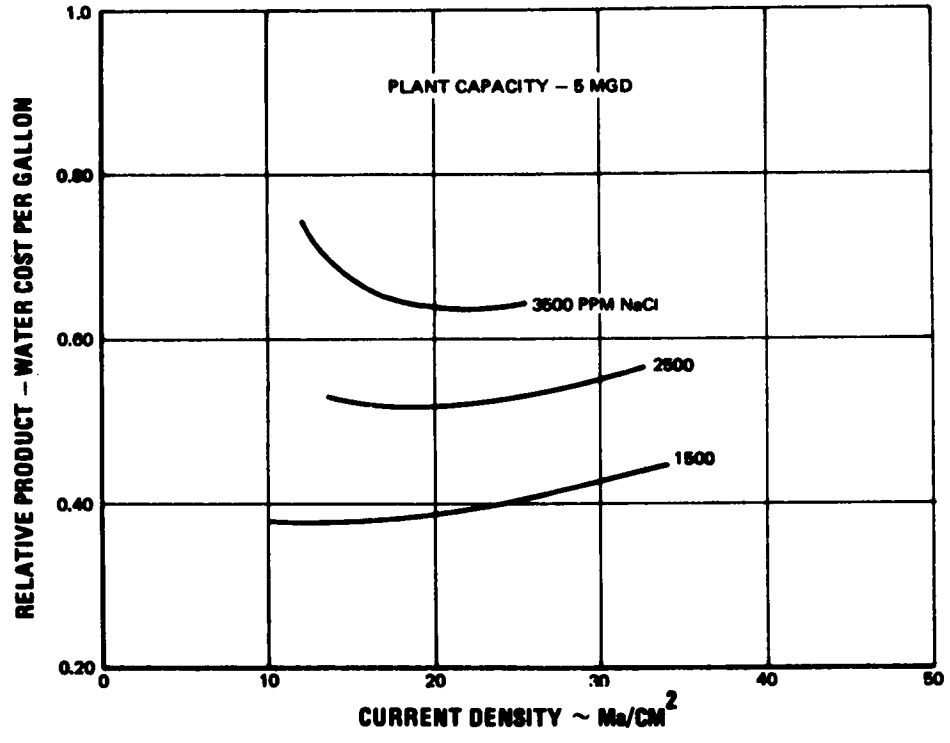

Figure 154 Product-Water Cost vs Current Density. Plant Capacity 5 MGD

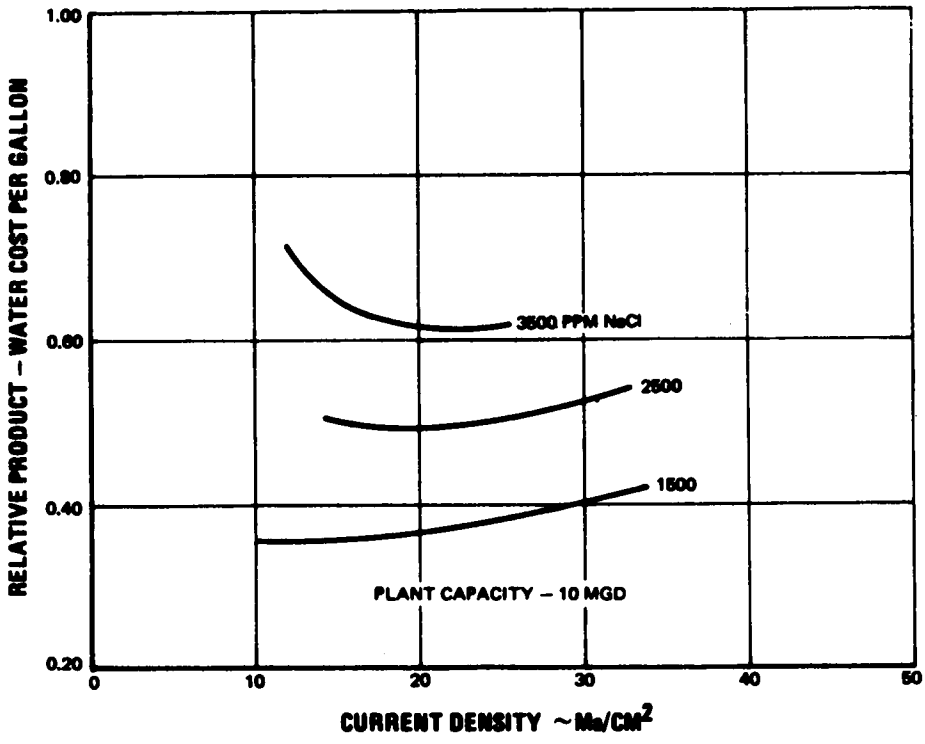

Figure 155 Product-Water Cost vs Current Density. Plant Capac ity 10 MGD

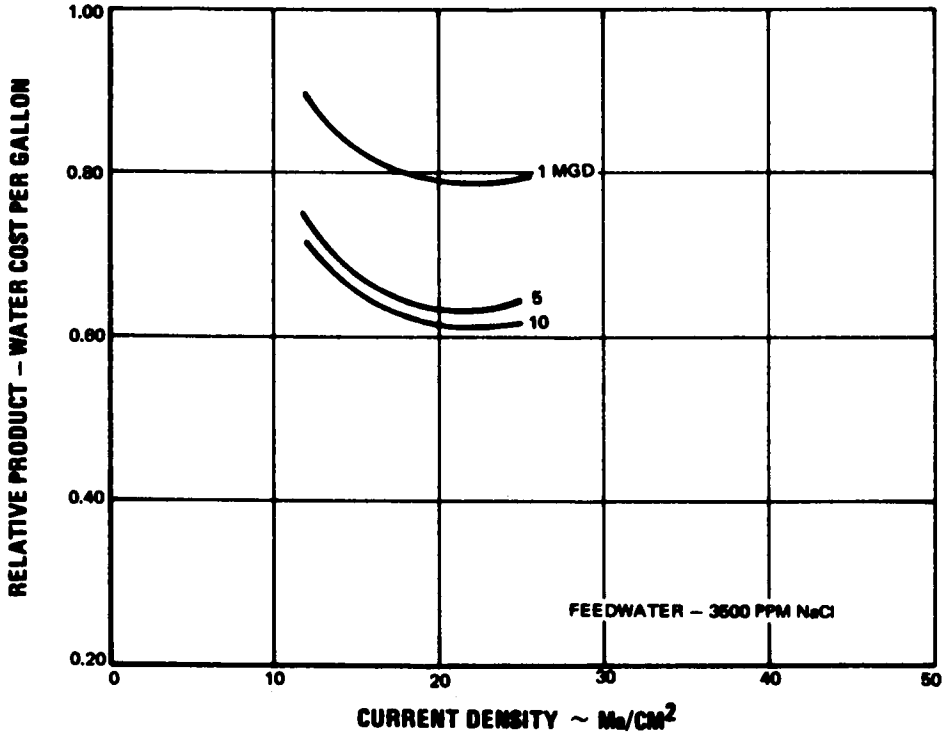

Figure 156 Product-Water Cost vs Current Density. Feedwater 3500 ppm NaCl

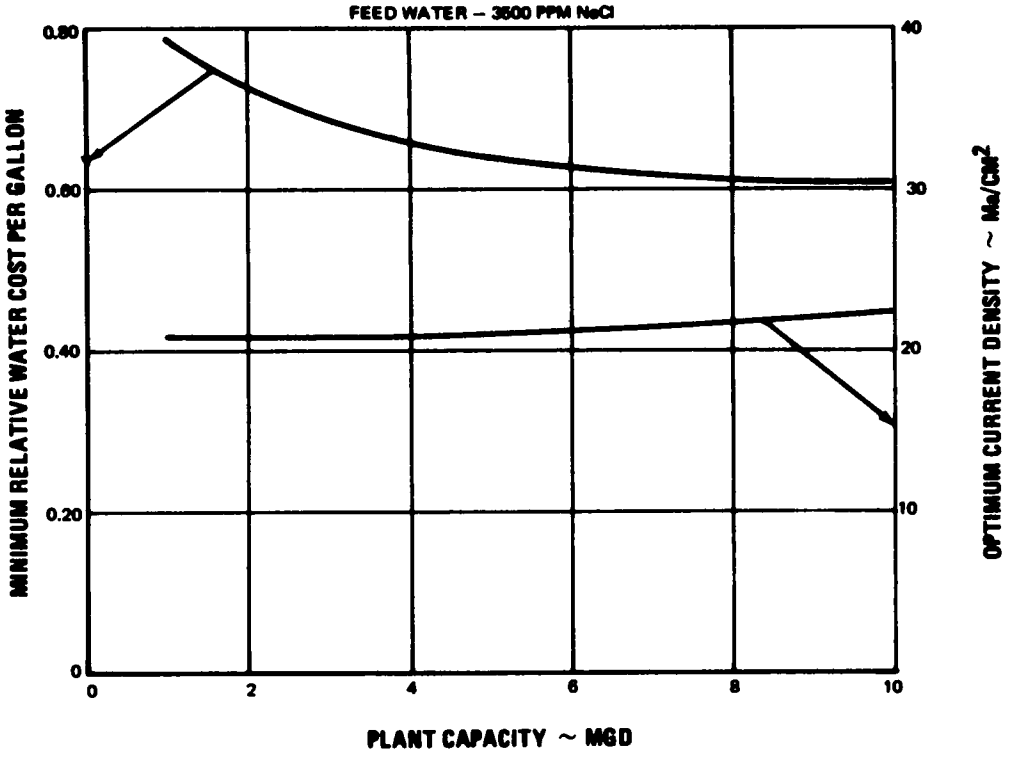

Figure 157 Optimum Current Density and Water Cost vs Plant Capacity. Feedwater 3500 ppm NaCl

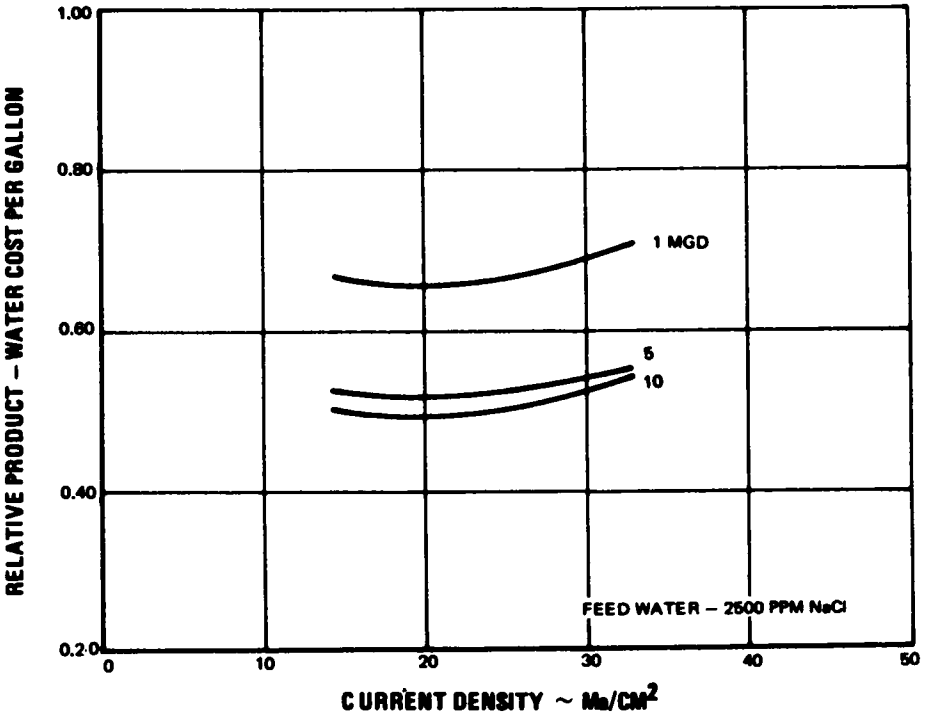

Figure 158 Product-Water Cost vs Current Density. Feedwater 2500 ppm NaCl

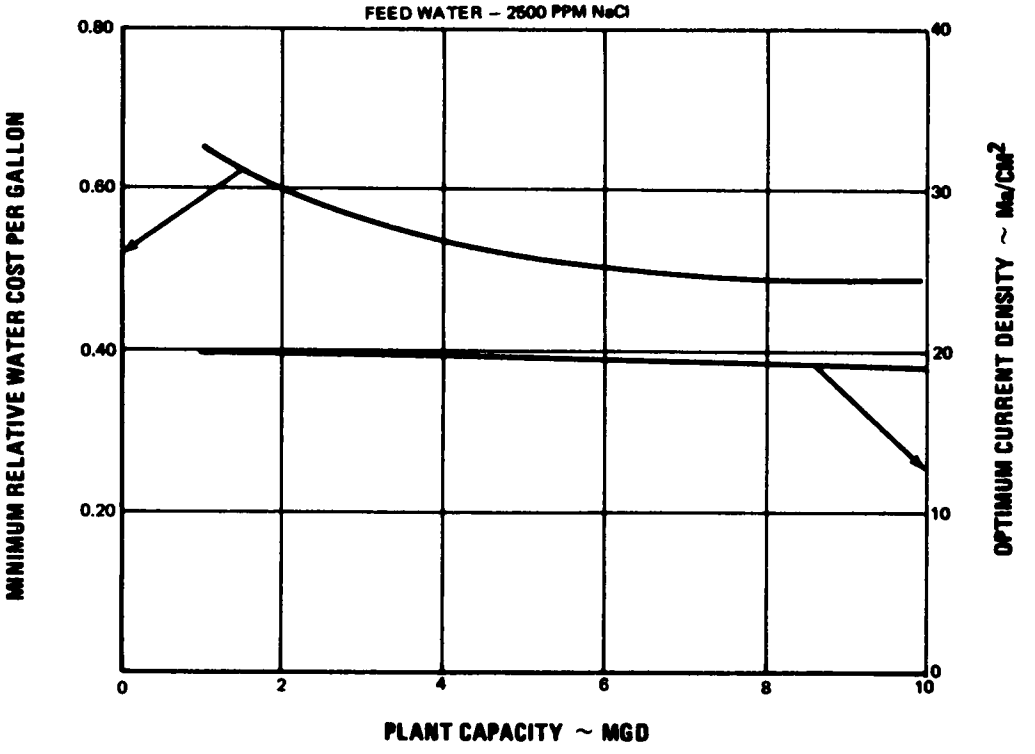

Figure 159 Optimum Current Density and Water Cost vs Plant Capacity. Feedwater 2500 ppm NaCl

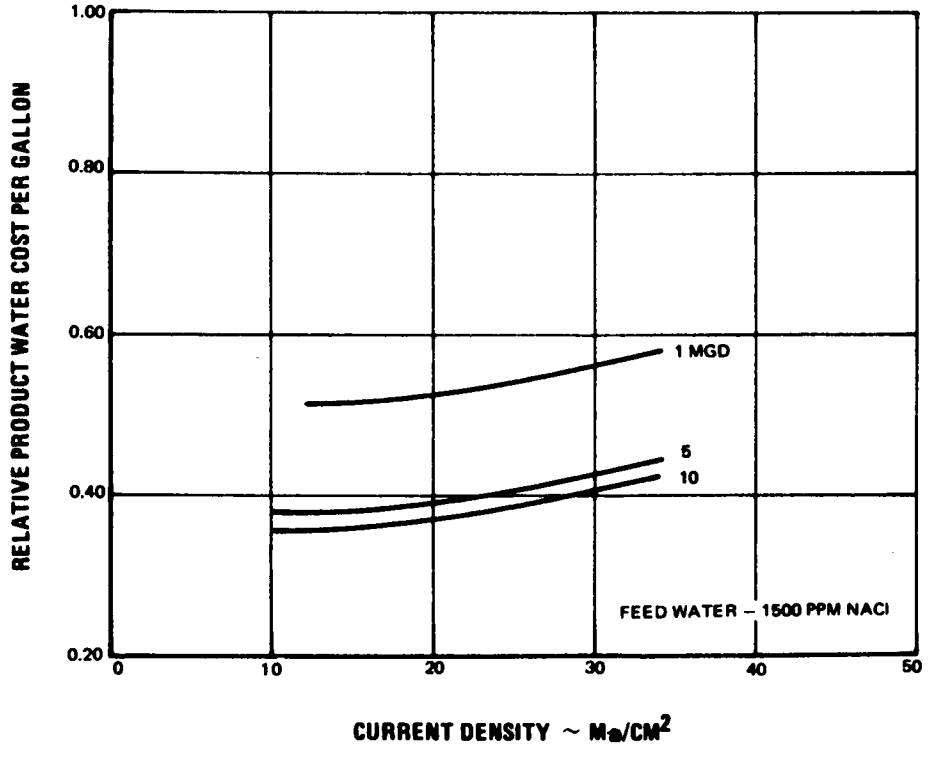

Figure 160 Product-Water Cost vs Current Density. Feedwater 1500 ppm NaCl

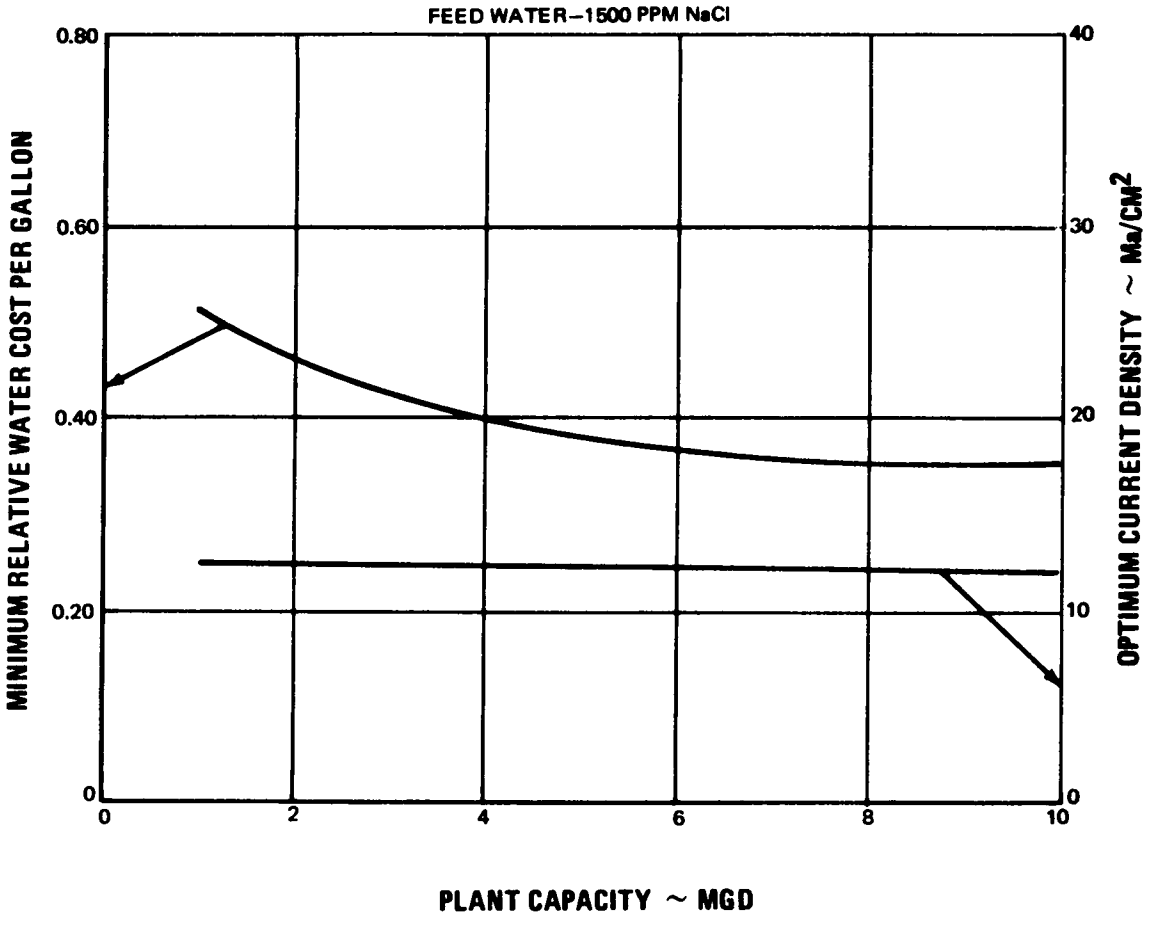

Figure 161 Optimum Current Density and Water Cost vs Plant Capacity. Feedwater 1500 ppm NaCl

C. Cost Estimates

The projected cost estimates for transport-depletion plants of 1, 5 and 10 mgd capacity generated by Stone and Webster Engineering are shown in Tables 17 through 22. The flow quantities for each plant size are shown on the material-balance sheet in Table 13. The flow streams in Table 13 refer to the process-flow diagram, Figure 149. The equipment list in Table 12 also shows the additional equipment required for the larger plant sizes. The staff requirements and salaries for the commercial-size plant are shown in Table 16.

The estimated costs, including the test-bed costs are summarized in Table 23.

TABLE 17

Estimate of Investment Costs for 1.0 MGD
Transport-Depletion Desalination Plant
(Stone & Webster Engineering Corporation table)

CONSTRUCTION

	Material Costs	Labor Costs	Total Costs
Direct Costs			
site development	750	3,050	$ 3,800
raw-water intake structures	–	Not included	–
plant buildings (including foundations, structures and painting	136,800	91,100	227,900
raw-water storage	–	Not included	–
raw-water treatment	132,000	8,050	140,050
raw-water pumps and strainers	1,050	300	1,350
chemical-feed equipment	30,100	4,100	34,200
treated-water pumps, filters, tanks and other equipment	8,350	750	9,100
transport-depletion cells, recirculation pumps and degasifier equipment	397,800	16,000	413,800
piping and covering	91,100	109,000	200,100
instrumentation (including pH control and air compressor equipment)	34,200	6,850	41,050
electrical equipment and wiring	152,000	42,600	194,600
product-water chlorination	6,100	450	6,550
product-water storage	6,100	450	6,550
waste-water and sludge-disposal equipment (not including brine)	9,250	600	9,850
total direct costs	$1,005,600	$283,300	$1,288,900
Distributable Costs			
office at works	$ 12,300	$ 60,800	$ 73,100
construction equipment, supplies and temporary construction	32,000	3,000	35,000
federal and state taxes, payroll burden and other distributables	–	73,000	73,000
total distributables	$ 44,300	$136,800	$ 181,100
TOTAL CONSTRUCTION COSTS			$1,470,000
Indirect Costs			
engineering and design	$ 104,000	$ 94,700	$ 198,700
allowance for indeterminants	50,200	43,000	93,200
fee	97,100	–	97,100
total indirect costs	$ 251,300	$137,700	$ 389,000
TOTAL CONSTRUCTION AND INDIRECT COSTS			$1,859,000
OWNERS COST			
land			$ 750
interest during construction @ 3.25% of total construction and indirect costs			40,300
spare parts inventory (includes one spare stack)			125,900
machine tools and laboratory supplies			7,900
furniture and furnishings			2,650
start-up labor and materials			73,550
miscellaneous (including legal, travel and public relations			3,950
Total Owners Costs			$ 255,000
TOTAL INVESTMENT COSTS			$2,114,000
ESTIMATED CONSTRUCTION PERIOD			8 Months

TABLE 18

Estimate of Annual Operating Costs for
1.0 MGD Transport-Depletion Desalination Plant
(Stone & Webster Engineering Corporation table)

FIXED OPERATING COSTS	
fixed charges on investment @ 5.27 percent + 0.25 percent for insurance	$116,700
operating labor	62,200
maintenance labor	15,000
general and administrative (overhead) including payroll burden	34,750
total fixed operating costs	$228,650
VARIABLE OPERATING COSTS	
membrane replacement	$ 5,120
maintenance supplies @ 0.5 percent of investment	10,700
chemical supplies	89,670
electrical energy @ $.007 per Kwhr	75,000
brine disposal @ $.03 per 1,000 gal	2,360
total variable operating costs	$182,850
TOTAL ANNUAL OPERATING COSTS	$411,500
UNIT PRODUCTION COSTS PER 1,000 GALLONS	$ 1.270

TABLE 19

Estimate of Investment Costs for 5.0 MGD
Transport-Depletion Desalination Plant
(Stone & Webster Engineering Corporation table)

CONSTRUCTION COSTS

	Material Costs	Labor Costs	Total Costs
Direct Costs			
site development	$ 2,000	$ 8,000	$ 10,000
raw-water intake structures	-	Not included	-
plant buildings (including foundations, structures and painting)	360,000	240,000	600,000
raw-water storage	-	Not included	-
raw-water treatment	347,000	21,000	368,000
raw-water pumps and strainers	2,800	800	3,600
chemical-feed equipment	79,100	10,800	89,900
treated-water pumps, filters, tanks and other equipment	22,000	2,000	24,000
transport-depletion cells, recirculation pumps and degasifier equipment	1,980,000	42,000	2,022,000
piping and covering	240,000	288,000	528,000
instrumentation (including pH control and air compressor equipment)	90,000	18,000	108,000
electrical-equipment and wiring	400,000	112,000	512,000
product-water chlorination	16,000	1,200	17,200
product-water storage	6,100	400	6,500
waste-water and sludge-disposal equipment (not including brine)	24,200	1,600	25,800
total direct costs	$3,569,200	$745,800	$4,315,000
Distributable Costs			
office at works	$ 32,000	$160,000	$ 192,000
construction equipment, supplies and temporary construction	84,000	8,000	92,000
federal and state taxes, payroll burden and other distributables		192,000	192,000
total distributables	$ 116,000	$360,000	$ 476,000
TOTAL CONSTRUCTION COSTS			$4,791,000
Indirect Costs			
engineering and design	$ 197,000	$182,000	$ 379,000
allowance for indeterminants	132,000	113,000	245,000
fee	216,000		216,000
total indirect costs	$ 545,000	$295,000	$ 840,000
Total Construction and Indirect Costs			$5,631,000
OWNERS COST			
land			$ 2,000
interest during construction @ 3.25% of total construction and indirect costs			152,500
spare parts inventory (includes one spare stack)			132,500
machine tools and laboratory supplies			12,000
furniture and furnishings			5,000
start-up labor and materials			280,000
miscellaneous (including legal, travel and public relations)			5,000
Total Owners Costs			$ 589,000
TOTAL INVESTMENT COSTS			$6,220,000
ESTIMATED CONSTRUCTION PERIOD			10 Months

TABLE 20

Estimate of Annual Operating Costs for
5.0 MGD Transport-Depletion Desalination Plant
(Stone & Webster Engineering Corporation table)

FIXED OPERATING COSTS	
fixed charges on investment @ 5.27 percent + 0.25 percent for insurance	$ 343,900
operating labor	119,200
maintenance labor	41,000
general and administrative (overhead) including payroll burden	72,100
total fixed operating costs	$ 576,200
VARIABLE OPERATING COSTS	
membrane replacement	$ 25,600
maintenance supplies @ 0.5 percent of investment	31,000
chemical supplies	448,300
electrical energy @ $.007 per Kwhr	375,000
brine disposal @ $.028 per 1,000 gal	11,000
total variable operating costs	$ 890,900
TOTAL ANNUAL OPERATING COSTS	$1,467,100
UNIT PRODUCTION COSTS PER 1,000 GALLONS	$.906

TABLE 21

Estimate of Investment Costs for 10.0 MGD
Transport-Depletion Desalination Plant
(Stone & Webster Engineering Corporation table)

CONSTRUCTION COSTS

	Material Costs	Labor Costs	Total Costs
Direct Costs			
site development	$ 3,100	$ 12,100	$ 15,200
raw-water intake structures	–	Not included	–
plant buildings (including foundations, structures and painting)	545,000	362,000	907,000
raw-water storage	–	Not included	–
raw-water treatment	526,000	32,000	558,000
raw-water pumps and strainers	4,200	1,200	5,400
chemical-feed equipment	120,000	16,300	136,300
treated-water pumps, filters, tanks and other equipment	33,200	3,000	36,200
transport-depletion cells, recirculation pumps and degasifier equipment	3,943,100	63,700	4,006,800
piping and covering	362,000	435,000	797,000
instrumentation (including pH control and air compressor equipment)	136,200	27,300	163,500
electrical-equipment and wiring	605,000	170,000	775,000
product-water chlorination	24,300	1,800	26,100
product-water storage	24,300	1,800	26,100
waste-water and sludge-disposal equipment (not including brine)	36,800	2,400	29,200
total direct costs	$6,363,200	$1,128,600	$ 7,491,800
Distributable Costs			
office at works	$ 48,600	$ 242,000	$ 290,600
construction equipment, supplies and temporary construction	12,700	11,900	24,600
federal and state taxes, payroll burden and other distributables	–	291,900	291,000
total distributables	$ 61,300	$ 544,900	$ 606,200
TOTAL CONSTRUCTION COSTS			$ 8,098,000
Indirect Costs			
engineering and design	$ 261,000	$ 238,000	$ 499,000
allowance for indeterminants	126,000	108,000	234,000
fee	360,000	–	360,000
total indirect costs	$ 747,000	$ 346,000	$ 1,093,000
Total Construction and Indirect Costs			$ 9,191,000
OWNERS COST			
land			$ 3,000
interest during construction @ 3.25% of total construction and indirect costs			299,000
spare parts inventory (includes two spare stacks)			260,000
machine tools and laboratory supplies			20,000
furniture and furnishings			6,000
start-up labor and materials			514,000
miscellaneous (including legal, travel and public relations)			10,000
Total Owners Costs			$ 1,112,000
TOTAL INVESTMENT COSTS			$10,303,000
ESTIMATED CONSTRUCTION PERIOD			12 Months

TABLE 22

Estimate of Annual Operating Costs for
10.0 MGD Transport-Depletion Desalination Plant
(Stone & Webster Engineering Corporation table)

FIXED OPERATING COSTS	
fixed charges on investment @ 5.27 percent + 0.25 percent for insurance	$ 569,000
operating labor	159,200
maintenance labor	41,000
general and administrative (overhead) including payroll burden	90,090
total fixed operating costs	$ 859,290
VARIABLE OPERATING COSTS	
membrane replacement	$ 51,200
maintenance supplies @ 0.5 percent of investment	50,000
chemical supplies	896,866
electrical energy @ $.007 per Kwhr	750,000
brine disposal @ $.025 per 1,000 gal	19,650
total variable operating costs	$1,767,710
TOTAL ANNUAL OPERATING COSTS	$2,627,000
UNIT PRODUCTION COSTS PER 1,000 GALLONS	$.811

TABLE 23

Summary of Projected Cost Estimates

plant capacity	0.5 MGD	1 MGD	5 MGD	10 MGD
total investment costs	$\$1.4017 \times 10^6$	$\$2.114 \times 10^6$	$\$6.220 \times 10^6$	$\$10.303 \times 10^6$
unit production costs per 1000 gallons	\$1.81	\$1.270	\$0.906	\$ 0.811

These values can be used to normalize the parametric data and determine the effect of feed-water salt concentration on the actual unit cost of water.

X. CONCLUSIONS AND RECOMMENDATIONS

This section summarizes the significant results of an eighteen-month engineering-development program for the Office of Saline Water. The major findings are noted and the areas requiring further investigation to properly evaluate the transport-depletion process for desalting brackish waters are identified.

1. The transport-depletion process offers several important potential advantages over the conventional electrodialysis process, including higher current densities, lower cell-pair resistance, no membrane fouling, and less costly neutral membranes.

   Some of these have been demonstrated. Additional tests are required to clearly demonstrate others. Tests with the pilot plant showed that high current densities are possible with no indications of boundary-layer polarization. The maximum measured current density of 50 ma/cm^2 represents a pilot-plant power-supply current limitation only, and there was no indication that higher current densities could not be achieved. The pilot-plant tests also demonstrated relatively-low cell-pair resistance. High cell-pair resistance occurred only with very low product-stream concentrations, and appeared to be the result of high bulk-solution resistance, as opposed to boundary-layer resistance.

2. Preliminary tests indicate that minimum cost to purify brackish water will be achieved at process-stream velocities between 4 and 5 inches/sec and at a process-stream path length of about 100 inches.

3. Most investigations to date have been done using a synthetic Na Cl feed solution. With the exception of some SRI tests, the limited number of brachish-water tests that have been made, used stacks designed for the conventional electrodialysis process, and do not permit optimum conditions for transport depletion. Comparative tests are desirable between NaCl solutions and typical brachish waters using the same stack and membrane-pair type in order to separate the effects on performance of feed-solution quality from those of stack design and membrane type.

4. An improved neutral membrane is required to maintain a reasonable current efficiency (above 55 percent) at low solution concentrations. The present neutral membrane of regenerated cellulose becomes increasingly cationic as solution concentration is decreased. Perhaps an anion membrane with a constant near-neutral transport number is required. Such a membrane should be free from fouling and of reasonable cost in order to realize all the potential advantages of the transport-depletion process.

5. The test-bed and commercial-plant cost studies show that a significant portion of the cost of water from a transport-depletion plant is associated with the cost of pretreatment and related chemicals. Further studies and long-term tests are required using actual brachish waters to determine the minimum and most economical pretreatment requirements for the transport-depletion process.

6. Tests on simulated and/or real brackish waters are required to assess the economic potential of the transport-depletion process. These tests should include long-time operation to establish membrane-replacement frequency.

XI. SUBJECT INVENTIONS

The following is a complete list of all subject inventions resulting from the work performed under this contract:

Neutral Electrodialysis Stack Spacer
Gasket Spacer - Turbulator
Membrane Stack Arrangement
Water Desalting Step-Flow Module
Four-Stack Desalting Module
External Manifold (for T.D. Screen)
Frame Assemblies

Full information relative to these subject inventions was submitted in Pratt & Whitney Aircraft letters dated October 10, 1967, December 1, 1967 and May 15, 1968.

☆ U. S. GOVERNMENT PRINTING OFFICE : 1971 O - 426-334